ROLE OF FRACTURING FLUID ON THE BREAKDOWN PRESSURE OF TIGHT SANDSTONE ROCKS

BY

Arqam Muqtadir

A Thesis Presented to the

DEANSHIP OF GRADUATE STUDIES

KING FAHD UNIVERSITY OF PETROLEUM & MINERALS

DHAHRAN, SAUDI ARABIA

In Partial Fulfillment of the

Requirements for the Degree of

MASTER OF SCIENCE

In

PETROLEUM ENGINEERING

December 2017

KING FAHD UNIVERSITY OF PETROLEUM & MINERALS

DHAHRAN- 31261, SAUDI ARABIA

DEANSHIP OF GRADUATE STUDIES

This thesis, written by **Arqam Muqtadir** under the direction of his thesis advisor and approved by his thesis committee, has been presented and accepted by the Dean of Graduate Studies, in partial fulfillment of the requirements for the degree of **MASTER OF SCIENCE IN PETROLEUM ENGINEERING.**

Dr. Abdulazeez Abdulraheem
(Advisor)

Dr. Dhafer A. Al-Shehri
Department Chairman

Dr. Salaheldin Elkatatny
(Co-Advisor)

Dr. Salam A. Zummo
Dean of Graduate Studies

عمادة الدراسات العليا
DEANSHIP OF GRADUATE STUDIES

Dr. Mohamed Mahmoud
(Member)

٧/١/١٨

Date

Dr. Dhafer A. Al Shehri
(Member)

Dr. Michael Fraim
(Member)

© Arqam Muqtadir
2017

Dedication

To my beloved parents, sister and brothers

To my nephews Abdurrahman and Mishary

ACKNOWLEDGEMENTS

Thanks to Almighty Allah for giving me the strength to complete this thesis. A heartfelt thanks goes to my family for their endless support, patience and sound advice at every stage of the Master's program.

I express my sincere gratitude to my advisor, Dr. Abdulazeez Abdulraheem for generously sharing his wealth of knowledge and experience. I would also like to thank my Co-Advisor Dr. Salaheldin Elkatatny for dedicating his tireless efforts. Special thanks goes to my committee members Dr. Mohamed Mahmoud, Dr. Dhafer Al Shehri and Dr. Michael Fraim for their insightful comments and discussions.

I would like to acknowledge the efforts of Dr. Ahmed Gomaa (BP, Houston) for assisting in this thesis, Abdulwahab Zaki Ali for providing access to the Geomechanical facility at CIPR, Mobeen Murtuza for assisting in the preparation of the Fracturing Cell setup, Rizwanullah Hussaini and Hani Al Mukainah for conducting CT Scans and Shujath Ali (Baker Hughes) for UCS and Brazilian tests. I would also like to thank Abdulhameed Al Rumaih, Abdulsamed Iddris, Abdulrahim Muhammadain, Assad Barri, Ahmad Mahboob, Sarmad Zafar Khan, Louie Panoy, Ahmad Adewunmi, Lionel Talley, Eassa Abdullah, Rahul Babu, Saud Al-Dughaimi, Abbas Al Abdullah, Redha Al-Abdrabalnabi and Abdelmjeed Mohamed for their efforts.

Thanks to my friends Faisal Ramzan, Mohammad Al Fattah, Muhammad Hassan, Zeeshan Tariq, Ahmed Sadeed, Hasan Islam and Mohammad Abdelwahab for their support and guidance, without which this thesis would be incomplete.

TABLE OF CONTENTS

LIST OF TABLES

LIST OF FIGURES

LIST OF ABBREVIATIONS

BHT	:	Bottomhole Temperature
BHP	:	Bottomhole Pressure
BPM	:	Barrels per minute
CMHEC	:	CarboxyMethyl HydroxyEthyl Cellulose
CMHPG	:	CarboxyMethyl HydroxyPropyl Guar
cP	:	Centipoise
d	:	Diameter (mm)
ft	:	Foot
GPT	:	Gallons per thousand gallons
GLDA	:	Glutamic Acid – Diacetic Acid
HHP	:	Hydraulic Horse Power
HEC	:	HydroxyEthylCellulose
HPG	:	HydroxyPropylGuar
l	:	Length (mm)
lb	:	Pounds

mD	:	millidarcy
NMR	:	Nuclear Magnetic Resonance
P	:	Failure load (N)
PAM	:	Polyacrylamide
PPG	:	Pounds per gallon
PPT	:	Pounds per thousand gallons
psi	:	Pounds per square inch
RCA	:	Routine Core Analysis
TEA	:	TriEthanol Amine
UCS	:	Unconfined Compression Strength
VES	:	Viscoelastic Surfactant
XRD	:	X-Ray Diffraction
XRF	:	X-Ray Fluorescence
Zr	:	Zirconium
E_{dyn}	:	Dynamic Young's modulus (GPa)
E_{static}	:	Static Young's modulus (GPa)

ρ_b	:	Bulk density (g/cc)
ν_{dyn}	:	Dynamic Poisson’s Ratio
ν_{static}	:	Static Poisson’s Ratio
$\Delta\sigma_1$	:	Axial Stress (psi)
$\Delta\varepsilon_3$	:	Lateral Strain
$\Delta\varepsilon_1$	:	Axial Strain
σ_t	:	Brazilian tensile strength (MPa)
$V_{p,s}$	:	P or S wave velocity (m/s)

ABSTRACT

Full Name : Arqam Muqtadir

Thesis Title : Role of Fracturing Fluid on the Breakdown Pressure of Tight Sandstone Rocks

Major Field : Petroleum Engineering

Date of Degree : December 2017

Hydraulic fracturing is a well stimulation technique which increases the hydrocarbon production by inducing fractures in the rock formation. The induced fractures in the reservoir serve as highways for faster hydrocarbon movement. The process is carried out by injecting fracturing fluid which primarily contains gelling agent, crosslinker, bactericide, fluid loss additive, friction reducer, clay stabilizer, buffer, breaker and proppant mixed in a base fluid. Fracturing fluids are carefully selected for each rock formation.

A Tight gas reservoir is commonly referred to as a low-permeability reservoir. Tight gas accounts for about 7 % of the world's hydrocarbon resources which is about the same as the conventional gas (9 %). Enormous quantities of natural gas are present in these tight gas reservoirs. Unlocking these reservoirs is fairly challenging due to the amount of complexities associated with them. Geomechanics plays a key role in the extraction of hydrocarbon from tight gas reservoirs. Hydraulic fracturing is an integral part of geomechanics and is an essential operation to achieve economical production.

The importance of fully understanding the fracturing process is critical in properly developing an efficient hydraulic fracturing plan. It's a robust technique but there are still several uncertainties associated in its implementation. Therefore, this study aims to address some of the challenges for tight sandstone in the areas of geomechanics and hydraulic fracturing.

The objective of this research is to develop an efficient experimental setup to determine the breakdown pressure of tight sandstone rocks. Effect of the type of fracturing fluid on breakdown pressure, effect of saturating fluid on the breakdown pressure and the geomechanical properties of tight sandstone rocks is studied in this research.

ملخص الرسالة

الاسم الكامل : ارقم مقتدير

عنوان الرسالة : دور كسر السوائل على انهيار الضغط من الصخور الرملي المنخفضة النفاذية

التخصص : هندسة البترول

تاريخ الدرجة العلمية : ديسمبر 2017

التكسير الهيدروليكي هو تقنية تحفيز جيدة تزيد من إنتاج الهيدروكربونات عن طريق إحداث كسور في النسيج الصخري. إن الكسور المستحثة في الخزان تعمل كمسارات سريعة لحركة الهيدروكربونات. يتم تنفيذ العملية عن طريق حقن سائل التكسير الذي يحتوي في المقام الأول على عامل التبلور (crosslinker) و مبيد للجراثيم و اضافات لتقليل فقد السؤائل و مخفض الاحتكاك و متوازن ومضيفات للتكسير و صخور صغيرة لمنع اغلاق الكسور بعد العملية. يتم اختيار سوائل تكسير بعناية لكل نوع من الطبقات.

وتشكل خزانات الغاز المنخفضة النفاذية حوالي 7 ٪ من الموارد النفطية في العالم وهي تقريبا نفس الغاز التقليدي (9٪). وتوجد كميات هائلة من الغاز الطبيعي في خزانات الغاز المنخفضة النفاذية. احداث كسور في هذه الخزانات يشكل تحديا كبيرا نظرا لكمية التعقيدات المرتبطة بها. تلعب الجيومكانيكا دورا رئيسيا في استخراج الهيدروكربون من خزانات الغاز المنخفضة

النفاذية. و يعتبر التكسير الهيدروليكي هو جزء لا يتجزأ من الجيوميكانيك وهو عملية أساسية لتحقيق الإنتاج الاقتصادي.

أهمية الفهم الكامل لعملية التكسير أمر بالغ الأهمية في وضع خطة التكسير بشكل صحيح. انها تقنية قوية ولكن لا تزال هناك العديد من التساؤلات المرتبطة بتنفيذه. لذلك، تهدف هذه الدراسة إلى معالجة بعض التحديات التي تواجه خزانات الحجر الرملي المنخفضة النفاذية في مجالات الجيوميكانيكا والتكسير الهيدروليكي.

ان الهدف من هذا البحث هو تطوير المسار التجريبي لتحديد انهيار الضغط لصخور الحجر الرملي المنخفضة النفاذية. في هذا البحث تم دراسة تأثير نوع سائل التكسير على ضغط الانهيار وتأثير سائل التشبع على ضغط الانهيار والخصائص الجيوميكانية لصخور الحجر الرملي المنخفضة النفاذية.

CHAPTER 1

INTRODUCTION

1.1 Energy Demands

Energy delivered by non-fossil fuels are estimated to increase faster than fossil fuels, but that doesn't change the fact that fossil fuels are still dominant in energy supply. Recent forecasts by the U.S Energy Information Administration show that even by 2040, fossil fuels account for over two thirds of the energy consumption. Among the fossil fuels, the fastest growing element is Natural gas even though it has a low carbon intensity (Figure 1.1).

Shale gas, tight gas and coalbed methane are the key contributors to the higher consumption of Natural gas. Hydrocarbon extraction from these reservoirs is much more challenging than conventional oil and gas reservoirs. The technology involved in the extraction of such reservoirs generally increases the cost which requires us to consider investigating new tools and procedures.

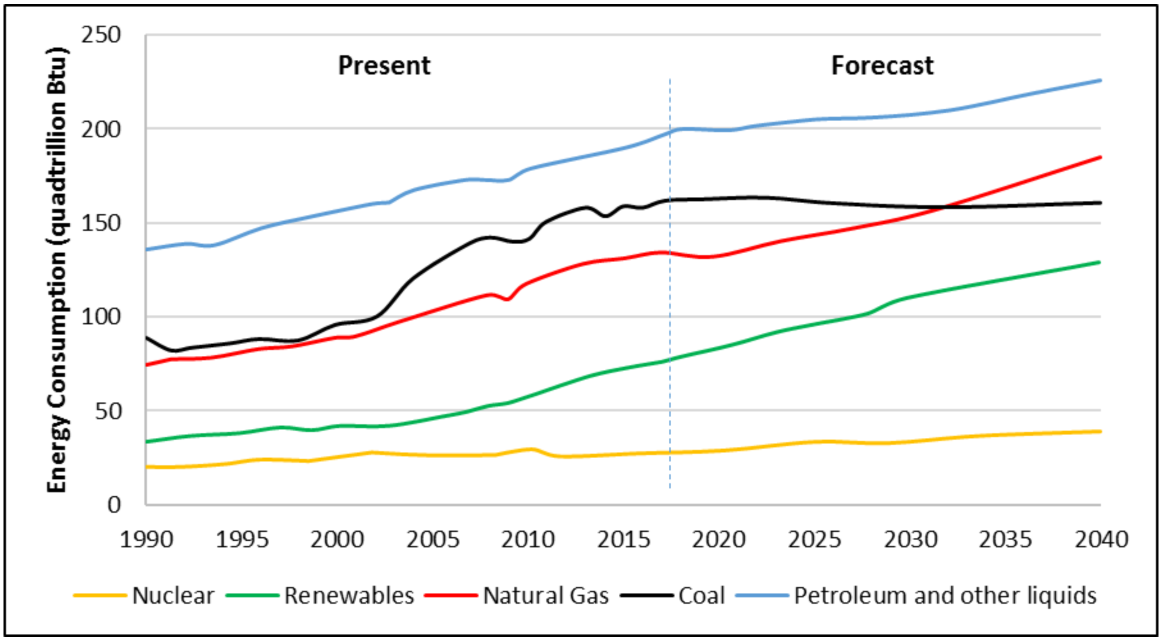

Figure 1.1 World Energy Consumption (EIA, 2017)

1.2 Background

Conventional hydrocarbon reservoirs are highly porous and permeable and therefore are easy to drill and produce. These reservoirs are driven by natural pressure and hence over a period of time, production declines. Techniques like artificial lift or fluid injections are used to help in increasing production. If methods beyond these artificial lift or traditional methods are used to surge production, the type of hydrocarbon produced is classified as unconventional.

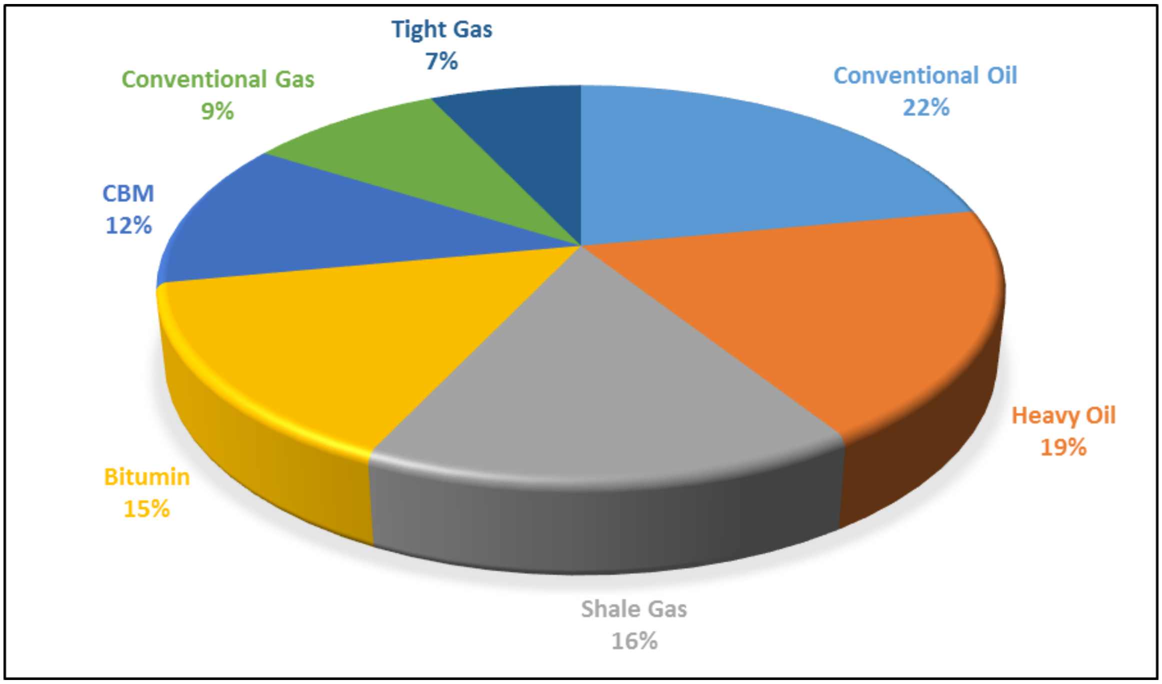

Figure 1.2 World Hydrocarbon Resources (Unconventional Resources, 2014)

Unconventional resources account for two thirds of the world's total hydrocarbon resources. Figure 1.2 (Unconventional Resources, 2014) shows the types of hydrocarbon resources in the world with their contributions. Tight gas accounts for about 7% of the world's hydrocarbon resources and is about the same as the conventional gas (9%). Enormous quantities of natural gas are present in these tight gas basins (Warpinski, 1991).

A Tight gas reservoir is commonly referred to as the low-permeability reservoir (Holditch, 2006). Saudi Aramco defines tight gas reservoir as the one having permeability less than 1 md, porosity less than 12% and requiring hydraulic fracturing to be commercially produced (Hayton et al., 2010).

Production from such a reservoir is fairly challenging due to the amount of complexities in the reservoir. Geomechanics plays a key role in the extraction of hydrocarbon from tight gas reservoirs. Geomechanics deals with the study of how rocks deform when they are subjected to stress, temperature and other environmental factors. Most of the failures witnessed in the life of a well are due to geomechanics. Tight gas reservoirs raise higher geomechanical concerns. Hydraulic fracturing is an integral part of geomechanics and is used to improve the productivity from such reservoirs.

Hydraulic fracturing technique is utilized to help in the economical production of hydrocarbons. The process involves inducing fractures in the rock formation to serve as highways for faster hydrocarbon travel. Hydraulic fracturing is done in both vertical and horizontal wells. The direction of the induced fracture is dictated by the direction of in situ stresses, natural fractures or other features.

The importance of fully understanding the fracturing process is critical in properly developing an efficient hydraulic fracturing plan. The industry today still lacks the knowledge of the process and faces difficulties in designing the hydraulic fracturing job (Syfan et al., 2013). As a result, improper designs have damaged many wells leading to uneconomical production rates. Thus, effort must be placed to understand the fracturing technique.

Therefore, this study aims to address some of the challenges for tight sandstone in the areas of geomechanics and hydraulic fracturing.

1.3 Problem Statement

Hydraulic fracturing is performed to enhance production in reservoirs with low permeability. It's a robust technique but there are still several uncertainties associated in its implementation. One of the uncertainties is the dependence of breakdown pressure on the type of fracturing fluid used. Therefore, this thesis sets out to determine the role of the type of fracturing fluid on the breakdown pressure of tight sandstone rocks.

1.4 Thesis Objective

The objective of this research is to develop an efficient experimental setup to determine the breakdown pressure of tight sandstone rocks and study the effect of the treatment design parameters on the tight sandstone breakdown pressure. Parameters investigated in this study were:

1. Effect of saturating fluid on the geomechanical properties of tight sandstone rocks
2. Determination of the breakdown pressure of tight sandstone rocks
   - Effect of the type of fracturing fluid on breakdown pressure
   - Effect of saturating fluid on the breakdown pressure

1.5 Approach

In order to perform this study, the following work flow will be used:

1. Characterization of the tight sandstone cores
2. Investigation of geomechanical parameters

3. Breakdown pressure determination using fracturing cell setup
4. Post-test analysis

1.6 Thesis Organization

This thesis is organized as per the guidelines stated by the Deanship of Graduate Studies of King Fahd University of Petroleum & Minerals. The thesis is divided into five chapters:

Chapter one states the introduction, problem statement and the approach taken for this research.

Chapter two contains the literature review on the types of fracturing fluids, fracturing fluid additives, the industry's methodology on determining breakdown pressure and effect of saturating fluid on the geomechanical properties of tight sandstone.

Chapter three defines the methodology for this research and states a step by step approach towards solving the problem.

Chapter four contains a detailed explanation of the results.

Chapter five winds up this thesis by stating the summary, conclusion and recommendations for future work.

CHAPTER 2

LITERATURE REVIEW

2.1 Hydraulic Fracturing

Hydraulic fracturing is a well stimulation technique to increase the production by inducing fractures in the rock formation by injecting pressurized fluid. The process is carried out by injecting fracturing fluid containing water, proppant and other materials (Gandossi and Von Estorff, 2015). Figure 2.1, shows a shale formation is being fractured through a horizontal well.

In 1947, Stanolind Oil and Gas, currently known as BP introduced "Hydrafrac" process to the oil and gas industry. Two years later, in 1949 the first commercial fracturing application was performed in the United States (Syfan et al., 2013). As described by J. B. Clark (1949) of Stanolind Oil & Gas Company, for a Hydrafrac process to be successful, the following criteria must be met:

1. The fracturing fluid must be viscous enough to be injected in the well at high pressures, enough to fracture the formation.

2. After the fracture is created, the fracture tends to close due to in situ stresses. Therefore, the fracturing fluid must carry some propping agents such as sand. These propping agents prevent the fracture from closing after fracking.
3. After the fracture is created, the fracturing fluid must not remain in the wellbore and block the formation but it must be thin enough to flow back out of the well.
4. Depending on the petrophysical properties of the rock, there must be sufficient pumping capacity to inject fracturing fluid faster than it leaks away into the formation.
5. The target formation must be sealed off from other formations using formation packers to avoid fracking other formations.

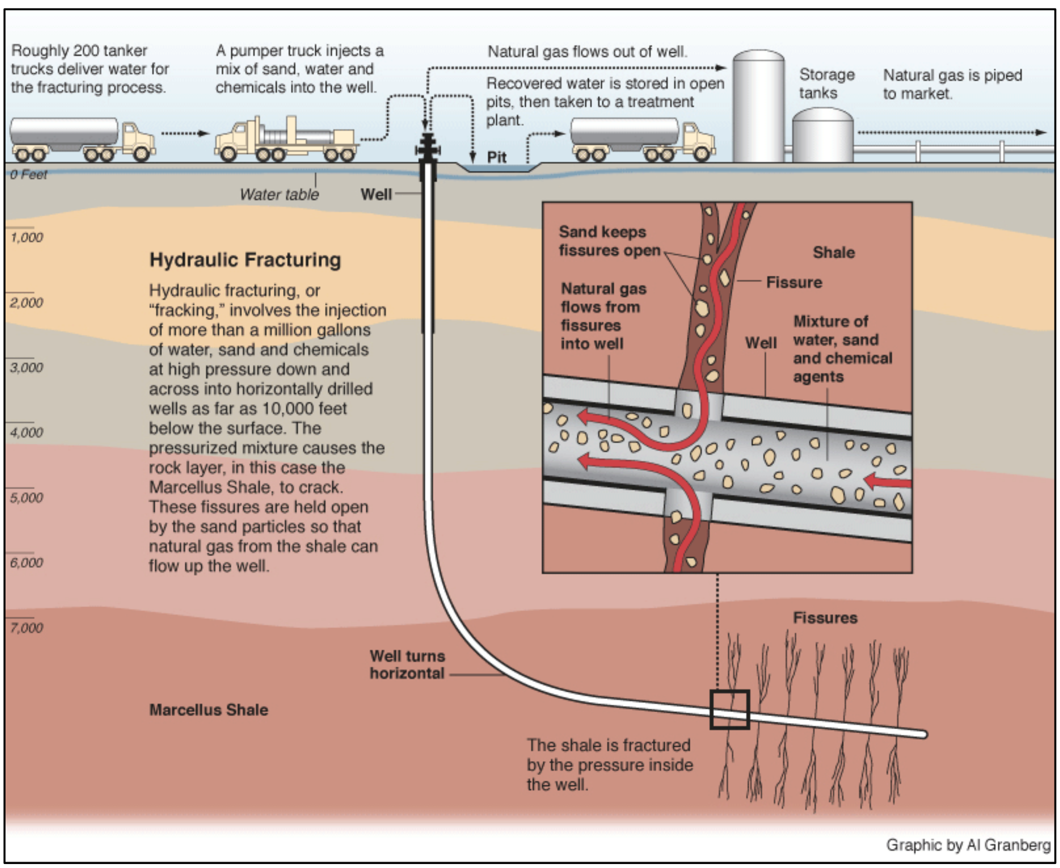

Figure 2.1 Hydraulic Fracturing process (Propublica)

In addition to the above-mentioned criteria, the fracturing fluid also must be

1. Environmentally Friendly: The constituents of the fluids must be least damaging to the environment as possible.
2. Safe: The fracturing fluid must be non-hazardous to the crew and pose a minimum damage if spilled.
3. Easy to Prepare: Preparing the fracturing fluid must be easy even under harsh environments.
4. Cost Effective: The fracturing fluid must be economical (less than $4.00 US/ gallon) and must have a good balance between cost and required objectives.

In 1980's and 1990's well known experts Holditch, Nolte, Warpinski, Veatch and others, considerably improved and aided the hydraulic fracturing process by defining critical fracture parameters and their effects on production. The result of their research impacted positively in the development of Bakken, Eagle Ford, Barnett, Haynesville, and Marcellus shales (Syfan et al., 2013).

It is evident that geomechanics dictates the fracture parameters like breakdown pressure, fracture length, height and width. As stated by Perkins and Kern (1961), if the formations overlaying and underlying the target formation exhibit higher in-situ stresses, the fracture well be contained in the intended formation and won't grow to the other formations. Without considering geomechanics, fracturing fluid parameters and fracture behaviors, the fracture maybe induced but result in a non-economical production.

It was reported in 2012 that there been over 2.5 million fracturing treatments pumped worldwide (King, 2012). No two reservoirs are the same and require tailored frac design to achieve effective fracturing. In essence, the Hydraulic fracturing process remains the same but is designed differently for different reservoirs.

The factors controlling the frac design are:

1. In-situ stresses
2. Permeability
3. Viscosity of reservoir fluids
4. Around wellbore damage or Skin factor
5. Initial Reservoir pressure
6. Reservoir depth
7. Wellbore parameters like (radius, friction, etc)

2.2 Fracturing Fluids

Designing of fracturing fluid is a crucial part of the hydraulic fracturing operations. For a fracturing fluid to be effective, several factors are to be considered. Some of them may not be easily controllable such as injection rate, fracturing fluid properties and proppant quality (Pye and Smith, 1973).

2.2.1 Types of Fracturing fluids

Several kinds of fracturing fluids are being used in the industry. Some of these fluids are:

1. Slickwater
2. Linear Gel
3. Cross-linked Gel

4. Oil-based Fluids
5. Foam/Poly Emulsions
6. Viscoelastic surfactants (VES)

The following paragraphs briefly describes each of these fluids.

Slickwater

The constituents which make up slickwater are water, clay stabilizer and friction reducer. To reduce water blocking effects and to not disturb the relative permeability, a Water Recovery Agent (WRA) is added.

There are numerous advantages of using slickwater as fracturing fluid. Slickwater is usually the most environmentally friendly and cost-efficient type of fracturing fluid due to its ability to be recovered and reused. High pumping rates can also be achieved by using lower hydraulic horse power (HHP) and can easily induce both tensile and shear fractures (Kennedy et al., 2012). It is also non-inflammable thus reducing on-site hazards.

The chief disadvantage of slickwater is its low viscosity. Effective proppant transport is dependent on viscosity making slickwater an inefficient proppant carrier. As a result, the fracture width is narrow and hydrocarbon production suffers. So, it may not be suitable for some cases (Kennedy et al., 2012). If slickwater isn’t adequate, hybrid fracs are suggested. In hybrid fracs, slickwater is injected (to fracture) in combination with viscous fracturing fluid to aid in the proppant placement (King, 2012).

Linear Gel

Linear gel contains water, clay stabilizers and gelling agents like Guar, HydroxyPropylGuar (HPG) or HydroxyEthylCellulose (HEC). Bactericides are added to the mixture since gelling agents promote bacteria growth. The damage to the proppant pack is controlled by using breakers (Gupta, 2009).

Linear gel's advantages are environment friendliness, easy mixing, low pumping rate and relatively less cost. As the fluid penetrates the formation, filter cake is formed and it helps in regulating fluid loss. The primary disadvantages include narrow fracture width due to low viscosity and the returned water contains the leftover breaker deeming it unfit for reusability.

Cross-linked Gels

Cross-linked gels are made up of the same ingredients as the Linear Gel with some additional additives. Crosslinker is added to increase the viscosity from about 30 cPs to more than 1000 cP. Higher viscosity tends to increase the fracture width and also contributes to carrying higher quantities of proppant. This further improves proppant transport to the fracture, minimalizes the fluid loss and reduces friction pressure. Once the formation is fractured, a breaker is set in place to reduce the viscosity and assist in withdrawing the fracturing fluid (Bennion et al., 2004).

Crosslinked fluids are environment friendly and the viscosity is stable for some of the crosslinked fracturing fluid which are borate based while it is unstable for titanium or zirconium based. Crosslinked fracturing fluids are often formation fluid compatible (Conway et al., 1983).

Oil-based

Oil-based fracturing fluids are used on water sensitive formations which undergo remarkable damage by using water-based fracturing fluids. Palm oil was used as the first viscosifier with Naphthenic Acid (Napalm) as crosslinker. Some crude oil additives have filter cake building tendencies which could control fluid loss, but fluid loss is mainly based on viscosity.

A field study showed that the use of water-based fracturing fluid caused water entrapment in the reservoir which interfered with the relative gas permeability restricting gas flow. On the other hand, when oil-based fracturing fluid was used, better permeability was seen i.e., little damage was done to the formation by oil-based fracturing fluid (Coskuner, 2006).

The major disadvantages include the flammable nature of oil and the extent of damage it can do to the on-site crew and the environment. High viscosity crude oils contain surfactants (naturally occurring) which potentially cause gelling problems. Some refined oils like diesel are obtained from refinery and could be very expensive but can be sold off to the market or reprocessed.

Foam/Poly Emulsions

Fracturing fluids containing ingredients which are immiscible in water are called Foam/Poly Emulsion fracturing fluids. Nitrogen, Carbon Dioxide, propane or diesel are the prime ingredients. Foam based fracturing fluids generally contain 65% to 80% of immiscible fluids. The range of the immiscible fluids is to determine the quality. Typically, these fluids provide an excellent proppant pack, proppant transport and breaking (due to gravity).

Nitrogen based fracturing fluids must be quickly flowed back due to its nature of dissipating quickly in the reservoir causing flow obstruction. Whereas, Carbon Dioxide based fracturing fluids are dense under most conditions and causes less dissipation. Another advantage of using Carbon Dioxide is that it dissolves in crude oil and it reduces its viscosity which helps in clean up. Fracturing fluids containing an excess of 80% of Nitrogen or Carbon Dioxide tends to have extremely low viscosity and is usually not deemed fit for fracturing purposes.

If the concentration of the immiscible fluids is about 20% to 30%, the type of fluid is called energized fluid. Nitrogen and Carbon Dioxide generally are used as “energizers” to energize fracturing fluids. Studies suggests that energized fluids have the potential to improve well performance by 1.1-2.2 times as compared to nonenergized solutions (Burke et al., 2011).

Apart from increasing hydrocarbon recovery, energized fracturing fluids reduces the water consumption, proppant required and injection rates. The created fractures are shorter and wider than in a nonenergized fluid. The major drawback for using such a system is the cost of Carbon Dioxide and Nitrogen supply and equipment needed at the well location (Friehauf and Sharma, 2009).

Emulsifying and keeping a hydrocarbon (diesel or condensate) as the external phase with water forms a Poly Emulsion fracturing fluid. By varying the ratio of hydrocarbon and water, the viscosity can be controlled. Drawback of using such fluids is the safety concern due to high pressure pumping and gelled propane which is flammable. Carbon Dioxide can cause additional problems due to its ability to form dry ice plugs as pressure is decreased.

Viscoelastic surfactants (VES)

Viscoelastic surfactants (VES) are known for their ability to provide high viscosity and by forming wormlike micelles and entangled structures in the formation rock. Increased viscosity further enhances the ability of proppant suspension, proppant transport and the ability to divert fluid in acidizing treatments (Yu and Nasr-El-Din, 2009). VES fluids have been used in various applications in the oil and gas industry for several decades. Only in the past decade VES has been used as a fracturing fluid (Gupta, 2009).

VES fracturing fluids contain surfactants or inorganic salts. Complex network of worm like micelles are formed when pH is increased and the surfactant molecules self-organize and align themselves due to intermolecular attractions and non-covalent bonds (Samuel et al., 1997). VES fracturing fluids can be used at high temperatures with addition of high temperature stabilizers. Their high viscosity can be broken by varying the pH or salinity or sometimes by introducing hydrocarbons. They are recyclable as well. The negatives of the VES fracturing fluid include high cost and questionable compatibility with formation fluid.

As witnessed above, a variety of fracturing fluids are available with different applications. The is no “best fracturing fluid”, each fracturing fluid has its benefits and shortcomings. Both water-based fracturing fluids and oil-based crosslinked fracturing fluids perform well in high temperatures with good proppant transport. VES may be used if formation compatibility issues arise due to using water-based fracturing fluid. VES may also be energized if needed. To reduce leak off, Nitrogen or Carbon Dioxide can prove helpful. If capillary pressure problems arise, methanol containing fracturing fluids can be used. It all depends on what the fracturing design team decides what could be the most efficient fracturing fluid system for the specific zone or reservoir.

2.2.2 Fracturing fluid Additives

Majority of the fracturing fluids used in the industry are water-based. To achieve the desired properties of the fracturing fluid, chemical additives are added to it. Additives contribute to about 0.1% - 0.5% of the total fracturing fluid volume (Arthur et al., 2009). To achieve the desired fracturing fluids properties, selection of each of the additives is critical (Jones and Britt, 2009).

Depending on the base fluid (water or oil) different type of additives are used. For instance, water-based fracturing fluids require higher interfacial tension and flow resistance reducing surfactants. But water-based fracturing fluids require less friction-loss reducers due to its friction reducing nature. Similarly, other fluids require additives to compensate for their limitations.

In general, additives are used for two main functions which are 1. Improving fracture creation and 2. Reducing formation damage (Conway et al., 1983). The different types of additives are discussed below:

Fluid loss additives

Fluid loss additives are mixed with the base fracturing fluid to restrict it from escaping the fracture. Fluid loss is a major concern since leakage of fluid through an unrestrained leak off potentially causes accumulation of proppant near the wellbore. This increase in concentration creates a “proppant bridge” that can restrict fracture propagation entirely (Harris, 1988). On the other hand, low fluid loss could initiate larger and deeper fractures (maybe undesired for certain formations).

Fluid loss additives are generally insoluble and remain in the fracture when the fracturing fluid leaks off into the formation (known as “spurt loss”). These remaining fluid loss additives form a filter cake and thus prevent further fluid loss in the formation. The filter cake remains in the fracture provided there is sufficient pressure. When the well starts to flowback, the filter cake re-disperses and escapes back to the borehole (Hawsey and Jacocks, 1961). The fluid lost per unit area prior to the formation of filter cake is known as Spurt and in naturally fractured reservoirs, its effect is significant (Jones and Britt, 2009).

Fluid loss additives raise some concerns as well despite their effectiveness. They significantly reduce fracture reduce formation permeability and fracture proppant conductivity which directly affect well productivity (Pye and Smith, 1973). Some examples of fluid loss additives are diesel, particulates and fine sand.

Bactericide/Biocides

Bacteria growth control is often required mainly for water-base fluids. Fracking with untreated water can cause bacteria growth (Howard and Fast, 1970). Viscosity of a fracturing fluid can be destroyed by aerobic bacteria in a matter of hours thus reducing the effectiveness of the fracturing fluid.

Anaerobic bacteria in the fracturing fluid have the potential to produce Hydrogen Sulphide (H_2S) within the reservoir. Both types of bacteria can be controlled by introducing chlorinated phenols, amide-type chemicals and quarternary amines in the fracturing fluid (Howard and Fast, 1970). Other examples are Chlorine dioxide, 2-Bromo-2-nitro-1,2-propanediol and gluteraldehyde

Breaker

Breakers are deployed to deoxidize the polymer molecule's backbone and as a result the fracturing fluid's viscosity is significantly reduced and is easily pulled out of the fracture. These additives primarily useful fracture cleanup and flowback. One area of concern with breakers is the time of breaking. If the breaker is deployed early, the well will experience significant fluid loss as well as ineffective fractures. If the breaker is deployed late, the viscous fracturing fluid could potentially cause invasion or plug the fracture (Fink, 2013).

For temperatures under 120°F and with a pH below 8.5 hemicellulose is used. At higher temperatures, ammonium and sodium persulfate are or with an activator at lower temperatures (Jones and Britt, 2009). Some example are Peroxydisulfates, Sodium or Ammonium persulfate.

Buffer

Some fracturing fluid additives require certain conditions to be fully active. Some properties are bacteria control, crosslinking, gel breaking, polymer gelation rate, stability of viscosity. For fracturing fluid, the common pH range is from 3 to 10. Additives like the crosslinkers require a pH sweet spot to fully attain the maximum viscosity of the fracturing fluid. For this purpose, buffers are used to adjusts pH of fracturing fluid. Buffers are produced by blending weak acids with weak bases (Harris, 1988). Some buffers have slow dissolving properties, allowing them to delay the properties associated with it (like crosslinking)

Some examples are Sodium carbonate, Sodium Hydroxide, Hydrochloric Acid, Acetic Acid, Potassium Carbonate and Formic Acid,

Clay stabilizer

Clay stabilizers are additives that help increase the formation and fracturing fluid compatibility. Some clay minerals present within most formations are sensitive to certain fracturing fluids (water-based mainly) and are vulnerable to migration and swelling. It is extremely important to prevent clay damage especially in tight, low pressured reservoirs since it adversely affects the capillary pressure (Anderson et al., 2010).

The aim of the clay stabilizers is to prevent the formation clays from enduring “ionic shock”. To facilitate this, the clay stabilizers are designed to provide high electrovalent strength. Potassium chloride, Sodium chloride, Tetramethyl ammonium chloride or Calcium Chloride are used as clay stabilizers. To control fine migrations, polymeric clay stabilizers are used which have the ability to attach anions on the clay. Fine migration is an important element to consider since proppant placement can be affected due to invasion of fines (Harris, 1988).

Corrosion inhibitor

To reduce chemical degradation, corrosion inhibitors are added to the fracturing fluid. Fracturing fluid which use acid (delayed acid gelling) can cause corrosion. Some examples of gel stabilizers are TriEthanol Amine (TEA), methanol, Ammonium Bisulfate and other inorganic compounds of Sulfur. Other corrosion inhibitors are available but a lot of them interfere with crosslinking of the fracturing fluid (Cassidy et al., 2011). Methanol is toxic, flammable, expensive and can cause reactor tower catalysts poisoning. TEA and sulfur stabilizers have none of those characteristics and hence have an advantage over methanol.

Crosslinker

The main purpose of the crosslinker is to provide high viscosity to the fracturing fluid. A crosslinker is a long chain chemical additive which bonds (either ionic or covalent) with the base fracturing fluid (Linear Gel) and alters the physical properties. Crosslinking is triggered by reaching certain temperature, pressure or change in pH. As a result, the viscosity is increased in the range of 2 to 3 orders of magnitude.

Metals like Zirconium, Titanium and Boron are used as crosslinkers. Chromium, Aluminum and Iron based crosslinkers are not preferred. Chemical stabilizers like as thiosulphate or methanol are added to maintain viscosity since these crosslinker decompose at high temperatures (over 225°F). As far as low temperatures (under 150°F) are concerned, aqueous solutions of the previously mentioned crosslinkers are employed (Harris, 1988). Instead of raising the polymer’s concentration, crosslinking using transition metal cations are done to significantly increase viscosity since they are more cost effective.

Some example are Potassium hydroxide and borate salts

Gelling agent

The most widely used types of polymers are Guar gum and cellulosic derivatives. These additives increase fracturing fluid viscosity, to help in carrying proppants.

Loyd Kern submitted the first patent on borate based guar in 1962 (US Patent # 3058909). By 1970, Guar gum was the most widely used gelling agent (Howard and Fast, 1970). HPG (Hydroxypropyl guar) and CMHPG (carboxymethyl hydroxypropyl guar) are produced by chemically altering the water-based polymers attained from guar. Cellulose or another natural source derived additives are Hydroxylethyl cellulose and carboxymethyl hydroxyethyl cellulose (CMHEC). These additives have a wide range of applicability in terms of temperature (60 F to 400 F).

The cellulosic based derivatives tend to be residue-free and therefore, decreases damage caused to the formation by the fracturing fluid. But they are difficult to disperse since they have a high hydration rate. Guar gum and its derivatives on the other hand are dispersed easily but some reside is left behind when broken.

Proppant

Proppants helps the fracture to remain open after the treatment is done. This allows the hydrocarbons to flow from the formation to the fracture and to the wellbore. Maximize fracture conductivity is the primary goal of and effective proppant performance us measured by how good is the fracture conductivity. Fractures tend to close after creation due to in-situ stresses thus making proppants an integral part of the fracturing fluid design.

Example include Sand (Sintered bauxite, ceramic beads, zirconium oxide) ceramic (glass beads), aluminum alloys, resin coated ceramic, plastics and nutshells. Strength and specific gravity are the main differentiators of proppants. Jones & Britt (2009) state that proppants are usually in the price range of about 5 to 10 times to that of sand.

Surfactants and Alcohol

Surfactants are commonly used in water-based fracturing fluids. Surfactants are additives which helps reduce interfacial tension, reducing capillary pressure as a result. As capillary pressure is reduced, less fluid will remain in the pores and thus, lower pressure is needed to flow back from tight reservoirs. So, it also enhances the compatibility enhances between reservoir fluids and fracturing fluids. Another use of surfactants is to stabilize foams (Harris, 1988).

Alcohol can also assist in lowering the interfacial tension but its use is looked down upon due to its negative effects on the fluid loss prevention and viscosity control (Howard and Fast, 1970). Moreover, it one of the most expensive additives.

Some examples are Ethoxylated alcohol, Methanol and isopropanol

Other fluid additives

Acid

Acid cleans borehole and surrounding formation to provide access path for the fracturing fluid. Some examples are Muriatic acid or HCl (concentration of 3% to 28%)

Friction reducer

Friction reducers reduces friction for better movement of fracturing fluid. Examples include Petroleum distillates and polyacrylamide (PAM).

Iron control

Iron control additives helps in preventing settling of carbonates and sulfates which could block the formation. Some examples are Ammonium chloride, ethylene glycol and polyacrylate.

2.3 Fracturing fluid for tight sandstone

Maplani (2006) performed an extensive literature review and performed interviews with numerous industry experts. His work provided a road map which helped operators to select the type of fracturing fluid. Eight parameters were used as key to select the fracturing fluid. The parameters were BHP, BHT, natural fractures, barrier types, geomechanical properties of the formation, thickness of pay zone and fracture half length. Figure 2.2 represents the road map. In Saudi Arabia, the formations such as Unayzah, Sarah and Qasim are important tight gas formations in Saudi Arabia. Unlocking them has been a challenge in the past. One such challenge is the high temperature (>300 °F) and depths (>15,000 ft) of the reservoirs. It’s clear from Figure 2.2 that crosslinked gel is suitable for these reservoirs.

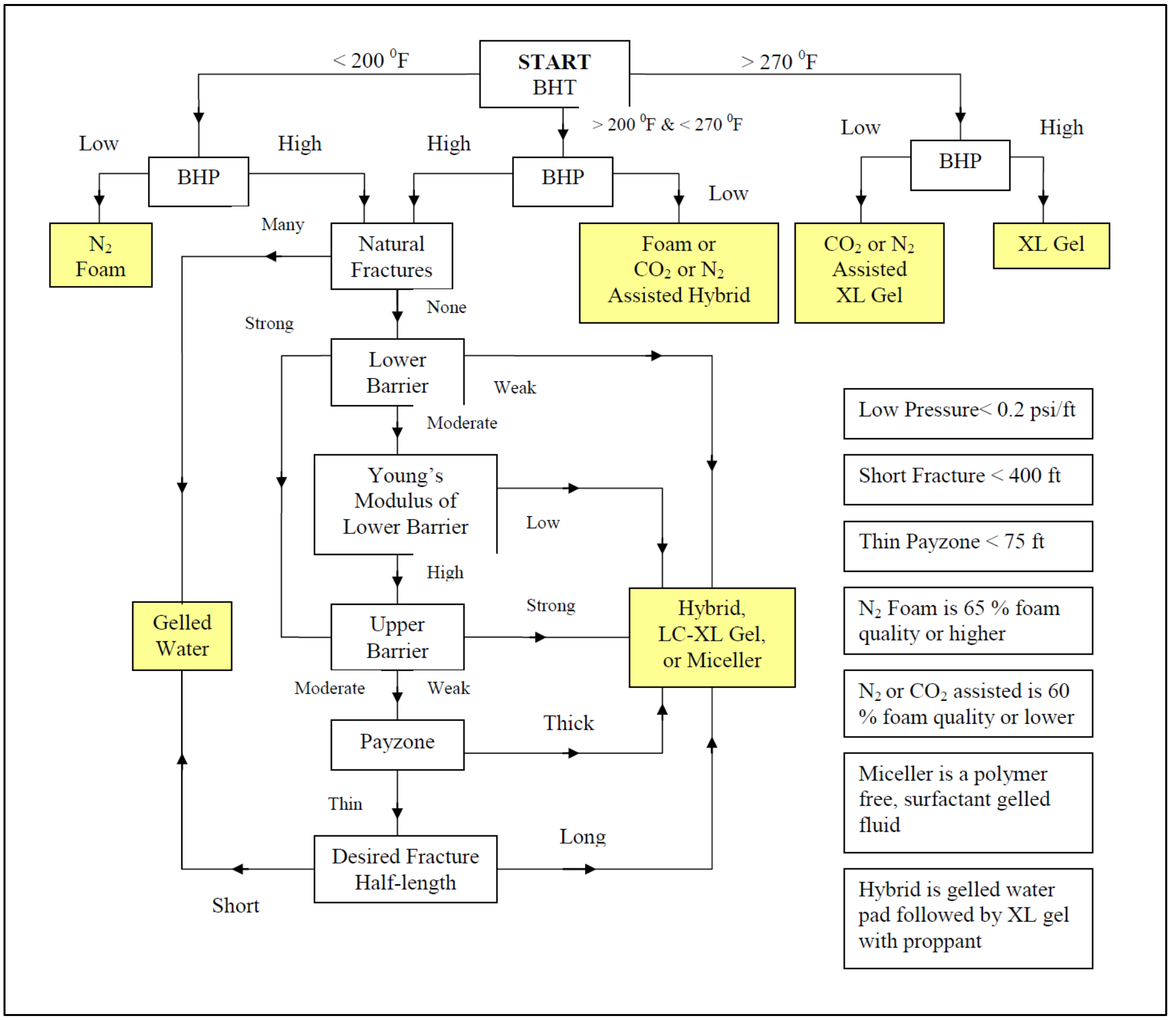

Figure 2.2 Fracturing fluid selection guide for tight sandstone reservoirs

Bu-Khamseen et al., (2010) described a successful hydraulic fracturing treatment conducted by LUKOIL. The Sarah formation of Saudi Arabia which is a tight sandstone reservoirs was treated. 20 ppt Linear gel was used to perform integrity tests and 50 ppt crosslinked gel was used to perform the minifrac test. Zirconium based crosslinker was used with 3% to 6% KCl or $NaBr$ brine (for high density).

Leal et al., (2014) discusses the usage of a novel hydraulic fracturing fluid recently used in Saudi Arabia. It consists of CMHPG guar crosslinked with a Zirconium based crosslinker. This is a delayed crosslinker which is fully active at high temperatures. The fluid is stablized at high temperatures by using gel stabilizer and optimum viscosity is achieved by adjusting the pH.

Al-Momin et al., (2015) describes some challenges faced during the hydraulic fracturing operation in an undisclosed tight gas reservoir in Saudi Arabia. In this study, 20ppt linear gel with 15% KCl brine was used to conduct the minifrac test while for the Main frac job, 45ppt Crosslinked gel with 15% KCl was used.

Al-Jalal et al., (2011) describes some fracturing jobs which were planned to be conducted on the Qasim, Sarah, Sharawra and Unayzah formations. Fracturing jobs were designed using fracture gradient as a key. If the fracture gradient was higher than 1 psi/ft, conventional fracturing fluid was used (crosslinked gel). As stated in section 2.2.1, these fluids are cost efficient, fairly compatible with the formation and easily flowed back. Pressure limitations arise when fracture gradients higher than 1 psi/ft are witnessed, hence high density fluids were used with VES. As stated in section 2.2.1, these fluids are expensive and usually incompatible with the formation.

Well B was completed in Qasim formation (Figure 2.3). The Qasim formation is comprised mostly of sandstone and siltstone containing quartz, mica, feldspar and a few traces of carbonate. The clay volume ranging is below 10%. There are two zones in this formation namely Lower and Upper Qasim. The Lower Qasim has 6% porosity with 0.013 mD permeability and 50% water saturation. The Upper Qasim also has 6% porosity with 0.01 mD permeability and 37% water saturation.

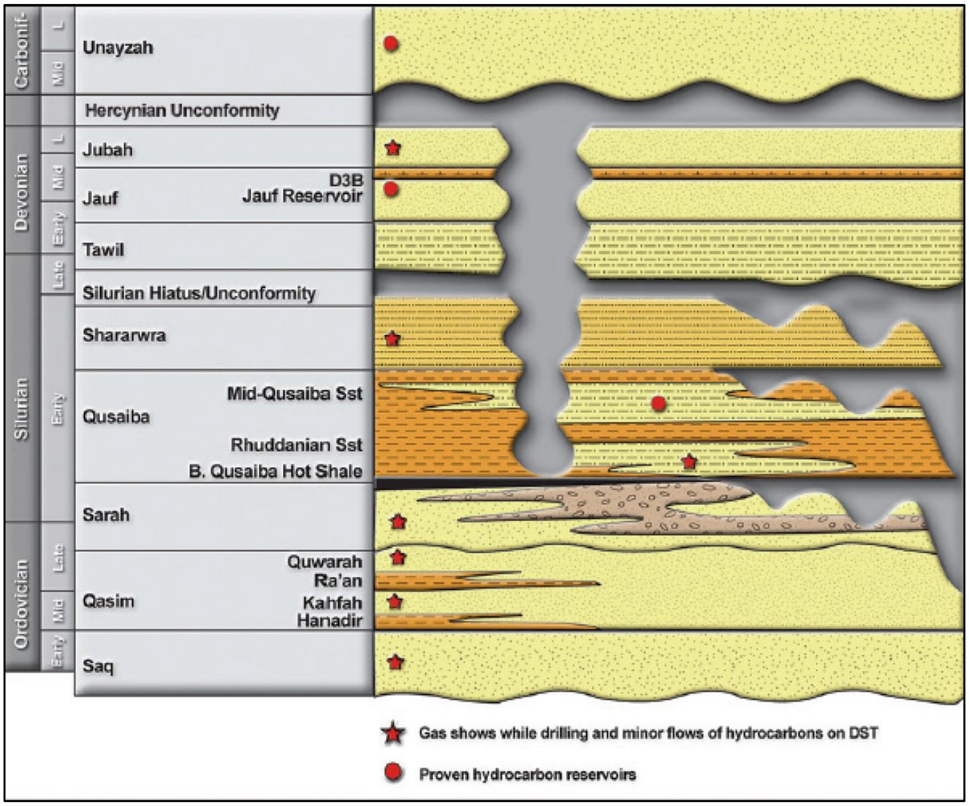

Figure 2.3 Stratigraphic Column of Lower Paleozoic Succession (Hayton et al. 2010b)

First the lower Qasim Zone was treated. The fracture gradient in this zone is 0.94 psi/ft which is lower than 1 psi/ft but it was decided to use VES with high density (11.4 ppg) $CaCl_2$ brine as base fluid. During the operation, the maximum achieved pumping rate was 26 bpm and breakdown pressure was 19,287 psi with 12,757 psi at the wellhead.

After flowing back the well, an emulsion was seen. Upon further studying and conducting laboratory tests, it was found that the emulsion was generated due to the interaction between the fracturing fluid and the iron in the tubulars. The production improved significantly.

The Upper Qasim Zone was treated next. The fracture gradient in this zone is also 0.94 psi/ft which is lower than 1 psi/ft but this time it was decided to go with the conventional fracturing fluid with 45 lb crosslinked gel (borate) with 8.6 ppg KCl brine as base fracturing fluid. During the operation, the maximum achieved pumping rate was 26 bpm and breakdown pressure was 23,088 psi with 14,716 psi at the wellhead.

As witnessed from the two fracturing jobs (summarized in Table 2.1) in the same formation with about the same properties, the breakdown pressure is affected by the type of fracturing fluid used.

Table 2.1 Summary of the fracturing job in Qasim formation

Zone / ***Parameter***	**Lower Qasim**	**Upper Qasim**
Permeability (mD)	0.013	0.01
Porosity	6%	6%
Water Saturation	50%	37%
Fracture Gradient (psi/ft)	0.94	0.94
Fracturing Fluid	VES with 11.4 ppg $CaCl_2$	Borate Crosslinked Gel with 8.6 ppg KCl
Pumping Rate (bpm)	26	26
Breakdown Pressure (psi)	19,287	23,088

Furthermore, Well C was completed in the Qusaiba shale formation. The upper Rhuddanian (tight) sand interbedded with the Qusaiba shale was targeted in this job. Permeability and porosity were 0.035 mD and 7% respectively. The fracture gradient was higher than 1 psi/ft so it was decided to use a heavier fluid system. This time, a Zirconium based crosslinked (50 ppt) fracturing fluid with 12.3 ppg NaBr brine was used. The maximum pumping rate applied was 16.4 bpm with a maximum BHP of 21,600 psi. The job was cancelled due to BHP exceeding the safety limit of 22,000 psi. Better knowledge of the breakdown pressure can help avoid such situations.

2.4 Determination of Breakdown Pressure

Breakdown pressure of a rock formation is the pressure at which a fracture will be created in the formation. Determination of breakdown pressure and fracture analysis is important for drilling operations in the areas of Leak Off Test (LOT) analysis, casing design and for hydraulic fracturing operations in the area of mini frac analysis and determination of the horse power required (Detournay and Carbonell, 1997).

LOT’s are performed during the drilling operation to determine the integrity of the rock formation. A typical leak off test of Formation Integrity test (FIT) is performed when casing is placed and by using a heavier mud (which is required to drill the next formation) the formation integrity is tested. In this type of test, the formation is not fractured, but the drilling mud is tested if it can breakdown the formation or not (Postler, 1997).

Extended Leak Off Tests (XLOT) are similar to LOT tests but in this case the formation is fractured to determine the breakdown pressure and the minimum horizontal stress. As seen in Figure 2.4 the fluid starts to leak in the formation at the Leak Off Point (LOP) until its finally fractured at Fracture Breakdown Pressure (FBP). Minifrac tests are similar to XLOT tests but with more cycles. These tests are conducted only on very selective formations and are very expensive (Minifrac test) (Li et al., 2009).

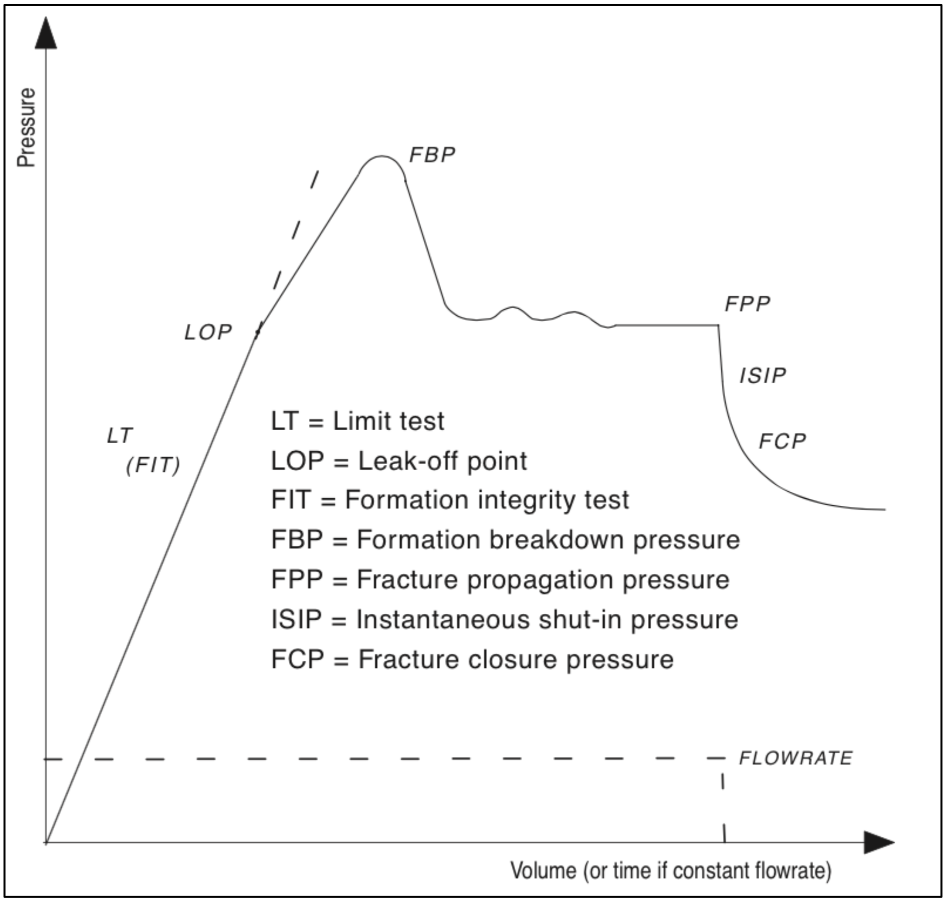

Figure 2.4 An Extended Leak Off Test (XLOT)

Generally, minifrac tests are subject to misinterpretation since they are conducted on cased hole. Having a lab based experiment to determine breakdown pressure can potentially save the high costs required to conduct these tests.

Zeng & Roegiers (2002) performed fracture breakdown pressure study with changing fracturing fluid injection rates. The study involved using a poly axial frame setup and used three large samples of sizes 5 in x 4 in x 4 in (and greater) of Jackford tight sandstone. Breakdown pressure increased as injection rate decreased. The tests were also validated against the Linear Elastic Fracture Mechanics (LEFM) model and matched well. But the study only used one type of fracturing fluid and also didn’t mention which type of fracturing fluid was used in the study.

Gunawan et al., (2012) evaluated the Fracture Assisted Sandstone Acidizing (FASSA) technique. A hydraulic fracture was created, then an acidizing job was performed. Apart from treating the skin, the acid aids in creating a conductive path for the fluid to flow. But FASSA treatment is only effective for Sandstone reservoirs having permeability of 20 to 60 mD. For reservoirs with permeability below 10 mD, the treatment isn’t very effective.

Brenne et al., (2013) investigated relation between breakdown pressure and Acoustic Emissions of 6 different rock types in a modified Hoek’s Cell for hydraulic fracturing. Samples of diameters 1.5 in. and 2.4 in. with lengths ranging from 2.25 in. to 5.1 in. and drilled hollow from the center with a diameter of 0.25 in. Their only drawback is that they used distilled water to frac and didn’t investigate the effect of other fracture fluids.

Fortin & Stanchits (2015) performed hydraulic fracturing on a pre-fractured shale outcrop with dimensions 279 x 279 x 381 mm on a poly axial frame. A high viscous fracturing fluid was used to frac the block. Acoustic sensors were used to find fracture propagation velocity. Since the fracturing fluid was very viscous, detection of acoustics was easy. This test is very expensive to perform and it’s difficult to perform sensitivity analysis for type of rocks and fluids.

Dehghan et al., (2016) 300 mm cubic cement blocks were used to study the induced hydraulic fractures. For the block with no natural fractures, the hydraulic fracture was straight and bi-wing propagating in the direction along the direction of the least principle stress. But for the block with a natural fracture, the fracture propagated in the same direction of the natural fracture and decreased the fracture initiation and propagation pressures.

Gomaa et al., (2014) introduced a new experimental setup for 2 in. x 2 in. Mancos shale cores with a 0.25 in. diameter hole in the center from which fracturing fluid was injected. Effect of fracturing fluid was investigated but it wasn't performed on any tight sandstone cores.

Majority of the literature covers lab based hydraulic fracturing on poly axial frames using one fluid. But only a few investigate the effect of fracturing fluid itself. The poly axial tests are difficult to perform due to sample preparation, test procedure complexities and are very expensive. Moreover, the effect of fracturing fluid on breakdown pressure for tight sandstones is not witnessed. Therefore, a small setup is proposed to study the fracture breakdown pressure and fracture complexity for tight sandstones.

2.5 Effect of Saturating Fluid on Geomechanical Properties

The elastic properties of geomechanics are divided into two categories namely, static and dynamic. Static properties are more accurate but are destructive, meaning the rock should be tested till failure (Fjaer et al., 2008). Dynamic on the other hand are non-destructive and are fast. Both types of tests have their advantages and disadvantages and are listed in Table 2.2.

Table 2.2 Differences between static and dynamic properties

Static	***Dynamic***
Direct determination (lab test only)	Indirect (logs, ultrasonic lab test)
Actual Value	Overestimated (1.5 to 1.8 times)
Destructive	Non-destructive
Expensive	Cost effective
Tedious lab work	Easy and fast
Discrete data based on coring	Continuous data with depth
Accurate and reliable	Affected by environments
Used directly	Calibration required
Pore collapse, crack sliding and dilatancy	Low amplitude, high frequency and low affected mass

The stiffness of a material when stress is applied to it is described by Young's Modulus (E). If a higher Young's modulus is seen, the less elastic (higher stiffness) the rock is (Zoback, 2010).

Poisson's ratio (ν) is defined as the negative ratio of radial strain to axial strain. It's a measure of how much the material can expand laterally when compressed axially. Poisson's ratio ranges from $\nu=0.5$ (incompressible material) to $\nu=0$ (showing very little lateral expansion when compressed) (Zoback, 2010). These elastic parameters are responsible for most of the geomechanical modelling including hydraulic fracturing.

As the water saturation changes in the rock, the geomechanical parameters are affected. As the water saturation increases, a reduction in the UCS (Yagiz and Rostami, 2012) and

Young’s modulus is seen, while Poisson’s ratios tends to increase (Widarsono et al., 2001). Usually sedimentary rocks are more affected by the water saturation than the igneous and metamorphic rock (Wong et al., 2016).

For carbonates, DeVilbiss (1984) partially saturated limestone rock with water and saw an attenuation in the acoustic velocities. Brignoli et al., (1995) performed UCS on fully saturated limestones and saw a 15 to 20% reduction in the Young’s modulus. Fabricius & Eberli (2009) also saw a similar decrease.

Mc Carter (2010) and Perera et al., (2011) performed UCS on coal and sandstones and saw a decrease in UCS and Young’s modulus as water saturation increased. Labuz & Berger (1991) saw a decrease of 15 % in the Young’s modulus as water saturation increased in granite while Vasarhelyi (2003) saw the same effect in Hungarian volcanic rocks.

Widarsono et al., (2001) compared log calculated Young’s Modulus and Poisson’s ratio for in a sandstone reservoir with water saturation ranging from 20% to 90%. The reduction in the Young’s Modulus was up to 50% and the increase in Poisson’s ratio was 100%. Meng (2005), Gu (2008), Hawkins & McConnell (1992), Lashkaripour & Ajalloeian (2000) performed UCS on sandstones and mudstones and saw a decrease in UCS and Young’s Modulus.

As seen in the literature, the fluid saturation affects the geomechanical properties of the rock. As a result, fracturing operation is affected. To further understand the interaction of the fracturing fluid in the reservoir, the tight sandstone cores will be subject to both oil and brine saturation to investigate the effect of the saturating fluid on geomechanical properties and breakdown pressure.

CHAPTER 3

METHODOLOGY

As mentioned in the first chapter, the research is broken down in the following workflow:

1. Characterization of the tight sandstone cores
2. Investigation of geomechanical parameters
3. Breakdown pressure determination using fracturing cell setup
4. Post-test analysis

Before describing the details of the workflow, the experimental requirements and materials are given first. The first section therefore covers the experimental requirements for each set of experiments, the second section contains the materials and from the third section onward, the workflow is described.

3.1 Experimental Requirements

The equipment to be used are:

1. For sample preparation:
    a. End face grinding machine (Figure 3.1)

This machine is vital to prepare samples for geomechanical tests. It grinds the ends of the samples with very high precision to ensure extremely smooth surfaces.

b. Drill press (Figure 3.2)

By using a special concrete bit, the drill press was used to drill hole into the samples required for the breakdown pressure test.

Figure 3.1 End face grinding machine

Figure 3.2 Drill press

2. For geomechanical tests:

    a. AutoLab 1500 for tri-axial and ultrasonic testing (Figure 3.3)

    The AutoLab 1500 is a state of the art geomechanical testing equipment designed for conducting both static and dynamic test. It can provide confining and axial pressures up to 10,000 psi.

    b. Brazilian Disc Testing Machine (Figure 3.4)

    This machine is used for estimating the tensile strength of the rock.

Figure 3.3 NER AutoLab 1500

Figure 3.4 Brazilian Disc Testing Machine

3. For Breakdown Pressure test:

    a. ISCO dual syringe pump (Figure 3.5)

    b. Fracturing fluid accumulator holding up to 1,000 ml (Figure 3.6)

    c. Modified ageing cell (described in section 3.5) (Figure 3.7)

    d. Pressure transducer connected to data acquisition to record the injection pressure as a function of time

Figure 3.5 ISCO dual syringe pump

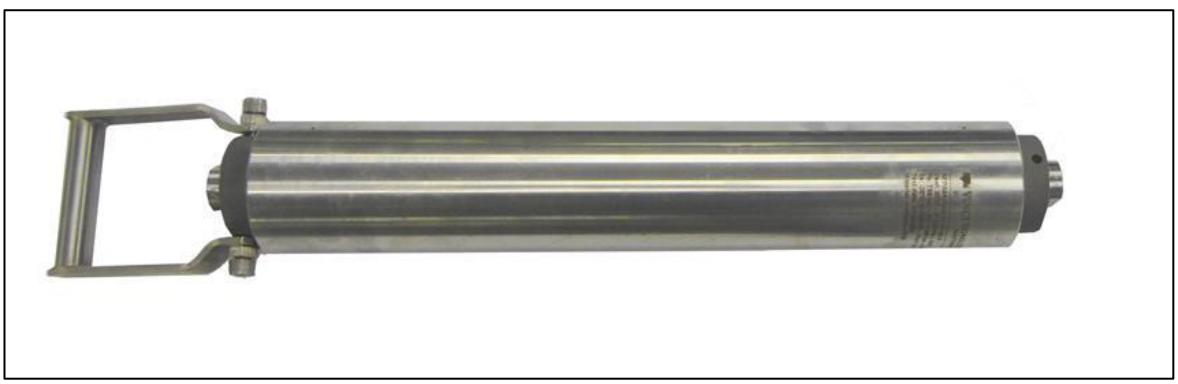

Figure 3.6 Fluid Accumulator

Figure 3.7 Ageing cell

4. For NMR experiments: Oxford NMR GeoSpec2 (Figure 3.8)

Figure 3.8 Oxford NMR GeoSpec2

5. For saturation

    a. ISCO dual syringe pump (same as for the breakdown pressure test)

    b. Accumulator cell (same as for the breakdown pressure test)

    c. Saturation cell (Figure 3.9)

Figure 3.9 Saturation cell

6. For preparation of Fracturing fluid

    a. Cole-Parmer variable speed Mixer (Figure 3.10)

    b. pH meter (Figure 3.11)

    c. Water bath (Figure 3.12)

    d. Grace m3600 viscometer (Figure 3.13)

    e. Weighting balance (Figure 3.14)

Figure 3.10 Cole-Parmer mixer

Figure 3.11 Benchtop pH meter

Figure 3.12 Water bath

Figure 3.13 Grace m3600 viscometer

Figure 3.14 Weighting balance

7. For CT scanning: Toshiba Alexion TSX-032A medical X-ray CT (Figure 3.15)

Figure 3.15 Toshiba Alexion TSX-032A medical X-ray CT

3.2 Materials

3.2.1 Tight Sandstone Cores

Samples form Scioto tight sandstone outcrop were used in this study. Due to a wide range of experiments conducted, a variety of cores were required for each experiment. The 12 in. by 12 in. block of tight sandstone was first cut into smaller blocks (Figures 3.16 and 3.17). Then one of the smaller blocks was sent to Schlumberger facility to be cored into smaller cores (Figure 3.18).

Figure 3.16 Large rock cutter

below:

Figure 3.17 Block cut into smaller blocks

Figure 3.18 Two different sizes of core plugs were obtained as per test requirements

The requirements of core samples are different for different type of tests, as described below:

1. 1.5 in. diameter with 3 in. length for geomechanical tests (Samples 1-1 to 1-15).
2. 2 in. diameter with 2 in. length for fracturing test (Samples 2-1 to 2-23). A hole of 0.25-in. in diameter and 0.75-in. length is drilled on one face of each core. A 0.25-in. OD tube is placed and fixed inside the hole at depth of 0.25 in., leaving an open hole section of 0.5-in. length (Figure 3.19). The pipe was fixed using strong epoxy.
3. 1 in. diameter with 0.5 in. length for Brazilian tensile testing.
4. Total number of core plugs obtained was 38, out of which 23 are used for fracturing test and the remaining 15 were used for geomechanical tests.

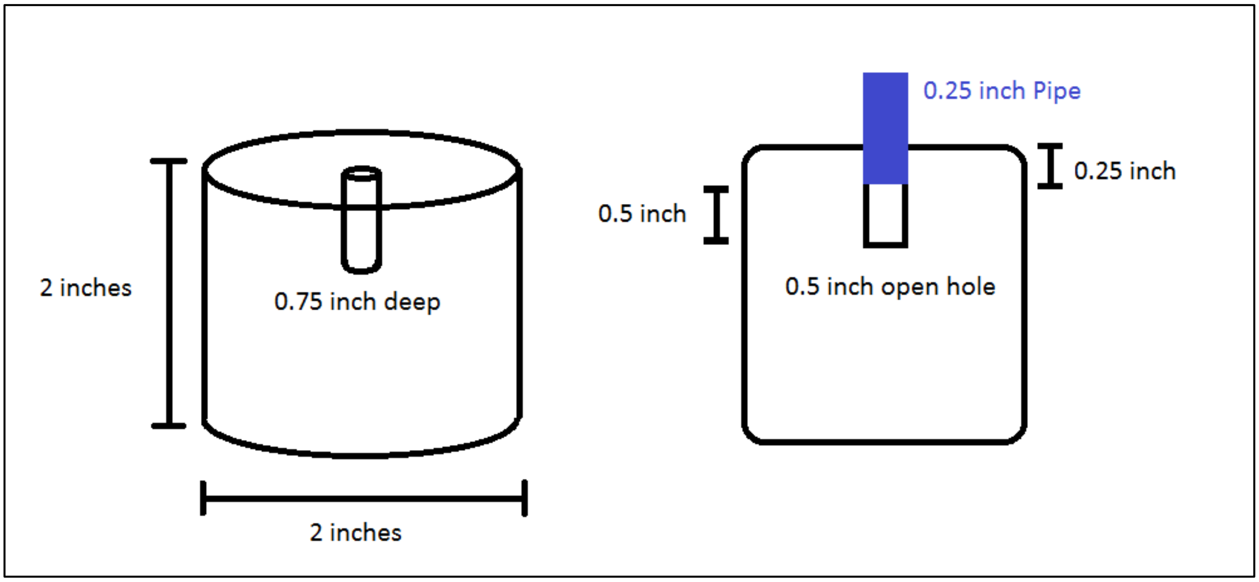

Figure 3.19 Core dimensions required for fracturing study

Drilling of the central hole was performed on a precise heavy duty drill press to maintain hole smoothness. The drill bit chosen for the job was a concrete drill bit with a round tip. It’s important for the bottomhole to be round to ensure test integrity. If the bottomhole is pointed, then the stress will be concentrated at the tip resulting in an abnormal propagation of the fracture as well as lower breakdown pressure. To ensure smooth bottom hole, CT scans were performed after drilling. It’s clear from Figure 3.20 that the pipe (bright white) is placed at a depth of 0.25 inch and 0.5 inch (black) is open hole as well as the bottomhole is round.

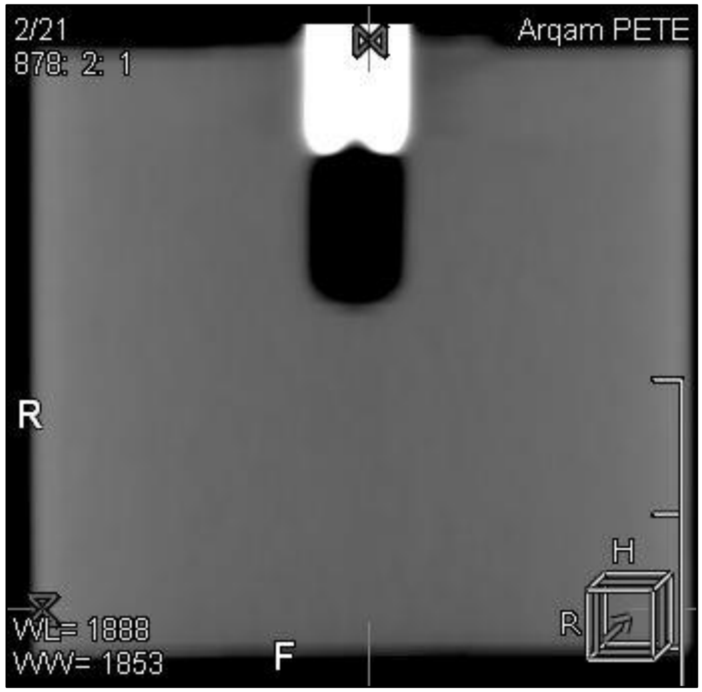

Figure 3.20 CT scan of sample 2-21 showing the placement of the pipe and roundness of the bottomhole.

3.3 Characterization of the Tight Sandstone Cores

In this section, the properties of the cores will be determined. First the Routine Core Analysis (RCA) is performed followed by special analysis by using Nuclear Magnetic Resonance (NMR) and CT scan. The aim of characterization of the cores is to determine the degree of homogeneity.

3.3.1 Routine Core Analysis (RCA)

RCA includes the determination of the petrophysical properties. Standard petrophysical equipment is used to determine the:

1. Permeability
2. Grain density
3. Porosity

Since the samples are tight sandstone rocks, the permeability and porosity values are expected to be low. This will help us in determining the type of fracturing fluid to be used.

3.3.2 Special Core Analysis (SCAL)

In order to have an even better understanding of the rock properties, special core analysis was performed. The SCAL includes NMR, CT Scan and XRD/XRF.

Nuclear Magnetic Resonance (NMR)

NMR is a powerful tool which can help in the determination of the different pore systems present in the sample. Few samples were saturated with brine and NMR was performed on them to understand the porosity, saturation profile, the pore systems and homogeneity.

CT Scan

Core imaging is an integral part of core analysis. It gives us eyes inside the core to explore features which are otherwise difficult to see. CT Scan was used to scan the samples for any significant features. All cores were CT scanned after coring. The methodology established for maintaining healthy cores was to conduct CT scan:

1. After plugging
2. After drilling central borehole
3. After running fracturing test

XRD

X-Ray Diffraction test measures the concentration of individual chemical compounds and determines the percentage of those compounds. Performing XRD on the tight sandstone samples will help us understand their constituents.

3.4 Investigation of Geomechanical Parameters

In this section, some of the crucial geomechanical parameters will be determined. The dynamic Young's Modulus and Poisson's Ratio will be determined by the ultrasonic test and the indirect tensile strength will be determined using the Brazilian test. Some cores were saturated to study the effect of saturation on the geomechanical parameters.

3.4.1 Ultrasonic Test

Ultrasonic tests were performed to get the dynamic geomechanical properties of the tight sandstone samples. The core plugs were placed within a rubber sleeve and placed in an ultrasonic core holder. The equipment used was the NER AutoLab 1500. The steps for the ultrasonic tests are as follows:

1. The required orientation of the sample is chosen and the sample is placed in a rubber sleeve.
2. The rubber sleeve (sample enclosed) is then placed on the ultrasonic core holders.
3. The core holder with the source crystal is placed at the bottom of the sample and the receiver at the top.
4. To avoid the confining oil to penetrate the sample, the system must be tightly sealed. To achieve a healthy seal, the rubber sleeve is tightly tied against the core holder by using wires.
5. The setup is then placed in the load cell of the AutoLab 1500 and the sensors connected.
6. The setup is then checked for any faults and then loaded into the triaxial cell to start testing.

7. Confining pressure is applied and the p and s waves are recorded.
8. Step 7 is repeated until necessary stages are complete.
9. In a typical test, the waves are recorded at increasing confining pressure and also while decreasing to investigate the hysteresis.

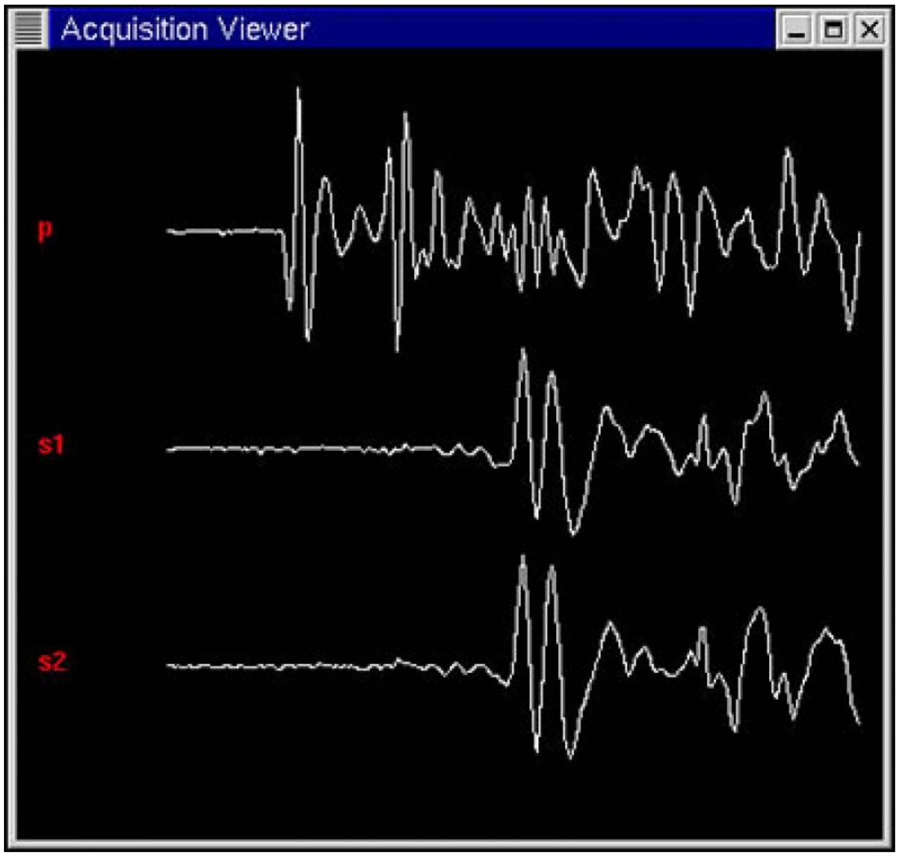

Figure 3.21 Typical response from an ultrasonic test

Figure 3.21 shows a typical response from an ultrasonic test. From this response we can quickly identify the arrival of sonic waves. The P and S- wave velocities are then calculated from the arrival time of the sonic waves by using:

$$V_{p,s} = \frac{sample\ length}{arrival\ time(p\ or\ s\ wave)} \tag{3.1}$$

$Where,$

$V_{p,s}$ p or s wave velocity (m/s)

Upon calculating the velocities, the dynamic geomechanical properties can be calculated by:

$$E_{dyn} = \frac{\rho_b * {V_s}^2 * (3 * {V_p}^2 - 4 * {V_s}^2)}{({V_p}^2 - {V_s}^2)} \tag{3.2}$$

$$\nu_{dyn} = \frac{{V_p}^2 - 2 * {V_s}^2}{2 * ({V_p}^2 - V_s)} \tag{3.3}$$

$Where,$

E_{dyn} Dynamic Young’s modulus (GPa);

ρ_b Bulk density (g/cc); and

ν_{dyn} Dynamic Poisson’s Ratio;

3.4.2 Unconfined Compression Strength (UCS) Test

UCS tests are conducted to determine the static geomechanical properties of the tight sandstone samples. In a UCS test, axial load is applied to the sample in the absence of confining pressure. The axial load is increased until the core plug is failed. The highest axial load is called the UCS. The equipment used was the NER AutoLab 1500. The steps for the UCS tests are as follows:

1. The required orientation of the sample is chosen and the sample is placed in a special rubber sleeve for destructive tests.
2. Both the radial and axial LVDT's (linear variable differential transformer) are set in place. LVDT's measure the change in length.
3. The setup is then placed in the load cell of the AutoLab 1500 and the sensors are connected.
4. The setup is then checked for any faults and then loaded into the triaxial cell to start testing.
5. Axial load is applied on the sample until the rock reaches failure.
6. The maximum axial load applied to the sample before it fails is the UCS of the sample.

The static Young's Modulus is the ratio of the change in axial stress by the change in axial strain. More specifically it is the slope of the stress strain curve and is given by:

$$E_{static} = \frac{\Delta\sigma_1}{\Delta\varepsilon_1} \tag{3.4}$$

$Where,$

E_{static}	Static Young's modulus (GPa);
$\Delta\sigma_1$	Axial Stress (psi); and
$\Delta\varepsilon_1$	Axial Strain;

The static Poisson's Ratio is given by:

$$\nu_{static} = -\frac{\Delta\varepsilon_3}{\Delta\varepsilon_1} \tag{3.5}$$

$Where,$

ν	Poisson's Ratio;
$\Delta\varepsilon_3$	Lateral Strain; and
$\Delta\varepsilon_1$	Axial Strain;

Or in simpler terms it is the ratio of the slopes of the axial stress vs strain curve and the axial stress vs lateral strain curve.

3.4.3 Brazilian Disc Test

The Brazilian Disc test is a simple and an inexpensive way to indirectly measure the tensile strength of a rock. Stress is applied on the diametrical plane of the disc until it is cracked (Figure 3.22). This test is more representative of the field cases due to the complicated stresses found in the field. The sample undergoes tensile failure while placed in a compressive stress environment (which is what happens is the field).

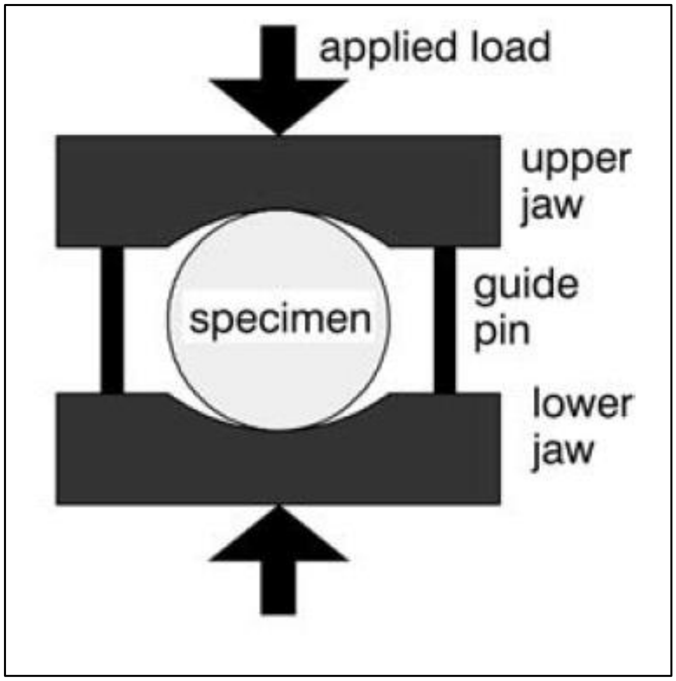

Figure 3.22 Brazilian Disc test

The Brazilian tensile strength can be calculated using the following equation

$$\sigma_t = \frac{2P}{\pi d l} \tag{3.6}$$

where:

σ_t	Brazilian tensile strength (MPa);
P	Failure load (N);
d	Diameter (mm); and
l	Length (mm).

As per the ASTM D3967 testing standard, the following is the procedure followed to conduct the Brazilian Disk test (indirect tensile test)

1. The sample is cut into a circular disc of diameter 1 inch and thickness of 0.5 inch. The thickness to diameter ratio is to be kept in the range of 0.2 to 0.75 as per ASTM D3967.
2. The sample is placed in the load frame.
3. Make sure the surfaces of the sample are in uniform contact with the load frame.
4. Load is applied at 0.027 mm/min. The pressure builds linearly until the sample is cracked.

3.4.4 Saturation of cores

In order to saturate the cores with the given liquid, the following procedure was followed:

1. Place the cores in the saturation cell and fill the empty space with spacers.
2. Vacuum the saturation cell for 5 hours.
3. Start pumping the saturation fluid in the saturation cell and apply pressure of 2000 psi.
4. Stop pumping and leave the saturation cell pressurized for 3 days.
5. Carefully open the valves to remove pressure. Drain the saturation cell and retrieve the cores.

3.5 Breakdown Pressure Determination Using Fracturing Cell Setup

An experimental setup was developed to determine the breakdown pressure of cores. The design and procedure to conduct this experiment are discussed in this section.

3.5.1 Developing the Fracturing cell

The ISCO pump provides pressure by pumping distilled water to the bottom end of an accumulator cell which contains the fracturing fluid on the other end. The accumulator cell is connected to the fracturing cell (modified ageing cell) as well as to the pressure gauge and the pressure transducer to record the pressure data (Figures 3.23 and 3.24).

The fracturing cell is actually an ageing cell with a pressure rating of 3000 psi which was modified to conduct the breakdown pressure test. Two inlets were added on top of the ageing cell (Figures 3.25 and 3.26). The inlet in the center is for the injection of the fracturing fluid and the other inlet is to provide confining pressure. The confining pressure is provided by means of Nitrogen gas (cylinder) which is connected to the fracturing cell.

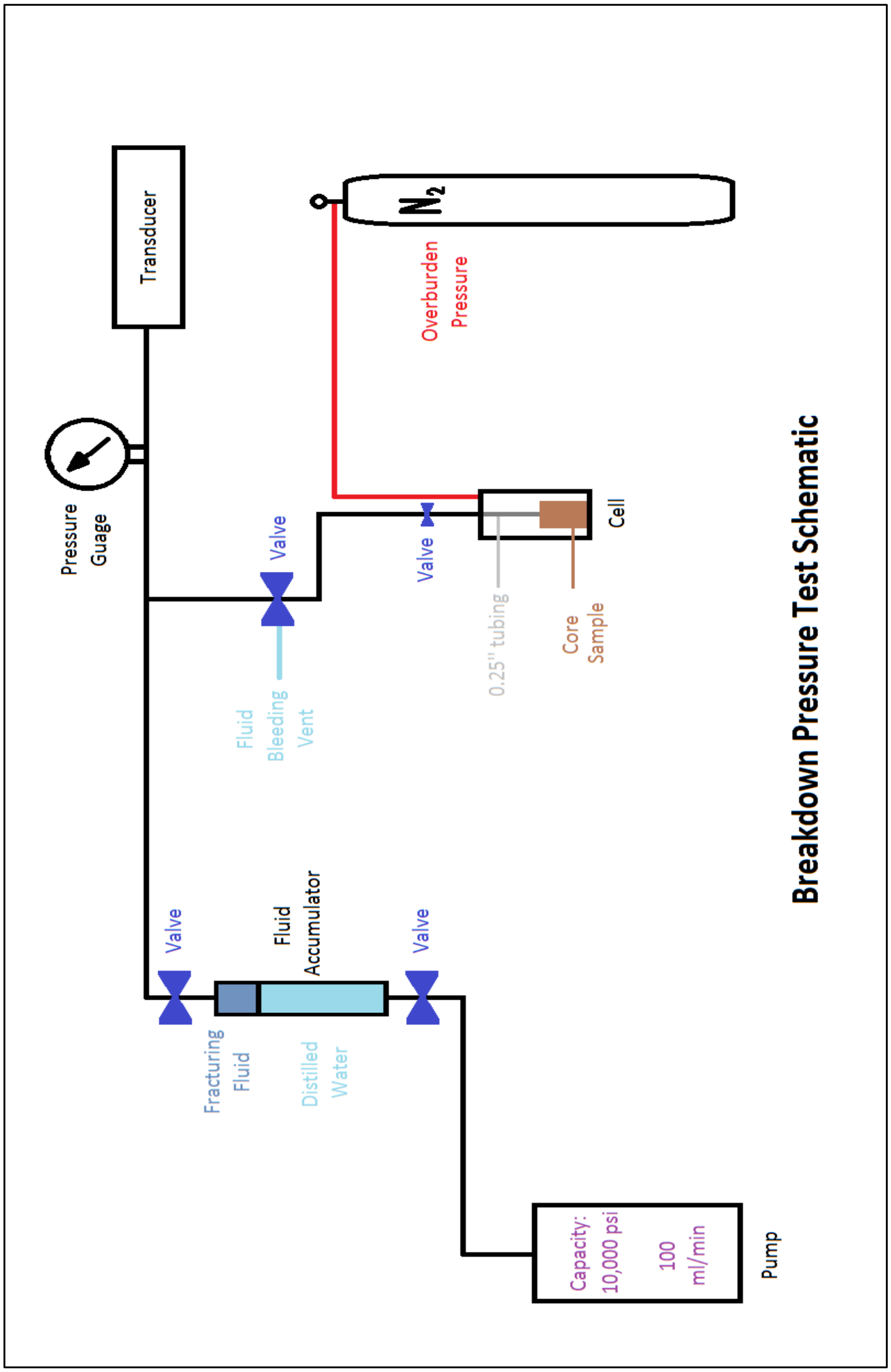

Figure 3.23 Breakdown Pressure Test Schematic

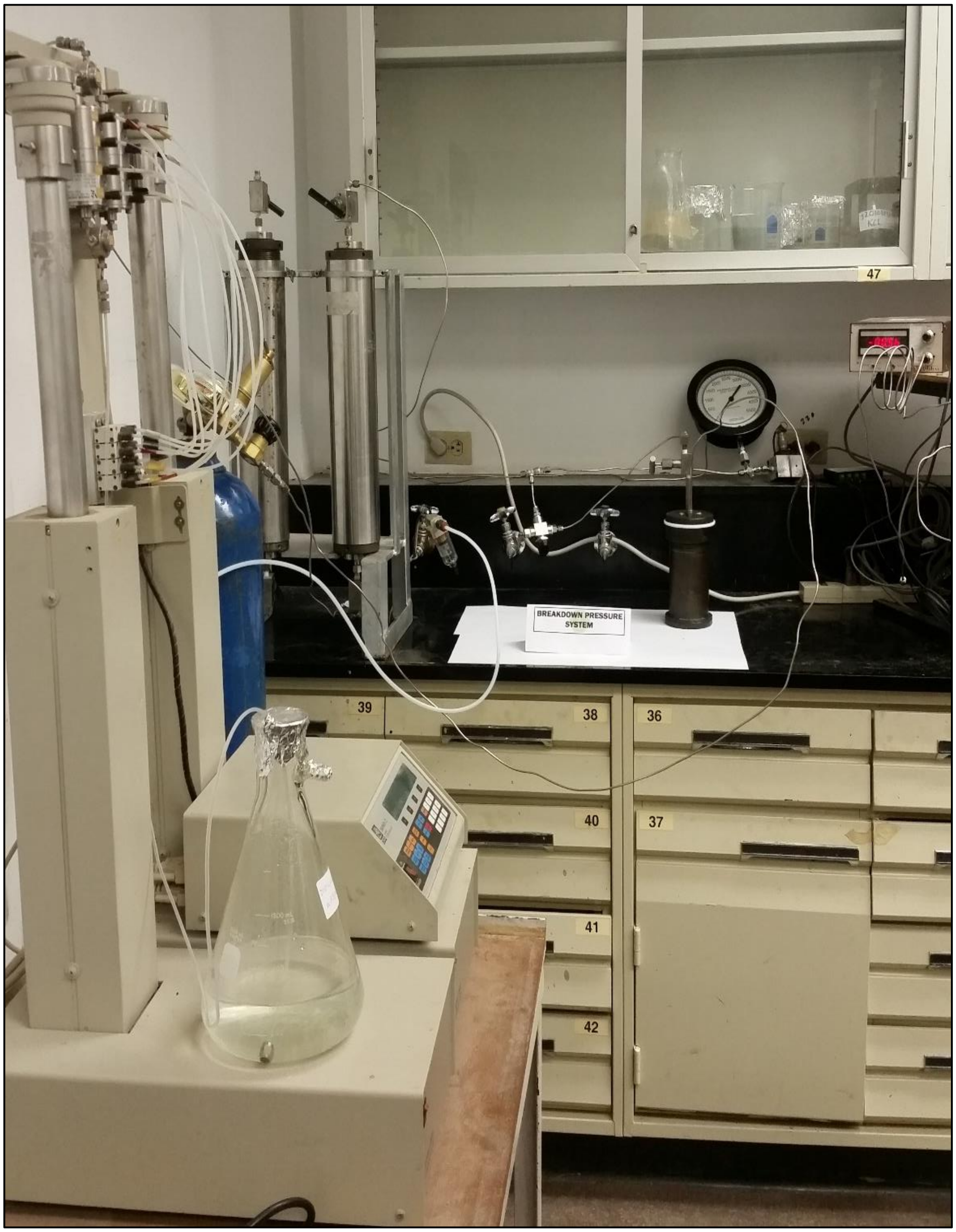

Figure 3.24 Breakdown Pressure System

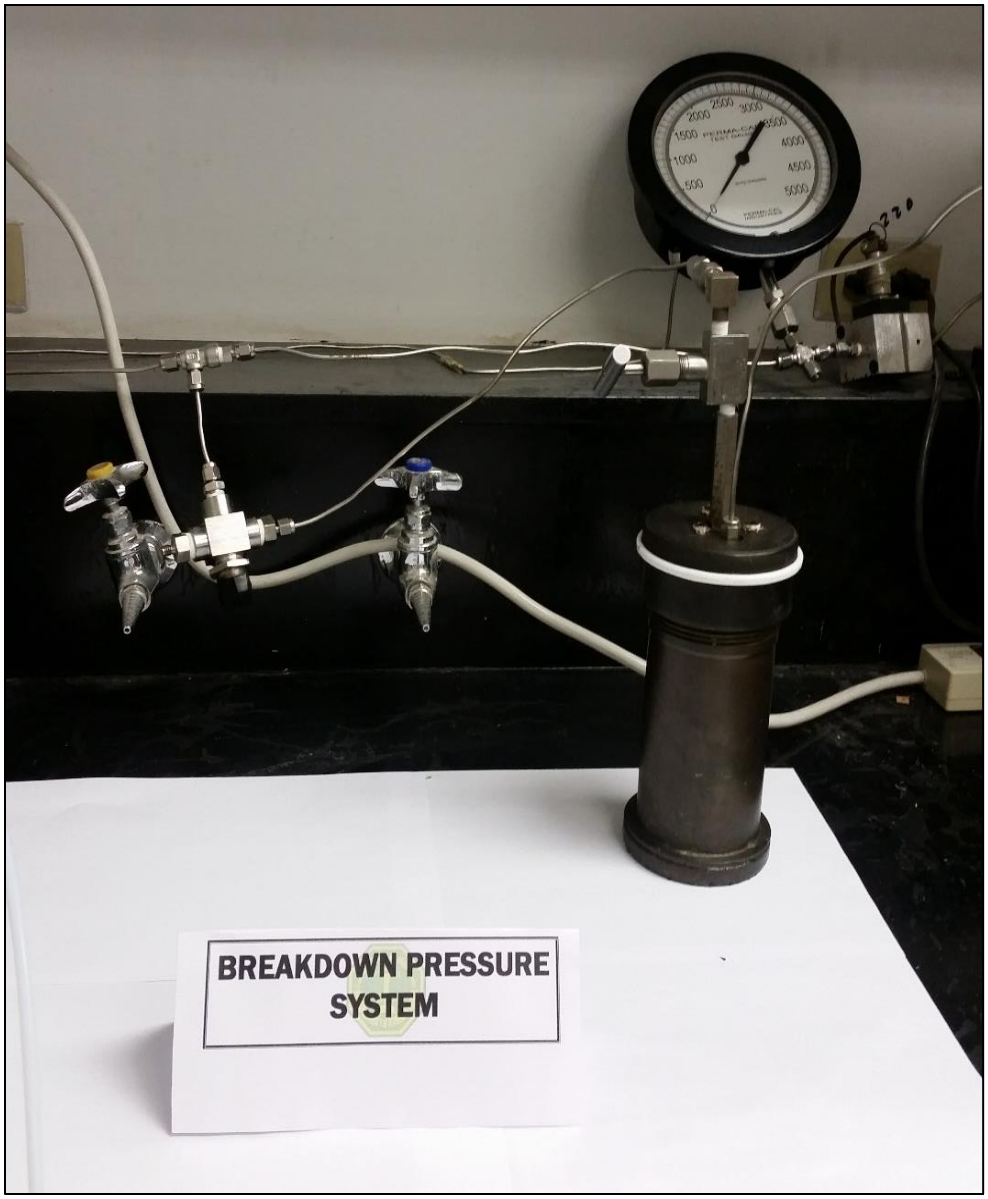

Figure 3.25 Fracturing cell

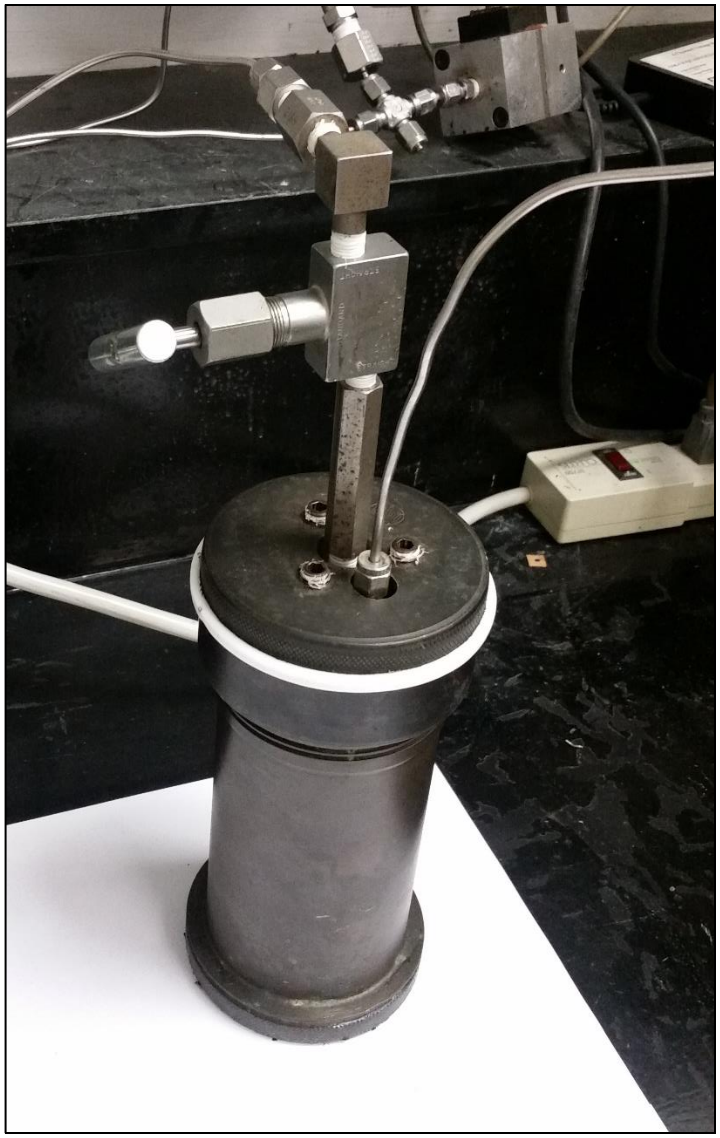

Figure 3.26 Fracturing cell showing the two inlets

3.5.2 Fracturing Fluid Preparation

The preparation of the fracturing fluid required precise measurements of the additives. The following are the different types of fracturing fluids and their preparing procedures:

1. Brine (3% Potassium Chloride)
    a. Pour 800 ml of distilled water into a clean 1000 ml volumetric flask.
    b. Measure 30 grams of Potassium Chloride using weight balance and add to the distilled water.
    c. Stir the mixture for 10 minutes on stirrer.
    d. After the Potassium Chloride was dissolved, add more distilled water till the 1000 ml mark.
2. Linear Gel
    a. Weigh 1000 (±1) grams of tap water using a 1000 ml beaker
    b. Place the beaker under the mixer and set the 1100 (±100) RPM on mixer to obtain vortex
    c. Using 10 mL cut off tip syringe slowly add the gelling agent (CMHPG) for
        i. 40 ppt add 10 ml CMHPG
        ii. 30 ppt add 7.5 ml CMHPG
        iii. 25 ppt add 6.25 ml CMHPG
    d. Increase mixing rpm to 2000 (±100) RPM.
    e. Start stopwatch to monitor and continue mixing for 20 minutes.
    f. Add 1.0 gpt of Clay stabilizer.
    g. Continue mixing for 10 more minutes.
    h. Measure the viscosity on Grace m3600 @ 100 s^{-1} shear rate.

3. Crosslinked Gel
    a. Set the water bath to 130°F and wait for it to warm up.
    b. Weigh 250 (± 0.5) grams of base gel into a beaker.
    c. Place the beaker under the mixer and set it to 2000 (±100) RPM .
    d. Slowly add Buffer to adjust the pH to 10.25 and continue mixing for 30 seconds.
    e. Add 1 gpt of crosslinker and continue to mix for 1 minute.
    f. Place the beaker into the water bath for 15 minutes (the crosslinker is a delayed crosslinker and fully active when the system heat above 130°F).
    g. Remove the beaker from the water bath and measure the viscosity on Grace m3600 @ 100 s^{-1} shear rate.
4. 20% GLDA with Guar Gum
    a. Weigh 223.05 grams of distilled water using a beaker.
    b. Add 1.95 grams of Guar and mix for 10 minutes.
    c. Add 225 grams of 40% GLDA and mix for another 10 minutes.
    d. Measure the pH and Viscosity.

3.5.3 Fracturing Test

1. Flush the system thoroughly with toluene and distilled water, then by air.
2. Clean the fluid accumulator and place the fracturing fluid in it and connect the lines.
3. Pump the fracturing fluid through the system and bleed it from all valves to make sure there is no air or any other fluid in them.
4. Pressurize the system to 2000 psi and make sure there are no leaks.

5. Once the system is full with the fracturing fluid, place the core in the rubber sleeve and tighten its ends to avoid confining fluid to enter the sample.
6. By means of a syringe, inject the fracturing fluid in the core through the pipe to make sure all the air in the borehole is replaced by the fracturing fluid.
7. Start the pump at the required rate and connect the core to the fracturing cell (continuous pumping is required to make sure there is no air in the system).
8. Secure the fracturing cell and tighten it.
9. Apply the required confining pressure. The pressure builds up until the core is fractured, then the pressure instantly falls to a significantly lower value.
10. The maximum pressure (before the pressure drops) is the breakdown pressure.
11. Stop the pump and the confining pressure.
12. Slowly release the confining pressure and disconnect the fracturing cell and retrieve the sample.
13. Conduct CT scan on the sample to identify the fracture behavior.

3.6 Post-Test Analysis

After the tests have been completed, the sample is examined for the fracture behavior and type. The sample is also CT scanned to see the extent of the fracture and the deformation, if any.

CHAPTER 4

RESULTS AND DISCUSSION

4.1 Characterization of Cores

As discussed in section 3.3, the cores will be characterized using numerous techniques. The obtained cores are divided into two groups and are tabulated in Table 4.1

Table 4.1 Types of cores

Geomechanical group	Fracturing Group
Samples 1-1 to 1-15	Sample 2-1 to 2-23
Size: 3” dia, 1.5” length	Size: 2” dia, 2” length

4.1.1 Routine Core Analysis (RCA)

RCA was performed on the geomechanical cores and the results are tabulated in Table 4.2. The tight sandstone cores have an average porosity is 13.31 %, average bulk density is 2.3 g/cc and an average permeability of 1.3 mD. It can be considered as a tight sandstone (Hayton et al., 2010).

Table 4.2 Routine Core Analysis

Sample Number	Bulk Density (g/cc)	Porosity (%)	Permeability (mD)
1-1	2.294	13.51	1.188
1-2	2.304	13.21	1.217
1-3	2.298	13.54	1.375
1-4	2.304	13.65	1.434
1-6	2.311	12.91	1.292
1-7	2.283	13.15	1.432
1-8	2.305	12.43	1.212
1-10	2.287	13.97	1.276
1-11	2.297	13.21	1.284
1-12	2.311	13.51	1.317
1-13	2.299	13.48	1.254
1-14	2.300	13.12	1.334

4.1.2 Special Core Analysis (SCAL)

NMR

Four cores (core number 1-1, 1-12, 1-13, 1-14) were selected and were fully saturated with brine (3% KCl). NMR was then performed on these samples.

Figures 4.1 to 4.4 represents the saturation profile of the cores. The saturation profile depicts how the total saturation is distributed along the length of the core starting from the top of the core till the bottom. It is evident from Figures that the cores are evenly saturated and are very identical and therefore, homogeneous.

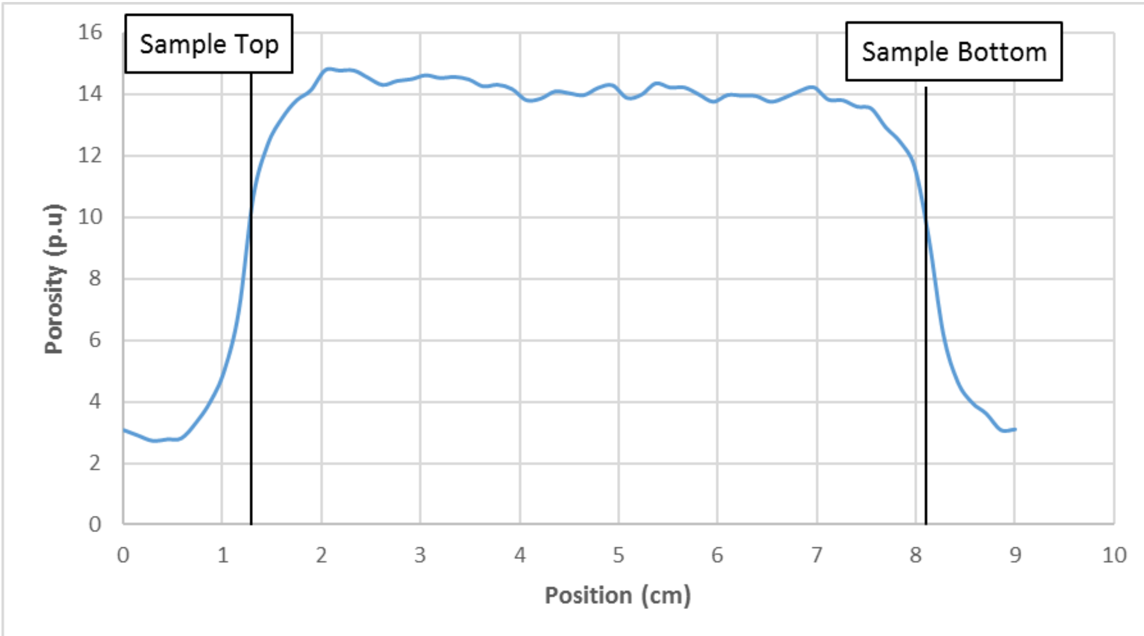

Figure 4.1 Saturation profile of sample 1-1

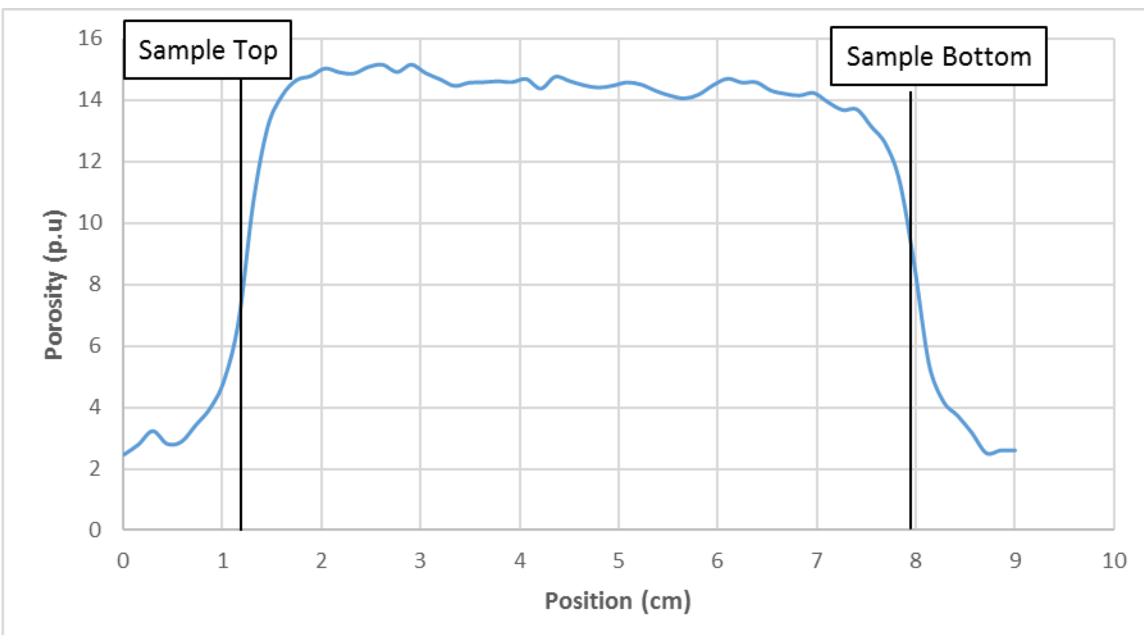

Figure 4.2 Saturation profile of sample 1-12

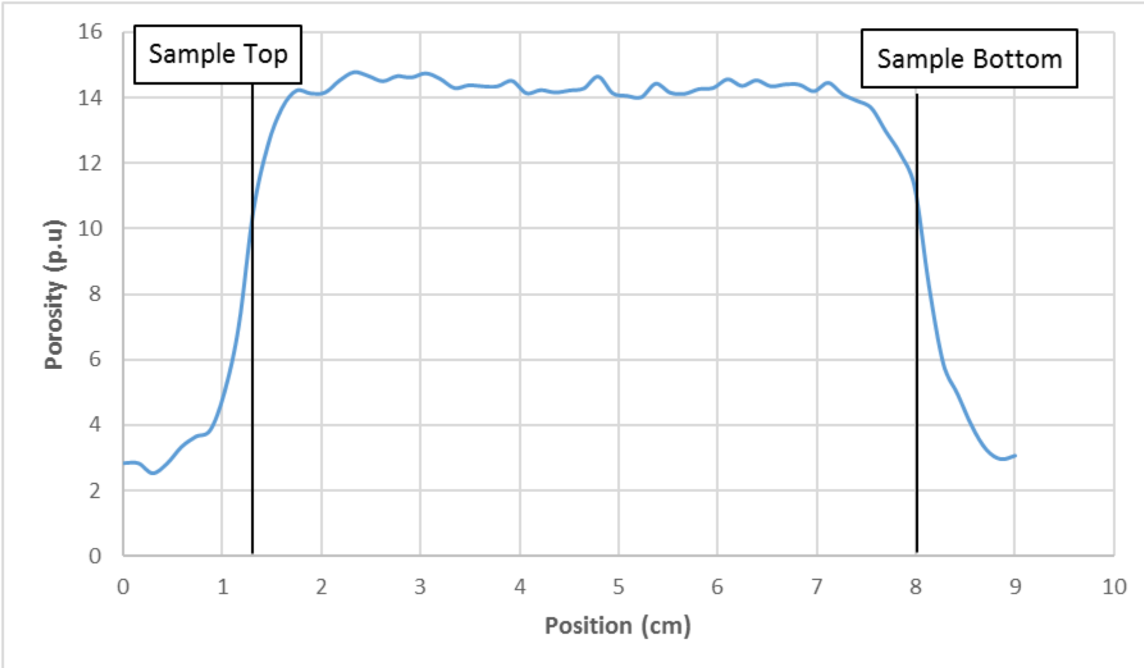

Figure 4.3 Saturation profile of sample 1-13

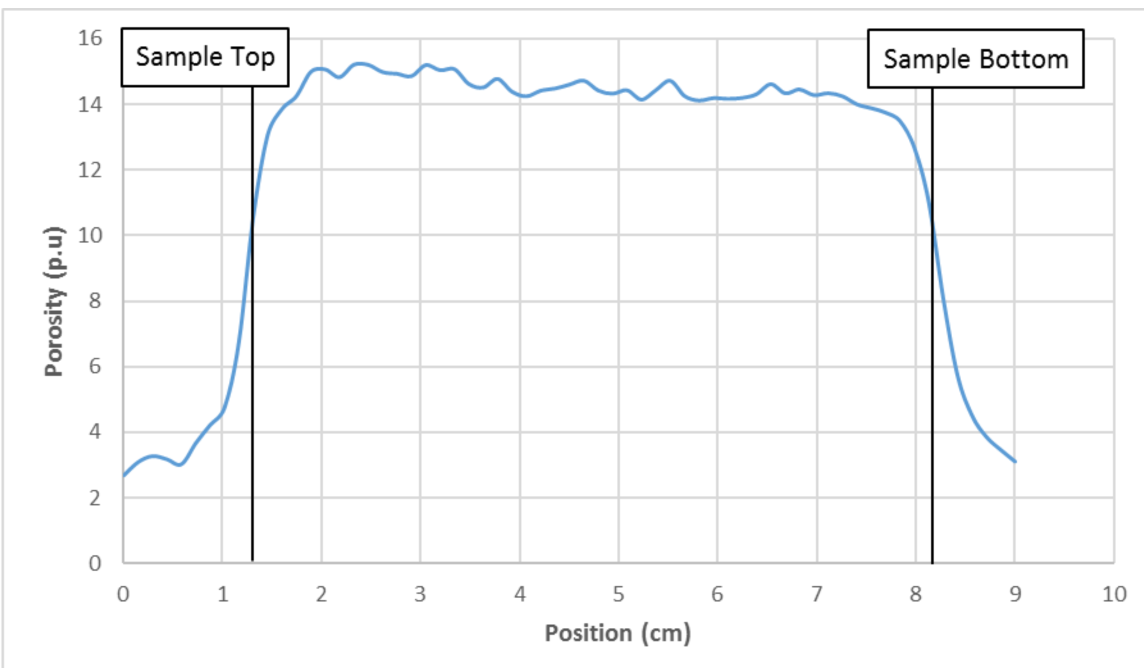

Figure 4.4 Saturation profile of sample 1-14

Figures 4.5 to 4.8 represents the NMR T2 Distribution results of the core plugs. The T2 distribution curves are skewed towards the left indicating presence of two pore systems namely Micropore and Mesopore systems. The Mesopore system is located towards the 20 ms T2 time, while the micropore system is located at the beginning of the T2 curve. The Mesopore system is the dominant system as seen from the Figure.

The porosity of the cores is also identical as see in Table 4.3. The range of the porosities are from 14.5% to 14.9%. The average porosity is 14.8%. This porosity is higher than what we saw in the RCA, but NMR is considered as the most accurate tool to determine porosity. Hence, this porosity will be for all samples

Table 4.3 NMR Results

Sample Number	***Porosity (%)***
1-1	14.5
1-12	14.8
1-13	14.8
1-14	14.9

Based on the results from NMR, we can conclude that:

1. The tight sandstone cores are homogeneous
2. Presence of two pore systems namely, Mesopores and Micropores.
3. Porosity for the cores is 14.8%

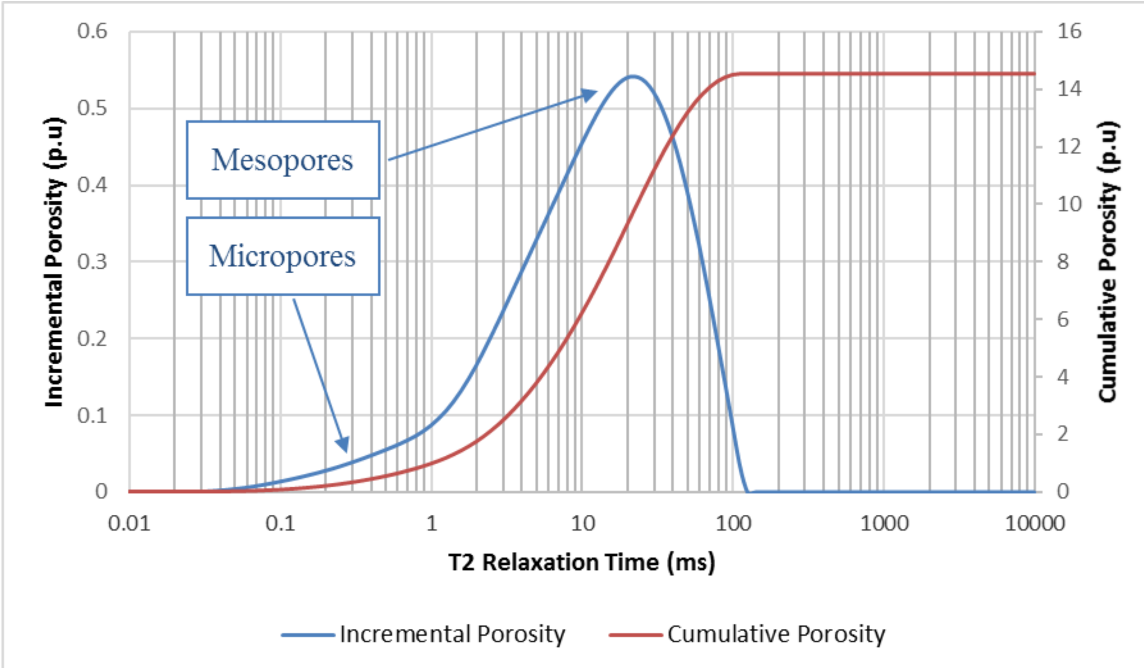

Figure 4.5 NMR T2 Relaxation of sample 1-1

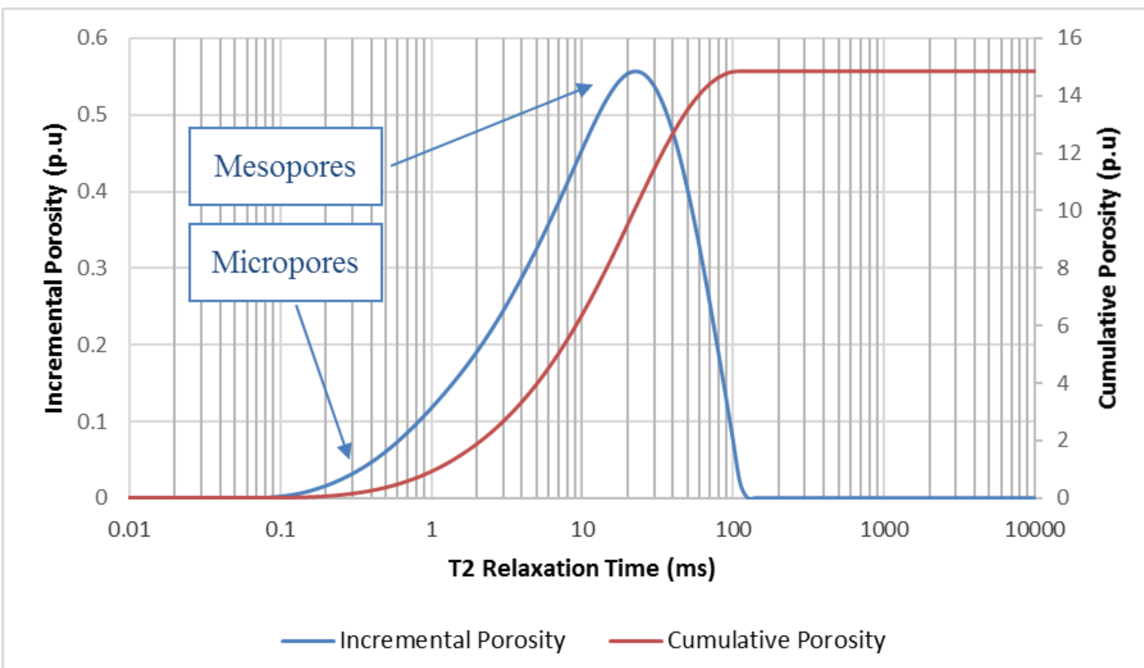

Figure 4.6 NMR T2 Relaxation of sample 1-12

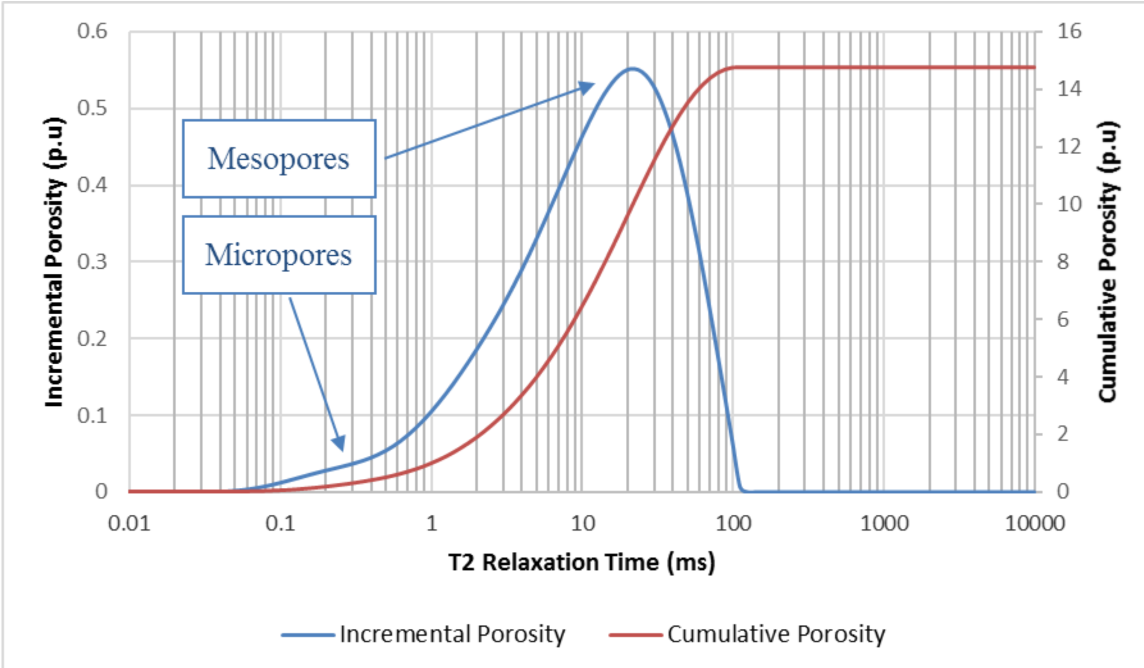

Figure 4.7 NMR T2 Relaxation of sample 1-13

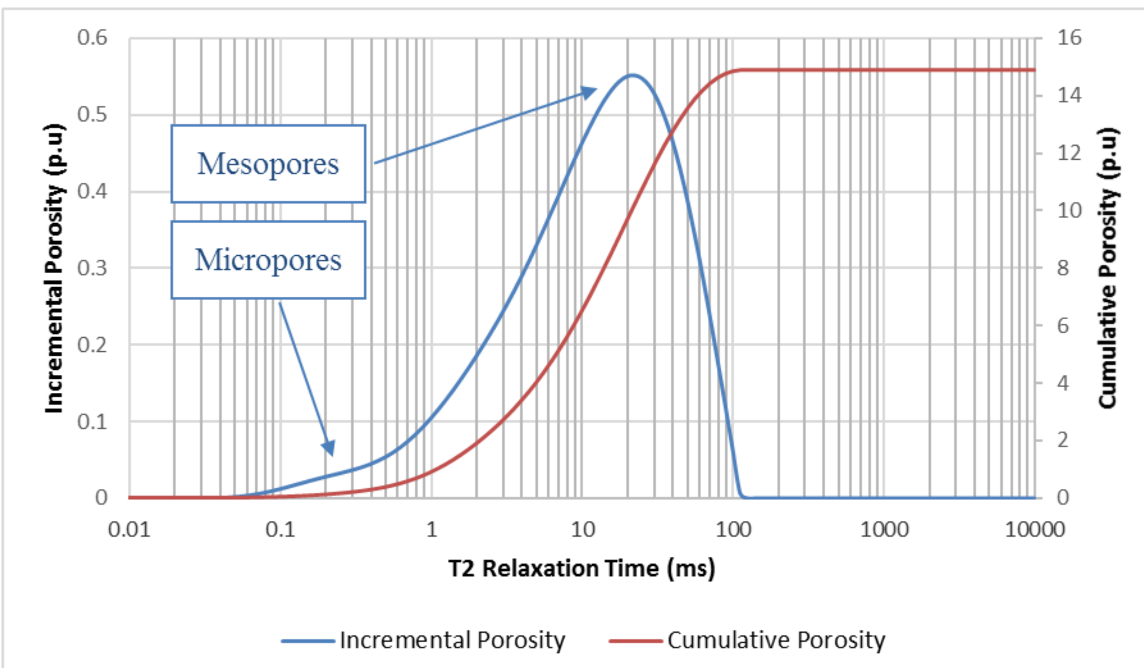

Figure 4.8 NMR T2 Relaxation of sample 1-14

CT Scan

All the core samples were scanned by using Medical CT scanner. The 23 cores for fracturing test were scanned 3 times while the 15 geomechanical cores were scanned once after plugging and once again after saturation as mentioned in section 3.3.2. The ranges of the CT scan were kept same throughout so it will be easier to identify the changes in them.

Figures 4.9 to 4.11 show a few samples from the fracturing test group. The Figures contain slice by slice images from the top of the samples to the bottom. It’s clear that the cores have no internal features like cracks or fractures and are homogeneous. But the bedding plane can be identified and hence the samples are horizontal. Figures 4.12 to 4.14 show the same samples after drilling a borehole in them. This is done to see if the hole is drilled smooth and if there are any affected areas due to drilling

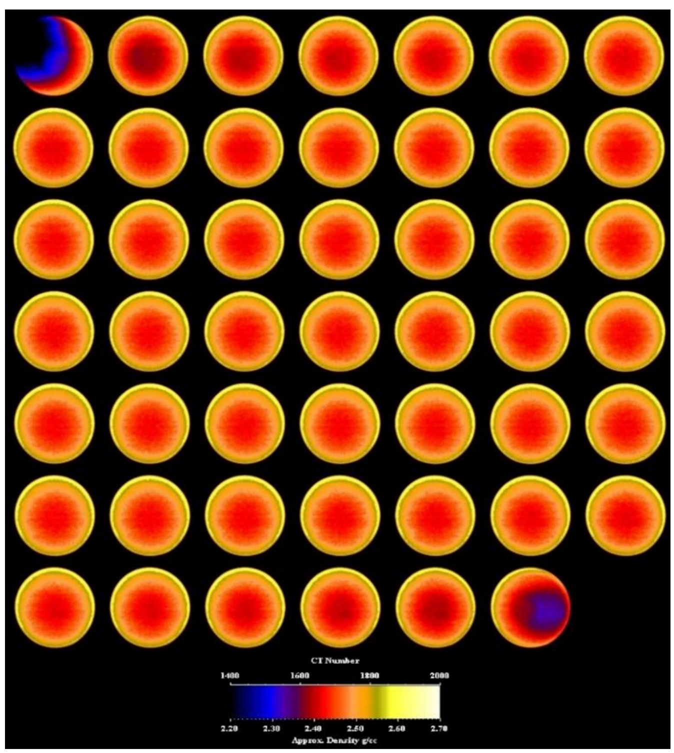

Figure 4.9 Sample 2-2 After plugging

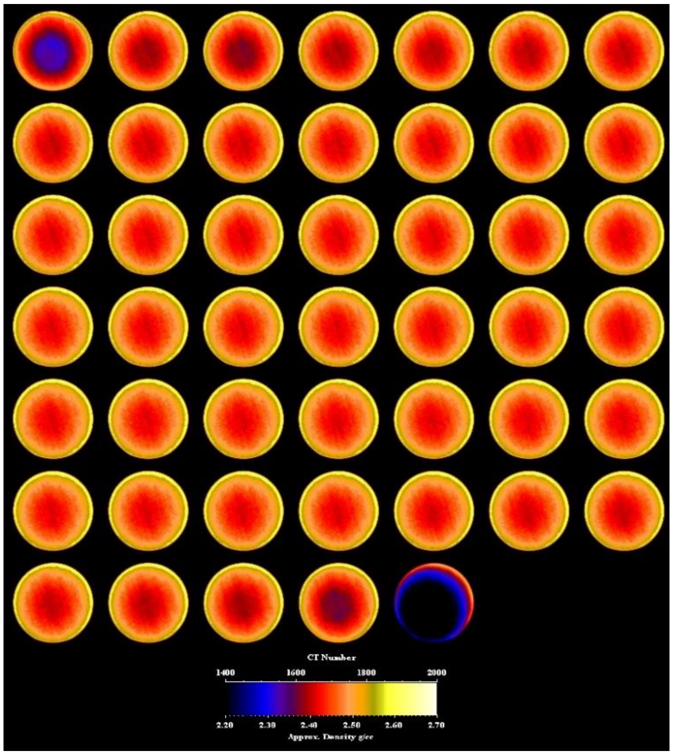

Figure 4.10 Sample 2-4 After plugging

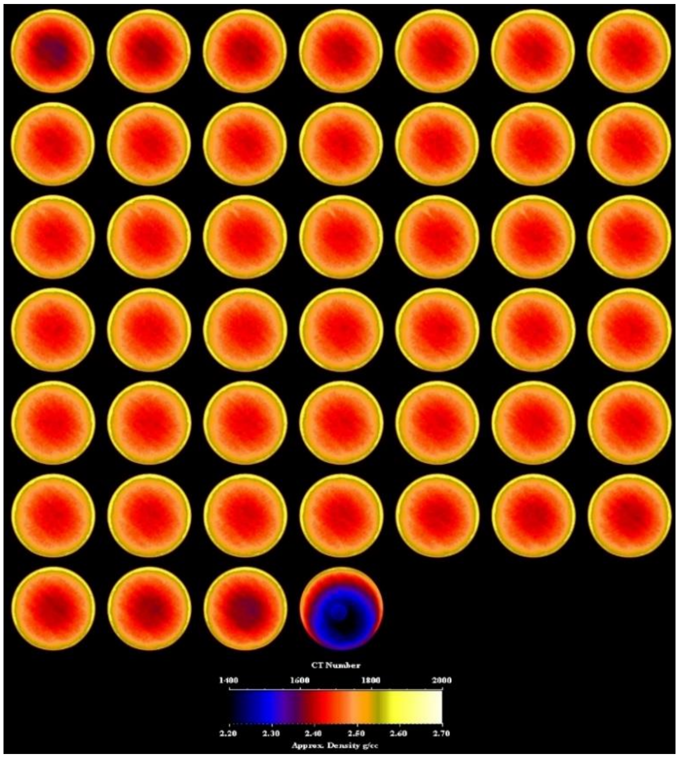

Figure 4.11 Sample 2-10 After plugging

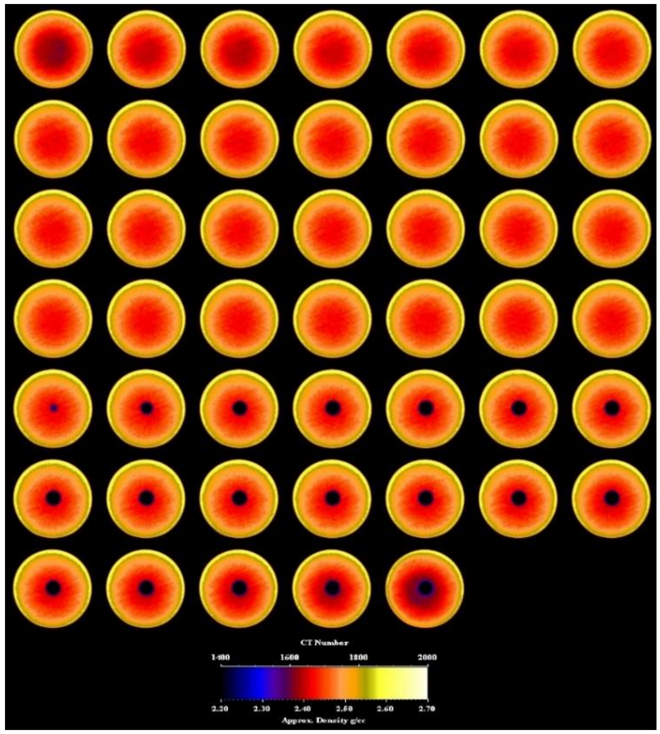

Figure 4.12 Sample 2-2 After drilling

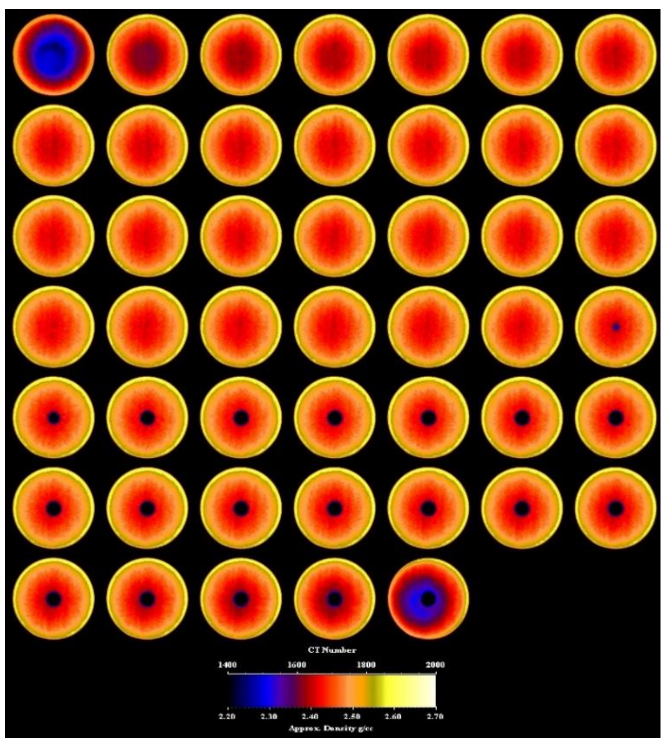

Figure 4.13 Sample 2-4 After drilling

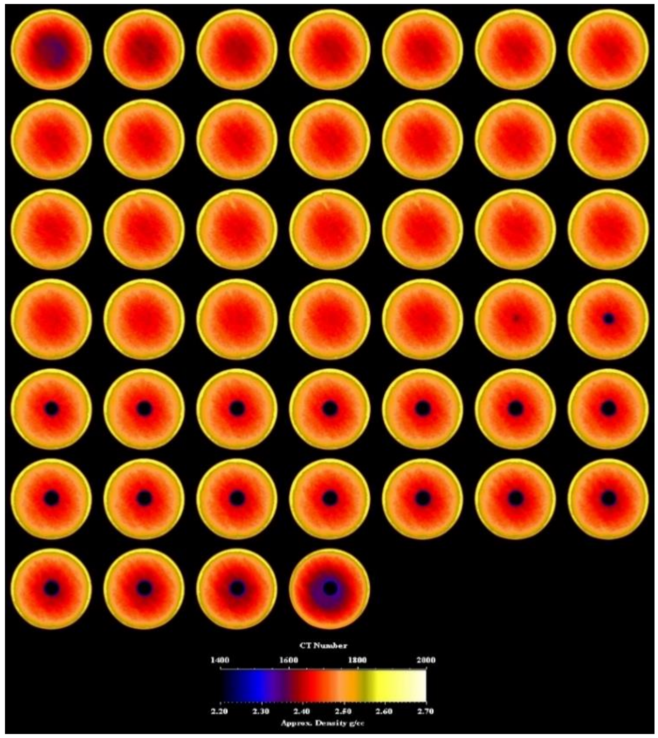

Figure 4.14 Sample 2-10 After drilling

Sample 1-1 has been displayed in dry and saturated (brine) conditions in Figures 4.15 and 4.16 respectively. An increase in CT number (approximate density) is seen as the core is saturated.

Figures 4.17 and 4.18 show sample 1-5 in both dry and saturated (oil) conditions. An increase in CT number is witnessed but it’s not as high as what we see in brine saturated sample. It can also be deduced that the samples are evenly saturated. The images of the rest of the samples can be seen in Appendix A.

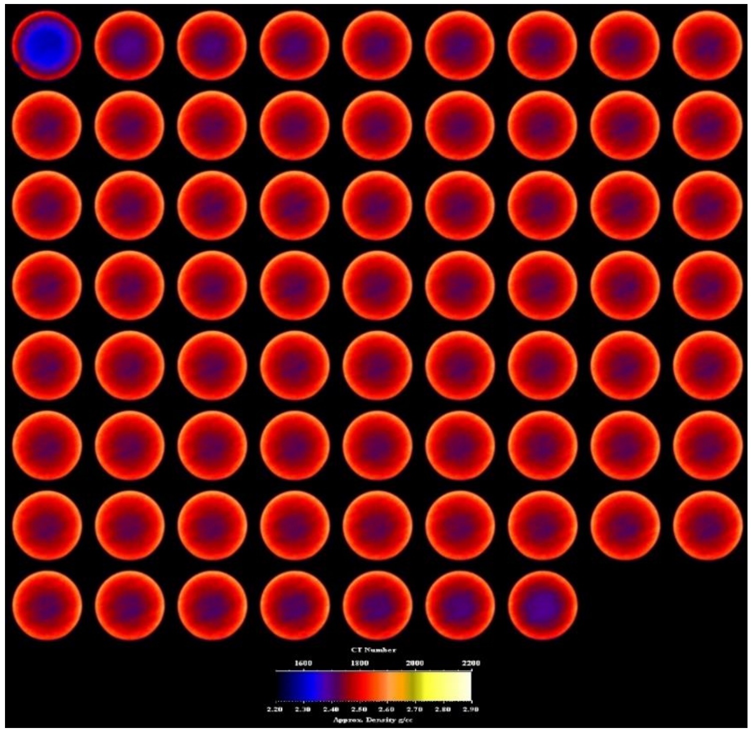

Figure 4.15 Sample 1-1 Dry

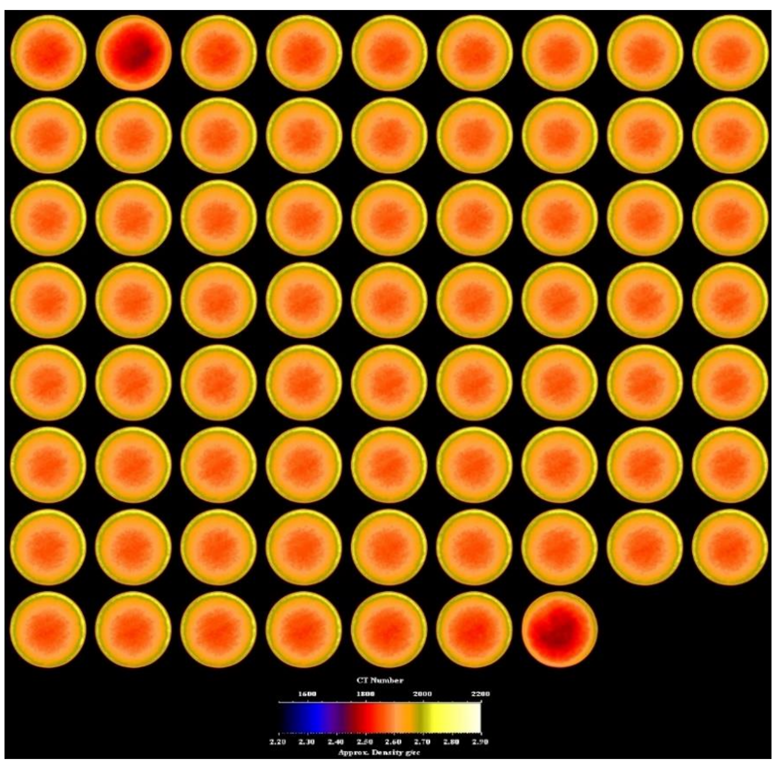

Figure 4.16 Sample 1-1 Brine Saturated

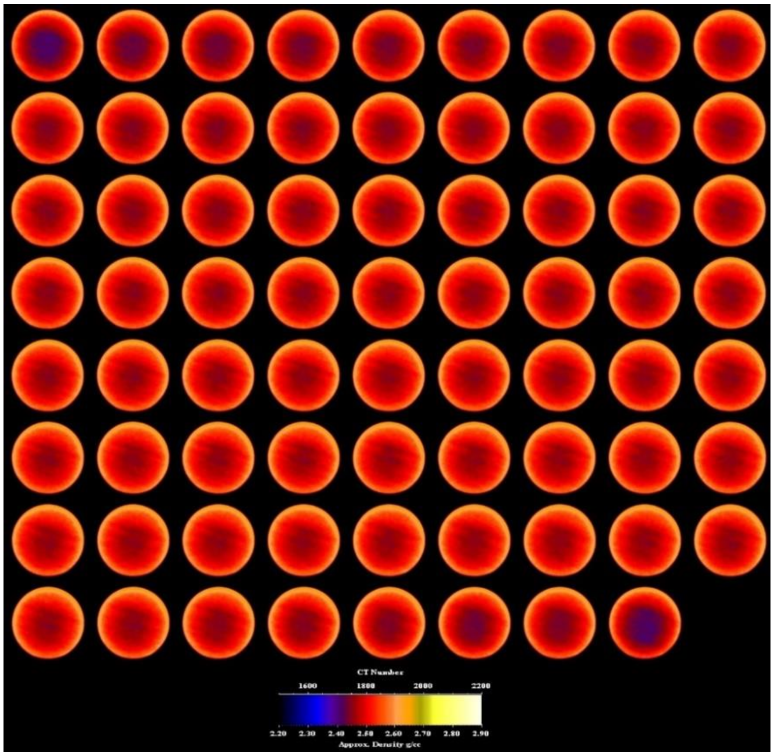

Figure 4.17 Sample 1-2 Dry

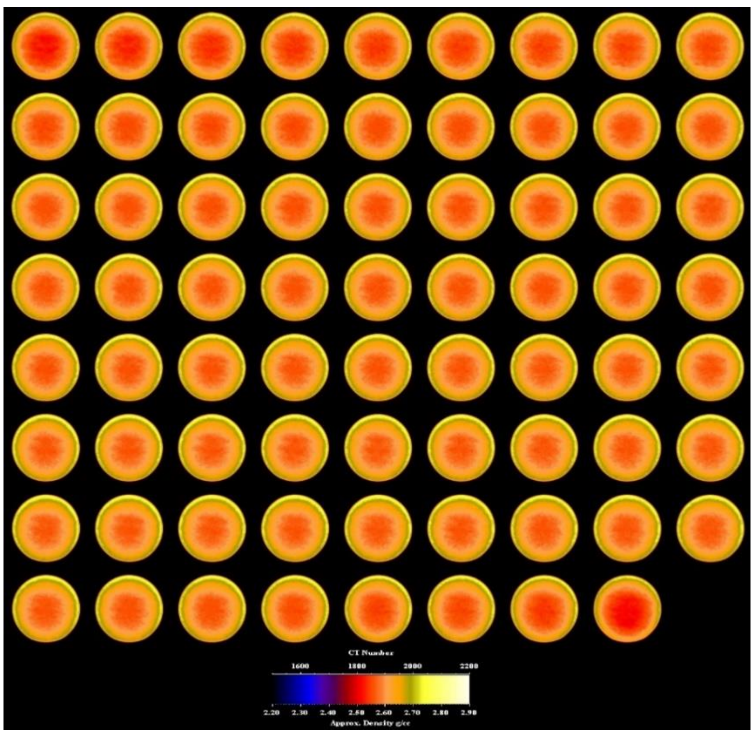

Figure 4.18 Sample 1-2 Oil Saturated

From the CT scans, an estimation of bulk density was calculated. The comparison of the dry and brine saturated sample is shown in Figure 4.19. The comparison for the dry and oil saturated sample is shown in Figure 4.20.

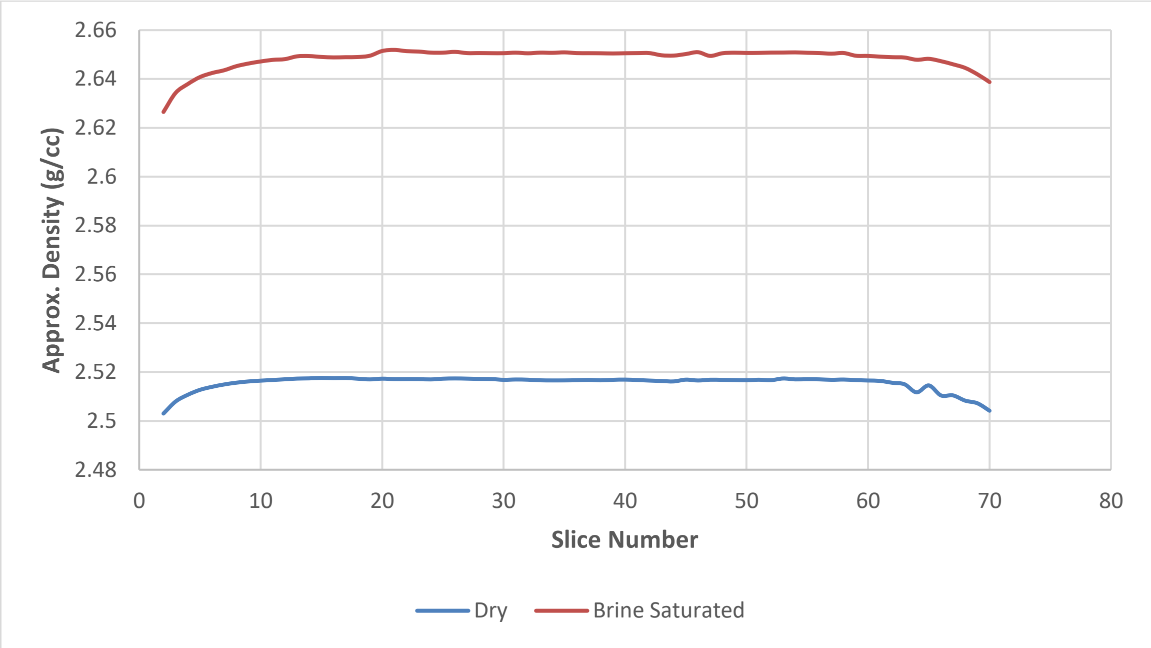

Figure 4.19 Approximate density comparison for dry and brine saturated sample (Sample 1-1)

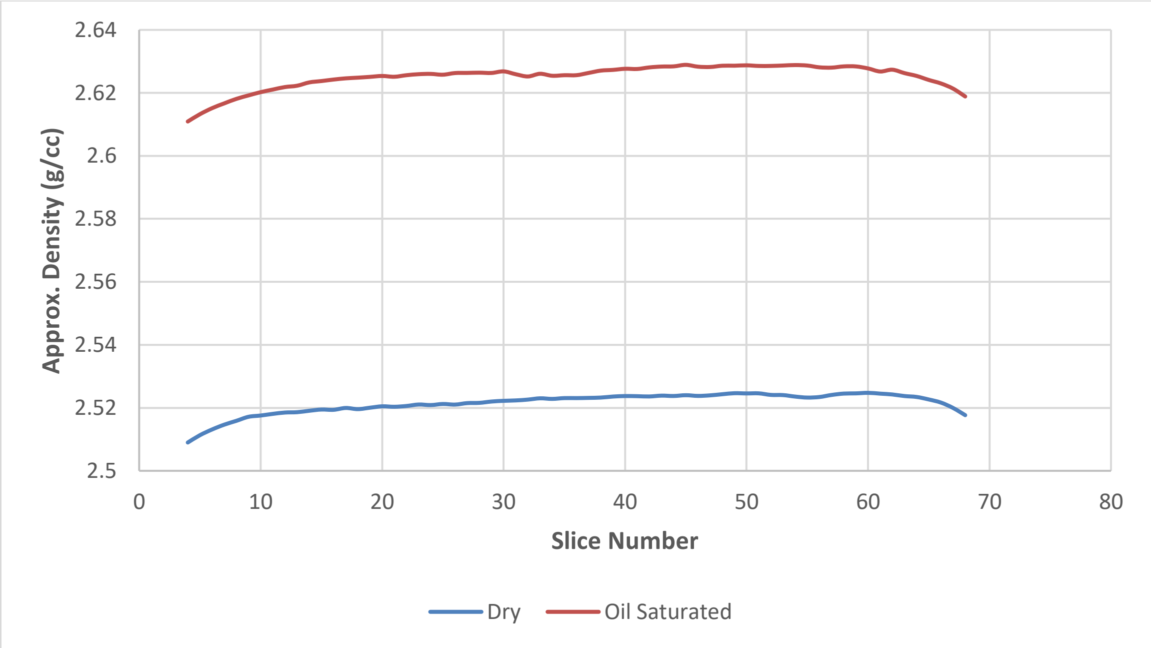

Figure 4.20 Approximate density comparison for dry and oil saturated sample (Sample 1-2)

The increase in the approximate density by saturating with brine was 0.13 g/cc. This increase in density can be converted to porosity by simply dividing by the density of the pore fluid (0.86 g/cc for oil and 1.03 for brine). The porosity for brine saturated sample was 12.6% and for the oil saturated sample was 12.1%. This comparison was done to confirm the complete oil saturation. The Approximate Density curves for the rest of the samples can be seen in Appendix A.

XRD

XRD for Scioto sandstone rocks was obtained from Mahmoud, M. A. et al., (2011). The XRD results show that it had 70% SiO_2 and about 22% clays and some traces of $CaCO_3$. The percentage concentration of each mineral is tabulated in Table 4.3.

Table 4.4 XRD Results

Mineral	**% Concentration**
Quartz (SiO_2)	70
Illite	18
Chlorite	4
Feldspar	2
Plagioclase	5
Calcite	Traces

4.2 Effect of Saturating Fluid on the Geomechanical Properties

Rock properties are affected by the fluids present in them. This is one of the cause of uncertainties in formation evaluation. Effect of saturating fluid on tight sandstone rocks is investigated in this section.

4.2.1 Ultrasonic test results

To understand the effect of saturating fluid on the geomechanical properties of tight sandstones, the dynamic properties of the dry were first measured at dry condition and later at saturated condition. Table 4.5 shows the cores and their saturating fluids.

Table 4.5 Cores with their saturating fluids

Sample Number	Saturating Fluid
1-1	Brine (3% KCl)
1-12	
1-13	
1-14	
1-2	Oil
1-5	
1-15	
1-16	

As mentioned previously, the ultrasonic test records the sonic waves with increasing and decreasing confining pressure at same intervals of time and same pressures. The dynamic properties of the samples were nearly identical for all the samples.

Figure 4.21 shows the change in Compressional Wave Velocity (V_p) with confining pressure. The blue circles represent the measured V_p with increasing confining pressure while the orange triangles represent V_p with decreasing confining pressure.

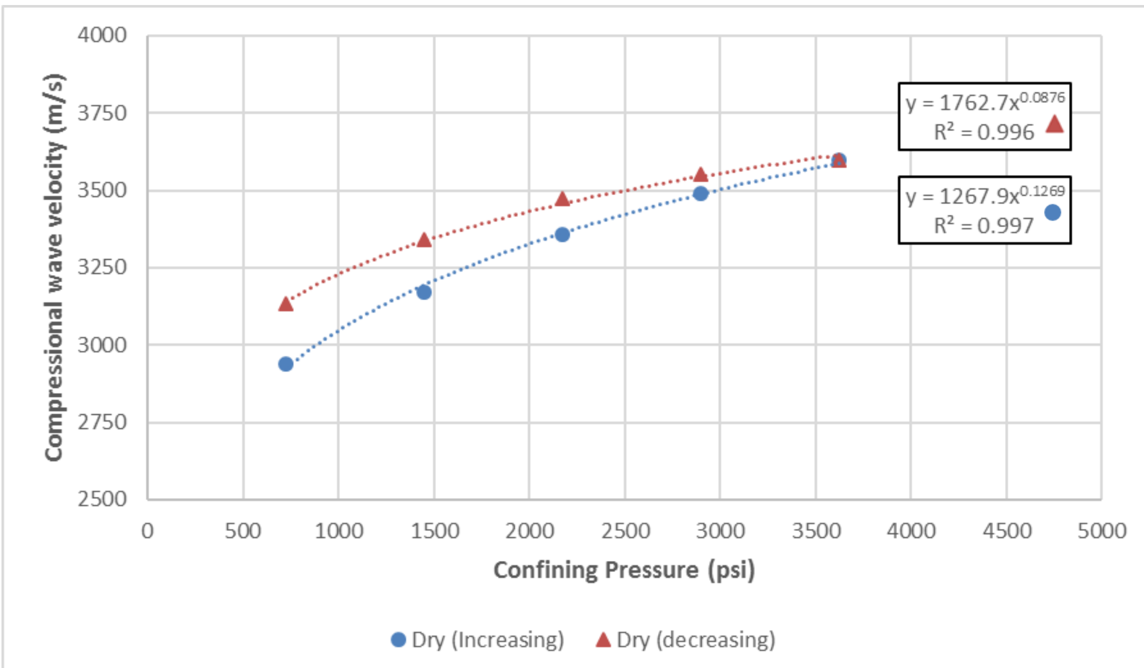

Figure 4.21 Compressional wave velocity vs Confining pressure (Sample 1-1)

As the confining pressure increases, the sample is squeezed and the grains are more tightly held together therefore, increasing the grain to grain contacts. This results in an increase of bulk density. V_p is directly proportional to bulk density, so as the confining pressure increases, V_p increases. A similar trend is witnessed for the V_s in Figure 4.22.

As explained previously, as the confining pressure increases, grains are held tightly together. This can potentially cause some reorientation of the grains and some minor deformation. As a result, when the confining pressure is released, the grains don't relax back to their original state and cause hysteresis.

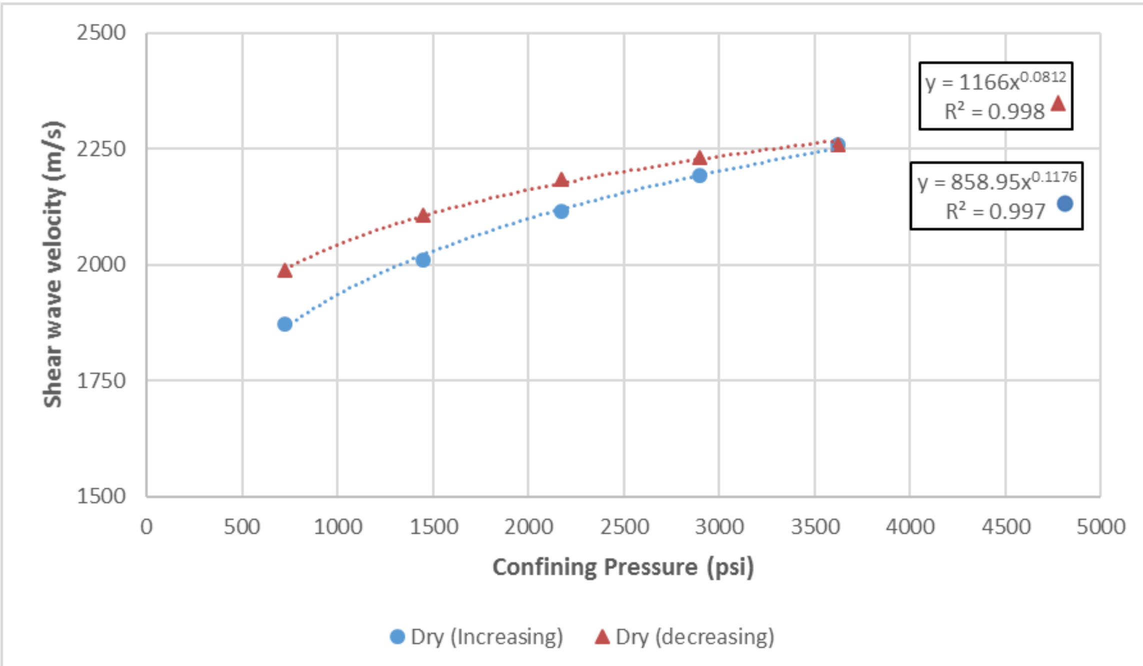

Figure 4.22 Shear wave velocity vs Confining pressure (Sample 1-1)

Figure 4.23 represents the effect of confining pressure on the Dynamic Young's Modulus (E_{dyn}). E_{dyn} increases when confining pressure is applied i.e., the rock tends to become less stiff as confining pressure increases. Hysteresis effect is clearly seen as the confining pressure is reduced. The Dynamic Poisson's ratio (ν_{dyn}) follows the same trend as seen in Figure 4.24.

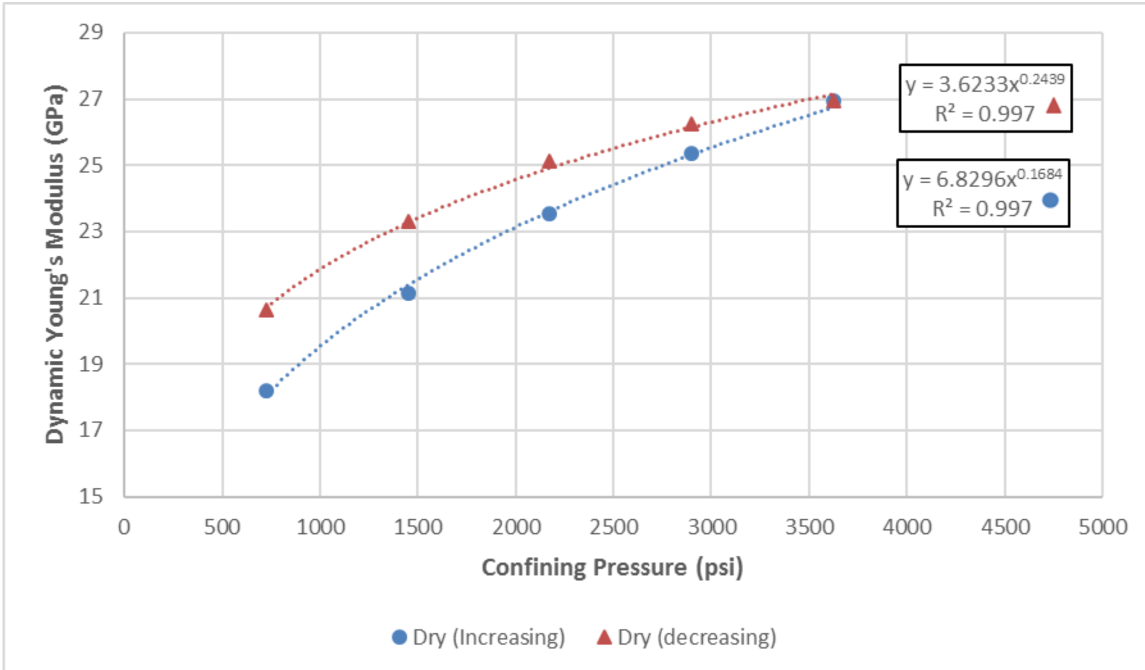

Figure 4.23 Young's Modulus vs Confining pressure (Sample 1-1)

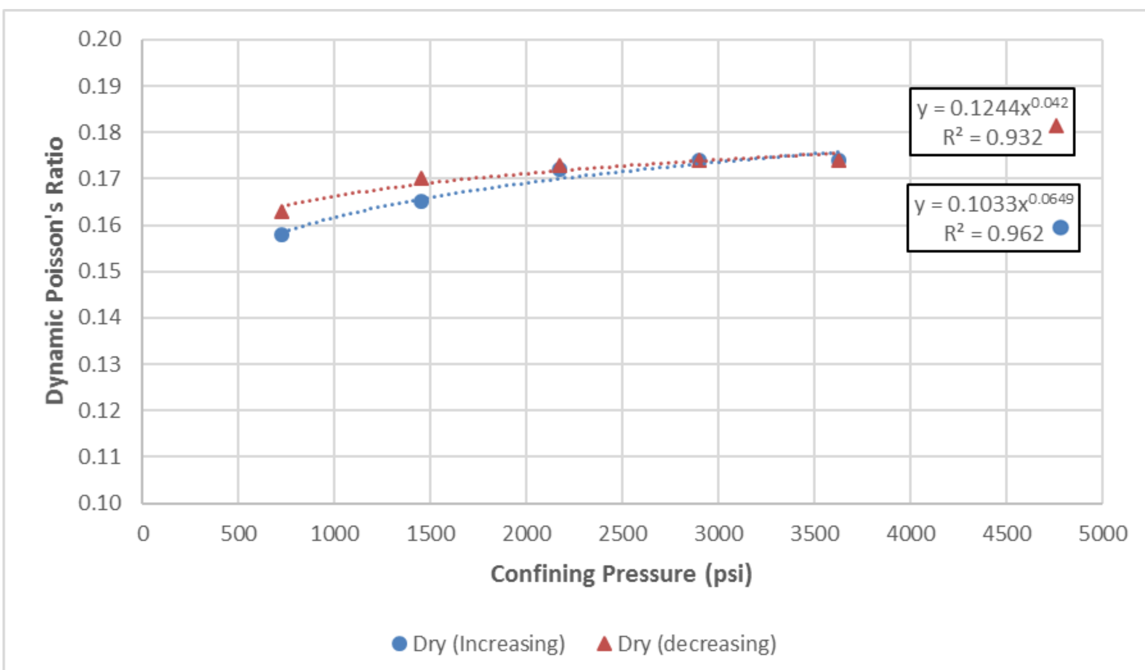

Figure 4.24 Poisson's Ratio vs Confining pressure (Sample 1-1)

Figures 4.25 to 4.28 represent the dynamic properties of sample 1-1 both in dry and brine saturated state. The V_p increases as the bulk density of the sample is increased. The V_s decreases due to the brine present in the pores. E_{dyn} for brine saturated sample is higher than dry at low confining pressure but the same at high confining pressure. This is due to the decreased V_s. 100% increase is seen in the ν_{dyn} due to the pores filled with brine. Brine is incompressible and this hinders the compaction of the rock, making the rock more incompressible as a whole. Due to this, hysteresis effect is also minimal.

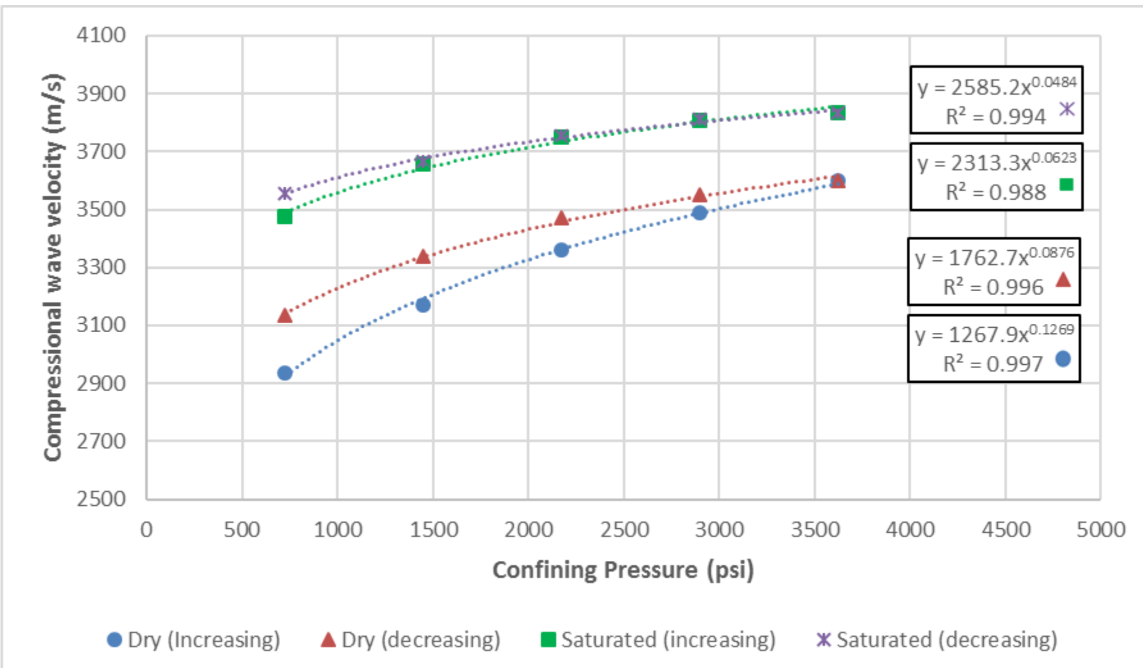

Figure 4.25 Comparison of Compressional wave velocity vs Confining Pressure, Dry vs Brine Saturated (Sample 1-1)

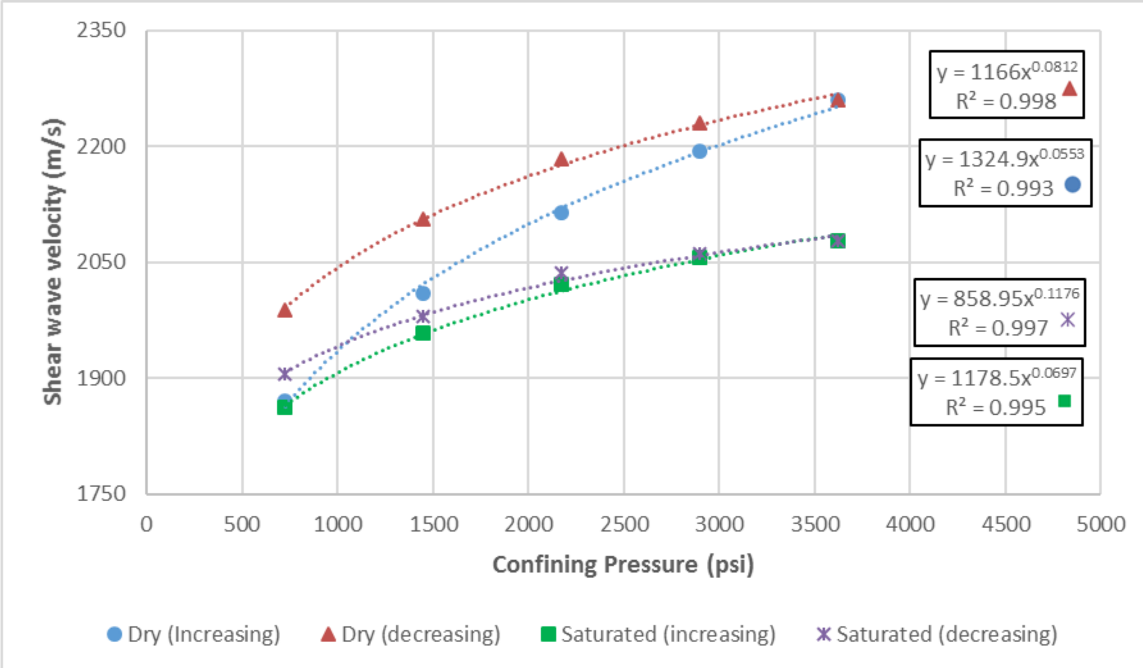

Figure 4.26 Comparison of Shear wave velocity vs Confining Pressure, Dry vs Brine Saturated

(Sample 1-1)

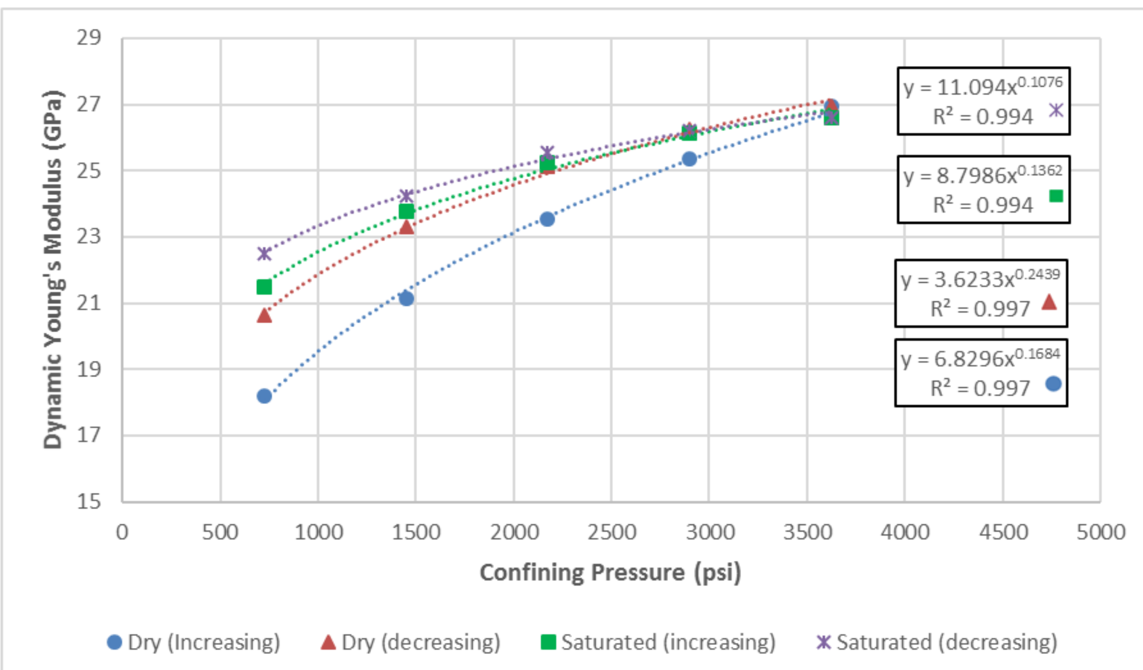

Figure 4.27 Comparison of Young's Modulus vs Confining Pressure, Dry vs Brine Saturated

(Sample 1-1)

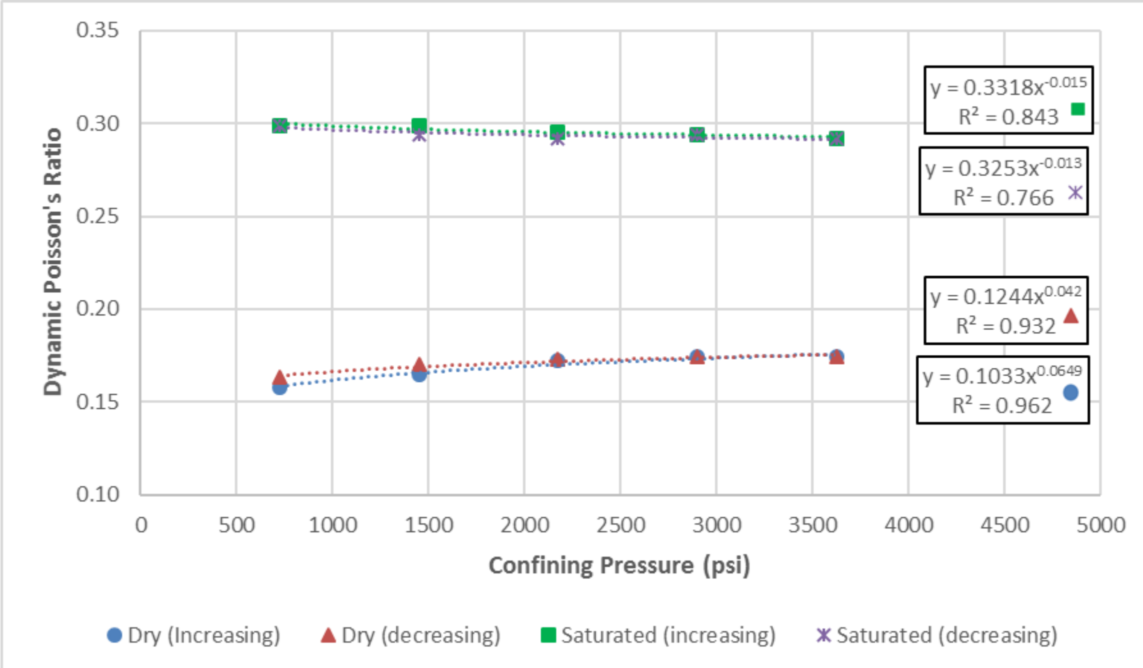

Figure 4.28 Comparison of Poisson's Ratio vs Confining Pressure, Dry vs Brine Saturated (Sample 1-1)

Figures 4.29 to 4.32 represent the comparison of the dynamic properties of an oil saturated sample with its dry state. The effect of hysteresis is higher than that of the brine saturated sample. This is due to the lower density of the oil. In the oil saturated sample, all the properties show an increase. The ν_{dyn} is decreased as the confining pressure is increased. The decrease in ν_{dyn} is much higher in the oil saturated sample than in the brine saturated sample. This is because of the slightly compressible nature of the oil and lower density.

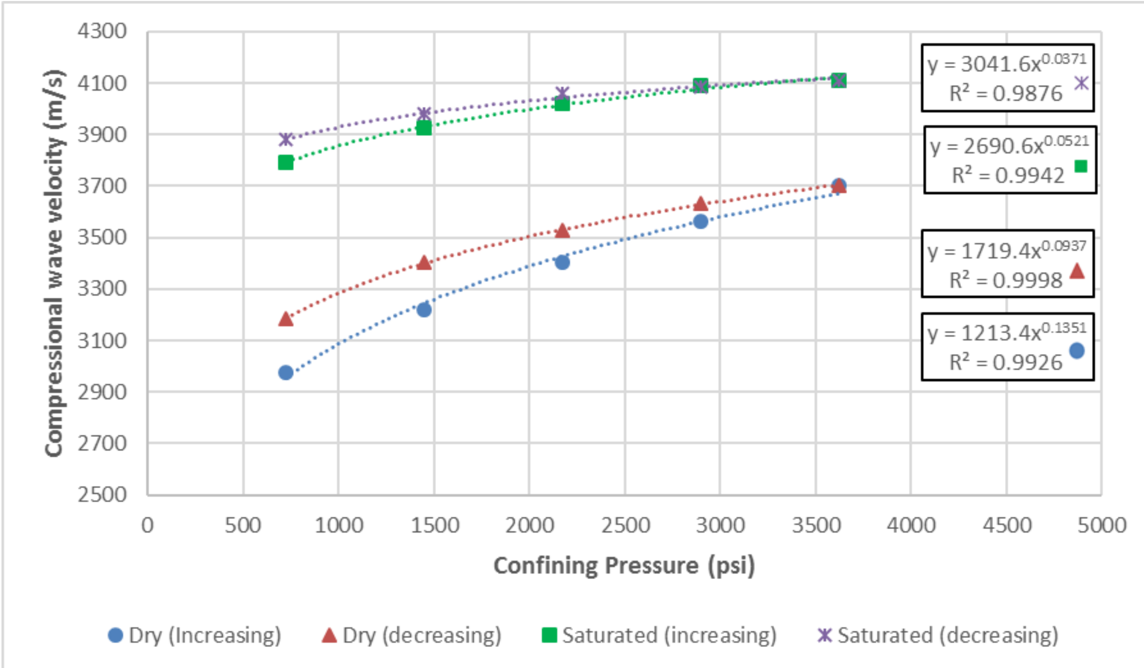

Figure 4.29 Comparison of Compressional wave velocity vs Confining Pressure, Dry vs Oil Saturated (Sample 1-2)

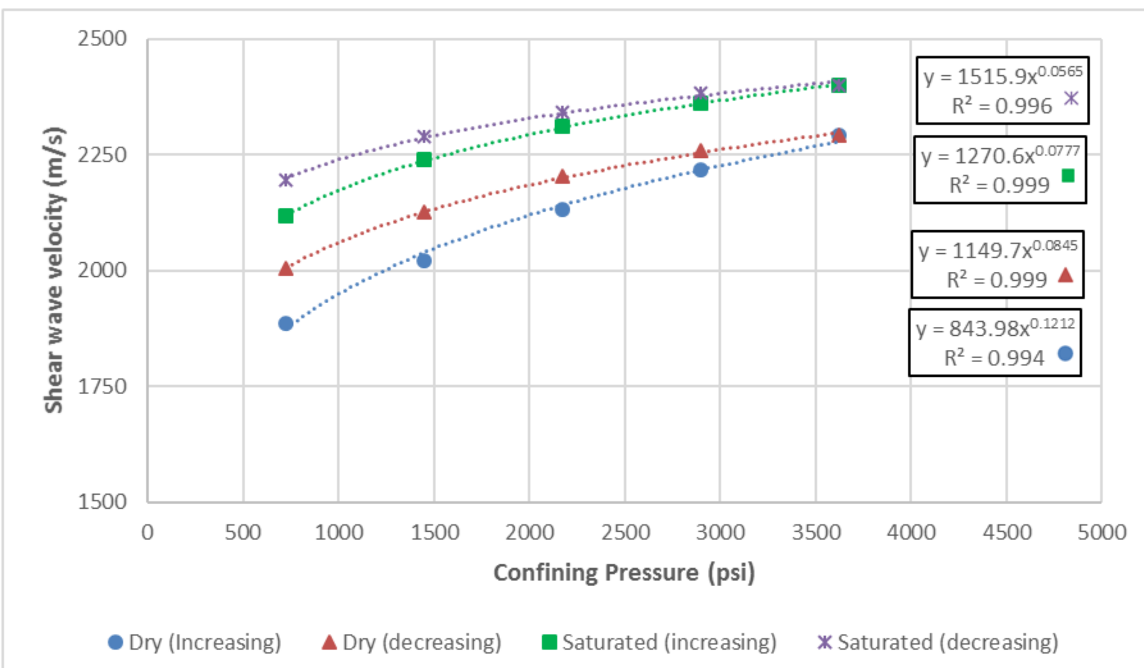

Figure 4.30 Comparison of Shear wave velocity vs Confining Pressure, Dry vs Oil Saturated (Sample 1-2)

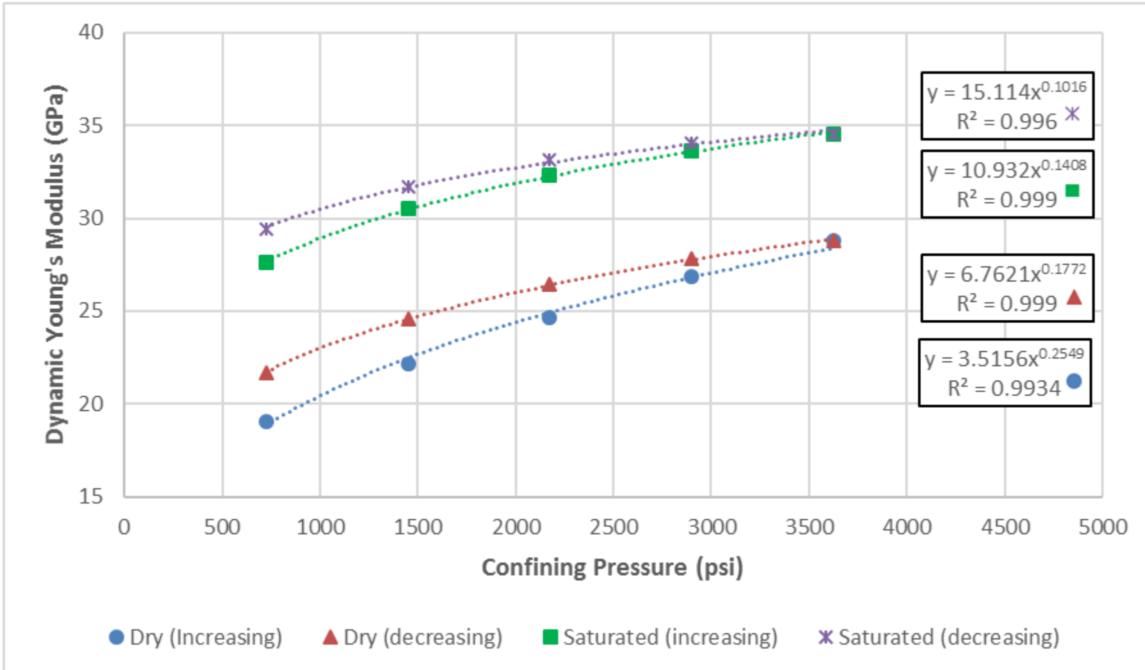

Figure 4.31 Comparison of Young's Modulus vs Confining Pressure, Dry vs Oil Saturated (Sample 1-2)

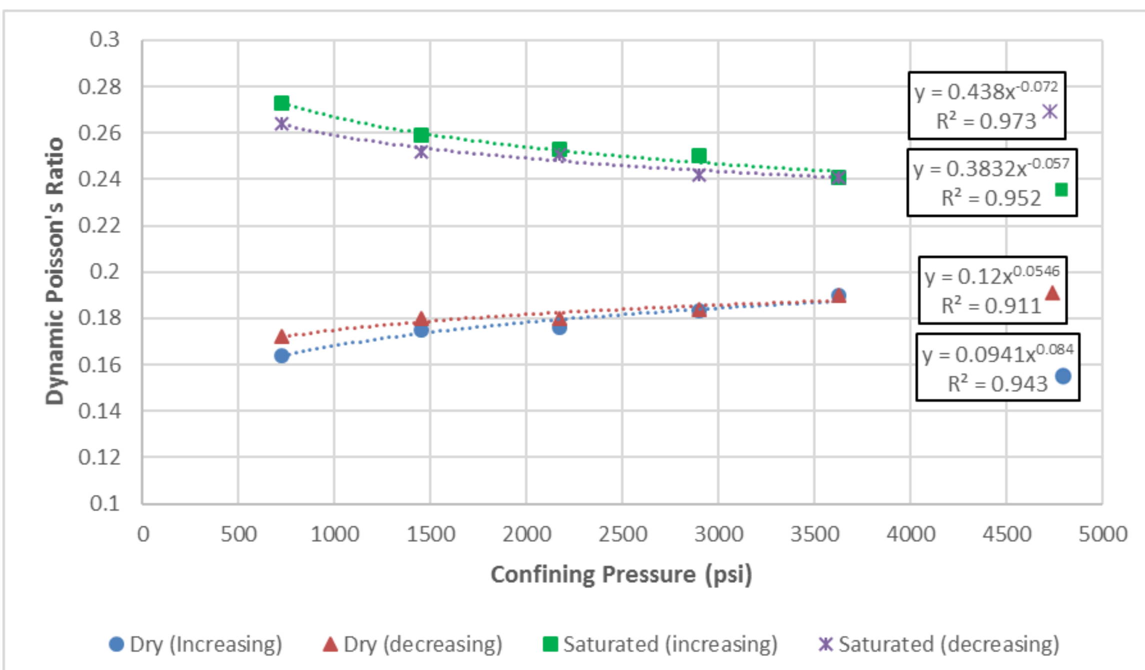

Figure 4.32 Comparison of Poisson's Ratio vs Confining Pressure, Dry vs Oil Saturated (Sample 1-2)

The effect of saturating fluid on the dynamic properties is summarized in Table 4.6. Regardless of the type of saturating fluid, all the properties increased except V_s which decreased for brine saturated sample. Also, the properties are much more effected in lower confining pressures.

Table 4.6 Effect of Saturating Fluid on the Dynamic rock properties

Property	**Percentage effect on the dynamic properties**			
	Low Confining Pressure		**High Confining Pressure**	
	Oil Sat.	**Brine Sat.**	**Oil Sat.**	**Brine Sat.**
$\boldsymbol{V_p}$	+ 24%	+ 20%	+ 10%	+ 8%
$\boldsymbol{V_s}$	+ 10%	**(-) 4%**	+ 2%	**(-) 8%**
$\boldsymbol{E_{dyn}}$	+ 39%	+ 21%	+ 16%	+ 1%
$\boldsymbol{\nu_{dyn}}$	+ 72%	+ 144%	+ 38%	+ 87%

The dynamic properties of other samples are displayed in Appendix B.

4.2.2 Unconfined Compressive Strength (UCS) test

UCS were performed in order to determine the change in strength and elastic properties due to saturating fluid. 3 samples were tested with different saturating fluids. The first sample was dry, followed by brine saturated and lastly oil saturated.

Dry Samples

1. Sample 1-11

Figure 4.33 shows the axial deformation with respect to the axial stress applied on it. This graph is referred to as the stress strain curve. Since this is an unconfined test, the initial behavior of the rock is seen to be less than ideal. The curve increases linearly after 4500 psi of axial stress is applied. The failure is at the highest point of the curve and the value at this point is known as the UCS. The UCS for this test was 11,457 psi. The slope at 50% of the UCS gives the static Young's Modulus (E_{static}) (Equation 3.4) which was $1.40 * 10^6$ psi or 9.65 GPa.

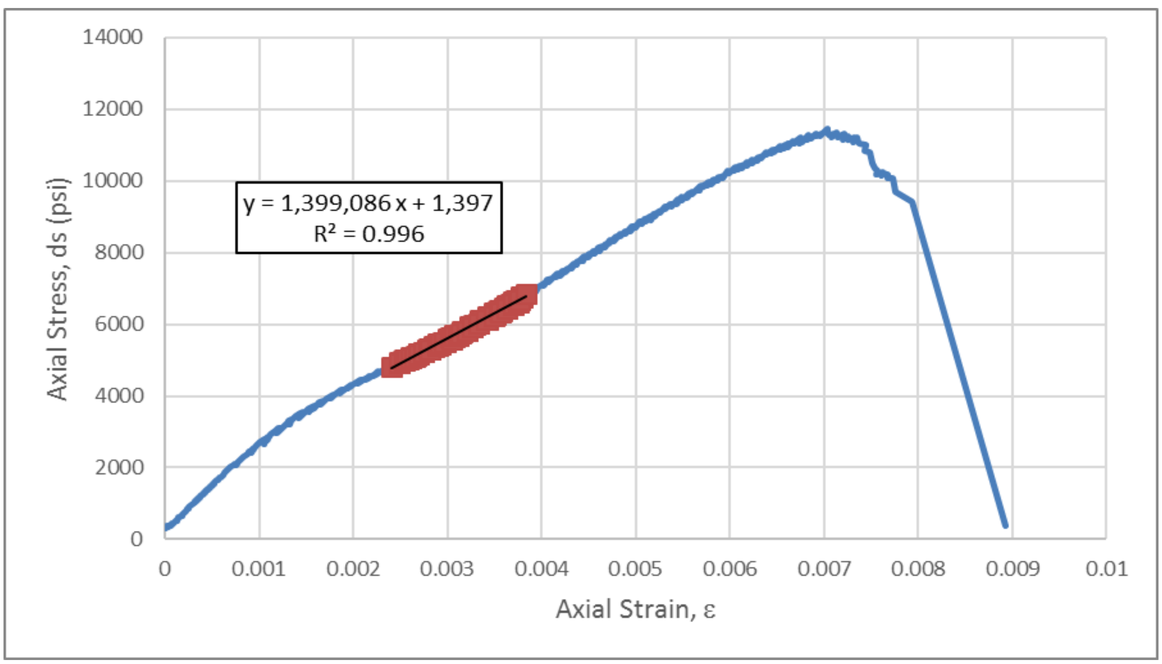

Figure 4.33 Axial Stress vs Axial Strain (Dry, Sample 1-11)

Figure 4.34 Failure pattern of Dry rock (Sample 1-11)

Figure 4.34 shows the failure pattern. Given the nature of the sample is horizontal, the shear failure between the bedding can be clearly seen.

2. Sample 1-7

As seen from Figure 4.35, the stress strain curve looks to be ideal and hence this sample will be considered for further analysis. The UCS was found to be 11,600 psi. The static Young's Modulus was $1.95 * 10^6$ psi or 13.43 GPa. The failure profile is shown in Figure 4.36.

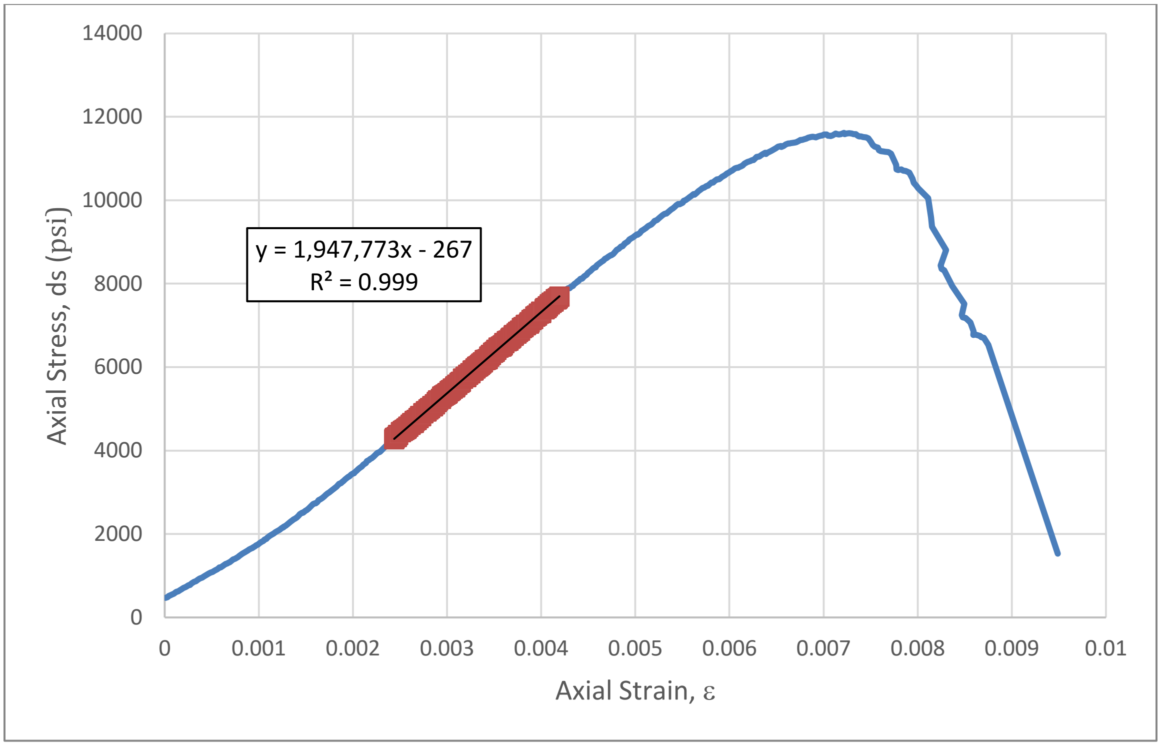

Figure 4.35 Axial Stress vs Axial Strain (Dry, Sample 1-7)

Figure 4.36 Failure pattern of Dry rock (Sample 1-7)

Brine Saturated Samples

1. Sample 1-14

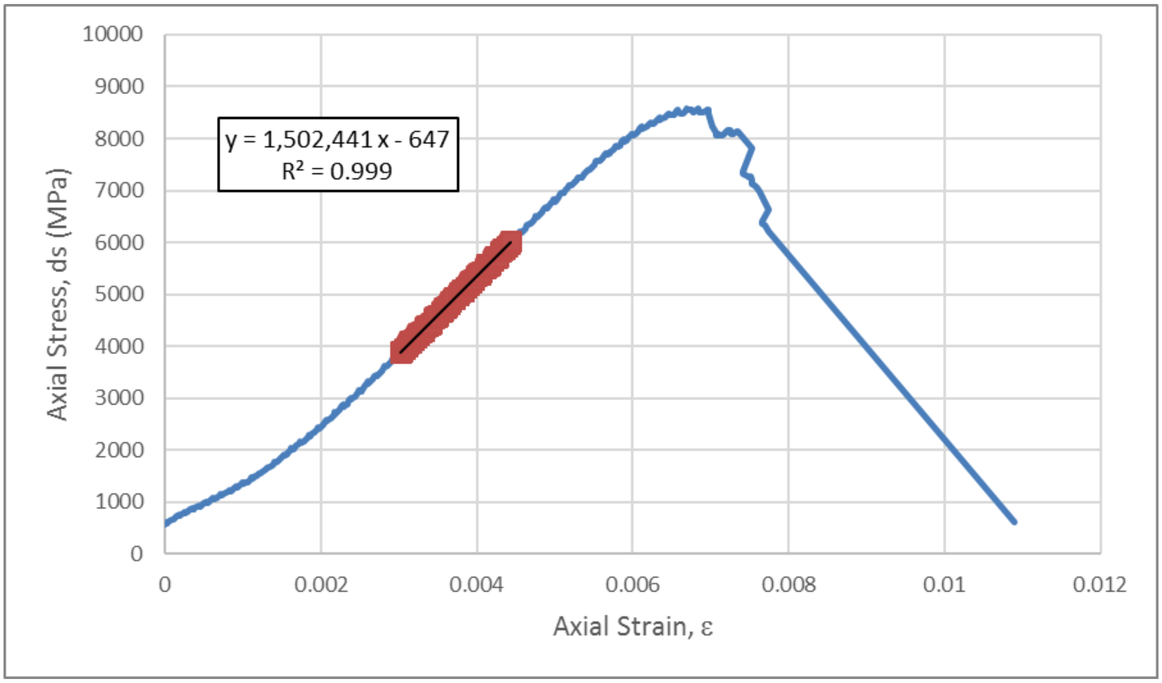

Figure 4.37 Axial Stress vs Axial Strain (Brine Saturated, Sample 1-14)

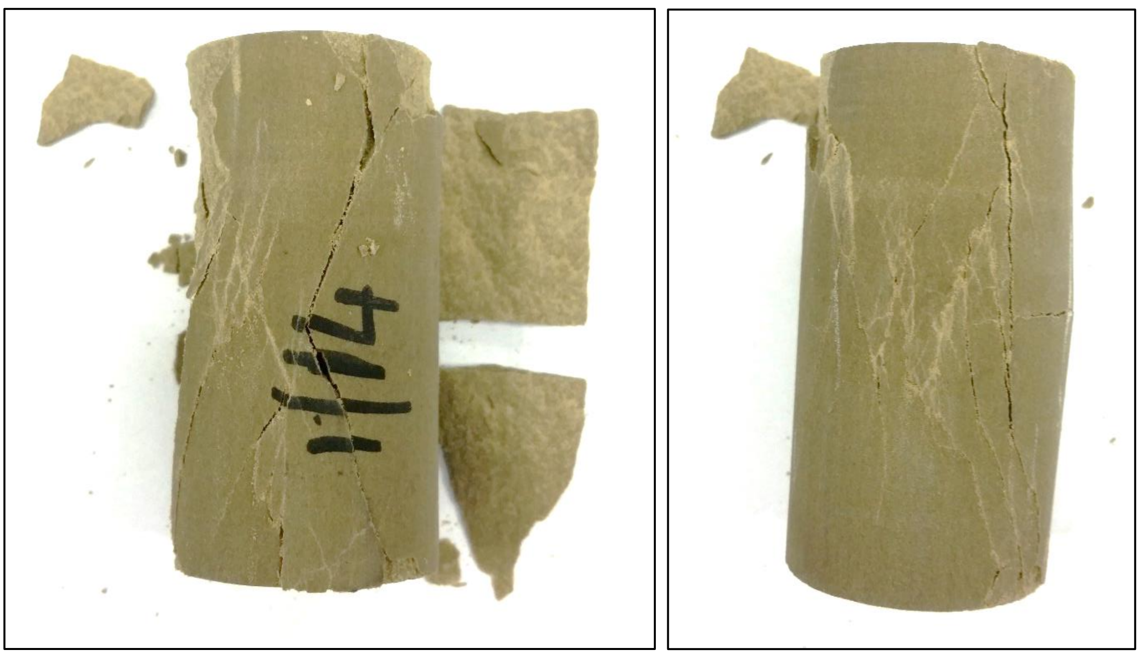

Figure 4.38 Failure pattern of Brine saturated rock (Sample 1-14)

Axial deformation with respect to the axial stress for sample 1-14 is shown in Figure 4.37. The UCS was 8,573 psi and the E_{static} = $1.50 * 10^6$ psi or 10.36 GPa. Figure 4.38 shows the failure pattern.

2. Sample 1-1

Figure 4.39 shows the stress train curve for sample 1-1. The UCS was 8,351 psi while the static Young's Modulus was $1.47 * 10^6$ or 10.2 GPa. The failure pattern is shown in Figure 4.40.

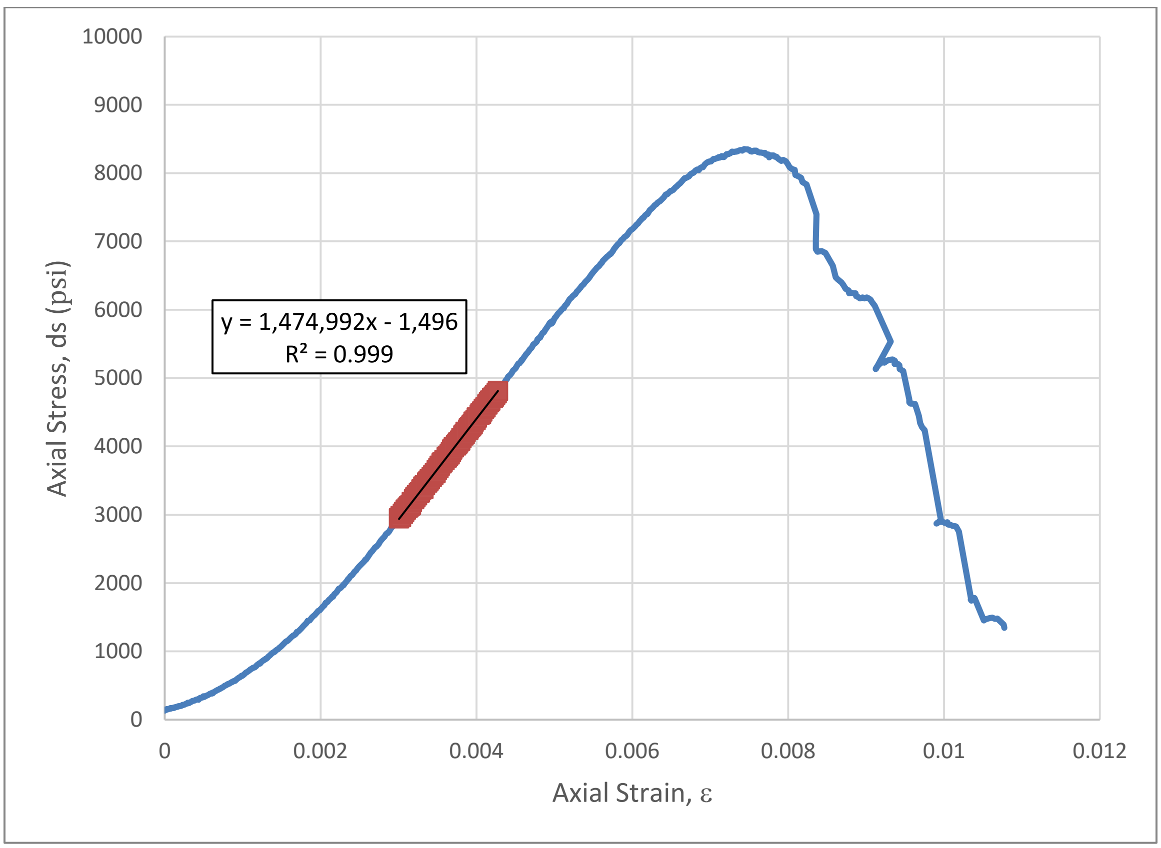

Figure 4.39 Axial Stress vs Axial Strain (Brine Saturated, Sample 1-1)

Figure 4.40 Failure pattern of Brine saturated rock (Sample 1-1)

Oil Saturated Samples

1. Sample 1-16

Figure 4.41 shows the axial deformation with respect to the axial stress applied on it. The UCS was 10,448 psi and the E_{static} is $1.68 * 10^6$ psi or 11.57 GPa. Figure 4.42 shows the failure pattern.

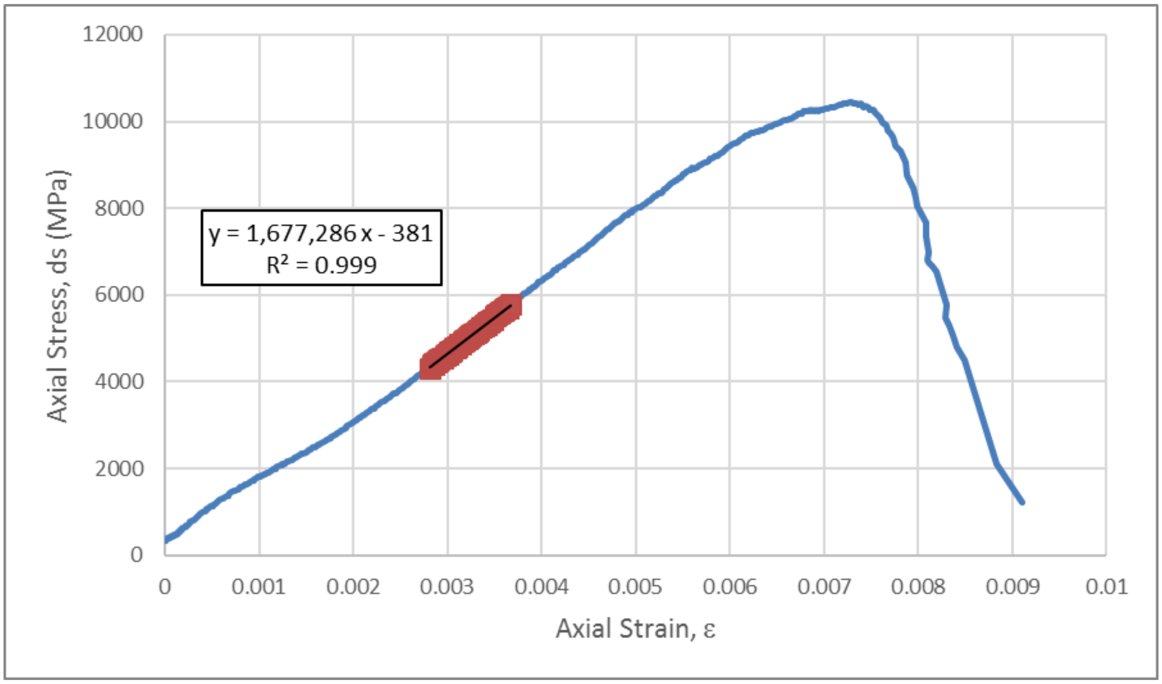

Figure 4.41 Axial Stress vs Axial Strain (Oil Saturated, Sample 1-16)

Figure 4.42 Failure pattern of Oil saturated rock (Sample 1-16)

2. Sample 1-5

Figure 4.43 shows the stress strain curve and Figure 4.44 shows the failure profile. The UCS was 10,357 psi and the static Young's Modulus was $1.74 * 10^6$ psi or 12 GPa.

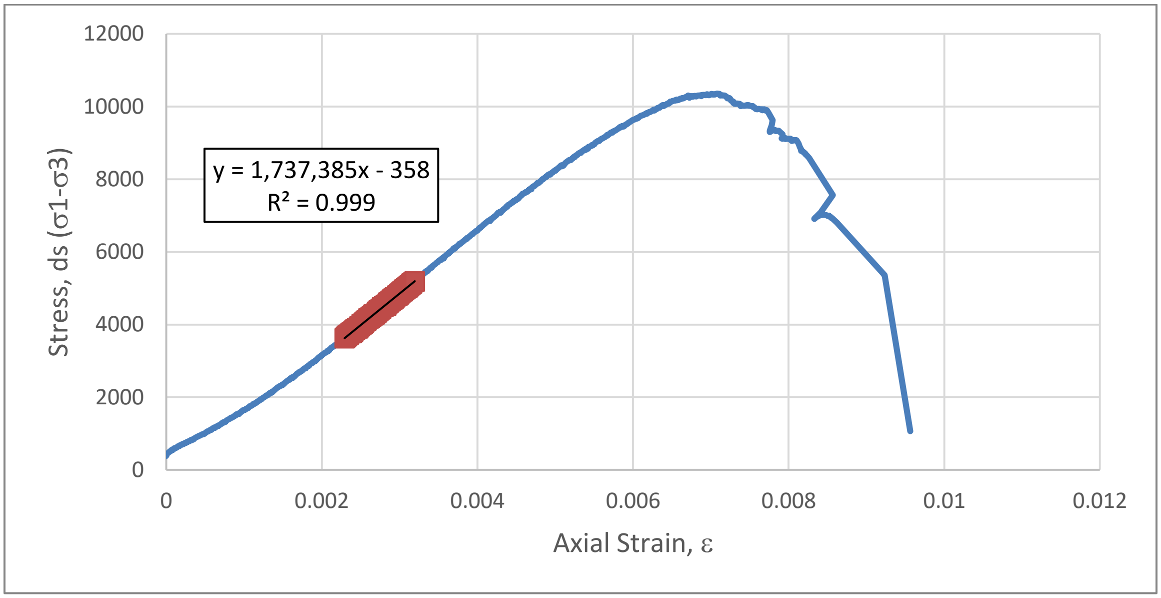

Figure 4.43 Axial Stress vs Axial Strain (Oil Saturated, Sample 1-5)

Figure 4.44 Failure pattern of Oil saturated rock (Sample 1-5)

The results of the UCS tests are summarized in Table 4.7 and graphically depicted in Figure 4.47. The UCS for the dry sample is the highest, followed by the oil saturated sample and then the brine saturated sample (Figure 4.45). The decrease in UCS in the oil saturated sample was 10% and brine sample was 25%. The decrease in E_{static} in the oil saturated sample was 13% and brine sample was 23% (Table 4.8). The decrease in the UCS is shown as a function of increasing bulk density in Figure 4.46. It is important to note that the increase in the bulk density is caused by fluid density. As the fluid density increases, the UCS decreases.

The degradation in the UCS and the E_{static} is in agreement with the literature. The decrease in UCS is observed due to the physico-chemical interactions between the grains of the sample and the fluid in the pores and the effective stress created by the fluid (Duda M. et al., 2012).

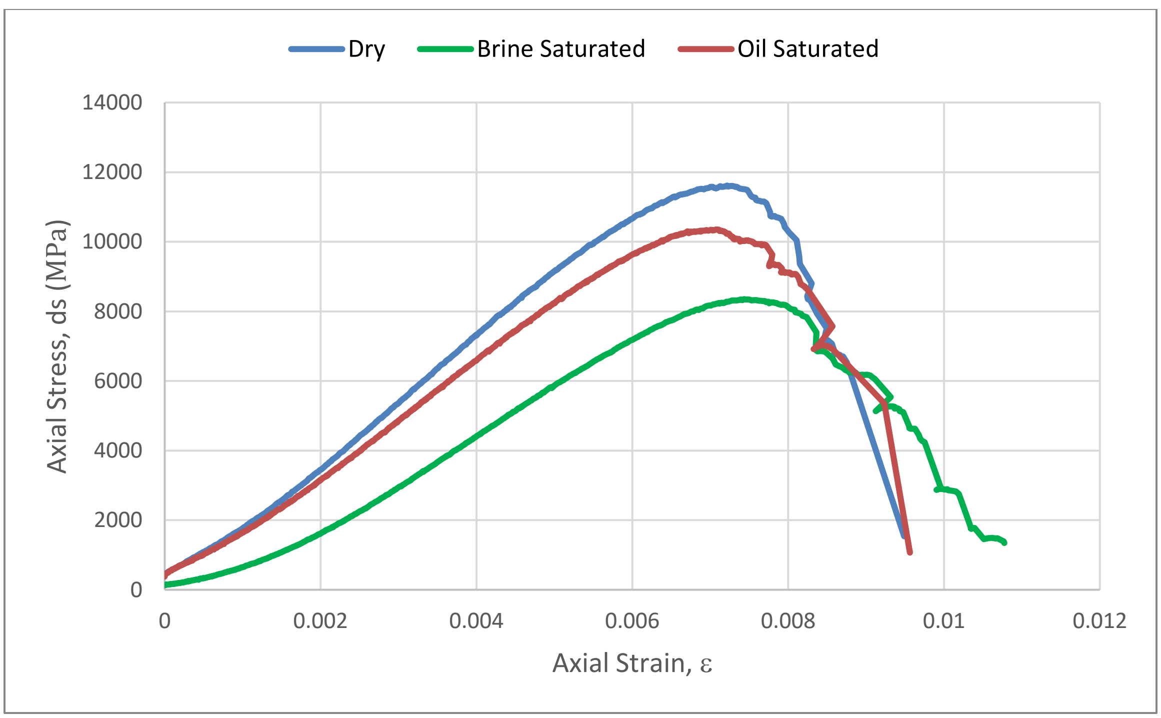

Figure 4.45 Effect of fluid saturation on UCS

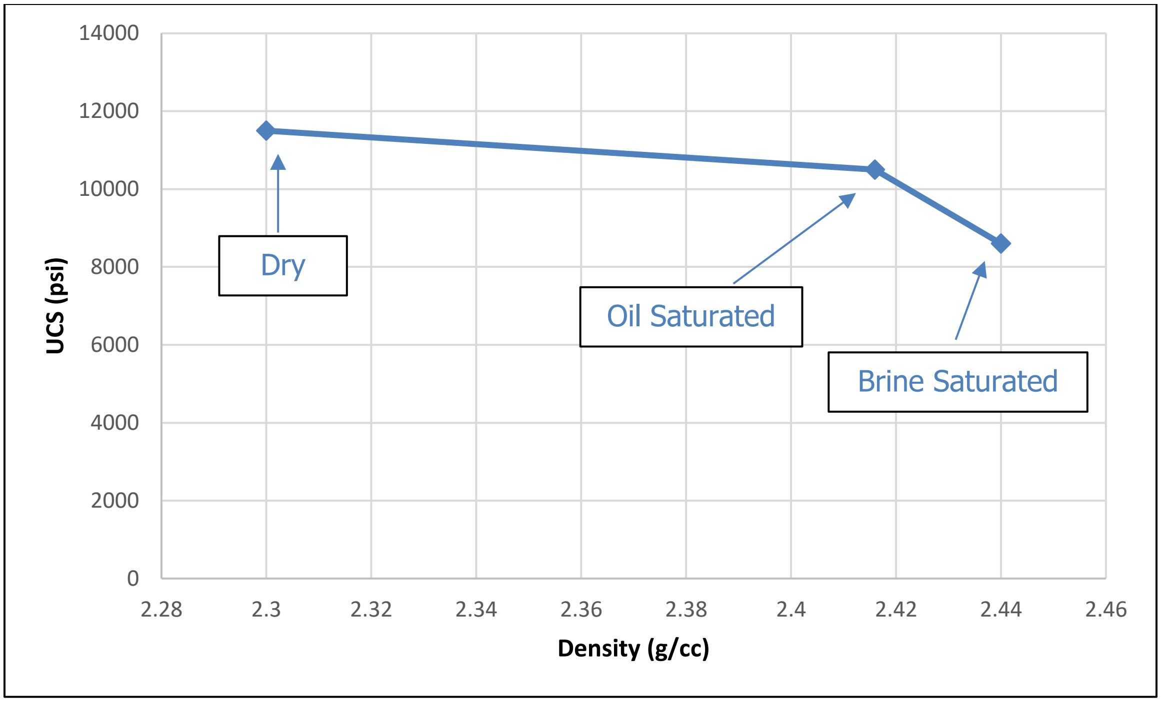

Figure 4.46 UCS comparison with increasing bulk density

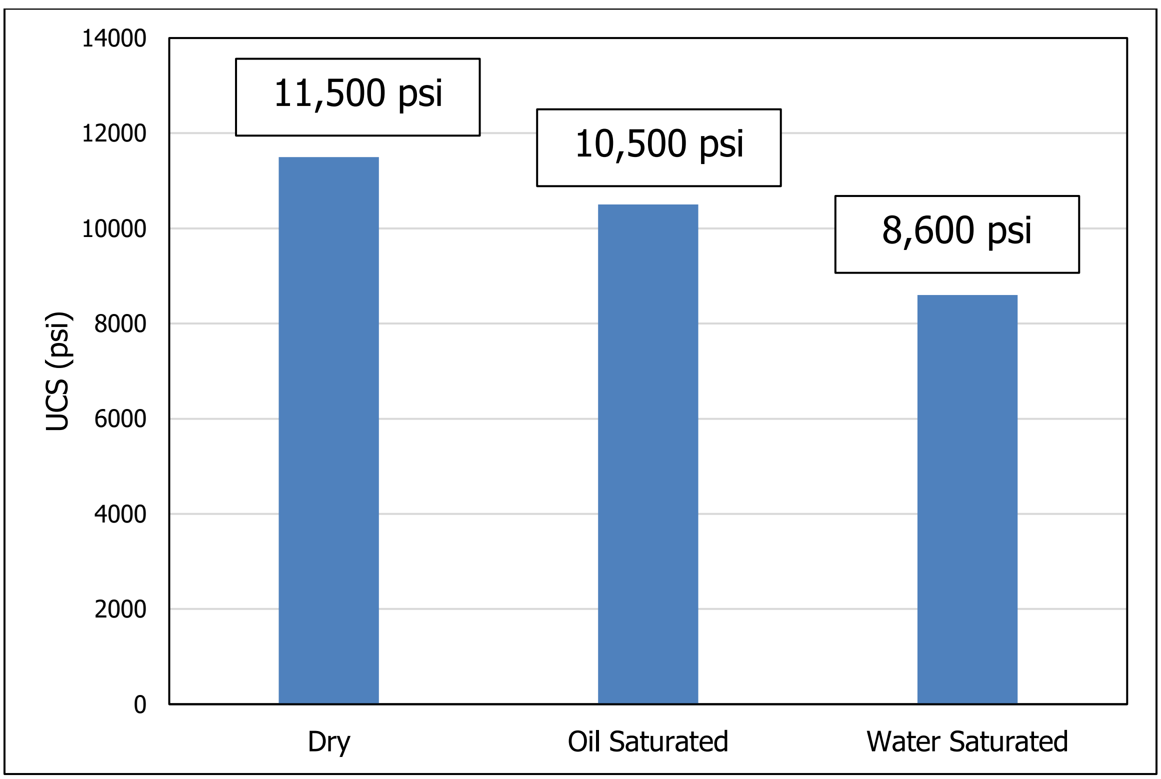

Figure 4.47 Effect of saturating fluid on the UCS

Table 4.7 Summary of the UCS tests

Property	Dry	Oil Sat.	Brine Sat.
UCS (psi)	11,530	10,400	8,500
E_{static} **(10^6psi)**	1.95	1.7	1.50

Table 4.8 Effect of Saturating Fluid on the Static Properties

Property	Percentage effect on the properties	
	Oil Saturated	**Brine Saturated**
UCS	(-) 10%	(-) 25%
E_{static}	(-) 13%	(-) 23%

4.3 Brazilian Tensile Test

Brazilian tensile tests were performed on a total of 11 samples out of which 3 were dry, 4 were saturated with oil and 4 samples saturated with brine.

4.3.1 Dry samples

a. Sample 17-A

The maximum load applied to the disc before undergoing tensile failure was at 2673 N. Figure 4.48 shows the loading profile for sample 17-A and Figure 4.51 shows the failure profile of the sample.

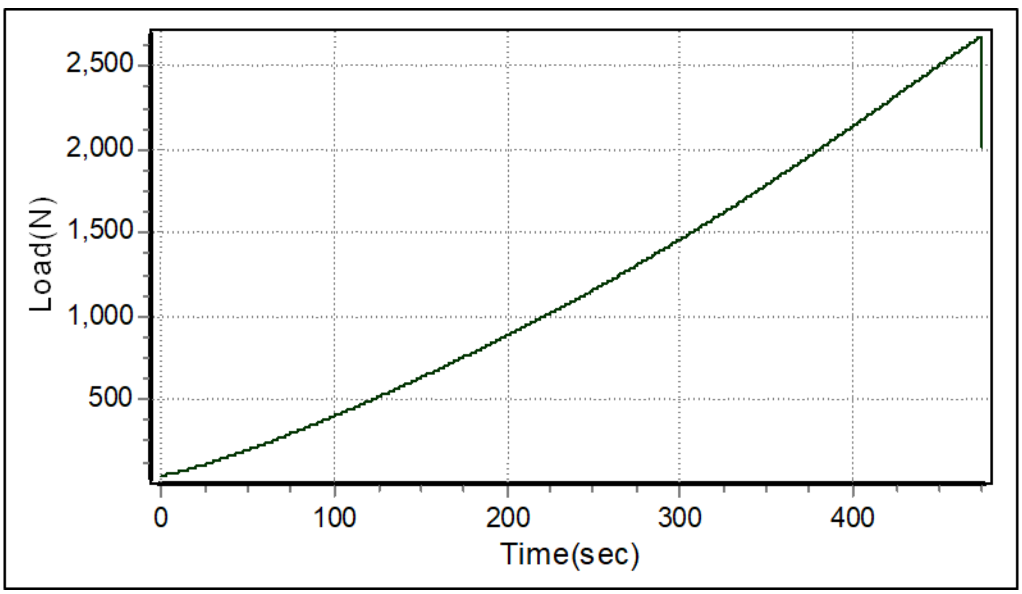

Figure 4.48 Computer generated Load profile (Sample 17-A, Dry)

b. Sample 17-B

Figure 4.49 shows the Brazilian Test for sample 17-B. The sample failed at 2287.8 N. Figure 4.51 shows the failure profile of the sample

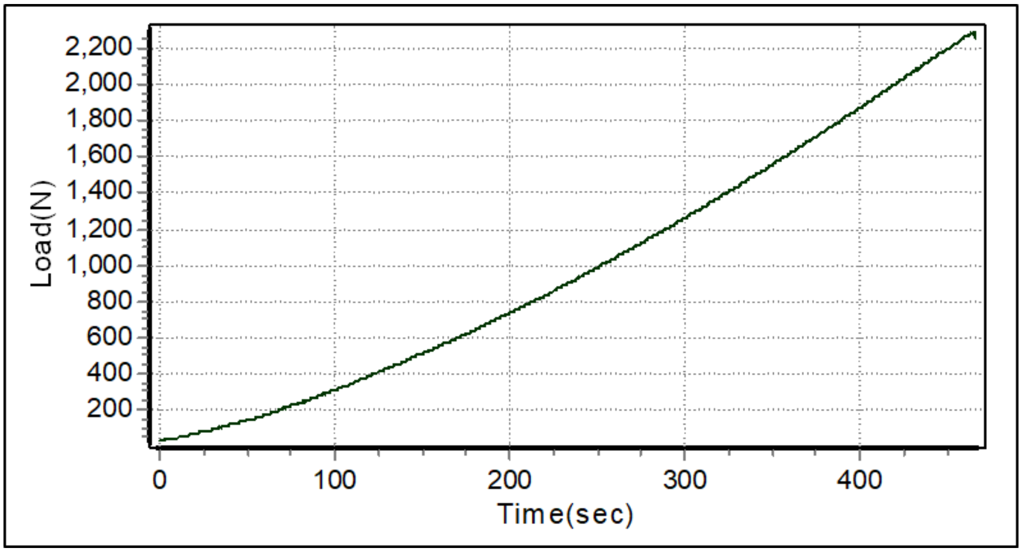

Figure 4.49 Computer generated Load profile (Sample 17-B, Dry)

c. Sample 1-17C

The tensile failure was achieved at 2637 N (Figure 4.50). The failure profile is shown in figure 4.51.

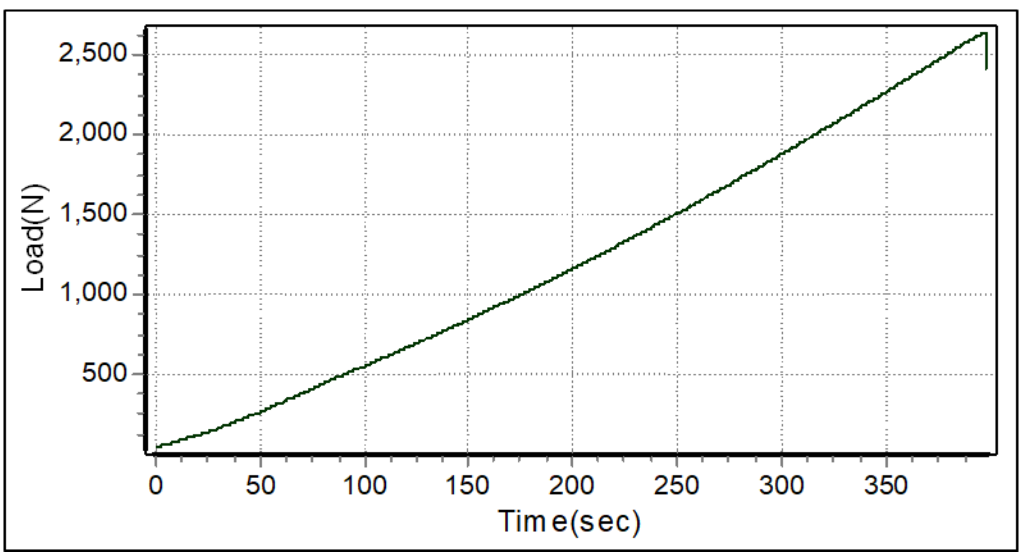

Figure 4.50 Computer generated Load profile (Sample 17-C, Dry)

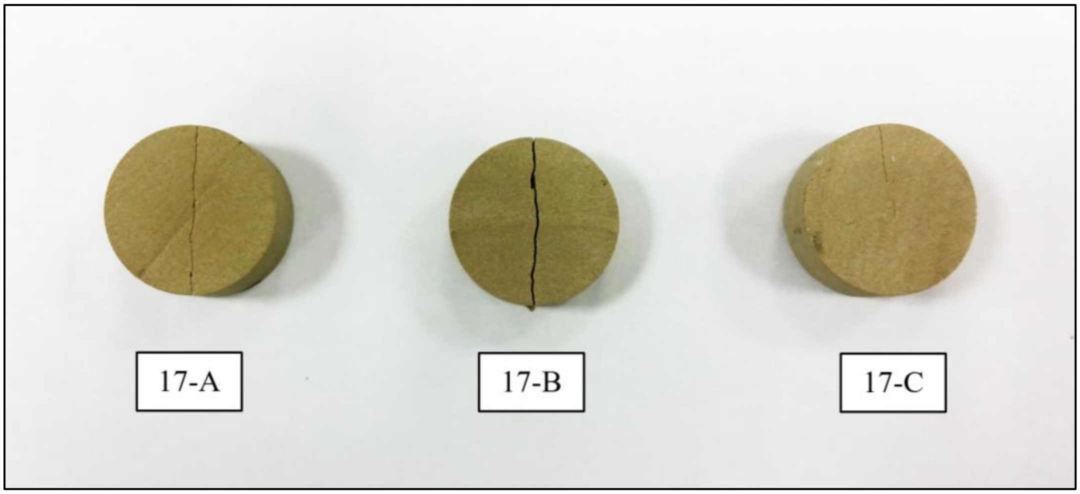

Figure 4.51 Tensile Failure Profile (Sample 1-A,B,C, Dry)

4.3.2 Brine Saturated

a. Sample 19-A

Figure 4.52 shows the Brazilian Test for sample 19-A. The tensile failure was seen at 1523.4 N. Figure 4.56 shows the failure profile of the sample.

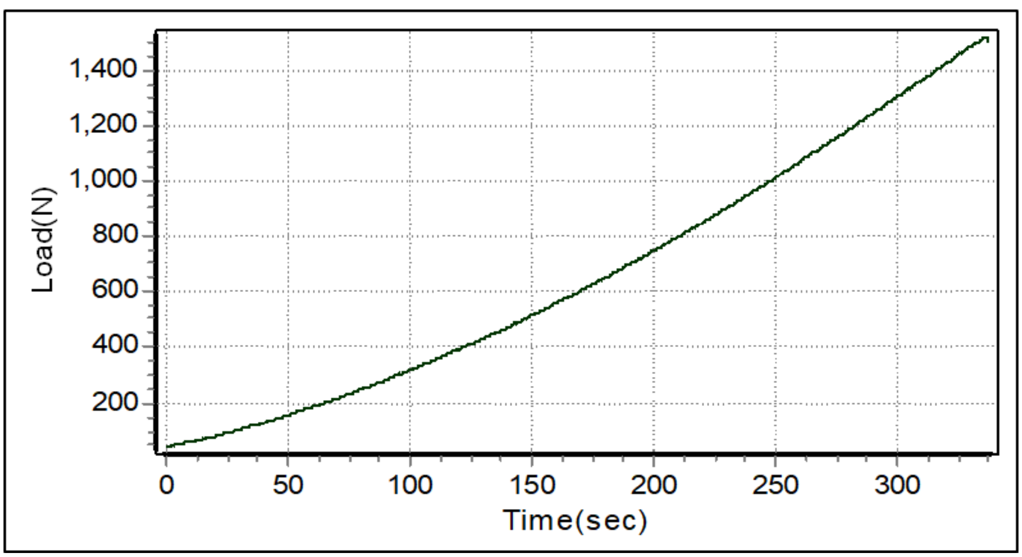

Figure 4.52 Computer generated Load profile (Sample 19-A, Brine Saturated)

b. Sample 19-B

The maximum tensile load of sample 19-B was 1381.8 N as seen in Figure 4.53. Figure 4.56 shows the failure profile of the sample.

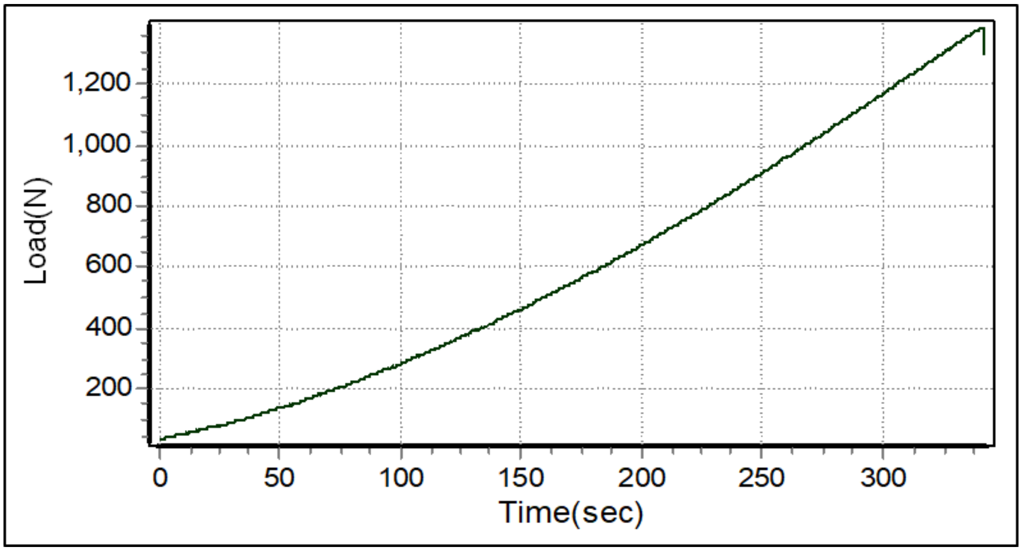

Figure 4.53 Computer generated Load profile (Sample 19-B, Brine Saturated)

c. Sample 19-C

The maximum load applied to the disc before undergoing tensile failure was 1616.4 N. Figure 4.54 shows the Brazilian Test for sample 19-C and Figure 4.56 shows the failure profile.

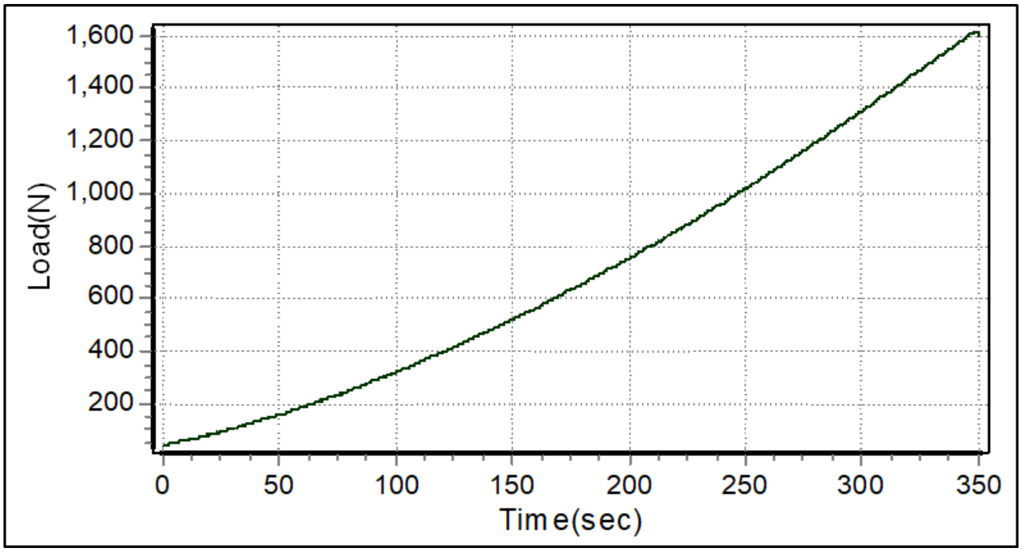

Figure 4.54 Computer generated Load profile (Sample 19-C, Brine Saturated)

d. Sample 19-D

The tensile failure of sample 19-D was achieved at 1606.2 N (Figure 4.55). the failure profile is shown in Figure 4.56.

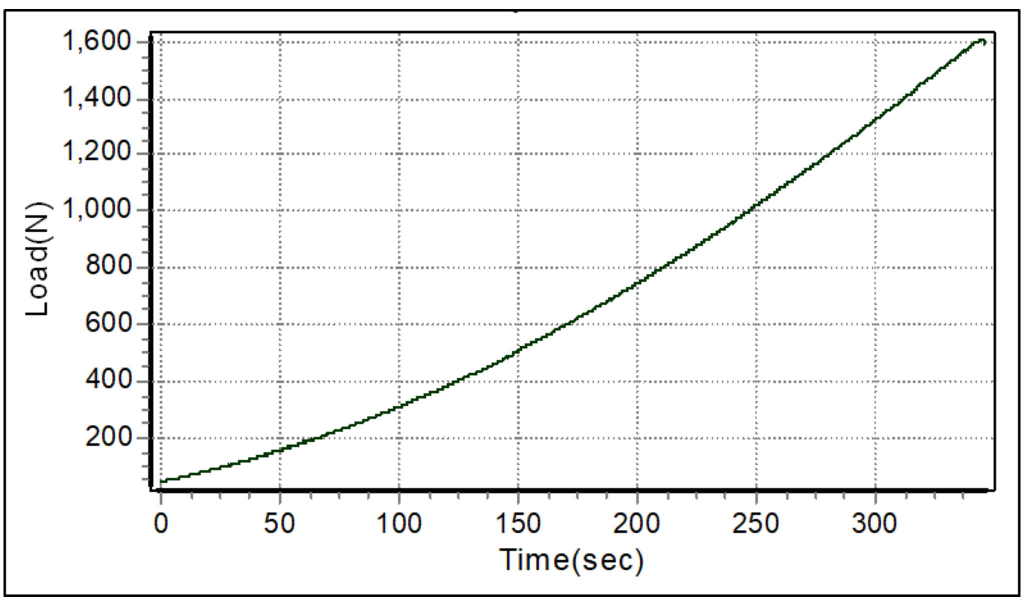

Figure 4.55 Computer generated Load profile (Sample 19-D, Brine Saturated)

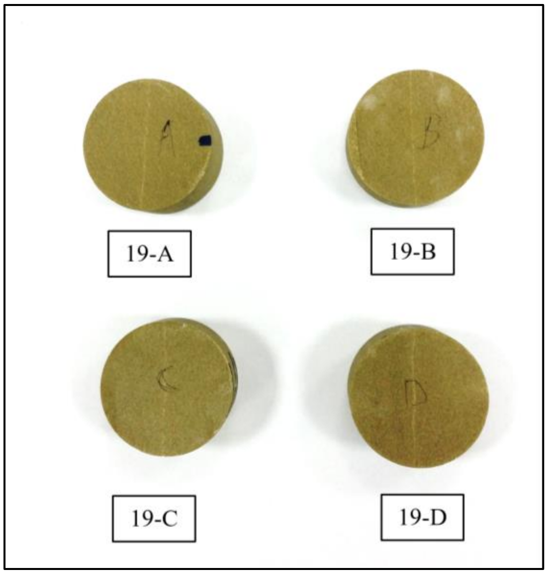

Figure 4.56 Tensile Failure Profile (Sample 1-A,B,C, Brine Saturated)

4.3.3 Oil Saturated

a. Sample 15-A

Figure 4.57 shows the tensile failure curve of sample 15-A. The tensile failure was at 1693.8 N. The failure profile of the sample is shown in Figure 4.61.

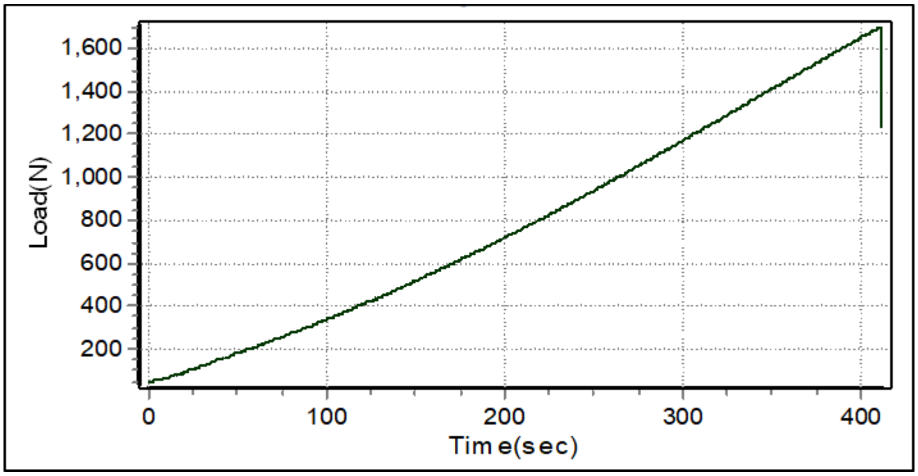

Figure 4.57 Computer generated Load profile (Sample 15-A, Oil Saturated)

b. Sample 15-B

Figure 4.58 shows the tensile failure of sample 15-B was achieved at 1962.6 N. Failure profile is shown in Figure 4.61.

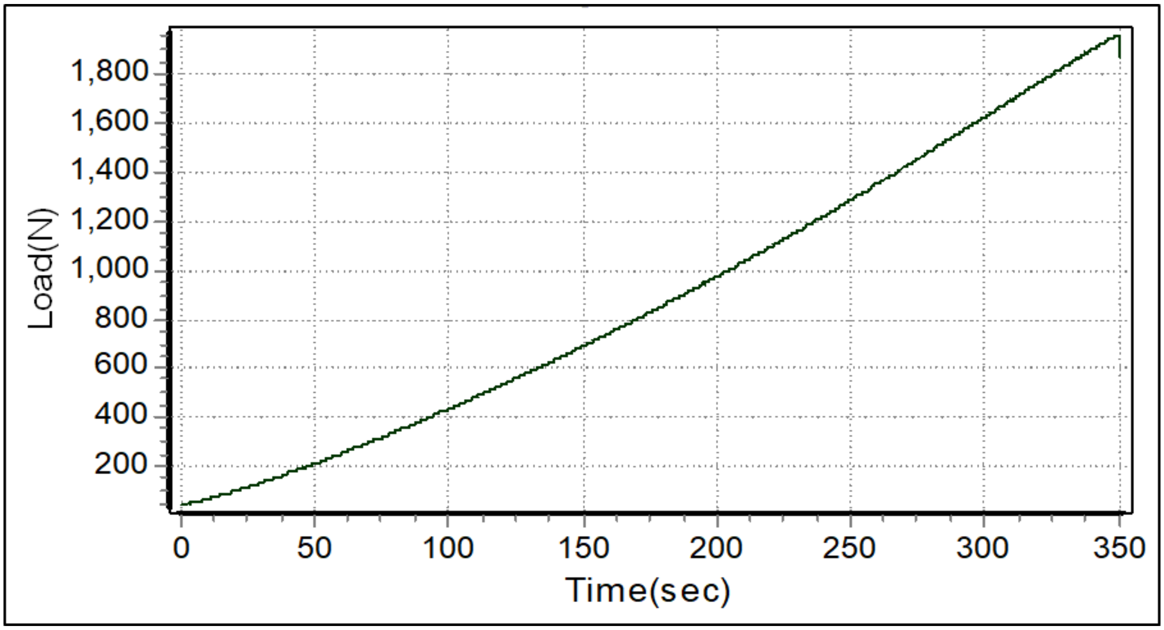

Figure 4.58 Computer generated Load profile (Sample 15-B, Oil Saturated)

c. Sample 15-C

Figure 4.59 shows the Brazilian Test for sample 15-C. The maximum load applied to the disc before undergoing tensile failure was 1983 N. Figure 4.61 shows the failure profile of the sample.

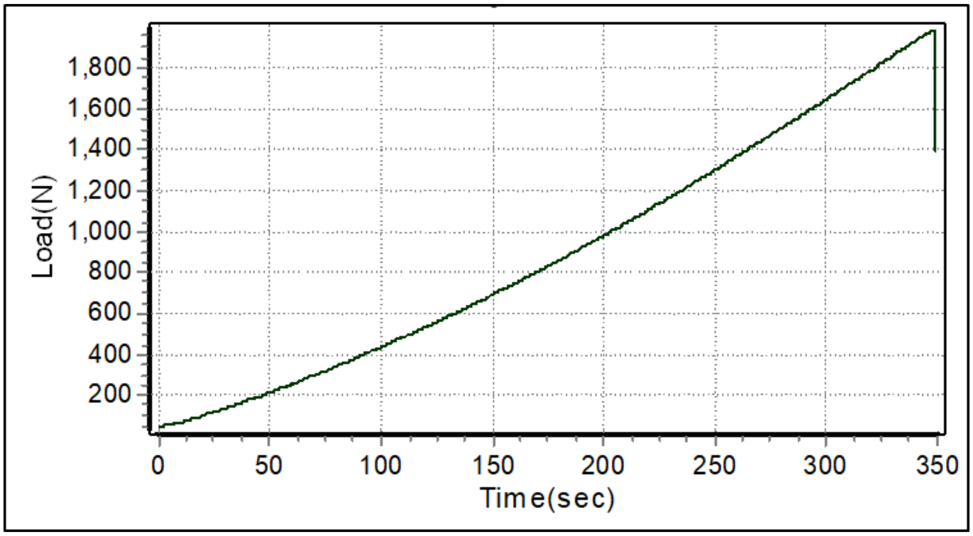

Figure 4.59 Computer generated Load profile (Sample 15-C, Oil Saturated)

d. Sample 15-D

The tensile failure of sample 15-D occurred at 2596.8 N (Figure 4.60). Failure profile of the sample is shown in Figure 4.61.

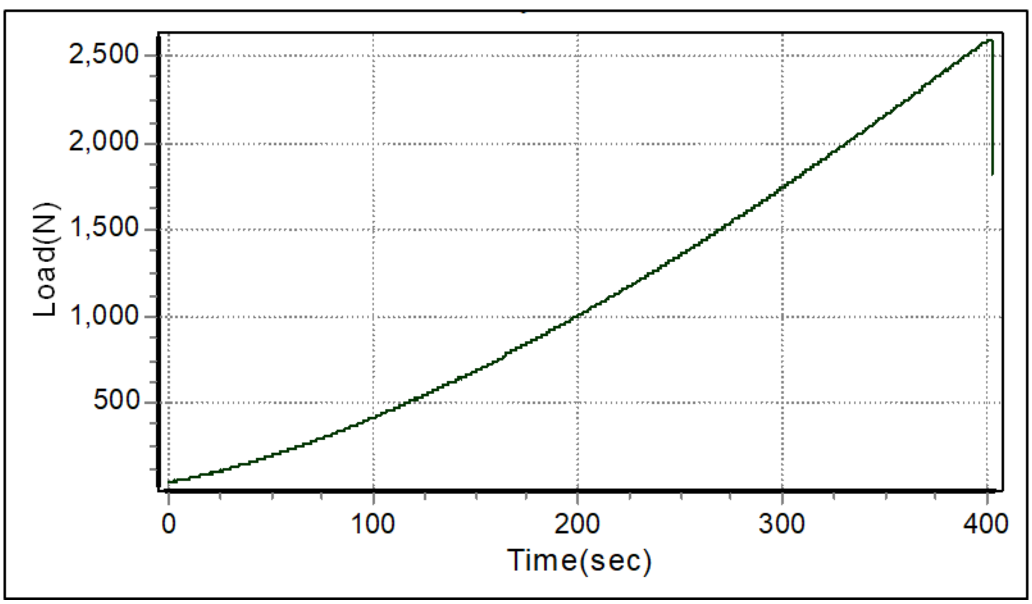

Figure 4.60 Computer generated Load profile (Sample 15-D, Oil Saturated)

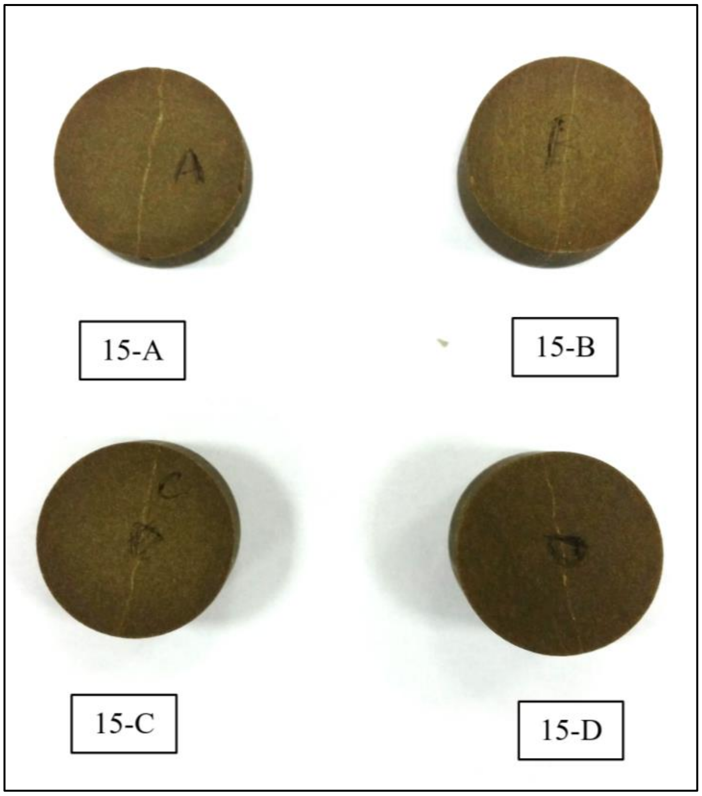

Figure 4.61 Tensile Failure Profile (Sample 1-A,B,C, Oil Saturated)

The results from all the Brazilian tests are tabulated in Table 4.9. The tensile strengths were calculated using Equation 3.6. The average tensile strength of the dry rocks is 768 psi, the average tensile strength of the brine saturated rocks is 447 psi while for the oil saturated rocks is 616 psi. It can also be seen from Figure 4.61 that the UCS and tensile strength is a function of bulk density.

Therefore, it can be concluded that as the density of the saturating fluid increases, the tensile strength (as well as UCS) of the rock decreases (Table 4.10 and Figure 4.62).

Table 4.9 Comparison of the Brazilian Tensile strengths of samples

	Sample	Diameter	Length	Load	Tensile Strength	
		mm	*mm*	*kN*	*MPa*	*psi*
Dry	***17-A***	25.2	12.7	2673.0	5.32	771
	17-B	25.3	10.8	2287.8	5.33	773
	17-C	25.4	12.6	2637.0	5.25	761
Oil Saturated	***15-A***	25.3	9.8	1693.8	4.35	631
	15-B	25.3	11.5	1962.6	4.29	623
	15-C	25.3	11.9	1983.0	4.19	608
	15-D	25.3	15.7	2596.8	4.16	603
Brine Saturated	***19-A***	25.3	12.4	1523.4	3.09	448
	19-B	25.4	11.6	1381.8	2.99	433
	19-C	25.3	12.8	1616.4	3.18	461
	19-D	25.3	13.2	1606.2	3.06	444

Table 4.10 Effect of saturating fluid on the Brazilian Tensile Strength of samples

Saturation	Density of Saturating Fluid (g/cc)	Average Tensile Strength (psi)	Percentage difference
Dry	Negligible	786	-
Oil	0.86	616	Reduced by 22%
Brine	1.03	447	Reduced by 43%

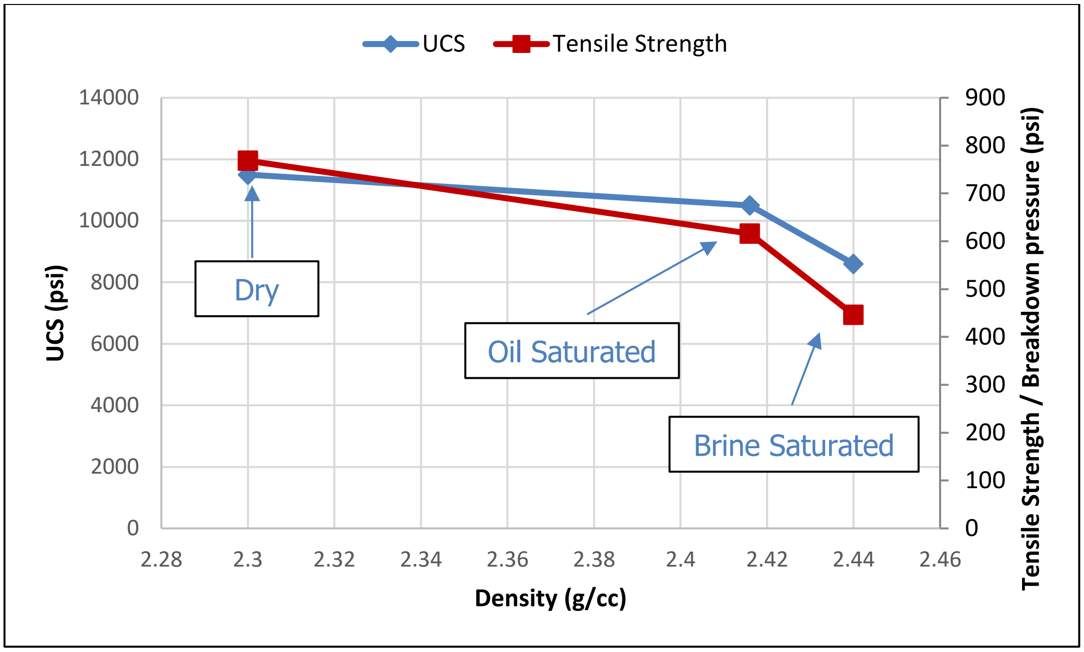

Figure 4.62 Strength comparison with increasing bulk density

4.4 Fracturing Fluid Rheology

Fracturing fluids were prepared as per the methodology described in Section 3.5.2. Rheological properties were studied for the frac fluids. Grace m3600 was used to perform the rheological study. Following are the steps used to measure the rheological properties:

1. 190 ml of fracturing fluid was measured and placed in the Grace m3600's cup
2. The viscosity was measured @ 100 s^{-1} shear rate
3. The pH was measured as well

The rheological properties of the different fracturing fluids are tabulated in Table 4.11

Table 4.11 Fracturing Fluid viscosity at 100 s^{-1}

Fracturing Fluid	Viscosity @100 s^{-1} (cp)	pH
Brine	1	7
25 ppt Linear Gel	45	8.66
40 ppt Linear Gel	86	8.68
20% GLDA with Guar Gum	120	3.71
25 ppt Crosslinked Gel	492	10.26
40 ppt Crosslinked Gel	1451	10.27

4.5 Breakdown pressure test

Breakdown pressure tests were conducted on 18 samples. Effect of the type of fracturing fluid on the breakdown pressure and the effect of the saturating fluid in the breakdown pressure is investigated in this section. All the tests were performed as per the methodology described in section 3.5.3. The confining pressure was kept constant in all tests (100 psi). the post-test analysis was conducted using CT Scan.

4.5.1 Effect of the type of fracturing fluid on the breakdown pressure

6 types of fracturing fluids were tested in this study. The number of samples used for this study were 16. All samples were tested under dry condition.

1. Brine (3% KCl)

Samples 2-21, 2-17 and 2-14 were used to determine the breakdown pressure using Brine as fracturing fluid. The viscosity of Brine was 1 cP.

a. Sample 2-21

The breakdown pressure curve of sample 2-21 is shown in Figure 4.63. As the brine was injected in the core, the pressure buildup was slow in the beginning followed by faster linear buildup. The pressure buildup decreased again before reaching the breakdown pressure. Breakdown was achieved at 550 psi and the fractured sample is shown in Figure 4.64.

Figure 4.65 shows the CT Scan of sample 2-21. The fracture produced was a bi-wing fracture and the fracture originated at the center of the borehole. The fracture was created parallel to the bedding plane. The fracture height is short and doesn't exceed below the borehole. The fracture width was small.

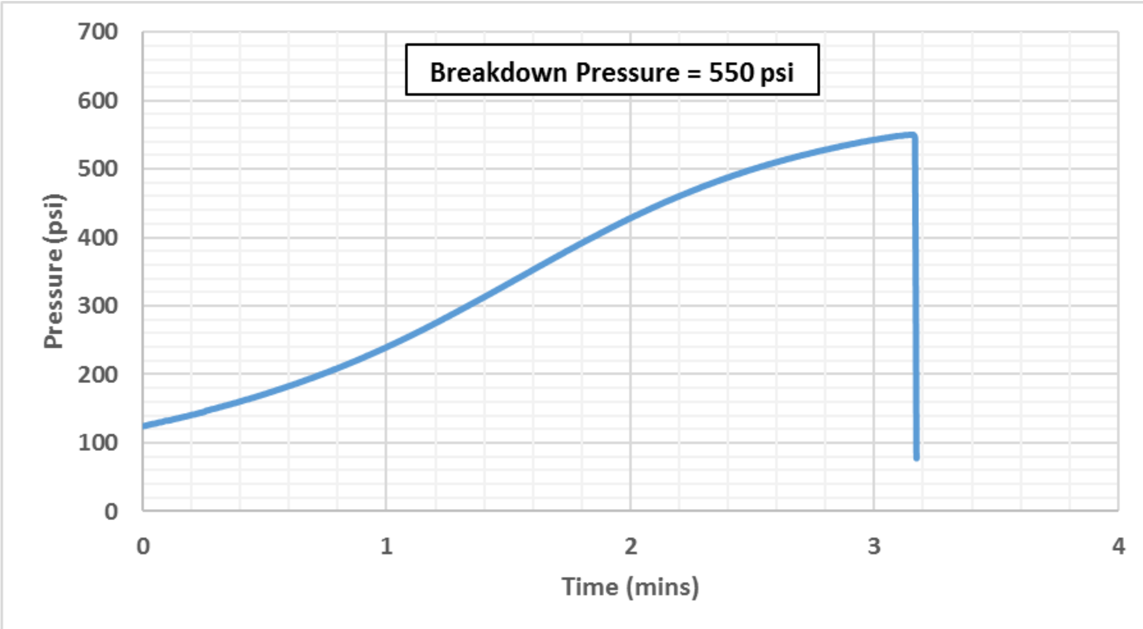

Figure 4.63 Breakdown Pressure curve (Brine, Sample 2-21)

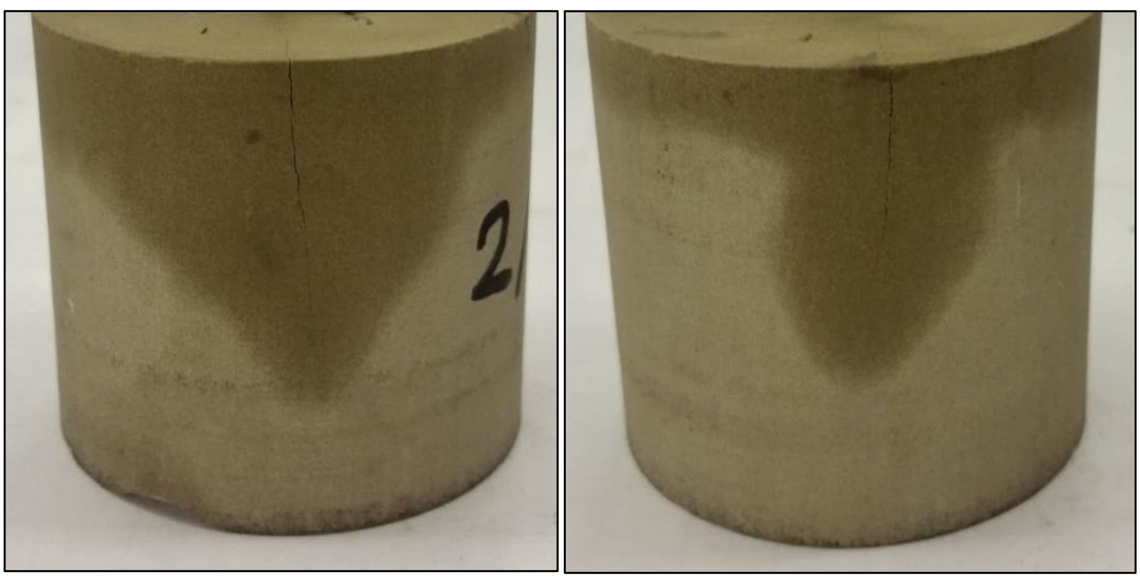

Figure 4.64 Fracture behavior (Brine, Sample 2-21)

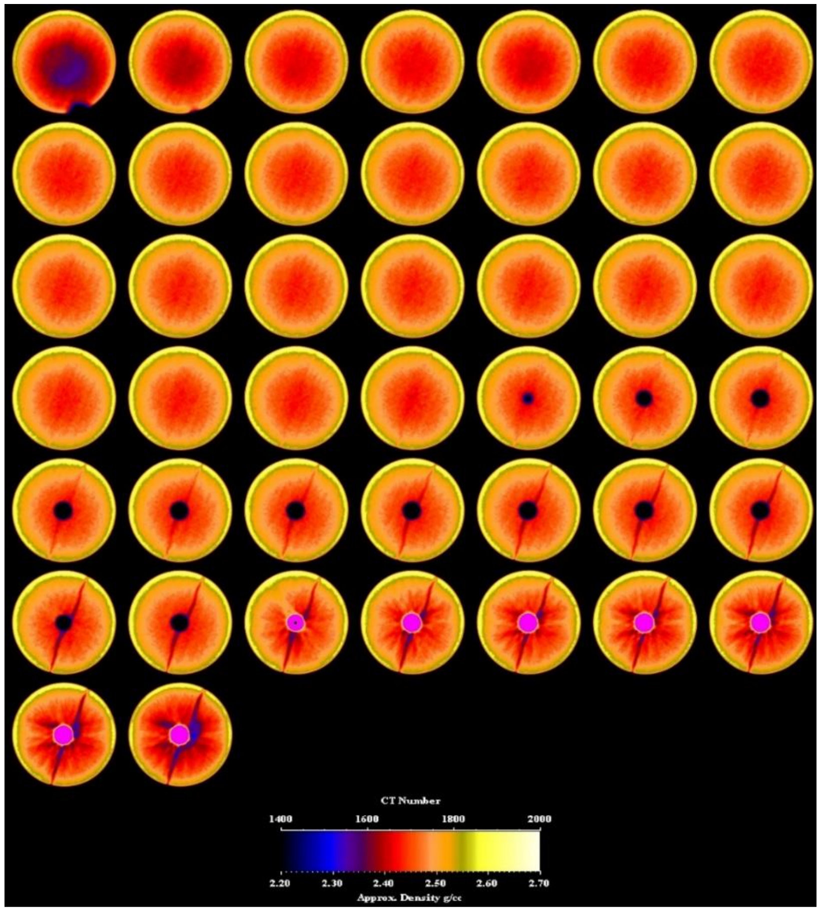

Figure 4.65 Fracture Behavior seen in CT Scan (Brine, Sample 2-21)

b. Sample 2-17

Figure 4.66 represents the breakdown pressure curve of sample 2-17 and Figure 4.67 shows the fractured sample. The breakdown pressure curve showed a similar behavior as Sample 2-21 with breakdown pressure of 617 psi.

Figure 4.68 shows the CT Scan of sample 2-17. This sample's fracture behavior was similar to the previous sample (sample 2-21) i.e., bi-wing fracture originating at the center of the borehole, parallel to the bedding plane with short fracture height and small fracture width.

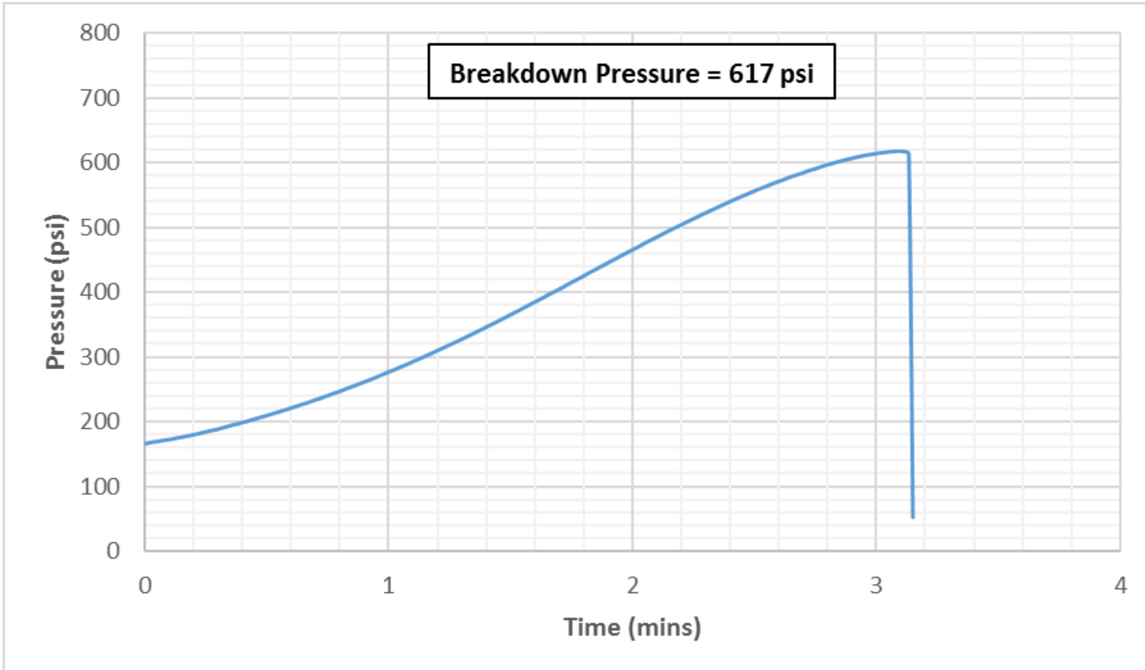

Figure 4.66 Breakdown Pressure curve (Brine, Sample 2-17)

Figure 4.67 Fracture behavior (Brine, Sample 2-17)

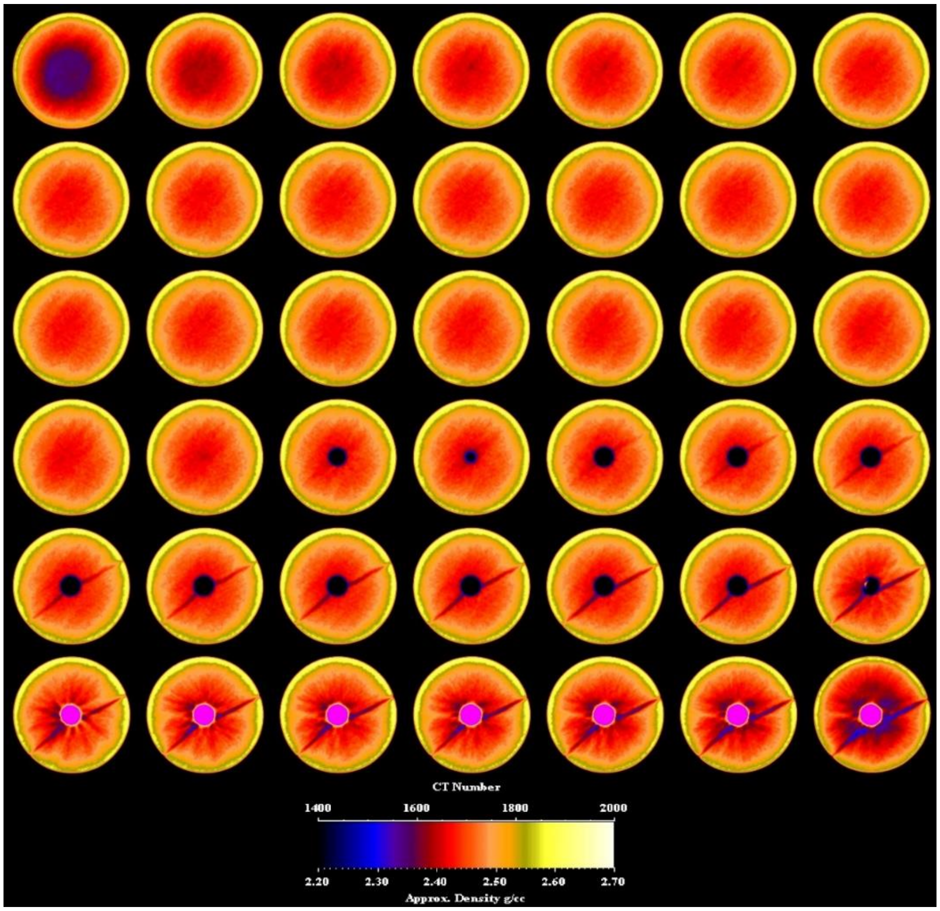

Figure 4.68 Fracture Behavior seen in CT Scan (Brine, Sample 2-17)

c. Sample 2-14

The breakdown pressure curve of sample 2-14 showed similar behavior as Samples 2-21 and 2-17 and is shown in Figure 4.69. Recorded breakdown pressure was 538 psi and the fractured sample is shown in Figure 4.70.

CT Scan of sample 2-14 is shown in Figure 4.71. The sample fractured differently than the previous samples. The fracture produced was a bi-wing fracture but the pipe along with a small portion of the rock were ejected out. This was caused because the pipe was placed at a depth of 0.2 inch rather than 0.25 inch. Also, the fracture height is shortest and the fracture width is smallest.

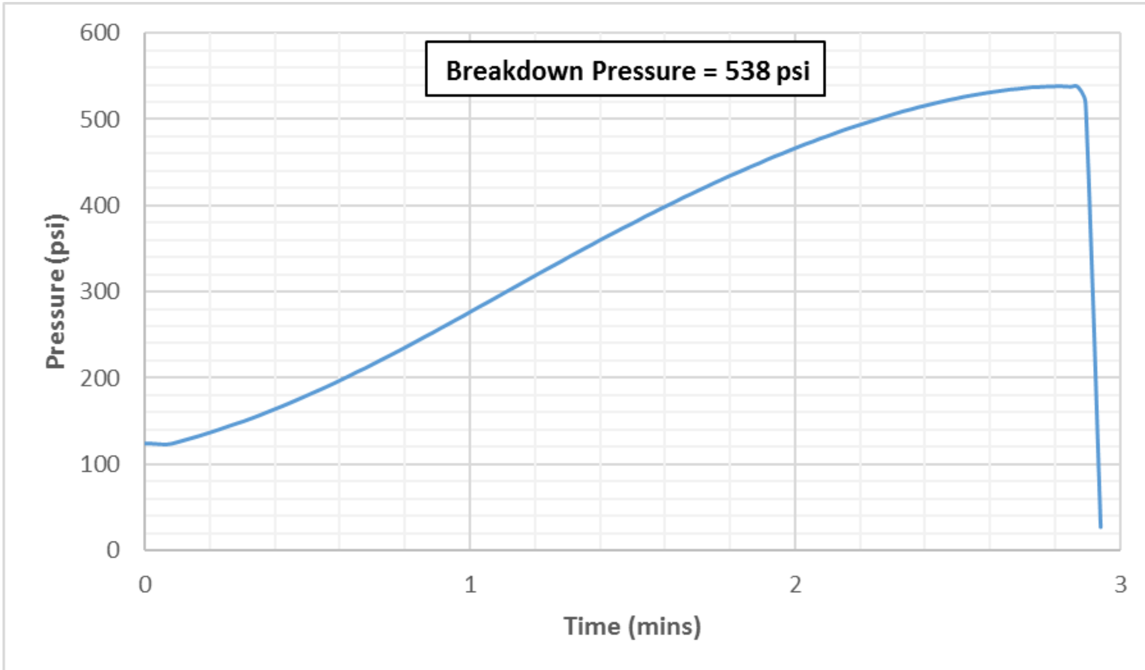

Figure 4.69 Breakdown Pressure curve (Brine, Sample 2-14)

Figure 4.70 Fracture behavior (Brine, Sample 2-14)

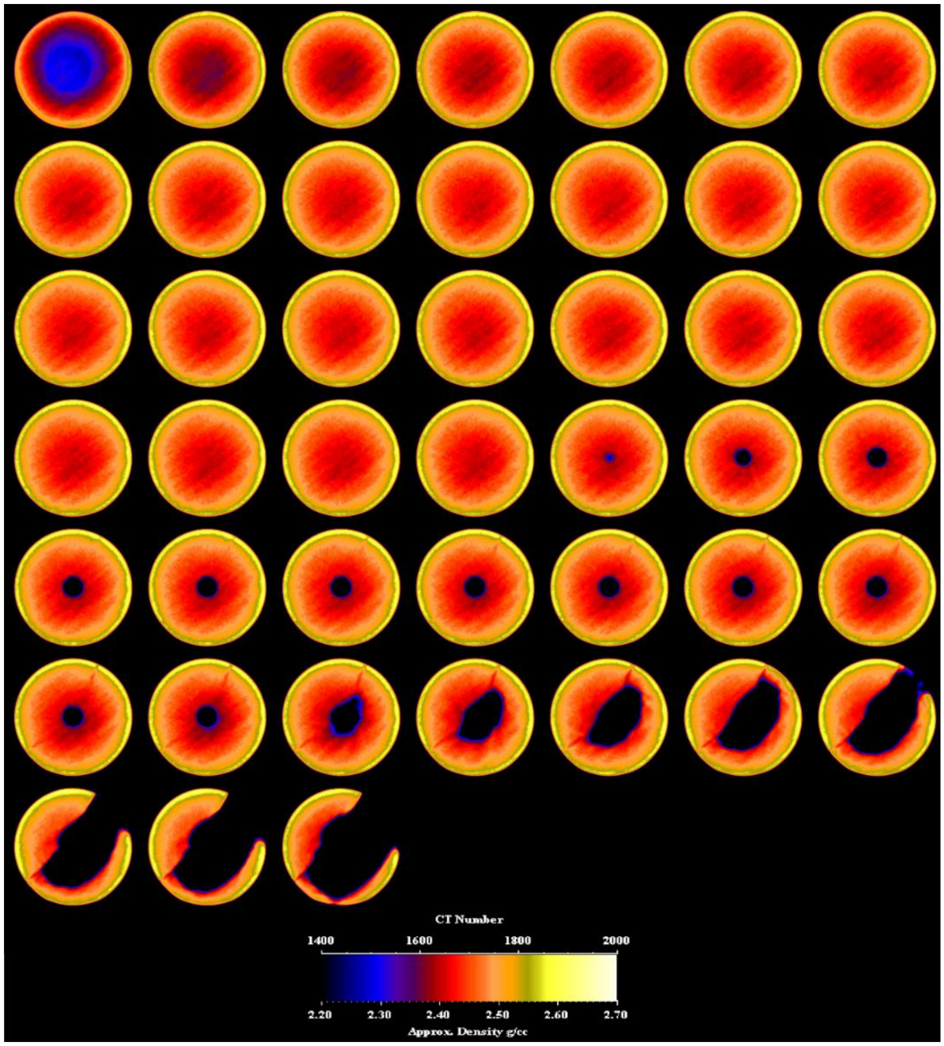

Figure 4.71 Fracture Behavior seen in CT Scan (Brine, Sample 2-14)

2. Linear Gel (25 ppt)

The viscosity of the 25 ppt Linear Gel was 45 cP. The samples used to study the breakdown pressure of this fracturing fluid were 2-7, 2-4 and 2-3.

a. Sample 2-7

Figure 4.72 represents the breakdown pressure curve of sample 2-7. As the 25 ppt Linear Gel was injected in the core, the pressure buildup was slow in the beginning followed by a faster but linear buildup. Breakdown was achieved at 1217 psi and the fractured sample is shown in Figure 4.73.

The fracture produced was a bi-wing fracture as seen in the CT Scan (Figure 4.74). It was also observed that one of the wing was weak. The fracture was created parallel to the bedding plane and had moderate fracture length exceeding the end of the borehole.

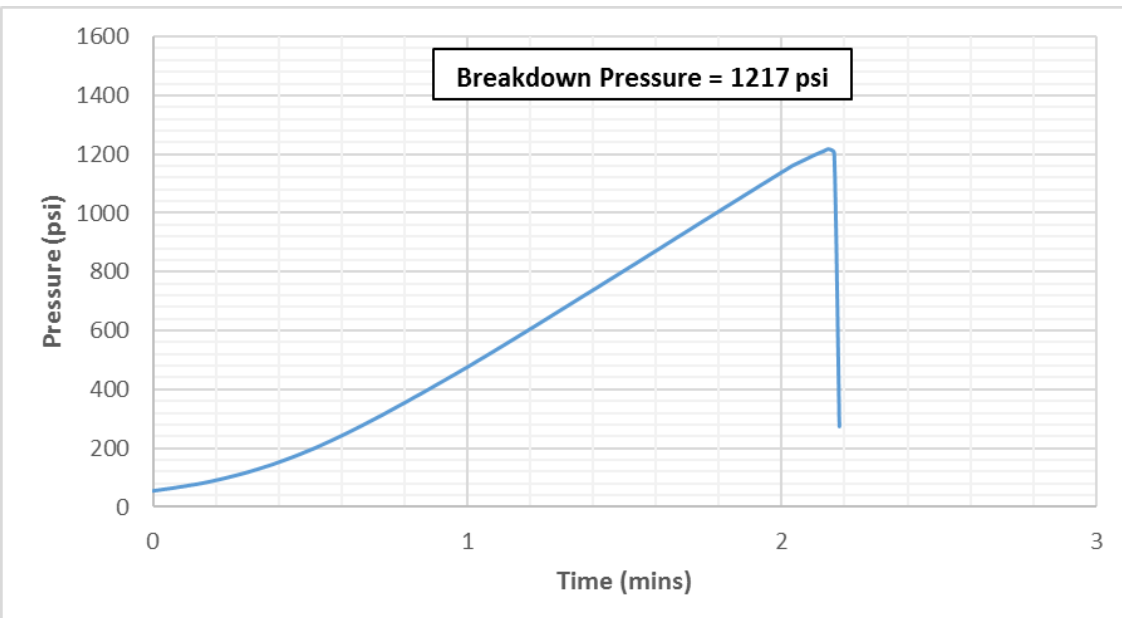

Figure 4.72 Breakdown Pressure curve (25 ppt Linear Gel, Sample 2-7)

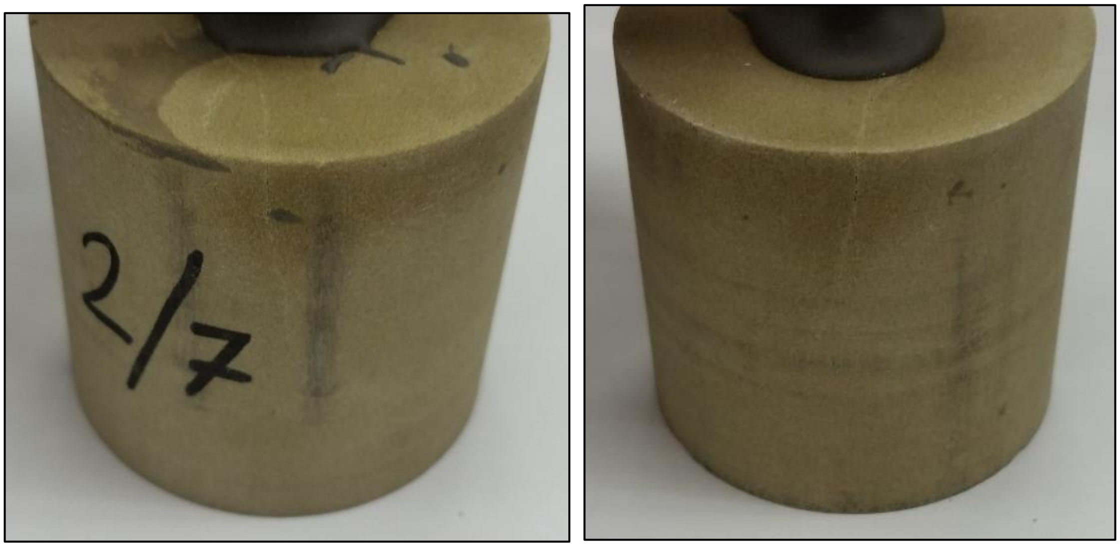

Figure 4.73 Fracture behavior (25 ppt Linear Gel, Sample 2-7)

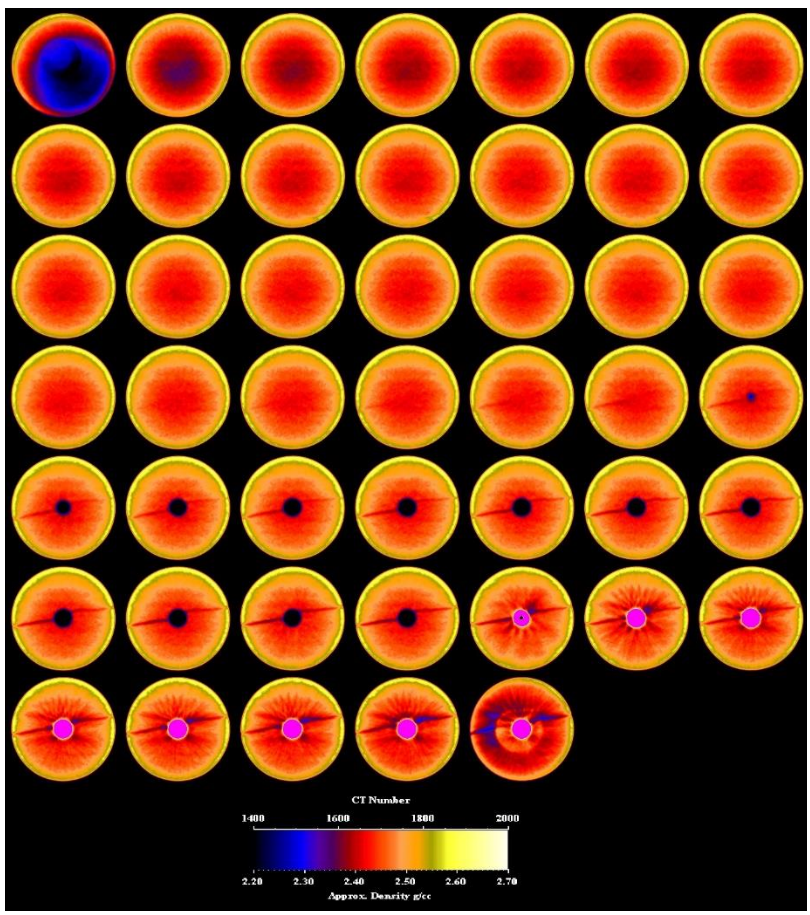

Figure 4.74 Fracture Behavior seen in CT Scan (25 ppt Linear Gel, Sample 2-7)

b. Sample 2-4

Similar pressure buildup was observed as the previous sample (sample 2-7) and the breakdown pressure of was 1234 psi (Figure 4.75). Breakdown was achieved at 1234 psi and the fractured sample is shown in Figure 4.76. The fracture produced was a bi-wing fracture. CT Scan couldn't be performed on the sample due to unavailability.

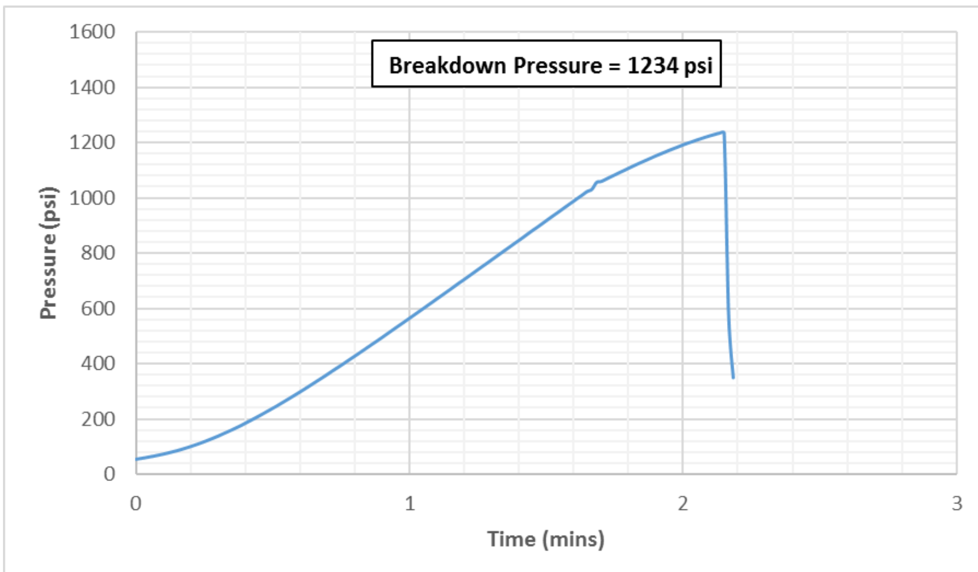

Figure 4.75 Breakdown Pressure curve (25 ppt Linear Gel, Sample 2-4)

Figure 4.76 Fracture behavior (25 ppt Linear Gel, Sample 2-4)

c. Sample 2-3

The breakdown pressure curve (Figure 4.77) showed a similar behavior as Sample 2-7. Breakdown was achieved at 1195 psi and Figure 4.78 shows the fractured sample.

The sample fractured differently than the previous samples. The fracture produced was only a single wing fracture even though the breakdown pressure is in the range of the previous samples. This could occur due to some structural defects in the borehole. The pressure will be concentrated at that point and would only create a fracture in that direction.

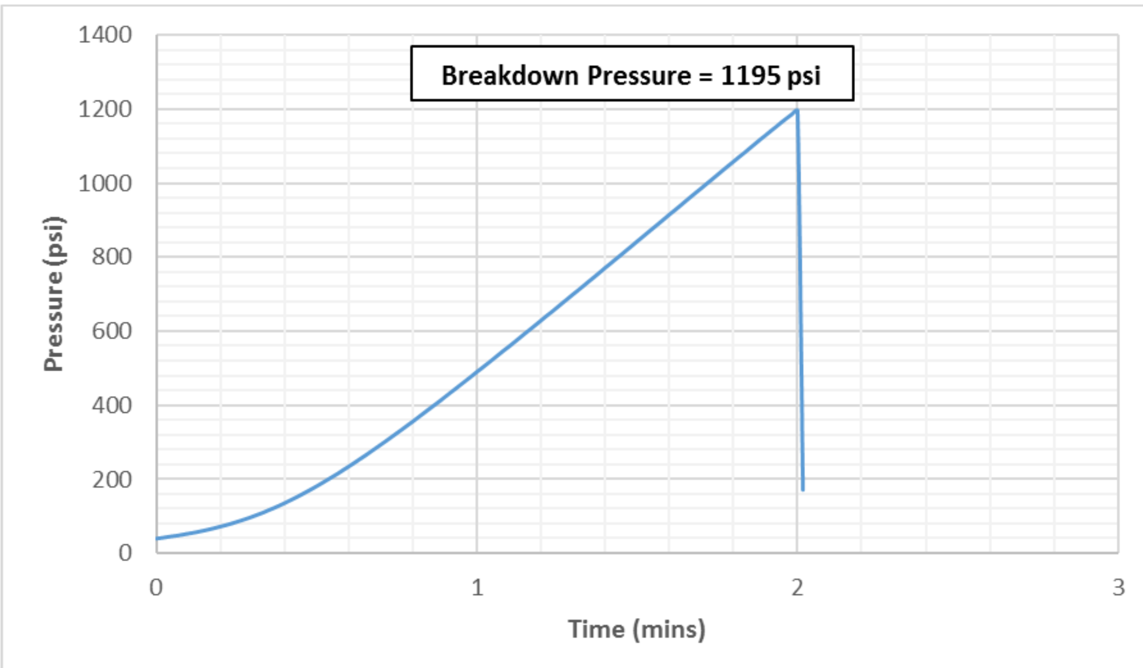

Figure 4.77 Breakdown Pressure curve (25 ppt Linear Gel, Sample 2-3)

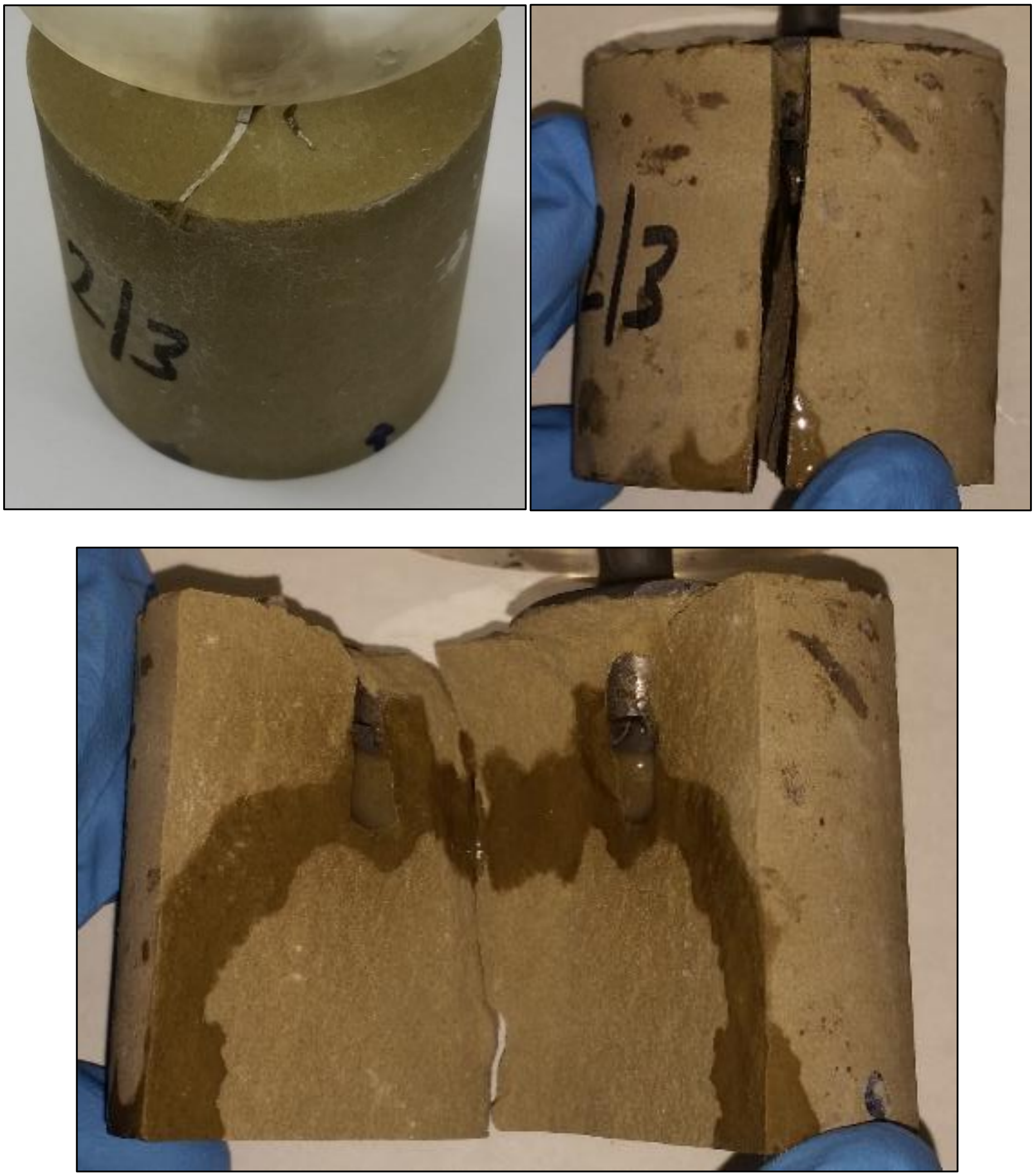

Figure 4.78 Fracture behavior (25 ppt Linear Gel, Sample 2-3)

3. Linear Gel (40 ppt)

Samples 2-10, 2-8 and 2-2 were used to determine the breakdown pressure using 40 ppt Linear Gel as fracturing fluid. The viscosity of the 40 ppt Linear Gel was 86 cP.

a. Sample 2-10

As seen in Figure 4.79 the pressure buildup was similar to the previous fluid (25 ppt Linear Gel). Breakdown was achieved at 1322 psi and the fractured sample is shown in Figure 4.69.

Figure 4.80 shows the CT Scan of sample 2-10. The fracture produced was a bi-wing fracture and the fracture originated at the center of the borehole. It was also seen that one of the wing was weak. The fracture was created parallel to the bedding plane and the fracture length was moderate. The fracture width was small.

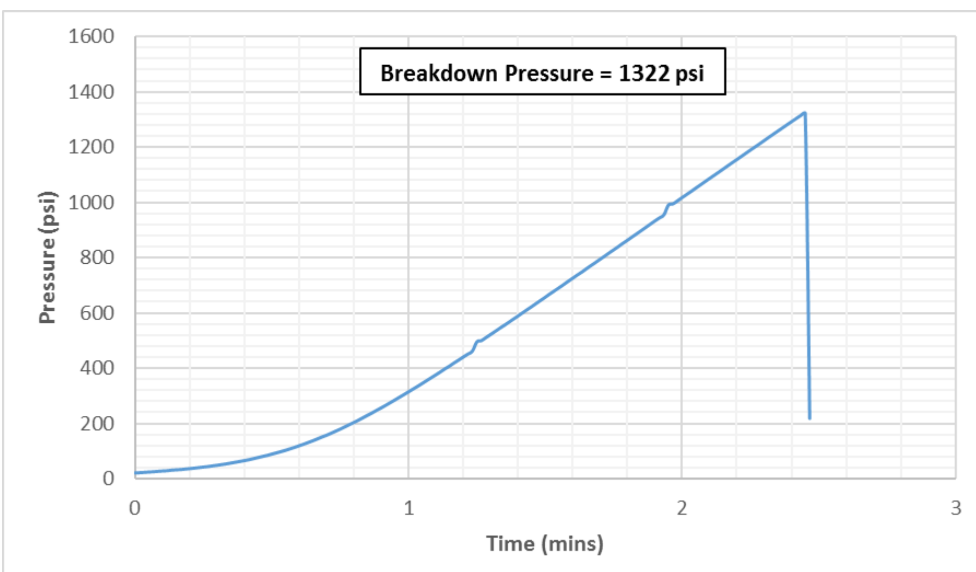

Figure 4.79 Breakdown Pressure curve (40 ppt Linear Gel, Sample 2-10)

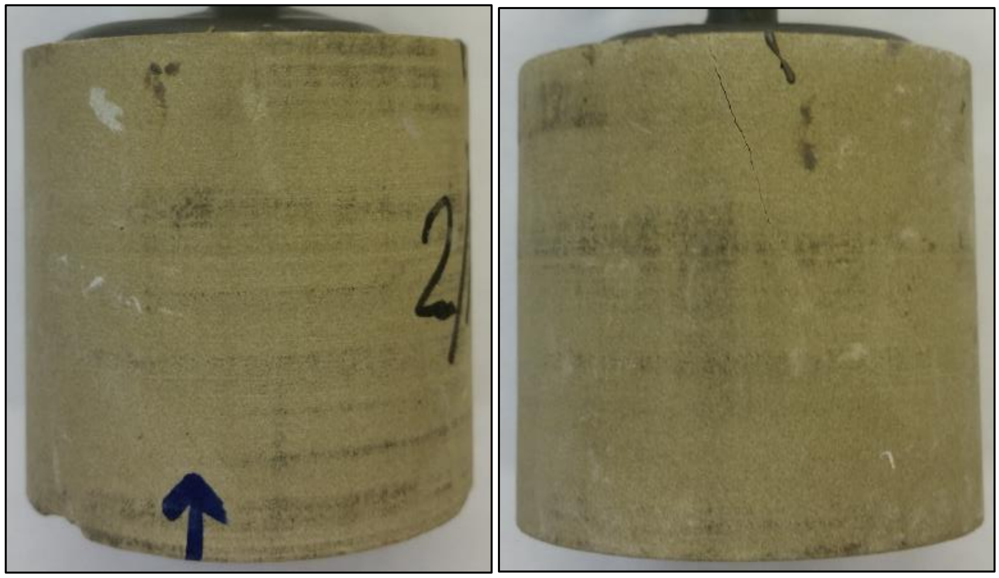

Figure 4.80 Fracture behavior (40 ppt Linear Gel, Sample 2-10)

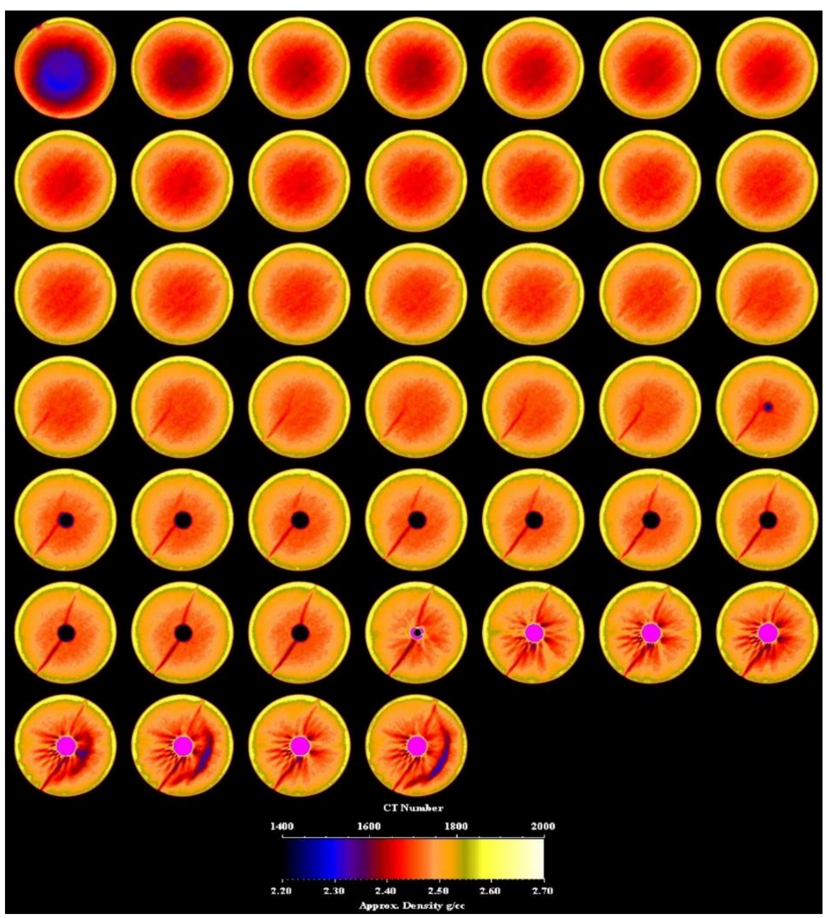

Figure 4.81 Fracture Behavior seen in CT Scan (40 ppt Linear Gel, Sample 2-10)

b. Sample 2-8

Breakdown was achieved at 1295 psi. The breakdown pressure curve showed a similar behavior as Sample 2-10 and the fractured sample is shown in Figure 4.82. Performing CT Scan (Figure 4.84) showed that the fracture was bi-wing, moderate heighted, with small to moderate width and was created parallel to the bedding plane.

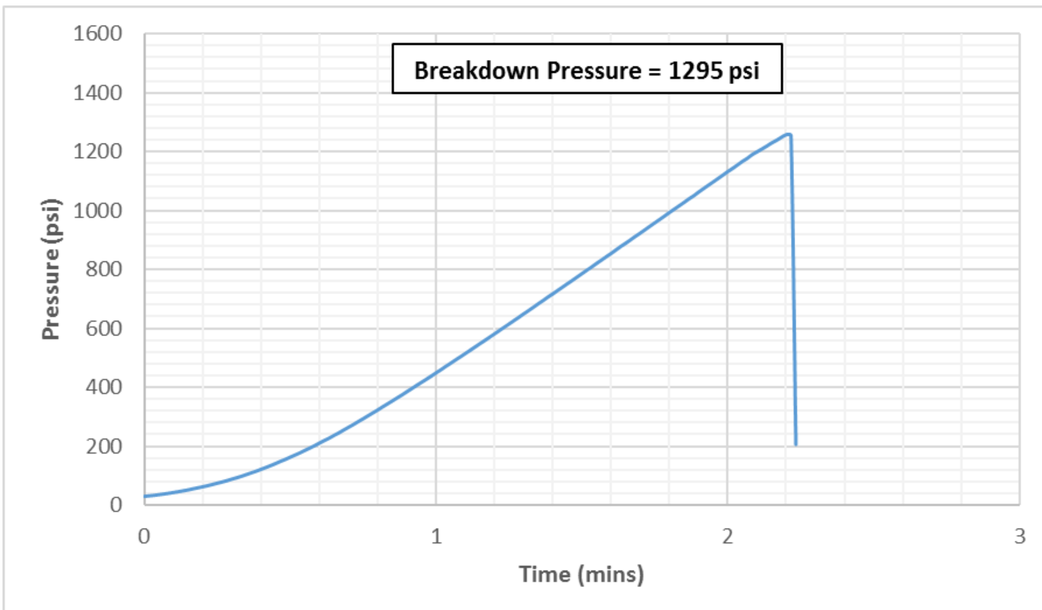

Figure 4.82 Breakdown Pressure curve (40 ppt Linear Gel, Sample 2-8)

Figure 4.83 Fracture behavior (40 ppt Linear Gel, Sample 2-8)

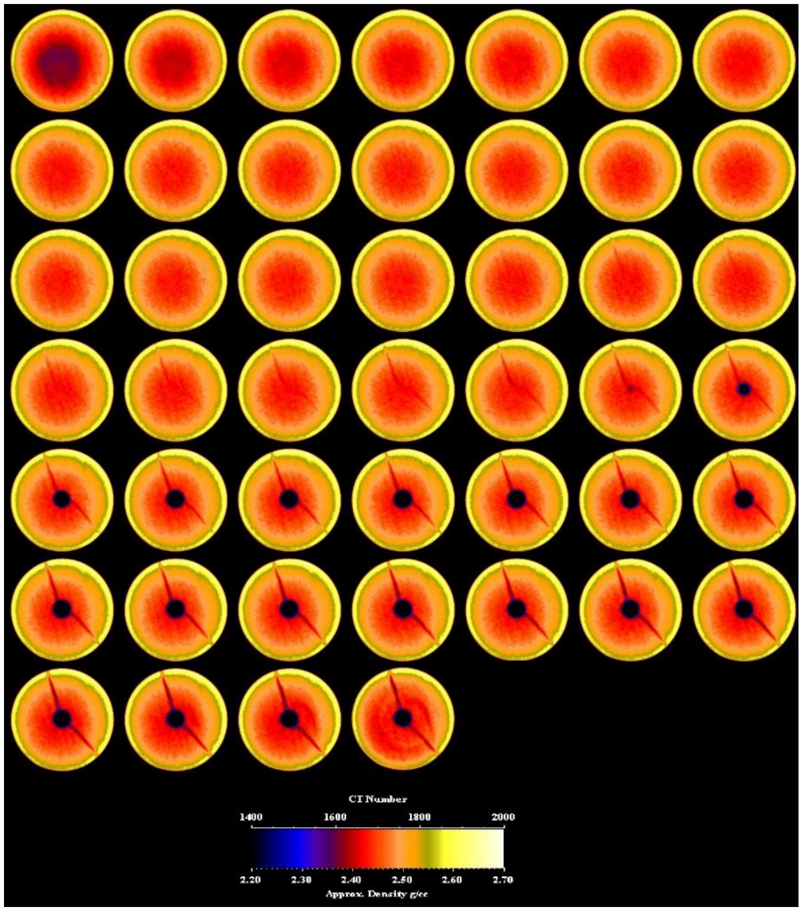

Figure 4.84 Fracture Behavior seen in CT Scan (40 ppt Linear Gel, Sample 2-8)

c. Sample 2-2

Figure 4.85 represents the breakdown pressure curve of sample 2-2. The breakdown pressure curve showed a similar behavior as Samples 2-10 and 2-8. Breakdown was achieved at 1290 psi and the fractured sample is shown in Figure 4.56.

Figure 4.87 shows the CT Scan of sample 2-8. The fracture produced was a bi-wing fracture and the fracture originated at the center of the borehole. The fracture created was of moderate height and parallel to the bedding plane with moderate width.

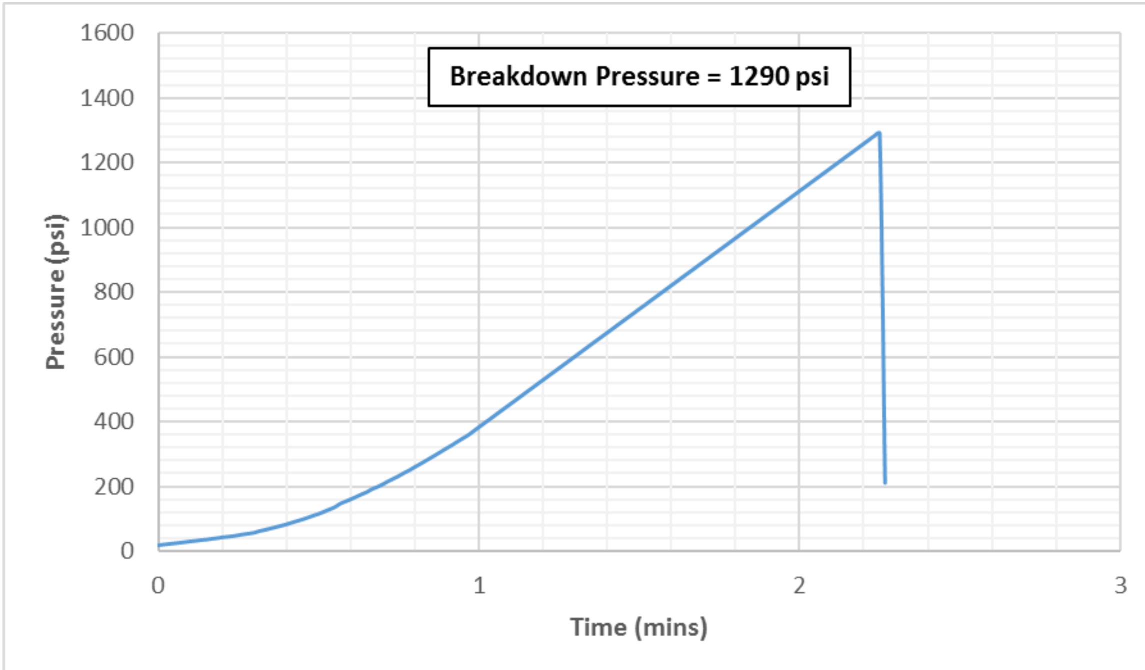

Figure 4.85 Breakdown Pressure curve (40 ppt Linear Gel, Sample 2-2)

Figure 4.86 Fracture behavior (40 ppt Linear Gel, Sample 2-2)

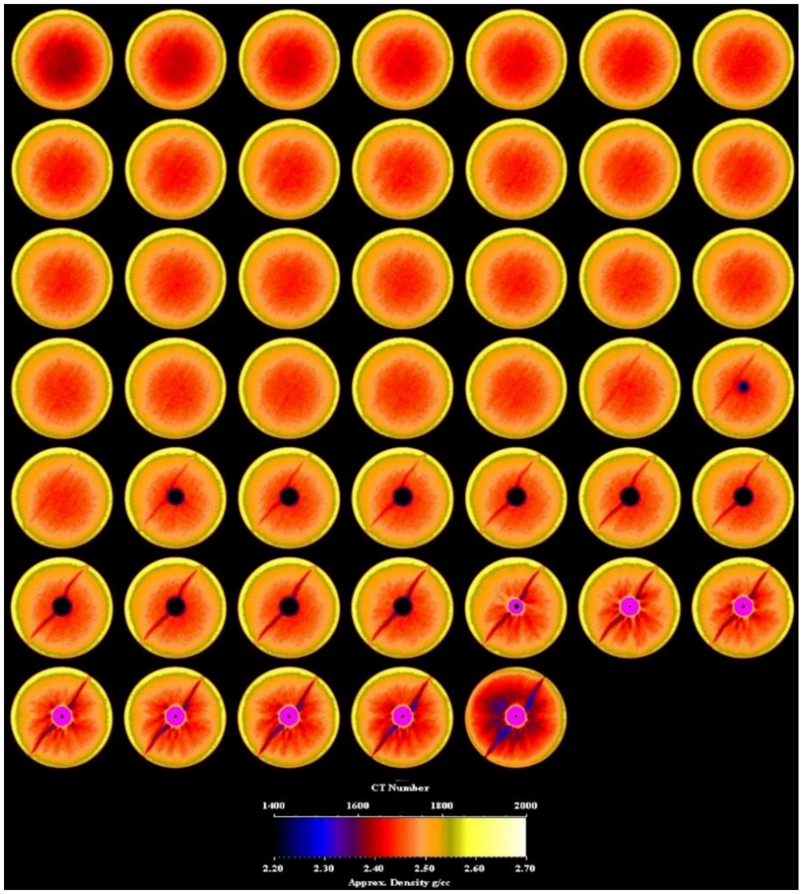

Figure 4.87 Fracture Behavior seen in CT Scan (40 ppt Linear Gel, Sample 2-2)

4. Crosslinked Gel (25 ppt)

The next fracturing fluid was 25 ppt Crosslinked Gel with viscosity 492 cP. Samples 2-16, 2-5 and 2-1 were used to determine its effect on the breakdown pressure.

a. Sample 2-16

As the 25 ppt Crosslinked Gel was injected in the core, the pressure buildup was slow in the beginning followed by a faster but linear buildup (similar to the Linear Gels) (Figure 4.88). The recorded Breakdown pressure was 1734 psi and Figure 4.89 shows the fractured sample.

Upon performing the CT scan (Figure 4.90), the fracture was Bi-wing and parallel to the bedding plane. The fracture length is long and it extends much further below the borehole with very thick fracture width. Formation of thick filter cake was seen at the bottomhole.

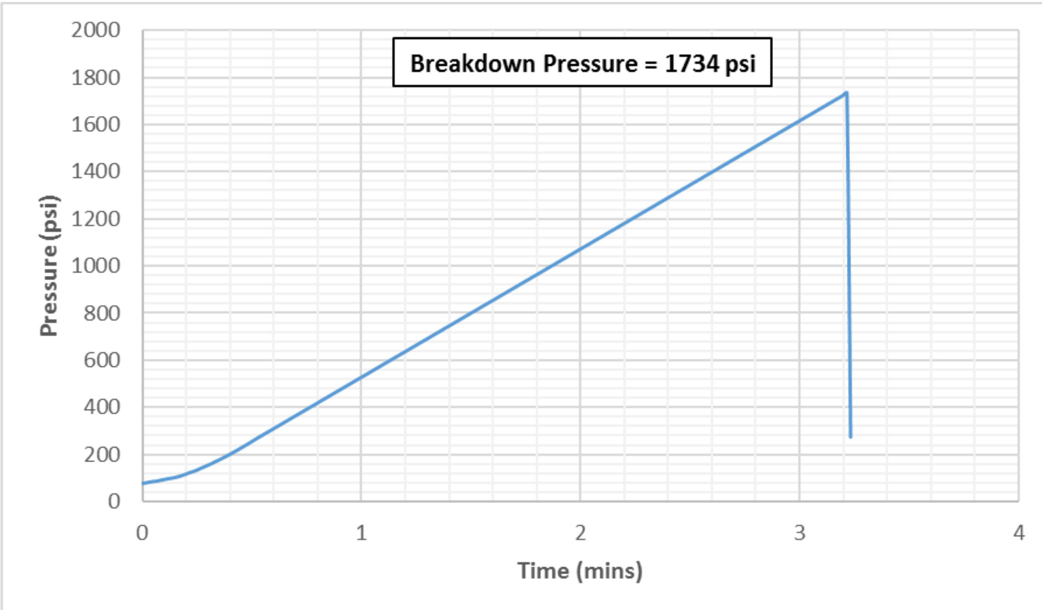

Figure 4.88 Breakdown Pressure curve (25 ppt Crosslinked Gel, Sample 2-16)

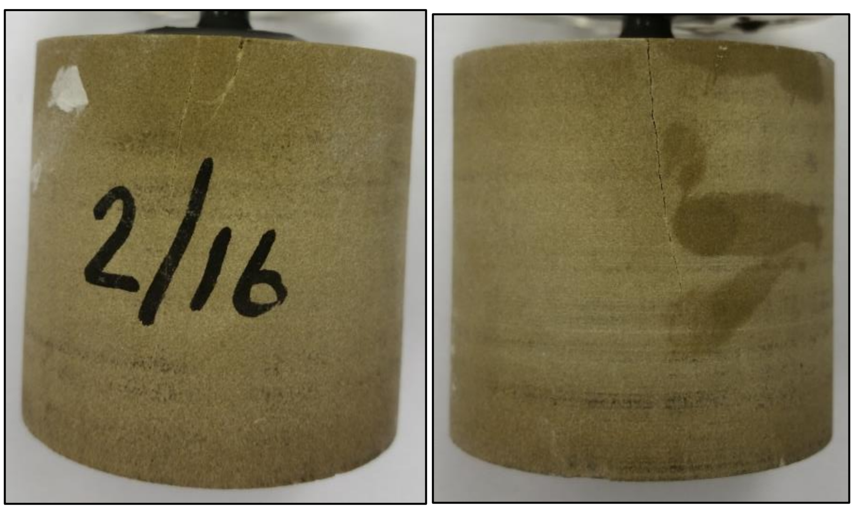

Figure 4.89 Fracture behavior (25 ppt Crosslinked Gel, Sample 2-16)

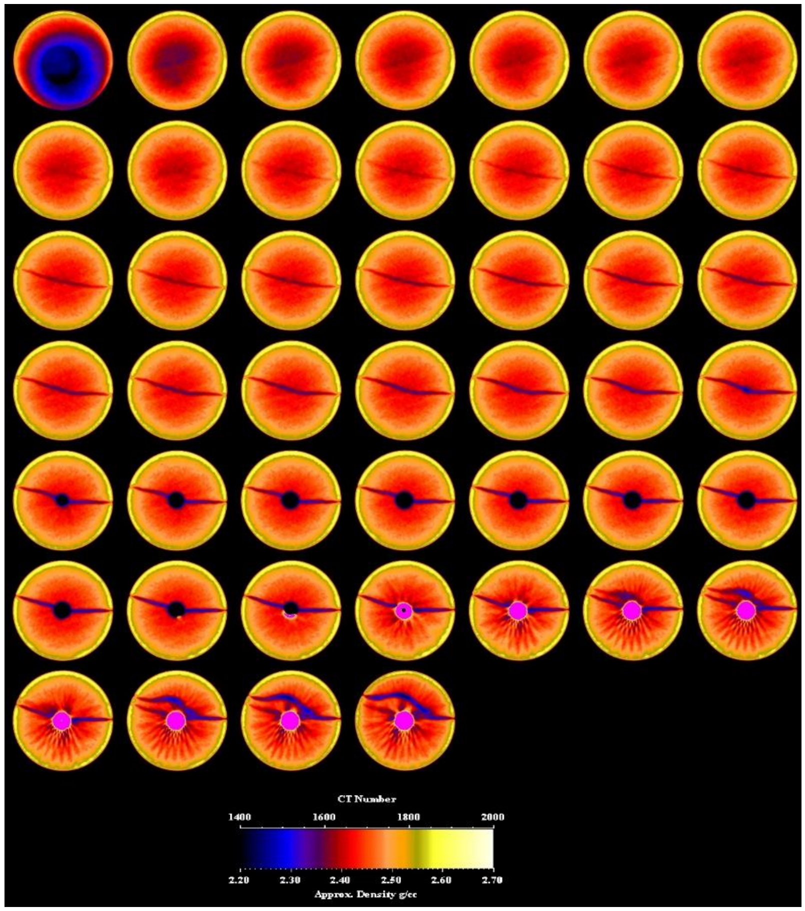

Figure 4.90 Fracture Behavior seen in CT Scan (25 ppt Crosslinked Gel, Sample 2-16)

b. Sample 2-5

Figure 4.91 represents the breakdown pressure curve of sample 2-5. As the 25 ppt Crosslinked Gel was injected in the core, the pressure buildup was slow in the beginning followed by a faster but linear buildup. At about 600 psi, the slope of the curve decreased until 1200 psi and then it linearly increased till breakdown. This was due to a small leak between the pipe and epoxy at the top of the sample. Recorded breakdown pressure 1656 psi and the fractured sample is shown in Figure 4.92.

Figure 4.93 shows the CT Scan of sample 2-5. A bi-wing fracture was formed parallel to the bedding plane. Fracture length was long and the width was very thick width. A thick filter cake was also formed at the bottomhole.

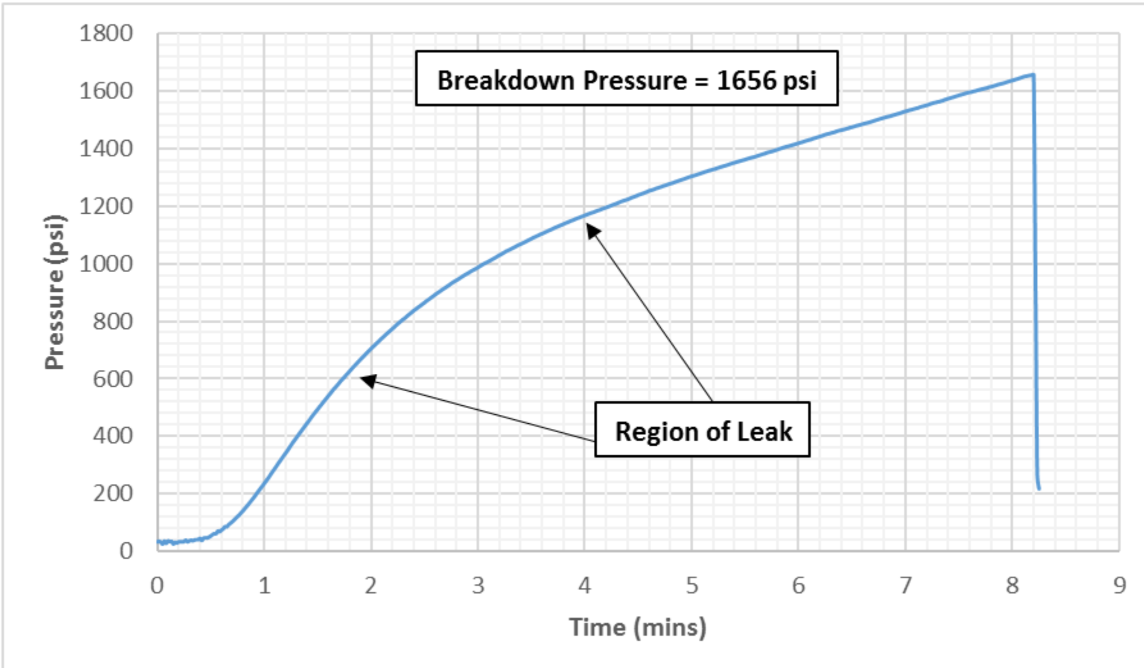

Figure 4.91 Breakdown Pressure curve (25 ppt Crosslinked Gel, Sample 2-5)

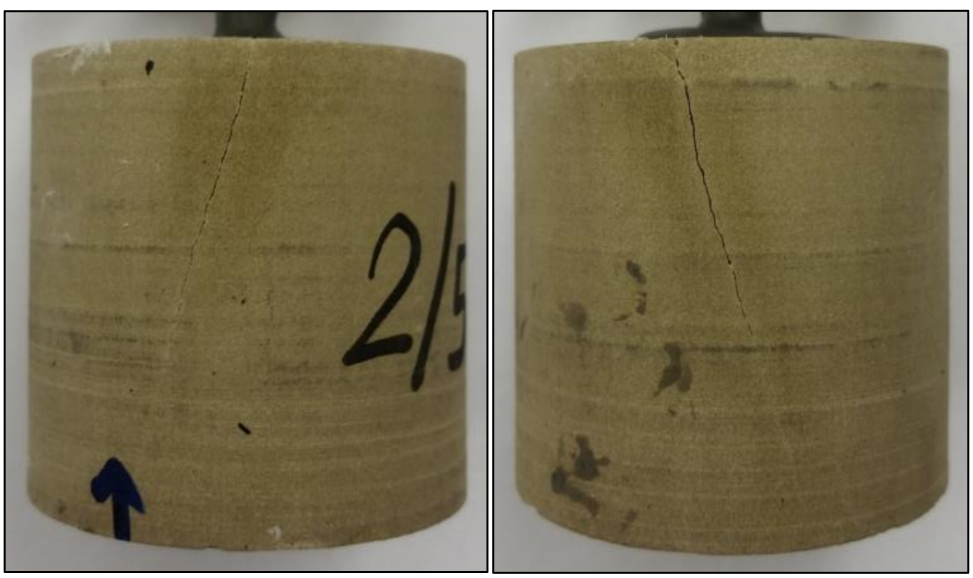

Figure 4.92 Fracture behavior (25 ppt Crosslinked Gel, Sample 2-5)

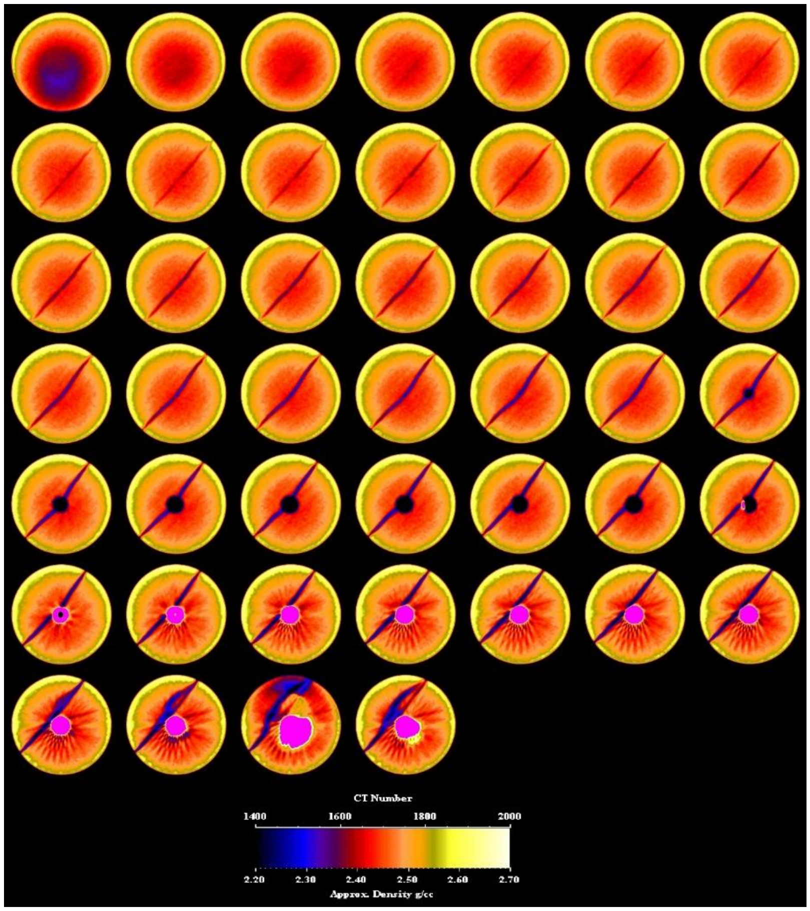

Figure 4.93 Fracture Behavior seen in CT Scan (25 ppt Crosslinked Gel, Sample 2-5)

c. Sample 2-1

The breakdown pressure curve of sample 2-1 is shown in Figure 4.94. The breakdown pressure curve showed a similar behavior as Sample 2-16. Breakdown was achieved at 1700 psi and the fractured sample is shown in Figure 4.95.

The fracture produced was a bi-wing fracture which fractured the whole core. A thick filter cake was also formed at the bottomhole.

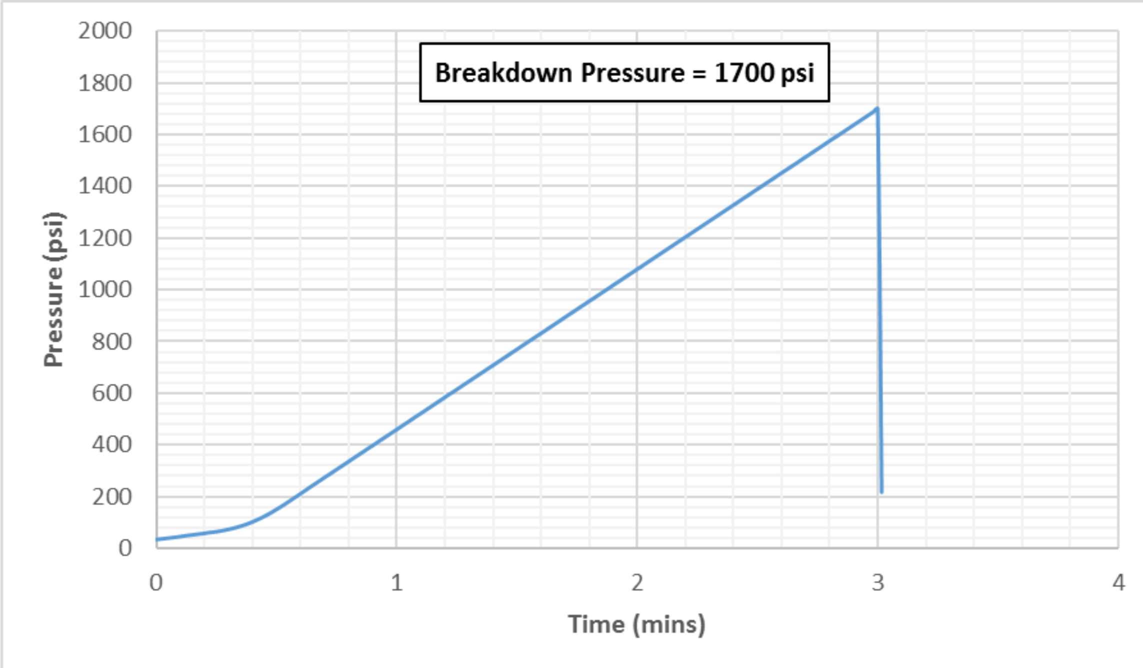

Figure 4.94 Breakdown Pressure curve (25 ppt Crosslinked Gel, Sample 2-1)

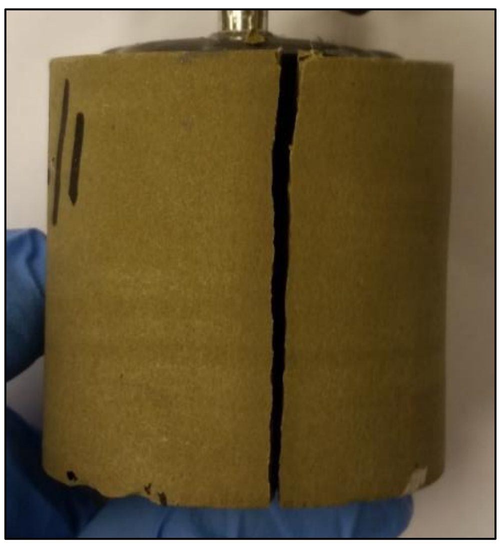

Figure 4.95 Fracture behavior (25 ppt Crosslinked Gel, Sample 2-1)

5. Crosslinked (40 ppt)

40 ppt Crosslinked Gel had a viscosity of 1451 cP. Samples 2-11, 2-9 and 2-13 were used to determine the breakdown pressure.

a. Sample 2-11

Figure 4.96 shows the breakdown pressure curve of sample 2-11. The breakdown pressure was 1940 psi and the fractured sample is shown in Figure 4.97.

Performing the CT scan showed that a bi-wing fracture was created along the bedding plane with long height and very thick width (Figure 4.98). At the bottomhole, a thick filter cake was also formed.

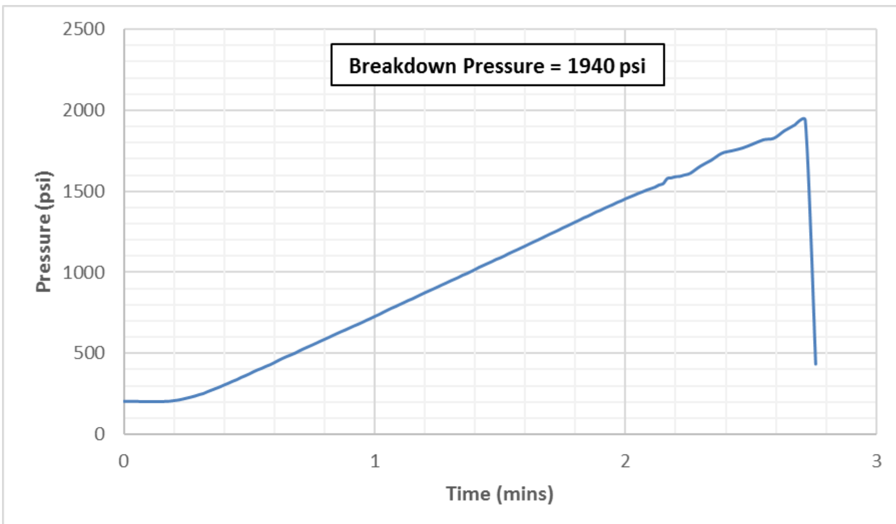

Figure 4.96 Breakdown Pressure curve (40 ppt Crosslinked Gel, Sample 2-11)

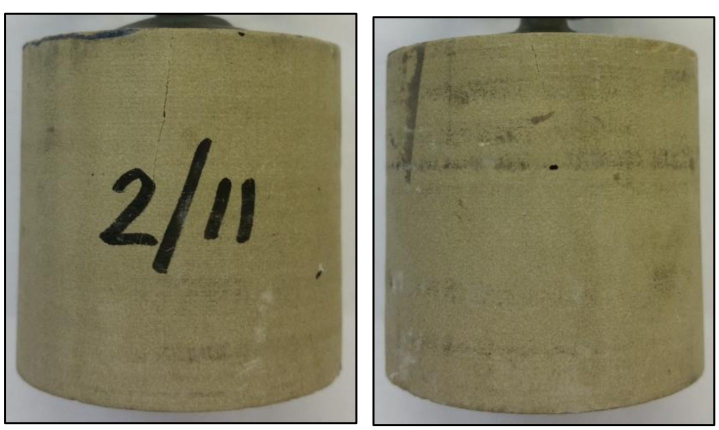

Figure 4.97 Fracture behavior (40 ppt Crosslinked Gel, Sample 2-11)

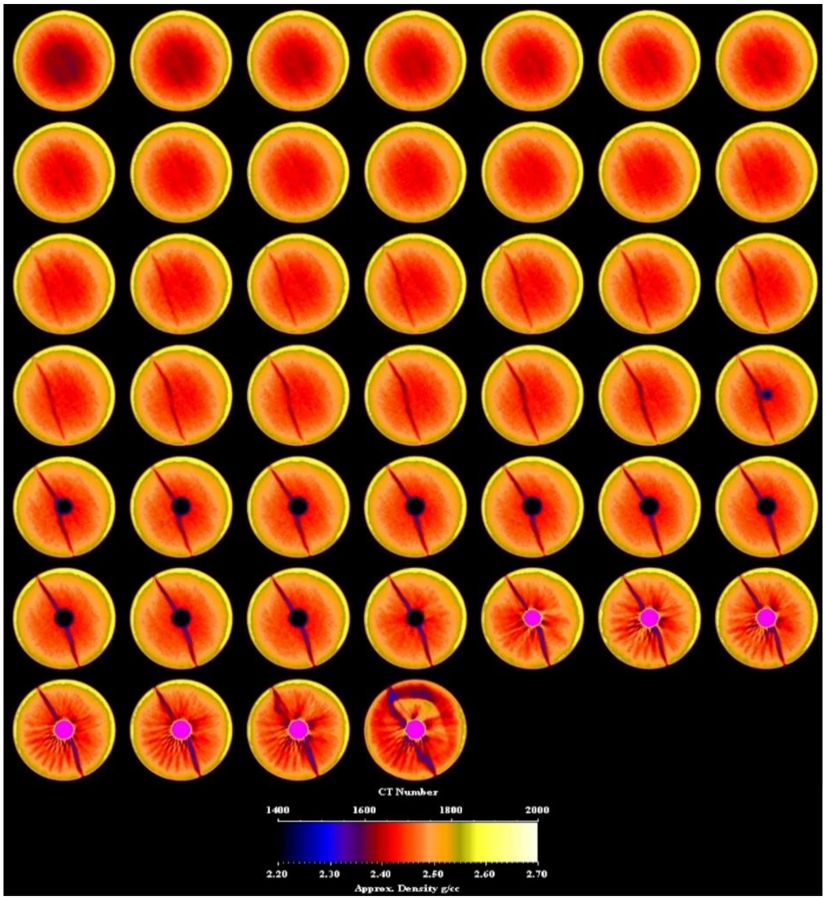

Figure 4.98 Fracture Behavior seen in CT Scan (40 ppt Crosslinked Gel, Sample 2-11)

b. Sample 2-9

Figure 4.99 represents the breakdown pressure curve of sample 2-9. As the 40 ppt Crosslinked Gel was injected in the core, the pressure buildup was slow in the beginning followed by a faster but linear buildup. At about 1500 psi, the pressure variably increased till breakdown. This could be due to a large leak between the pipe and epoxy. Recorded breakdown pressure 2034 psi and the fractured sample is shown in Figure 4.100.

The fracture produced was a bi-wing fracture. The fracture length was long the observed fracture width was the very thick. A thick filter cake was also formed at the bottomhole (Figure 4.100).

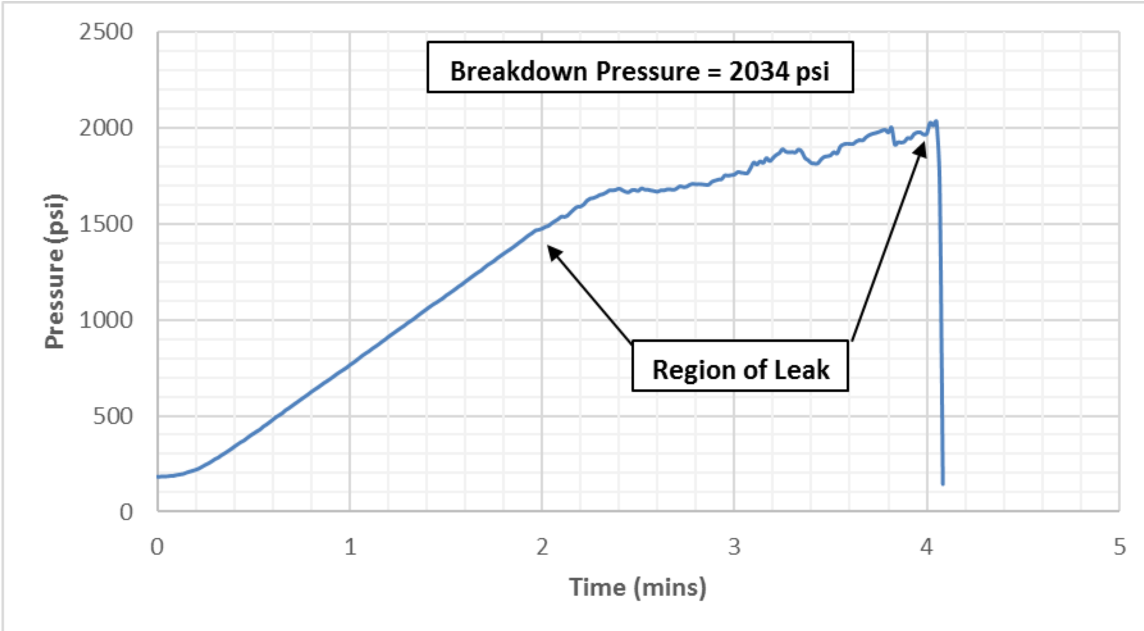

Figure 4.99 Breakdown Pressure curve (40 ppt Crosslinked Gel, Sample 2-9)

Figure 4.100 Fracture behavior (40 ppt Crosslinked Gel, Sample 2-9)

c. Sample 2-13

The breakdown pressure curve was similar to that of Sample 4.11 (Figure 4.101). The recorded breakdown pressure was 1837 psi and the fractured sample is shown in Figure 4.102.

CT Scan showed that only a single wing fracture even though the breakdown pressure is in the range of the previous samples (Figure 4.103). This could occur due to some structural defects in the borehole. The pressure will be concentrated at that point and would only create a fracture in that direction. The fracture was long with moderate width.

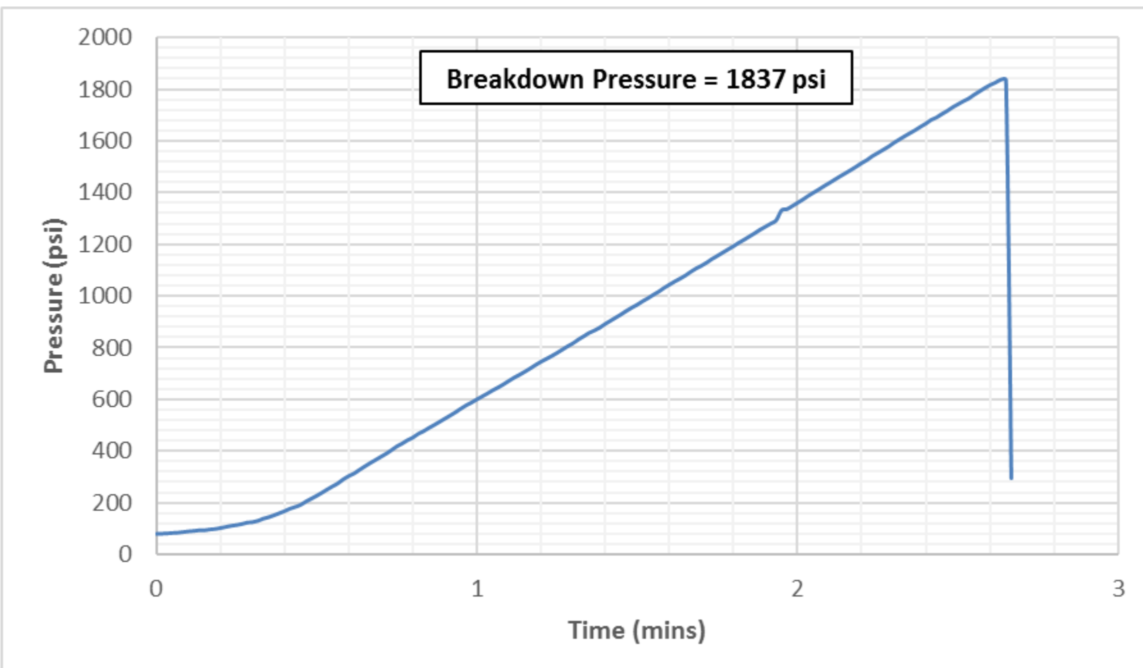

Figure 4.101 Breakdown Pressure curve (40 ppt Crosslinked Gel, Sample 2-13)

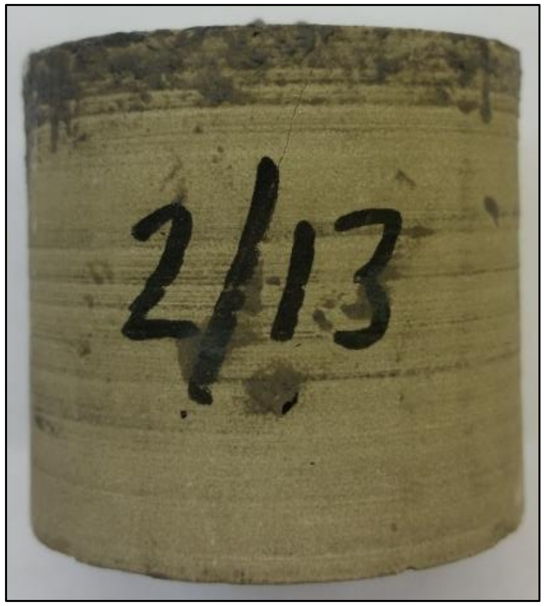

Figure 4.102 Fracture behavior (40 ppt Crosslinked Gel, Sample 2-13)

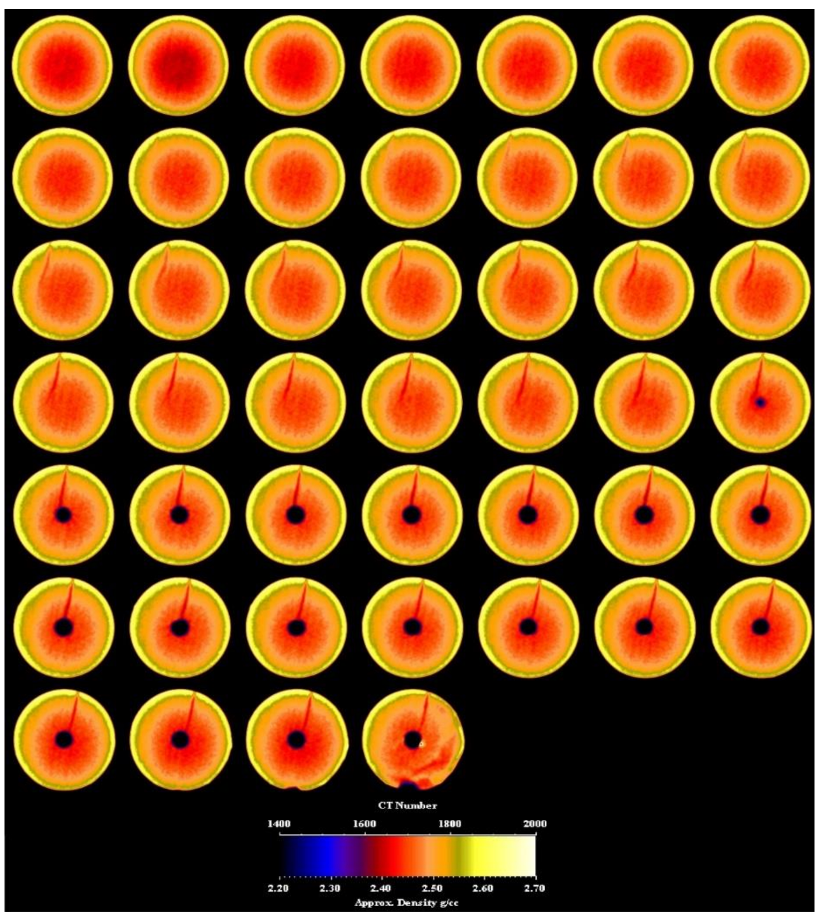

Figure 4.103 Fracture Behavior seen in CT Scan (40 ppt Crosslinked Gel, Sample 2-13)

6. 20% GLDA with Guar

Samples 2-19 was used to determine the breakdown pressure using 20% GLDA with Guar as fracturing fluid. The viscosity of the 20% GLDA with Guar was 121 cP.

The sample was fractured at 1493 psi (Figure 4.104). The fractured sample is shown in Figure 4.105. Upon performing CT Scan, it was found that the fracture was bi-wing with one weak wing (Figure 4.106). The fracture length is moderate and fracture width was small.

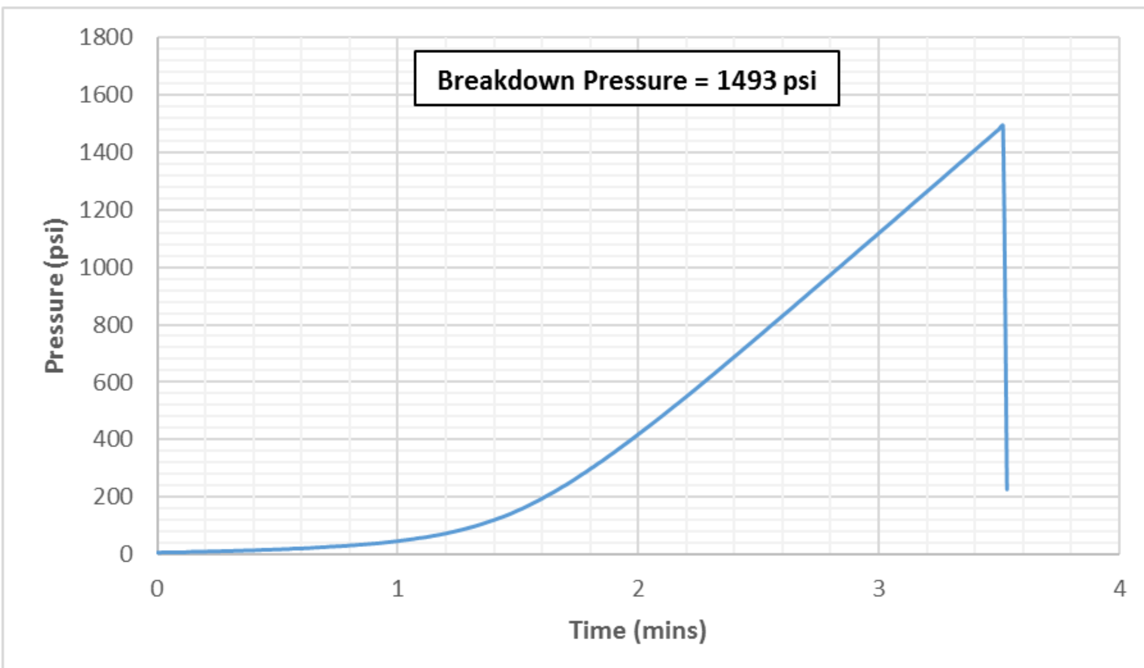

Figure 4.104 Breakdown Pressure curve (20% GLDA with Guar, Sample 2-19)

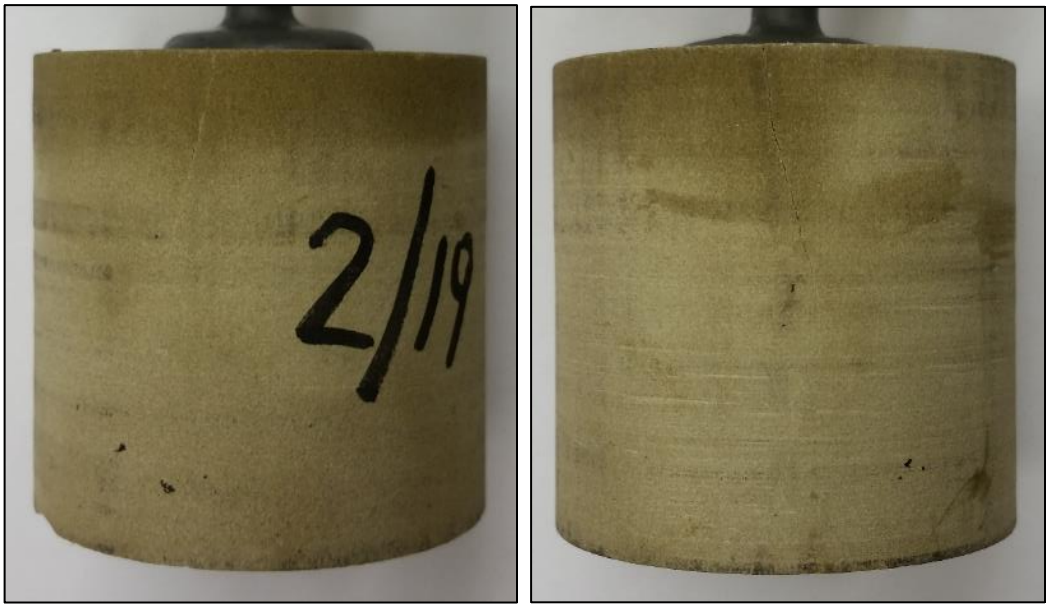

Figure 4.105 Fracture behavior (20% GLDA with Guar, Sample 2-19)

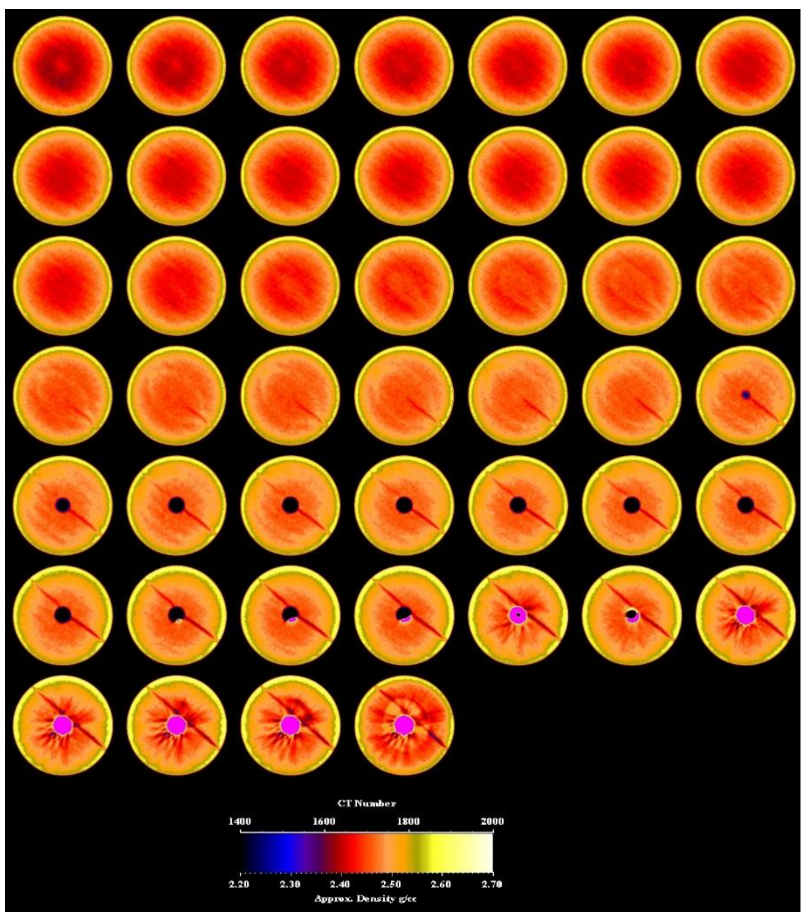

Figure 4.106 Fracture behavior seen in CT Scan (20% GLDA with Guar, Sample 2-19)

In this section, tests were performed to determine the effect of the type of fracturing fluid on the breakdown pressure of the tight sandstone rocks. The fluids used were brine, 25 ppt linear gel, 40 ppt linear gel, 25 ppt crosslinked gel and 40 ppt crosslinked gel. Each of these tests were performed thrice to prove the consistency. As a conformation, 20% GLDA with guar was also used. The post-test analysis conducted using CT Scan showed the fracture type, height and width. Table 4.12 summarizes the breakdown pressures of different fluids along with the type of fractures seen.

Table 4.12 Summary of the Breakdown Pressure tests

Fluid Type	**Viscosity @ 100 s^{-1} (cp)**	**Sample number**	**Fracture Characteristics**			**Breakdown pressure (psi)**
			Type[a]	**Height[b]**	**Width[c]**	
Brine (3% KCl)	1	2-21	Bi	1	2	553
		2-17	Bi	1	2	617
		2-14	Bi	1	1	538
Linear Gel (25 ppt)	45	2-7	Bi-1	2	2	1217
		2-4	Bi	3	-	1234
		2-3	S	2	1	1195
Linear Gel (40 ppt)	86	2-10	Bi-1	3	2	1322
		2-8	Bi	3	2	1295
		2-2	Bi	2	3	1290
20% GLDA with Guar	121	2-19	Bi-1	3	2	1490
Crosslinked Gel (25 ppt)	492	2-16	Bi	4	4	1734
		2-5	Bi	4	4	1656
		2-1	Bi	5	5	1700
Crosslinked Gel (40 ppt)	1451	2-11	Bi	4	4	1940
		2-9	Bi	4	4	2034
		2-13	S	4	2	1837

a- for fracture type: Bi stands for Bi-wing fracture, Bi-1 stands for Bi-wing fracture with 1 weak wing and S stands for single wing fracture. All fractures are along the bedding plane.
b- for fracture height: Range is set from 1 to 5. (Where 1 – very short – not exceeding bottomhole, 3 - moderate – exceeding bottomhole and 5 - full sample length)
c- for fracture width: Range is set from 1 to 5. (Where 1 – small, 3 – moderate and 5 – full fracture)

As seen in Table 4.12, the average breakdown pressure achieved by brine was 570 psi. The fractures created were Bi-wing with short height and small width. For the 25 ppt Linear Gel the average breakdown pressure was 1215 psi. Mostly short to moderate height, Bi-wing fractures with small width were produced. 40 ppt Linear Gel produced mostly Bi-wing fractures with moderate height and moderate width. The average breakdown pressure was 1302 psi. The breakdown pressure achieved by 20% GLDA with Guar was 1490 psi. The fracture was Bi-wing with 1 weak wing, moderate height and short to moderate width.

25 ppt Crosslinked Gel created fractures that were Bi-wing with mostly long height and mostly large width. The average breakdown pressure was 1700 psi. 40 ppt Crosslinked Gel also created Bi-wing fractures with long height and large width at an average breakdown pressure of 1937 psi. The fractures for all the fluid types were along the bedding plane.

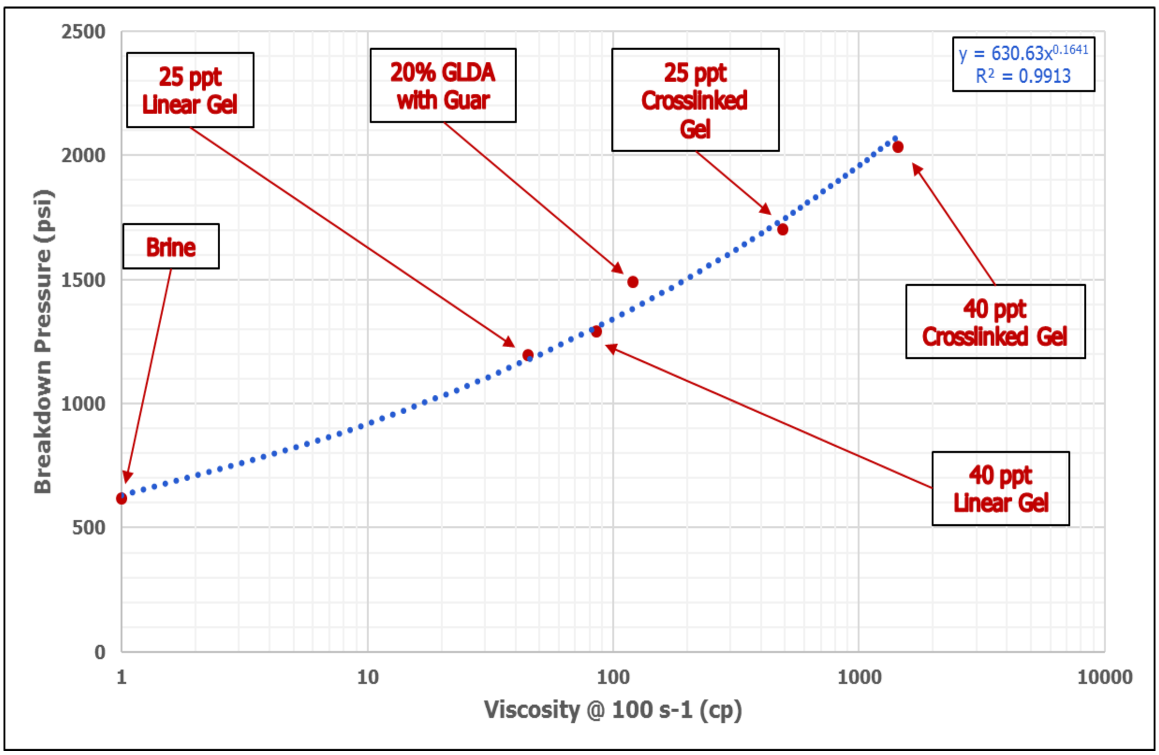

Figure 4.107 Effect of fracturing fluid viscosity on the breakdown pressure

Figure 4.107 shows the trend of the breakdown pressure vs viscosity @ 100 s^{-1}. Gomaa et al., (2014) found out that there is a strong power relation of fracturing fluid type with the breakdown pressure of Mancos shale outcrops in a similar study. In this study for Scioto tight sandstone outcrop, the breakdown pressure also has a strong power relation with the viscosity in tight sandstones. This confirms the dependence of the breakdown pressure with the type of fracturing fluid used.

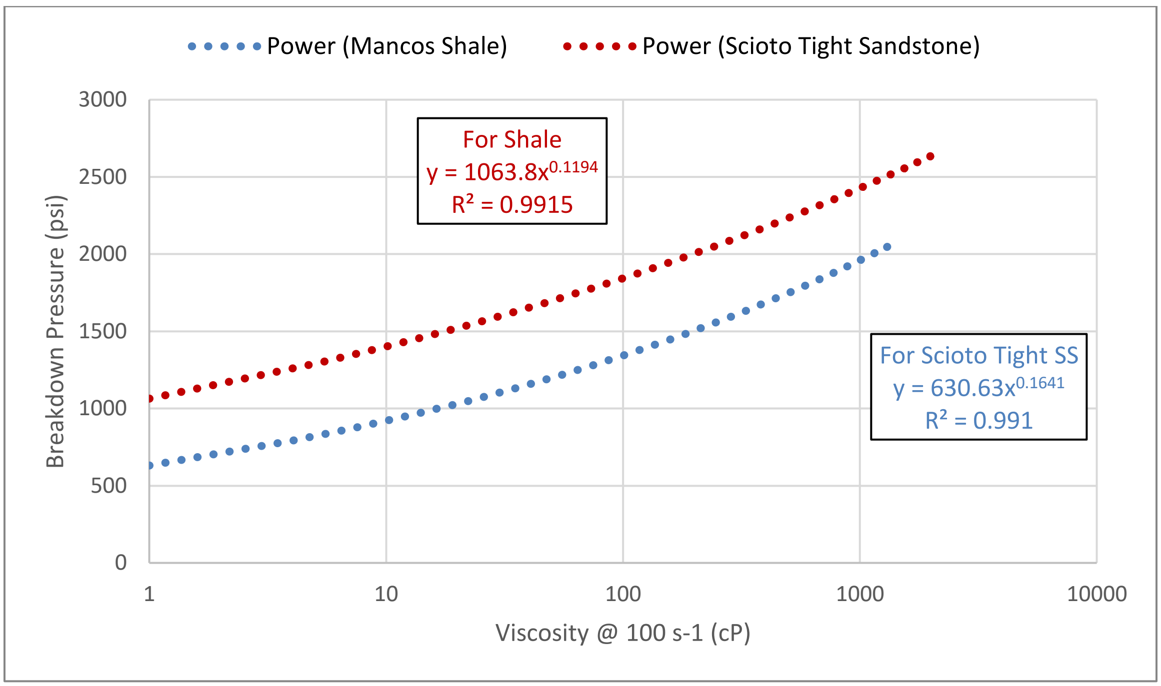

Figure 4.108 Validation with Mancos Shale Study (Gomaa et al., 2014)

A comparison has been made with the results from this study with the study of Gomaa et al., (2014). The trend is the same for both Mancos shale and Scioto tight sandstone (Figure 4.108.) It can be seen that the breakdown pressures of the Mancos shale cores are higher than that of the tight sandstone cores. This can be explained by either due to the difference in the geomechanical properties or the permeability-porosity of both rock types.

The tensile strength of the Mancos shales is much lower than that of Scioto sandstone (Lai, B. T et al., 2015). So the higher breakdown pressures in Mancos shale can be directly linked to its very tight nature. The permeability and porosity of the Mancos shale cores was 8-20 nD and 6.6% whereas for the sandstone cores 1.3 mD and 14.8% respectively.

4.5.2 Effect of the saturating fluid in the breakdown pressure

The sensitivity analysis on the breakdown pressure was done by using saturated samples. Sample 2-12 was saturated with brine (3% KCl) and sample 2-15 was saturated with oil. The fracturing fluid used in this study was 25 ppt Linear Gel.

1. Brine Saturated (Sample 2-12)

The pressure increases in the same manner as in dry samples (Figure 4.109), but the test is shorter and the breakdown pressure (752 psi) was much lower than that of the dry sample. The fracture produced was only a single wing fracture, but a small fracture opposite to it can be seen in Figures 4.110 and 4.111. This could occur due to some structural defects in the borehole. These structural defects are enhanced by the fluid saturation, making them even more weaker. As a result, the pressure will be concentrated at that point and would only create a fracture in that direction. The fracture is of moderate height and width and along the direction of the bedding plane.

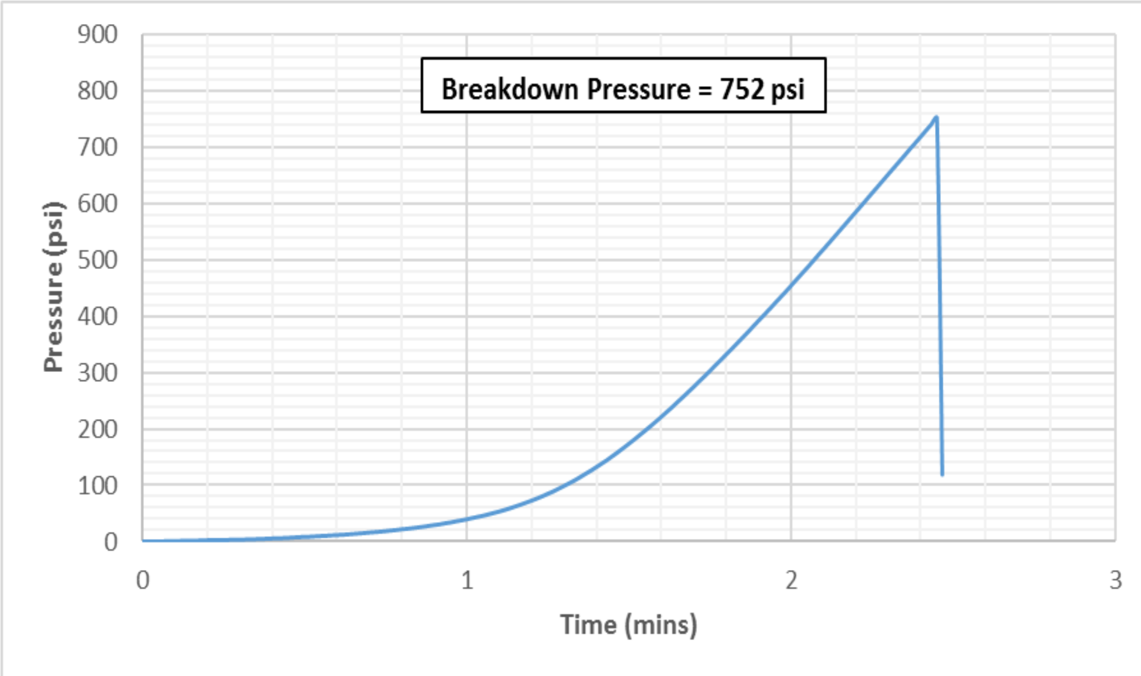

Figure 4.109 Breakdown Pressure curve (25 ppt Linear Gel, Brine Saturated Sample 2-12)

Figure 4.110 Fracture behavior (25 ppt Linear Gel, Brine Saturated Sample 2-12)

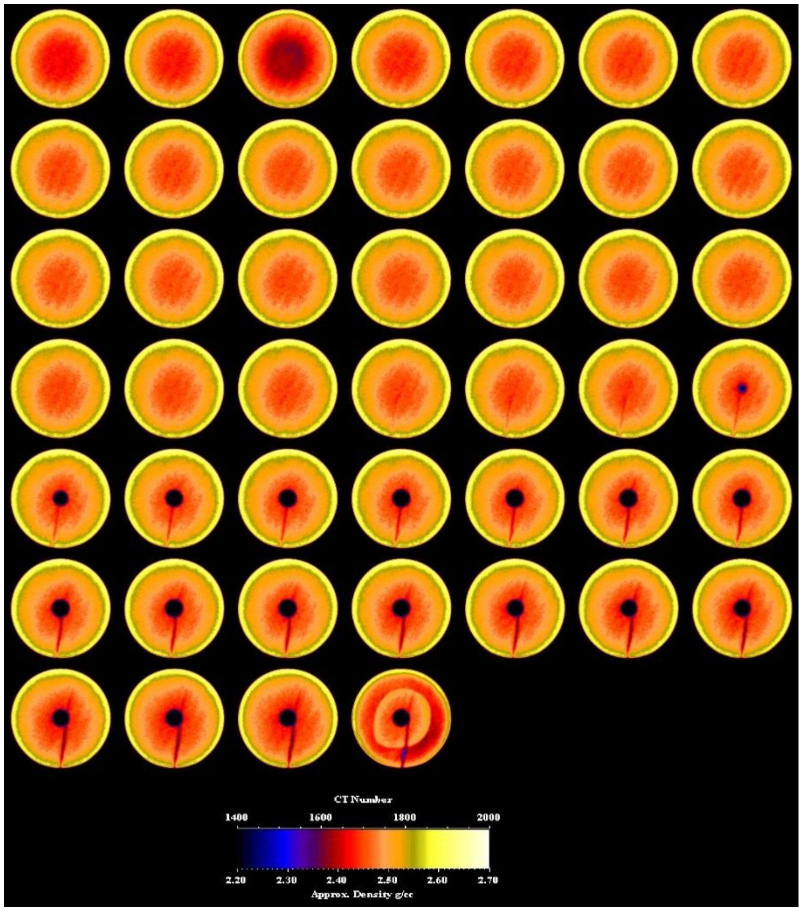

Figure 4.111 Fracture behavior seen in CT Scan (25 ppt Linear Gel, Brine Saturated Sample 2-12)

2. Oil Saturated (Sample 2-15)

Sample 2-15 was only partially saturated (porosity by weight difference was 9.2%). The pressure increases in the same manner as in dry samples and the brine saturated sample (Figure 4.112). The breakdown pressure was 1112 psi which was lower than that of the dry sample but higher than brine saturated sample.

The fracture produced was only a single wing fracture as seen in Figures 4.113 and 4.114. Both the fracture height and width were small.

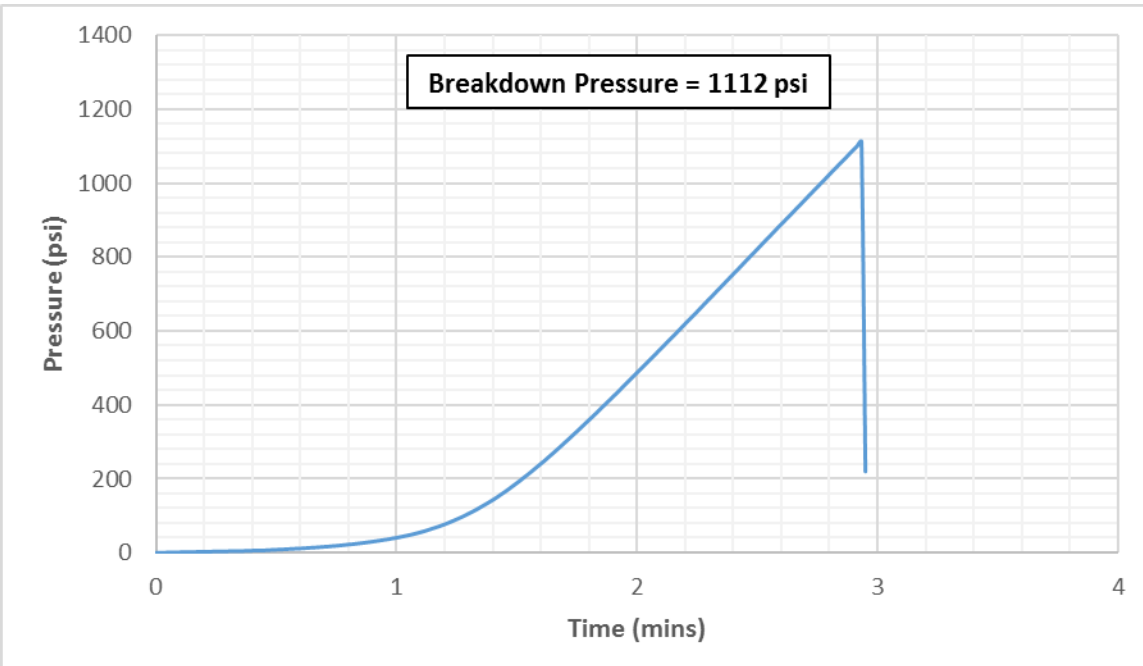

Figure 4.112 Breakdown Pressure curve (25 ppt Linear Gel, Oil Saturated Sample 2-15)

Figure 4.113 Fracture behavior (25 ppt Linear Gel, Oil Saturated Sample 2-15)

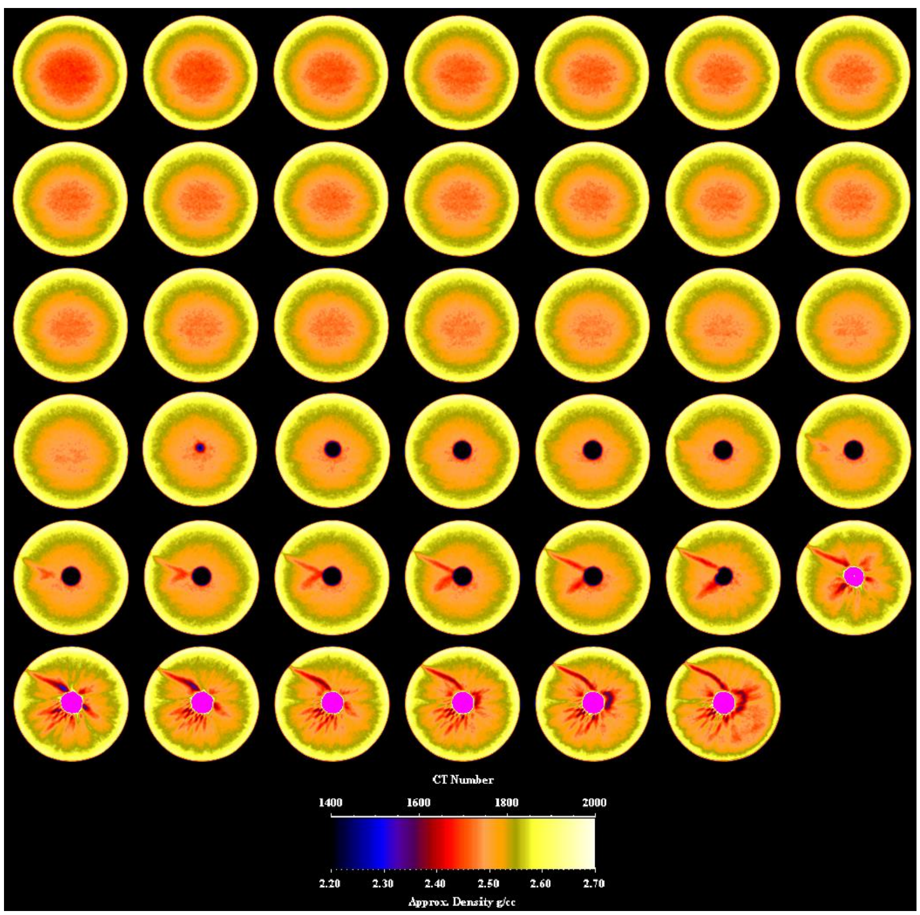

Figure 4.114 Fracture behavior seen in CT Scan (25 ppt Linear Gel, Oil Saturated Sample 2-15)

In this section, tests were performed to determine the effect of the type of saturating fluid on the breakdown pressure of the tight sandstone rocks. The saturating fluids used were oil and Brine (3% KCl). The fracturing fluid used was 25 ppt Linear Gel.

Table 4.13 quantifies the percentage of decrease in the breakdown pressure and Figure 4.115 graphically depicts it. Figure 4.116 shows the reduction in the breakdown pressure due to different saturating fluids. These values are in agreement with the geomechanical tests (Figure 4.117).

Table 4.13 Effect of saturating fluid on the breakdown pressure

Saturation	**Breakdown Pressure (psi)**	**Percentage difference**
Dry	Average - 1215	-
Brine	752	**(-) 38%**
Oil (partial)	1112	**(-) 8%**

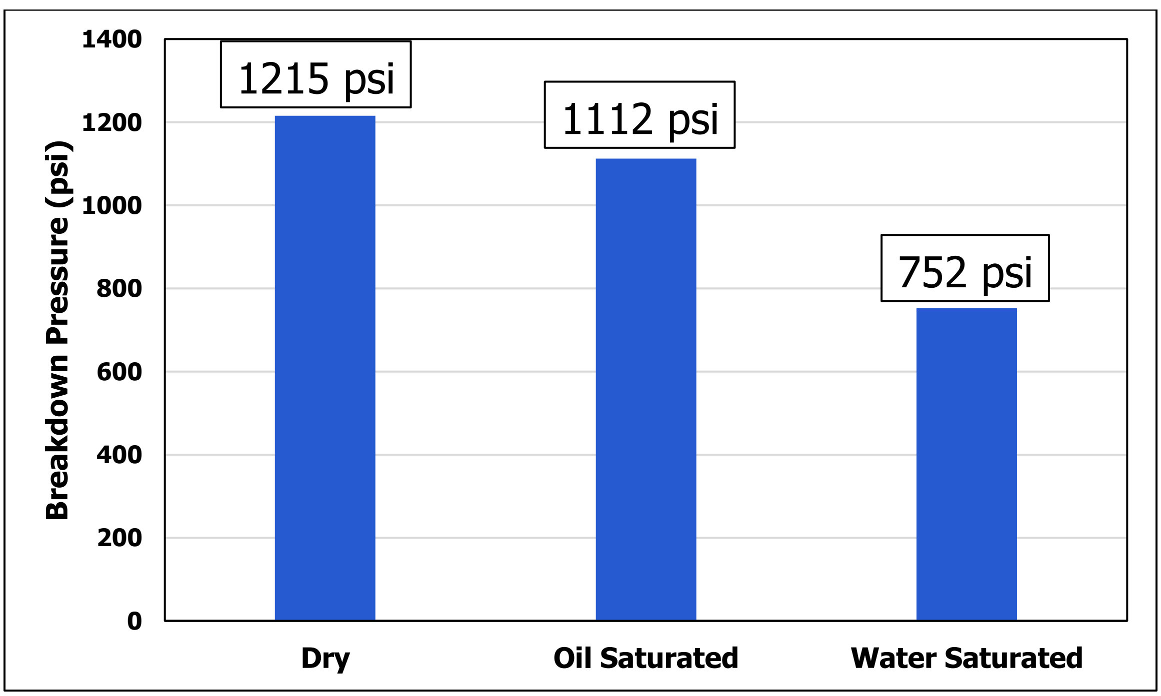

Figure 4.115 Reduction in the breakdown pressure due to fluid saturation

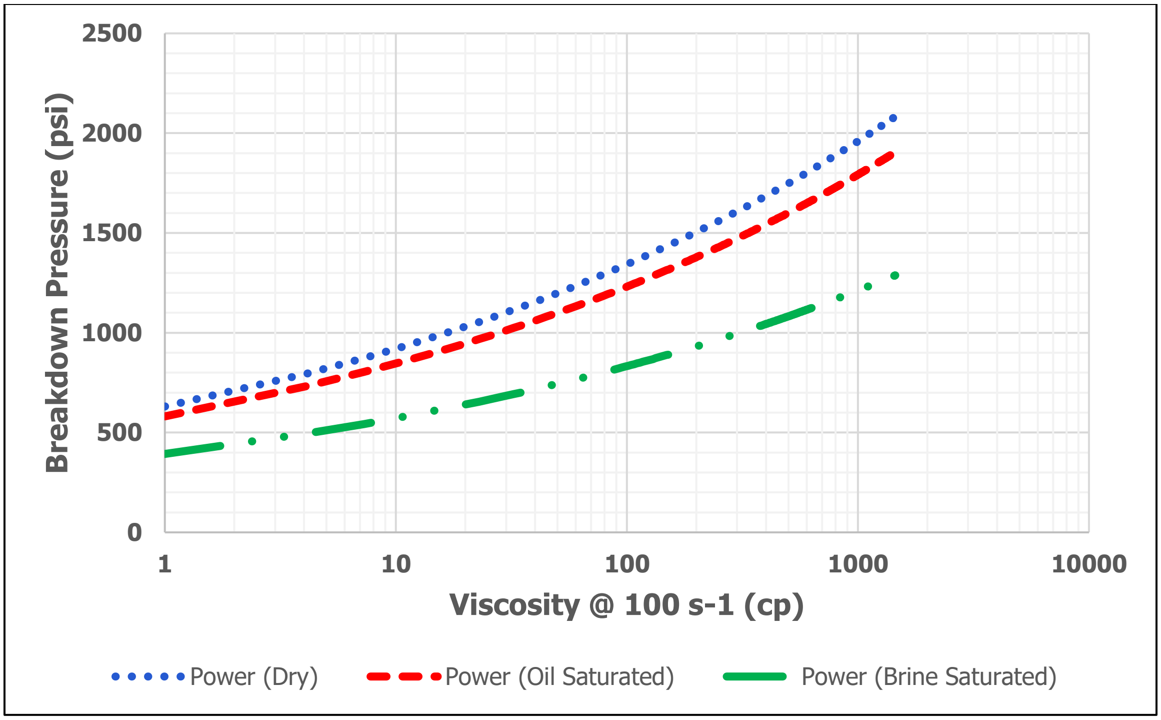

Figure 4.116 Effect of Saturating fluid on the breakdown pressure

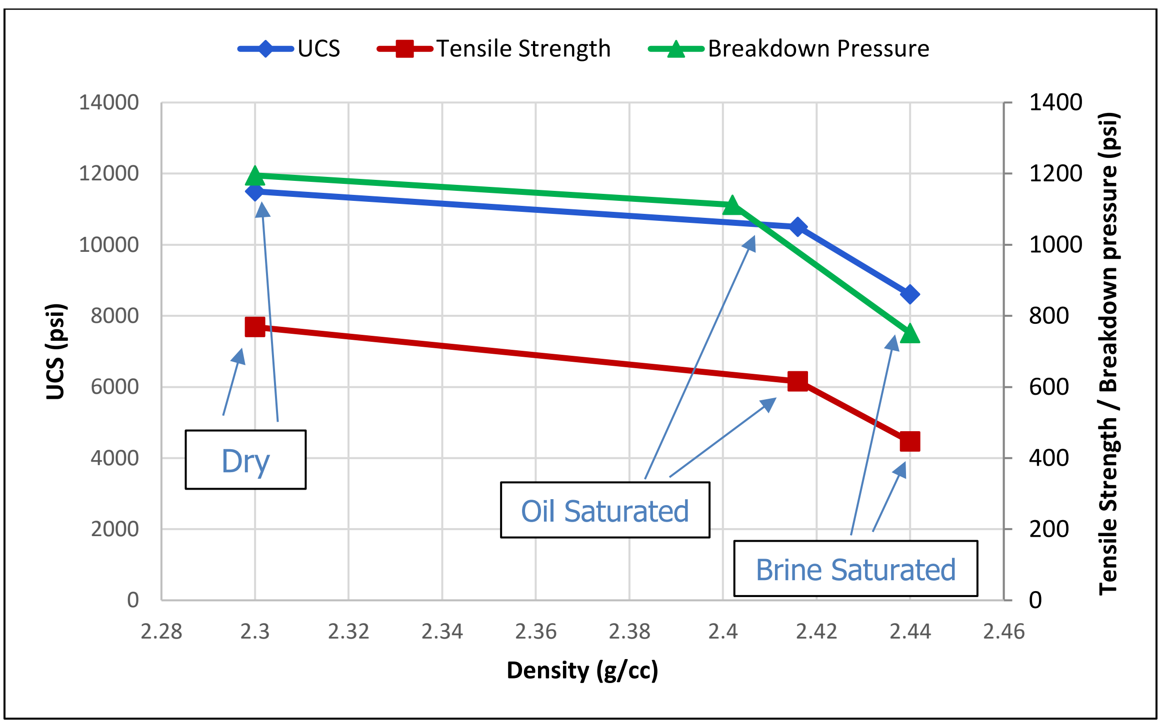

Figure 4.117 Reduction in the strength of the rock due to increasing bulk density

CHAPTER 5

CONCLUSIONS AND RECOMMENDATIONS

The objective of this thesis was to study the effect of fracturing fluid on the breakdown pressure of tight sandstone rocks. The conclusions and recommendations from this thesis are mentioned in this chapter.

5.1 Conclusions

The following conclusions are drawn from this thesis:

1. Studying the effect of saturating fluid on the geomechanical properties revealed that brine (3% KCl) saturated samples became significantly weaker. Oil saturated samples became moderately weaker. This behavior is witnessed due to the physico-chemical interactions between the grains of the sample and the fluid in the pores and the effective stress created by the fluid.
2. Breakdown pressure determination test setup was developed and the effect of fracturing fluid on the breakdown pressure was studied. A strong power relation between the viscosity and breakdown pressure was seen. This relation is in

agreement with some of the previous work in the literature. It was also seen that as the viscosity increases, the fracture width and height increased. For most tests, the fractures created were bi-wing fractures. Some single wing fractures were created due to deformities in the borehole.

3. The effect of the saturating fluids on the breakdown pressure was also studied. It was seen that the saturating fluids reduced the breakdown pressure. For partially saturated oil samples the breakdown pressure was reduced by 9% and for the brine saturated sample, the reduction was 43%. The reduction in these values are in agreement with the Brazilian tensile test results.

5.2 Recommendations for Future work

The work can be further extended on the following areas:

1. This thesis considers samples which are either dry or fully saturated. Further study can be performed on samples with intermediate saturations.
2. Elaboration of this study can be done by studying these effects on lower permeability sandstones, carbonates and shales.
3. Acoustic Emission can be applied since it is considered as a strong tool to determine the deformation, fracture initiation and fracture propagation.

References

Anderson, R.L., Ratcliffe, I., Greenwell, H.C., Williams, P.A., Cliffe, S., Coveney, P.V., 2010. Clay swelling — A challenge in the oilfield. Earth-Science Rev. 98, 201–216. https://doi.org/10.1016/j.earscirev.2009.11.003

Arthur, J.D., Bohm, B.K., Coughlin, B.J., Layne, M.A., Cornue, D., 2009. Evaluating the Environmental Implications of Hydraulic Fracturing in Shale Gas Reservoirs, in: SPE Americas E&P Environmental and Safety Conference. Society of Petroleum Engineers. https://doi.org/10.2118/121038-MS

Bennion, D.B., Thomas, F.B., Schulmeister, B.E., Sumani, M., 2004. Determination of True Effective In Situ Gas Permeability in Subnormally Water-Saturated Tight Gas Reservoirs. J. Can. Pet. Technol. 43. https://doi.org/10.2118/04-10-02

Brenne, S., Molenda, M., Stockhert, F., Alber, M., 2013. Hydraulic and Sleeve Fracturing Laboratory Experiments on 6 Rock Types, in: Effective and Sustainable Hydraulic Fracturing. InTech. https://doi.org/10.5772/56301

Brignoli, M., Santarelli, F., Papamichos, E., 1995. Capillary effects in sedimentary rocks: Application to reservoir water-flooding. American Rock Mechanics Association.

Burke, L.H., Nevison, G.W., Peters, W.E., 2011. Improved Unconventional Gas Recovery With Energized Fracturing Fluids: Montney Example, in: SPE Eastern Regional Meeting. Society of Petroleum Engineers. https://doi.org/10.2118/149344-MS

Cassidy, J.M., Kiser, C., Tucker, R., 2011. Corrosion-Inhibitor Design for Compatibility with Acid-Gelling Polymers, in: SPE International Symposium on Oilfield Chemistry. Society of Petroleum Engineers. https://doi.org/10.2118/141435-MS

Conway, M.W., Almond, S.W., Briscoe, J.E., Harris, L.E., 1983. Chemical Model for the Rheological Behavior of Crosslinked Fluid Systems. J. Pet. Technol. 35, 315–320. https://doi.org/10.2118/9334-PA

Coskuner, G., 2006. Completion Operations in Low Permeability Deep Basin Gas Reservoirs: To Use or Not to Use Aqueous Fluids, That is the Question. J. Can. Pet. Technol. 45. https://doi.org/10.2118/06-10-01

Dehghan, A.N., Goshtasbi, K., Ahangari, K., Jin, Y., 2016. Mechanism of fracture initiation and propagation using a tri-axial hydraulic fracturing test system in naturally fractured reservoirs. Eur. J. Environ. Civ. Eng. 20, 560–585. https://doi.org/10.1080/19648189.2015.1056384

Detournay, E., Carbonell, R., 1997. Fracture-Mechanics Analysis of the Breakdown Process in Minifracture or Leakoff Test. SPE Prod. Facil. 12, 195–199. https://doi.org/10.2118/28076-PA

DeVilbiss, J.W., 1984. Some effects of pore fluids on dispersion and absorption of viscoelastic waves, in: SEG Technical Program Expanded Abstracts 1984. Society of Exploration Geophysicists, pp. 347–350. https://doi.org/10.1190/1.1894012

M. Duda, J. Renner; The weakening effect of water on the brittle failure strength of sandstone, Geophysical Journal International, Volume 192, Issue 3, 1 March 2013, Pages 1091–1108, EIA, 2017. Energy Information Administration [WWW Document]. URL https://www.eia.gov/

Fabricius, I.L., Eberli, G.P., 2009. Dispersion of elastic waves in carbonate rocks., in: SEG Technical Program Expanded Abstracts 2009. Society of Exploration Geophysicists, pp. 1955–1959. https://doi.org/10.1190/1.3255238

Fink, J., 2013. Hydraulic Fracturing Chemicals and Fluids Technology, 1st Editio. ed.

Fjaer, E., Holt, R.M., Horsrud, P., 2008. Petroleum related rock mechanics, Second Edi. ed.

Fortin, J., Stanchits, S., 2015. What Can we Learn from Ultrasonic Velocities Monitoring During Hydraulic Fracturing of a Tight Shale. American Rock Mechanics Association.

Friehauf, K.E., Sharma, M.M., 2009. A New Compositional Model for Hydraulic Fracturing With Energized Fluids. SPE Prod. Oper. 24, 562–572. https://doi.org/10.2118/115750-PA

Gandossi, L., Von Estorff, U., 2015. An overview of hydraulic fracturing and other formation stimulation technologies for shale gas production. JRC Sci. Hub. https://doi.org/10.2790/379646

Gomaa, A.M., Qu, Q., Nelson, S., Maharidge, R., 2014. New Insights into Shale Fracturing Treatment Design, in: SPE/EAGE European Unconventional Resources Conference and Exhibition. Society of Petroleum Engineers. https://doi.org/10.2118/167754-MS

Gunawan, H., Susanto, H., Widyantoro, B., Noguera, J.A., 2012. Fracture Assisted Sandstone Acidizing, Alternative Approach To Increase Production in Tight Sandstone Reservoir, in: SPE Oil and Gas India Conference and Exhibition. Society of Petroleum Engineers. https://doi.org/10.2118/154947-MS

Gupta, D.V.S., 2009. Unconventional Fracturing Fluids for Tight Gas Reservoirs, in: SPE Hydraulic Fracturing Technology Conference. Society of Petroleum Engineers. https://doi.org/10.2118/119424-MS

Harris, P.C., 1988. Fracturing-Fluid Additives. J. Pet. Technol.

Hawkins, A.B., McConnell, B.J., 1992. Sensitivity of sandstone strength and deformability to changes in moisture content. Q. J. Eng. Geol. Hydrogeol. 25, 115–130. https://doi.org/10.1144/GSL.QJEG.1992.025.02.05

Hawsey, J.D., Jacocks, C.L., 1961. The Use Of Fluid-Loss Additives In Hydraulic Fracturing Of Oil And Gas Wells, in: SPE California Regional Meeting. Society of Petroleum Engineers. https://doi.org/10.2118/244-MS

Hayton, S., Heine, C., Gratto, B.E., 2010. Tight Gas Exploration in Saudi Arabia, in: SPE Deep Gas Conference and Exhibition. Society of Petroleum Engineers. https://doi.org/10.2118/131065-MS

Holditch, S.A., 2006. Tight Gas Sands. J. Pet. Technol. 58, 86–93. https://doi.org/10.2118/103356-JPT

Howard, G.C., Fast, C.R., 1970. Hydraulic fracturing. Society of Petroleum Engineers.

Jones, J.R., Britt, L.K., 2009. Design and Appraisal of Hydraulic Fractures. Society of Petroleum Engineers.

Kennedy, R.L., Gupta, R., Kotov, S.V., Burton, W.A., Knecht, W.N., Ahmed, U., 2012. Optimized Shale Resource Development: Proper Placement of Wells and Hydraulic Fracture Stages, in: Abu Dhabi International Petroleum Conference and Exhibition. Society of Petroleum Engineers. https://doi.org/10.2118/162534-MS

King, G.E., 2012. Hydraulic Fracturing 101: What Every Representative, Environmentalist, Regulator, Reporter, Investor, University Researcher, Neighbor, and Engineer Should Know About Hydraulic Fracturing Risk. J. Pet. Technol. 64, 34–42. https://doi.org/10.2118/0412-0034-JPT

Labuz, J.F., Berger, D.J., 1991. Moisture effects and the mechanical response of granite beams. Int. J. Rock Mech. Min. Sci. Geomech. Abstr. 28, A339. https://doi.org/10.1016/0148-9062(91)91195-W

Lashkaripour, G.R., Ajalloeian, R., 2000. The Effect Of Water Content On The Mechanical Behaviour Of Fine-Grained Sedimentary Rocks. International Society for Rock Mechanics.

Lai, B. T., Li, H., Liu, H. H., Zhang, J. L., & Georgi, D. (2015, November 9). Brazilian Tensile Strength Test of Orgainc-rich Shale. Society of Petroleum Engineers. doi:10.2118/177644-MS

Li, G., Lorwongngam, A., Roegiers, J.C., 2009. Critical Review Of Leak-Off Test As A Practice For Determination Of In-Situ Stresses. American Rock Mechanics

Association.

Mahmoud, M. A., Nasr-El-Din, H. A., & DeWolf, C. A. (2011, January 1). Removing Formation Damage and Stimulation of Deep Illitic-Sandstone Reservoirs Using Green Fluids. Society of Petroleum Engineers. doi:10.2118/147395-MS

Perera, M.S.A., Ranjith, P.G., Peter, M., 2011. Effects of saturation medium and pressure on strength parameters of Latrobe Valley brown coal: Carbon dioxide, water and nitrogen saturations. Energy 36, 6941–6947. https://doi.org/10.1016/j.energy.2011.09.026

Propublica. Hydraulic Fracturing. [URL] https://www.propublica.org/

Postler, D.P., 1997. Pressure Integrity Test Interpretation, in: SPE/IADC Drilling Conference. Society of Petroleum Engineers. https://doi.org/10.2118/37589-MS

Pye, D.S., Smith, W.A., 1973. Fluid Loss Additive Seriously Reduces Fracture Proppant Conductivity and Formation Permeability, in: Fall Meeting of the Society of Petroleum Engineers of AIME. Society of Petroleum Engineers. https://doi.org/10.2118/4680-MS

Samuel, M., Card, R.J., Nelson, E.B., Brown, J.E., Vinod, P.S., Temple, H.L., Qu, Q., Fu, D.K., 1997. Polymer-Free Fluid for Hydraulic Fracturing, in: SPE Annual Technical Conference and Exhibition. Society of Petroleum Engineers. https://doi.org/10.2118/38622-MS

Syfan, F.E., Palisch, T.T., Dawson, J.C., 2013. 65 Years of Fracturing Experience: The

Key To Better Productivity Is Not What We Have Learned, But What We Have Forgotten and Failed To Utilize!, in: SPE Annual Technical Conference and Exhibition. Society of Petroleum Engineers. https://doi.org/10.2118/166107-MS

Vasarhelyi, B., 2003. Some observations regarding the strength and deformability of sandstones in dry and saturated conditions. Bull. Eng. Geol. Environ. 62, 245–249. https://doi.org/10.1007/s10064-002-0186-x

Warpinski, N.R., 1991. Hydraulic Fracturing in Tight, Fissured Media. J. Pet. Technol. 43, 146–209. https://doi.org/10.2118/20154-PA

Widarsono, B., Wong, P.M., Saptono, F., 2001. Estimation of Rock Dynamic Elastic Property Profiles through a Combination of Soft Computing, Acoustic Velocity Modeling, and Laboratory Dynamic Test on Core Samples, in: Proceedings of SPE Asia Pacific Oil and Gas Conference and Exhibition. Society of Petroleum Engineers. https://doi.org/10.2523/68712-MS

Wong, L.N.Y., Maruvanchery, V., Liu, G., 2016. Water effects on rock strength and stiffness degradation. Acta Geotech. 11, 713–737. https://doi.org/10.1007/s11440-015-0407-7

Yagiz, S., Rostami, J., 2012. Indentation test for the measurement of rock brittleness. American Rock Mechanics Association.

Yu, M., Nasr-El-Din, H.A., 2009. Quantitative Analysis of Viscoelastic Surfactants, in: SPE International Symposium on Oilfield Chemistry. Society of Petroleum Engineers. https://doi.org/10.2118/121715-MS

Zeng, Z., Roegiers, J.-C., 2002. Experimental Observation of Injection Rate Influence on the Hydraulic Fracturing Behavior of a Tight Gas Sandstone, in: SPE/ISRM Rock Mechanics Conference. Society of Petroleum Engineers. https://doi.org/10.2118/78172-MS

Zoback, M.D., 2010. Reservoir Geomechanics. Cambridge University Press, Cambridge, pp. xi–xiv. https://doi.org/10.1017/CBO9780511586477.001

Appendix A

CT Scan of samples from fracture test group

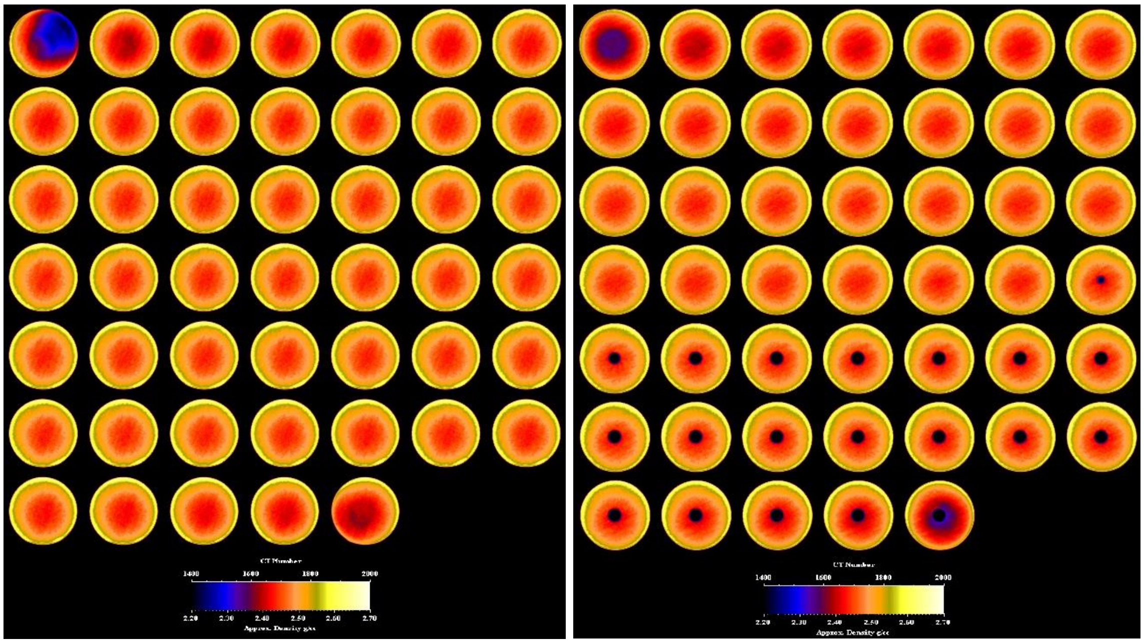

Figure A. 1 CT Scan of Sample 2-1 (before and after drilling)

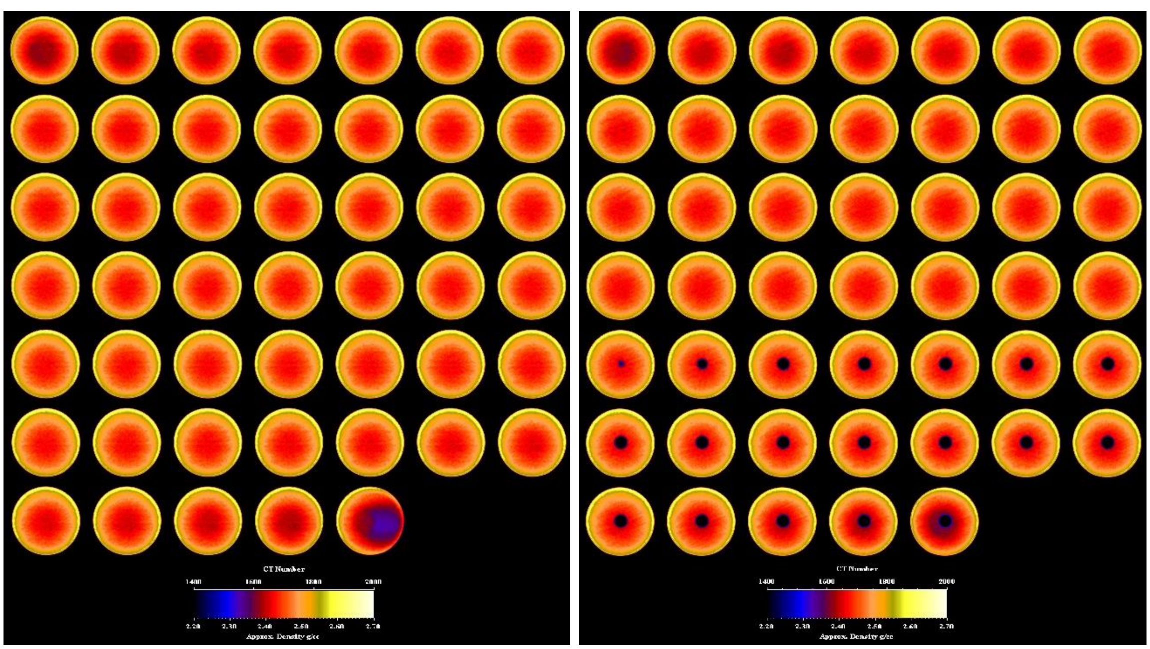

Figure A. 2 CT Scan of Sample 2-2 (before and after drilling)

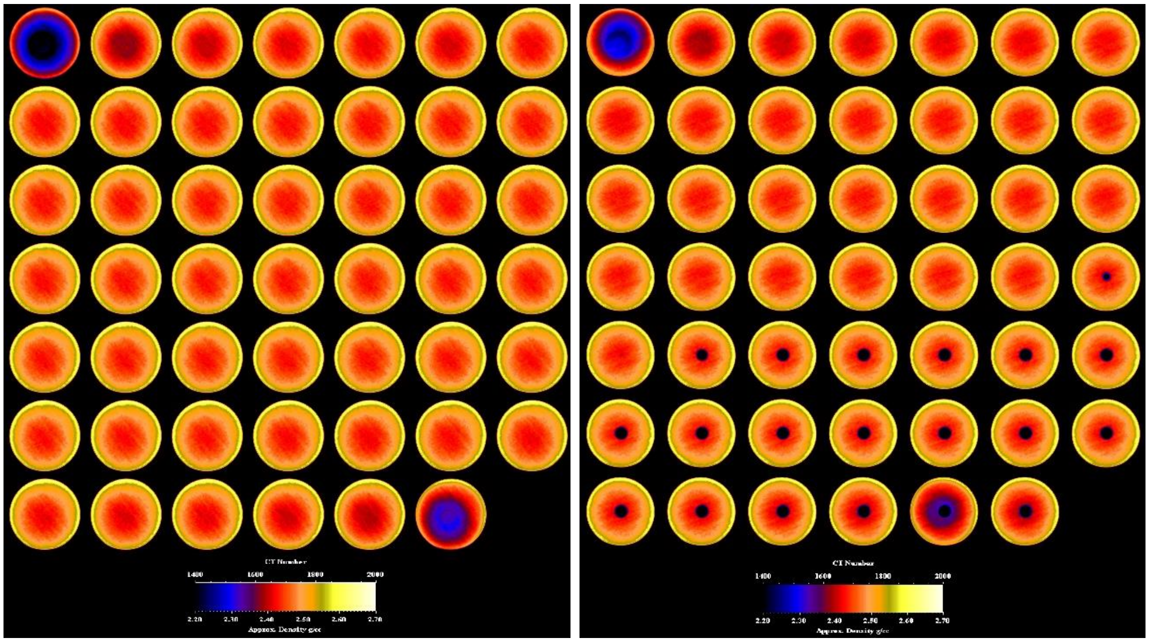

Figure A. 3 CT Scan of Sample 2-3 (before and after drilling)

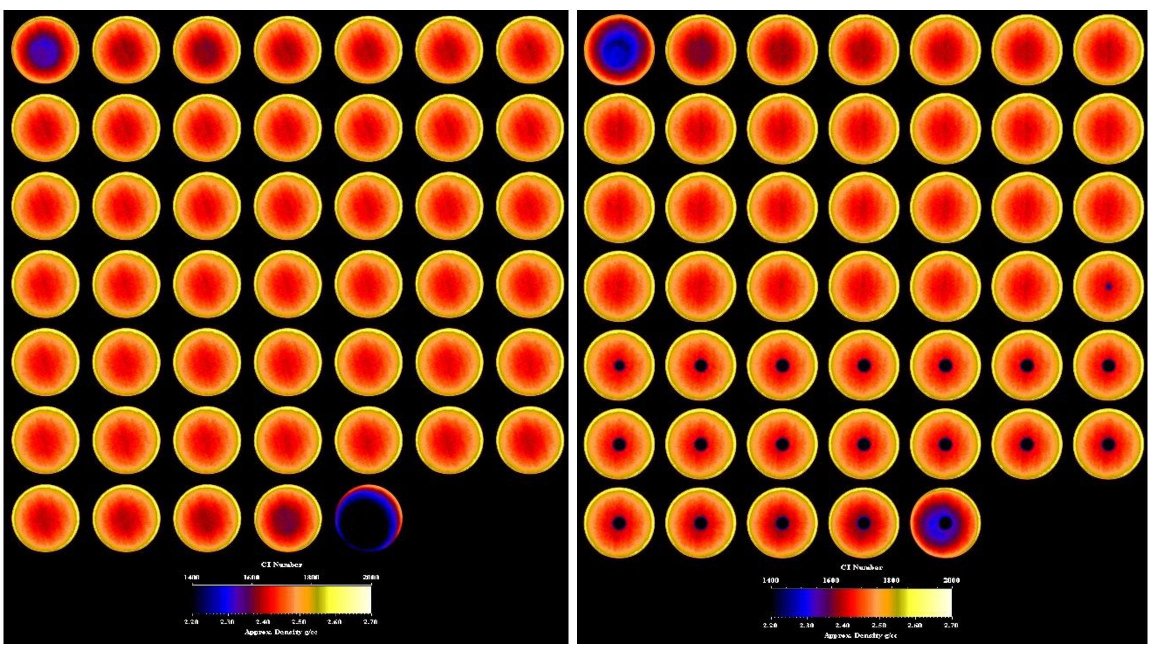

Figure A. 4 CT Scan of Sample 2-4 (before and after drilling)

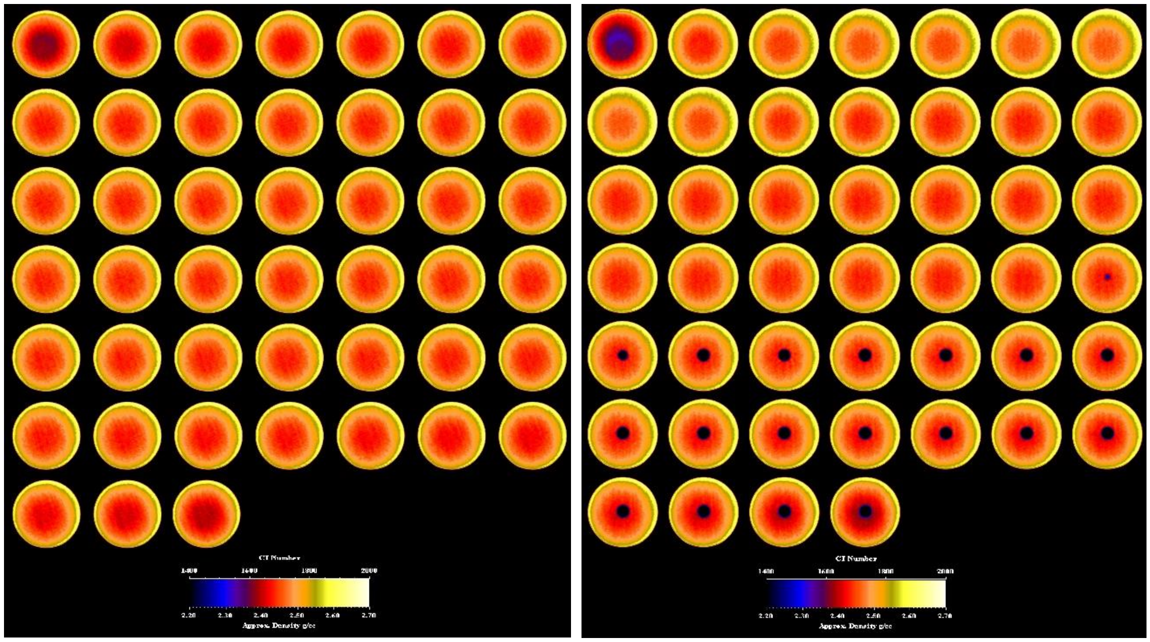

Figure A. 5 CT Scan of Sample 2-5 (before and after drilling)

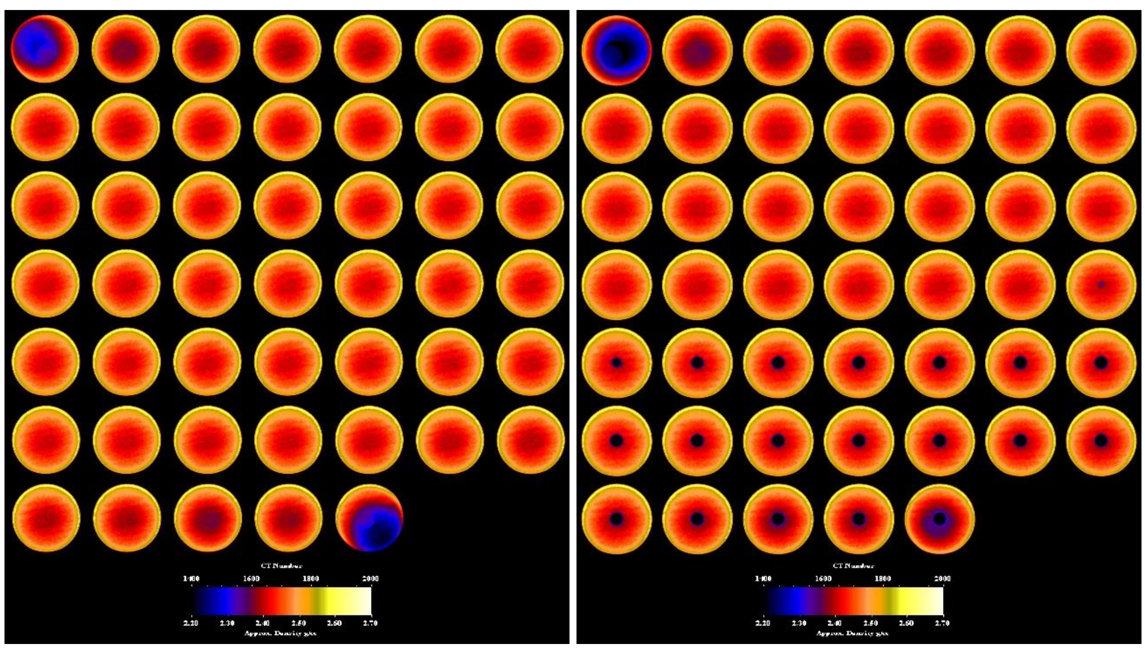

Figure A. 6 CT Scan of Sample 2-7 (before and after drilling)

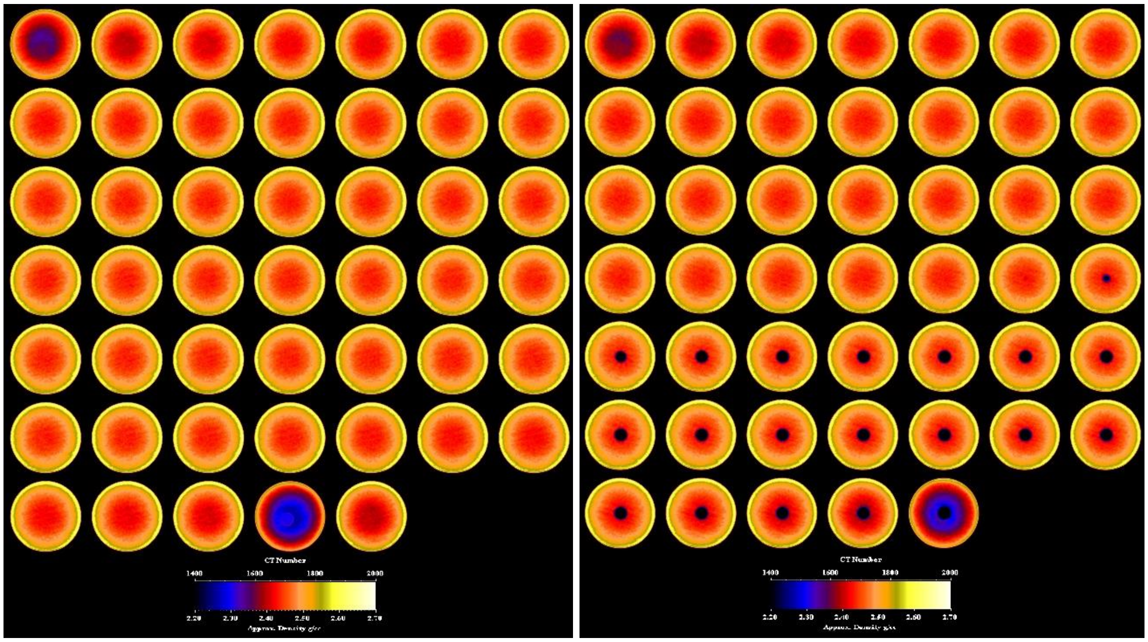

Figure A. 7 CT Scan of Sample 2-8 (before and after drilling)

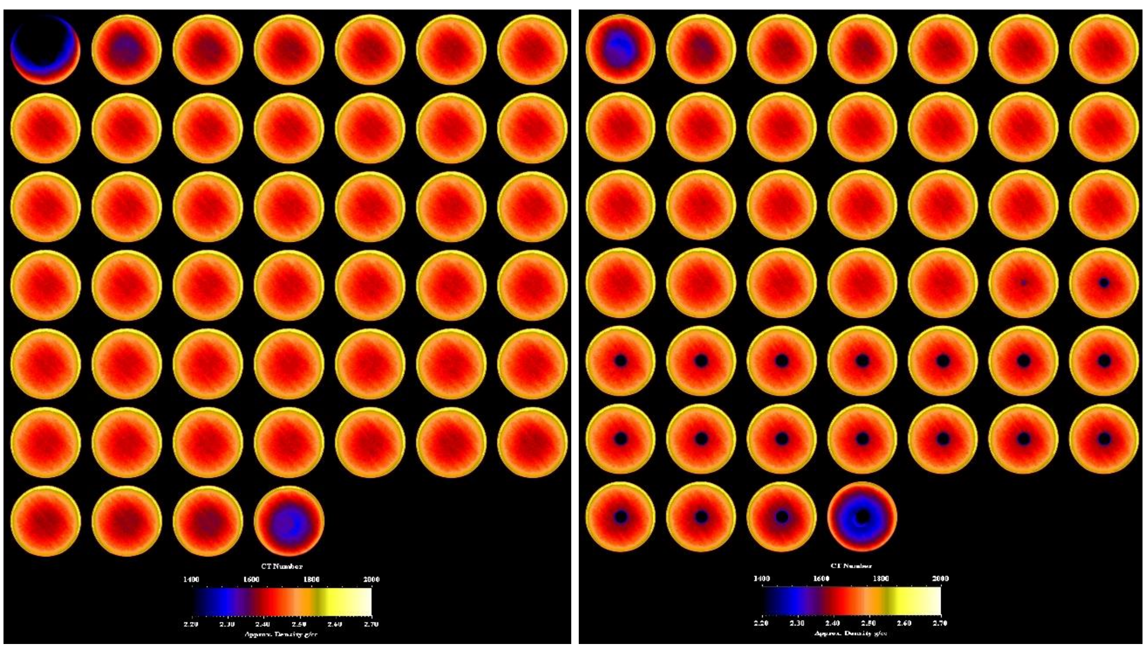

Figure A. 8 CT Scan of Sample 2-9 (before and after drilling)

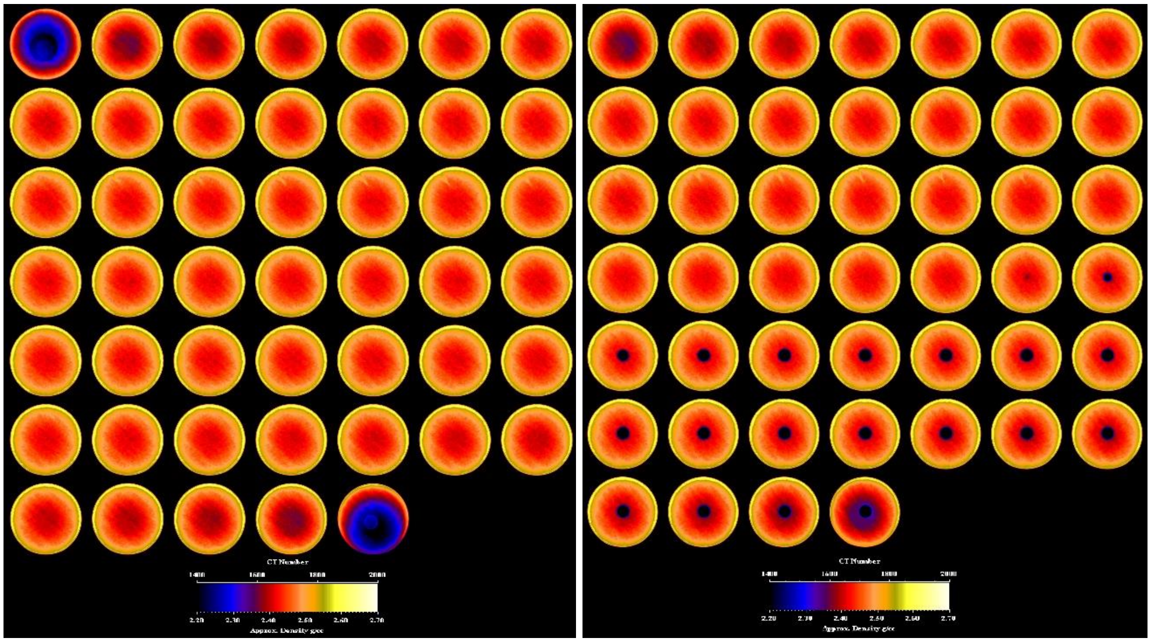

Figure A. 9 CT Scan of Sample 2-10 (before and after drilling)

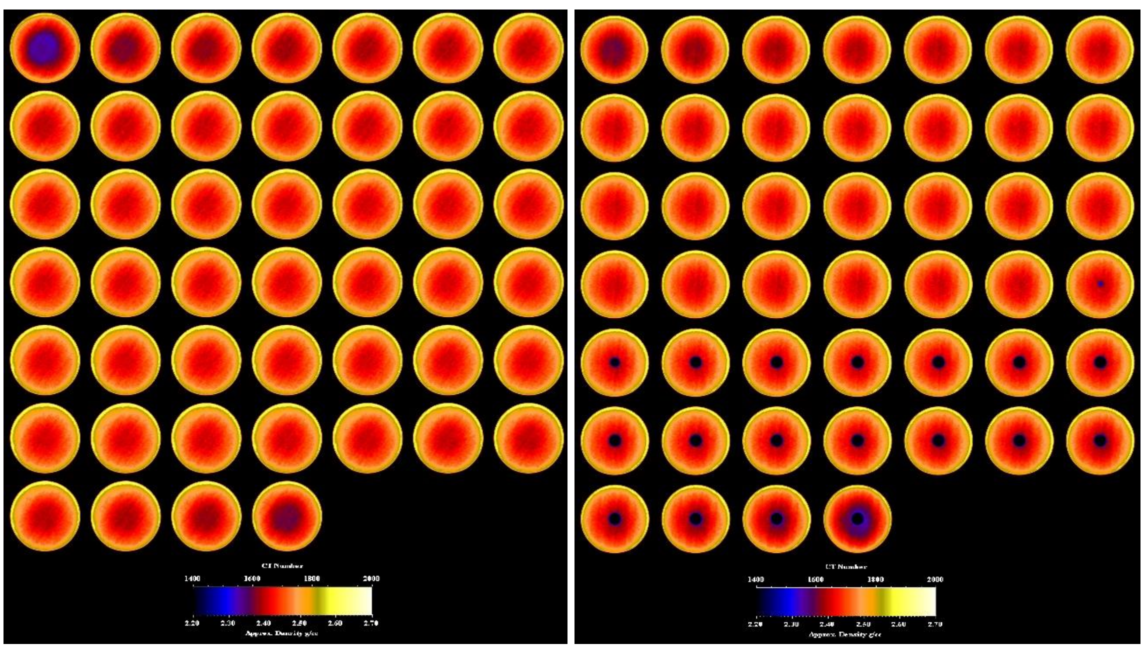

Figure A. 10 CT Scan of Sample 2-11 (before and after drilling)

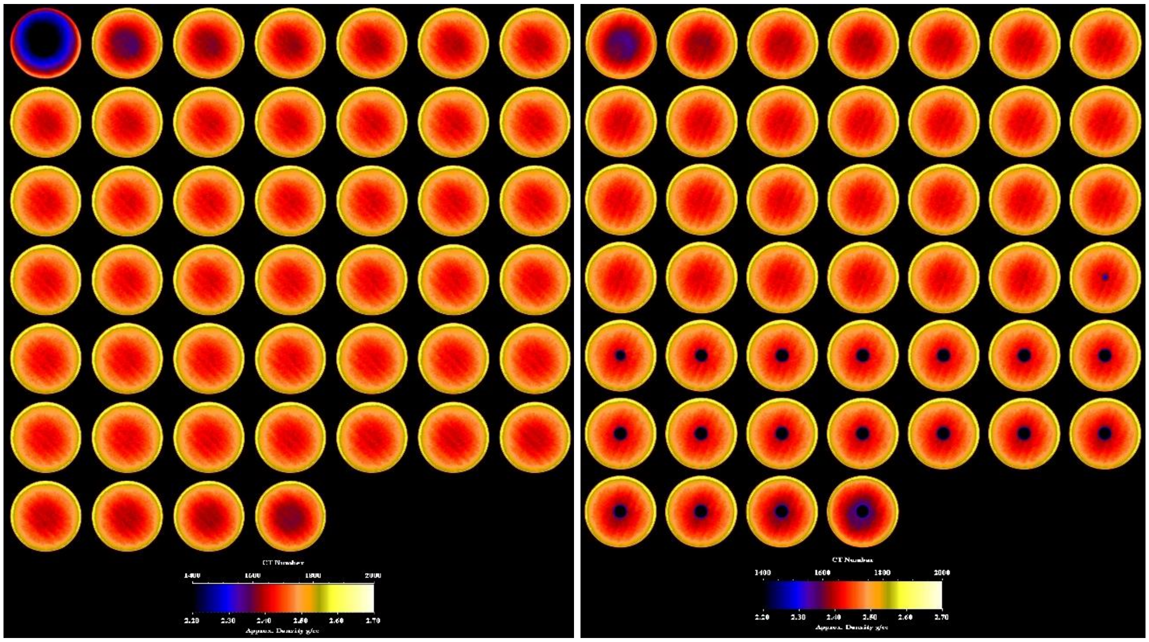

Figure A. 11 CT Scan of Sample 2-12 (before and after drilling)

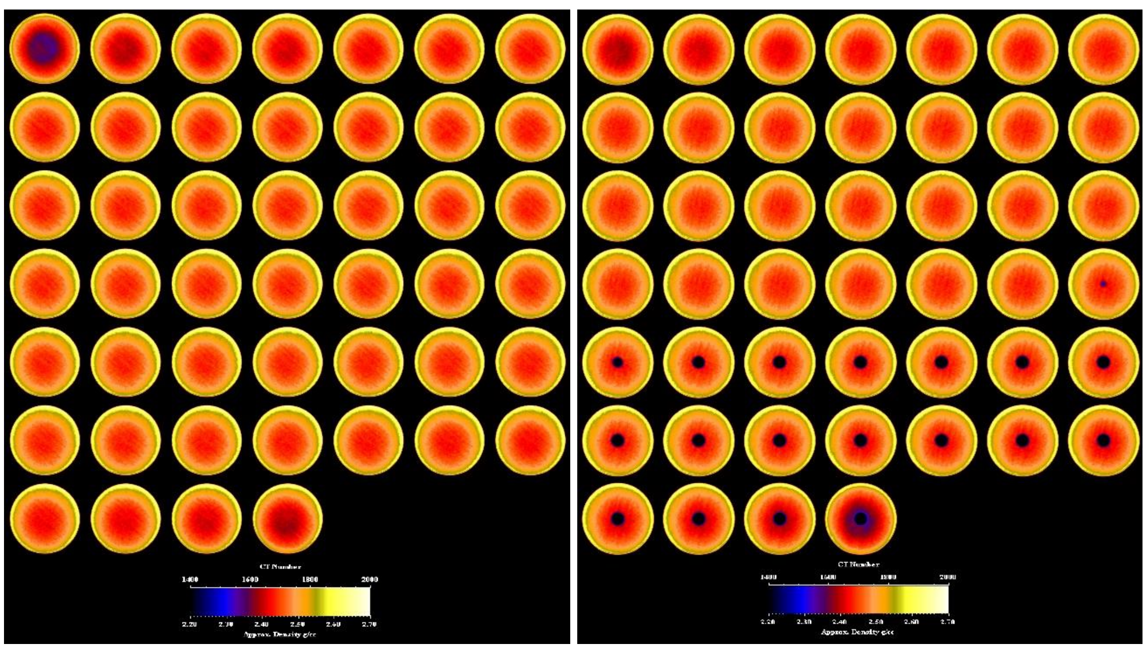

Figure A. 12 CT Scan of Sample 2-13 (before and after drilling)

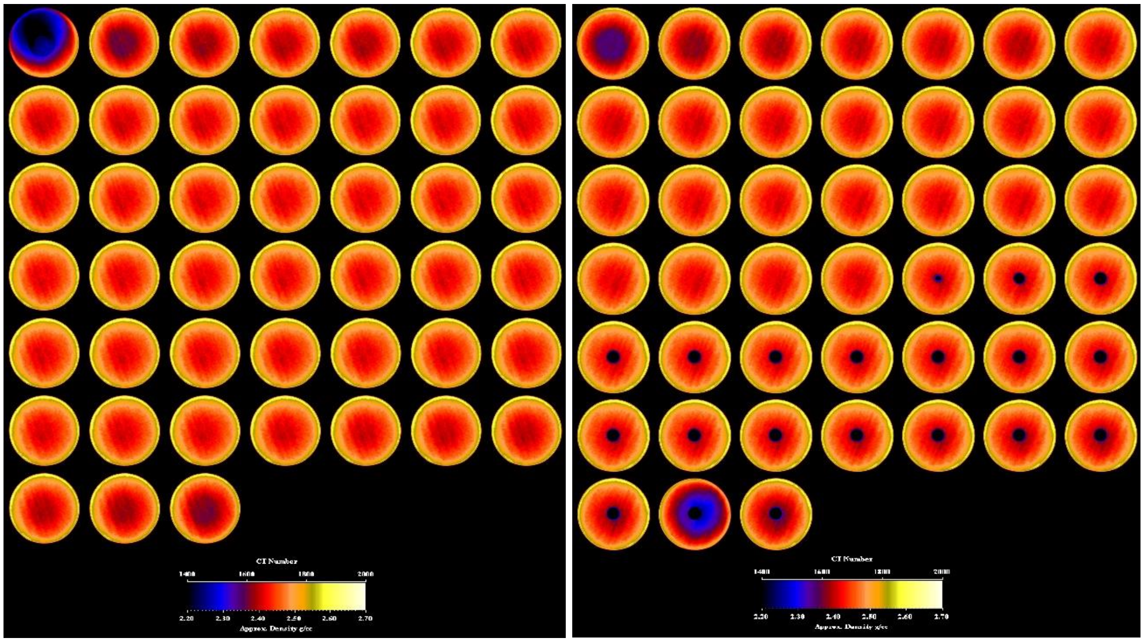

Figure A. 13 CT Scan of Sample 2-14 (before and after drilling)

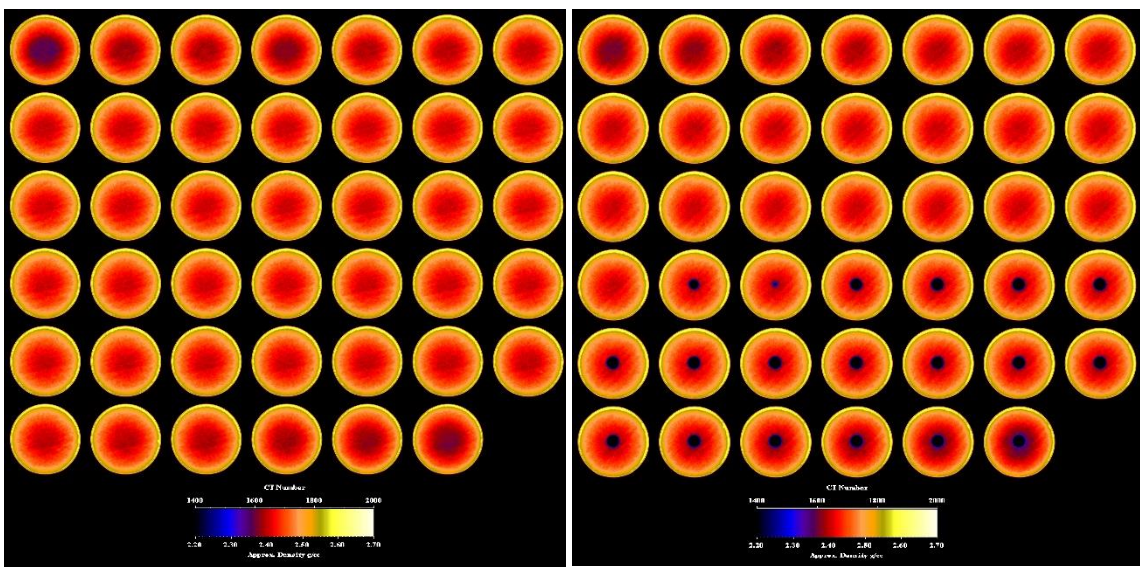

Figure A. 14 CT Scan of Sample 2-15 (before and after drilling)

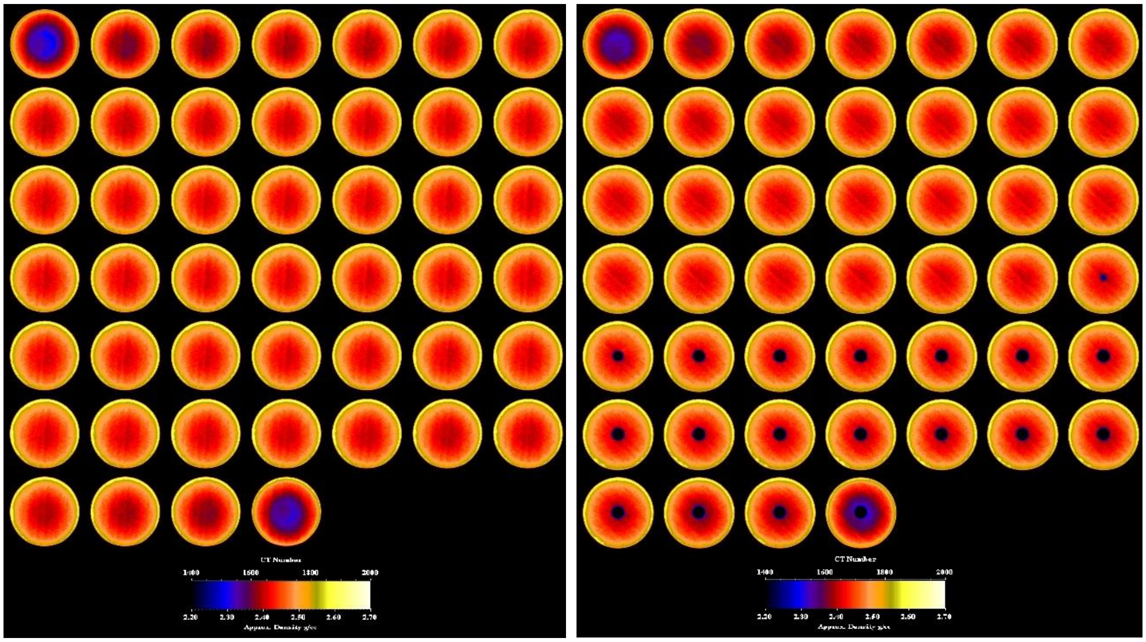

Figure A. 15 CT Scan of Sample 2-16 (before and after drilling)

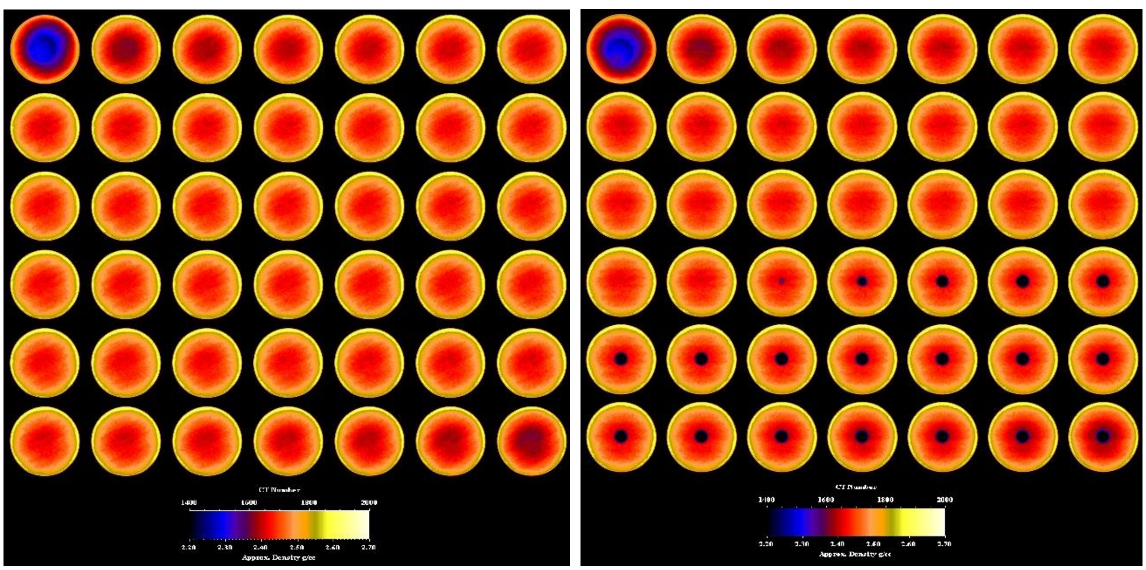

Figure A. 16 CT Scan of Sample 2-17 (before and after drilling)

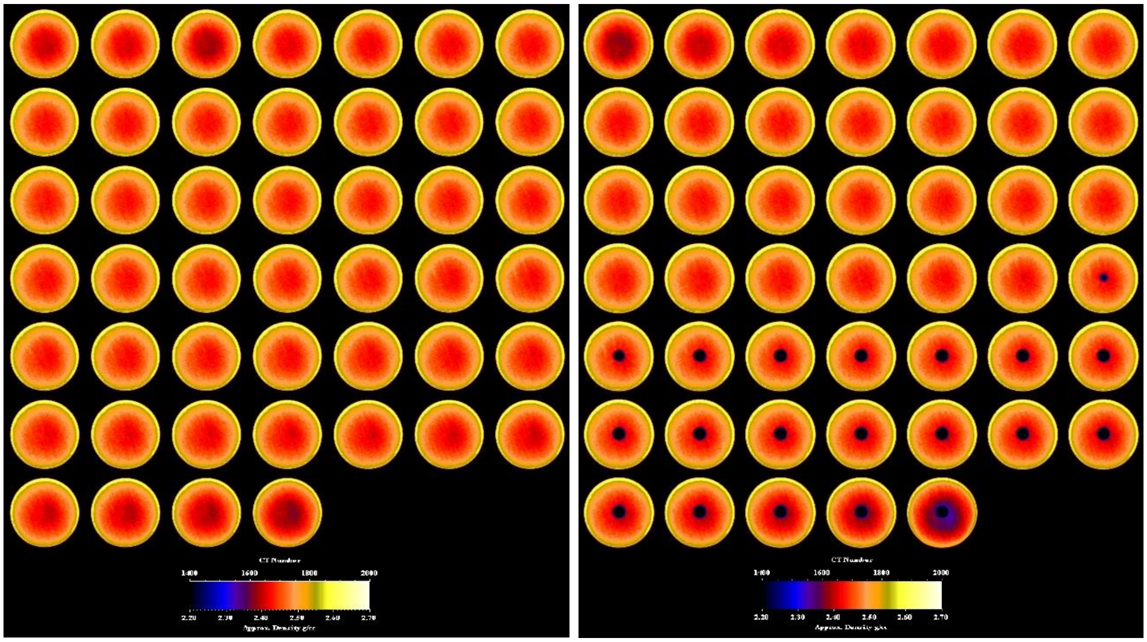

Figure A. 17 CT Scan of Sample 2-18 (before and after drilling)

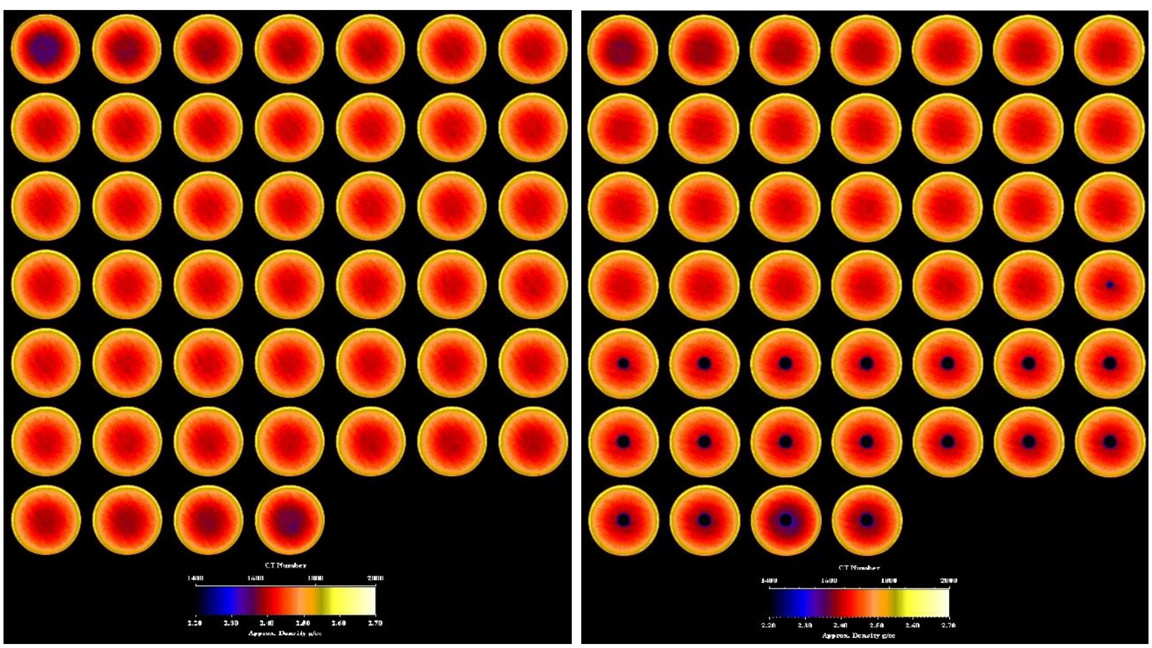

Figure A. 18 CT Scan of Sample 2-19 (before and after drilling)

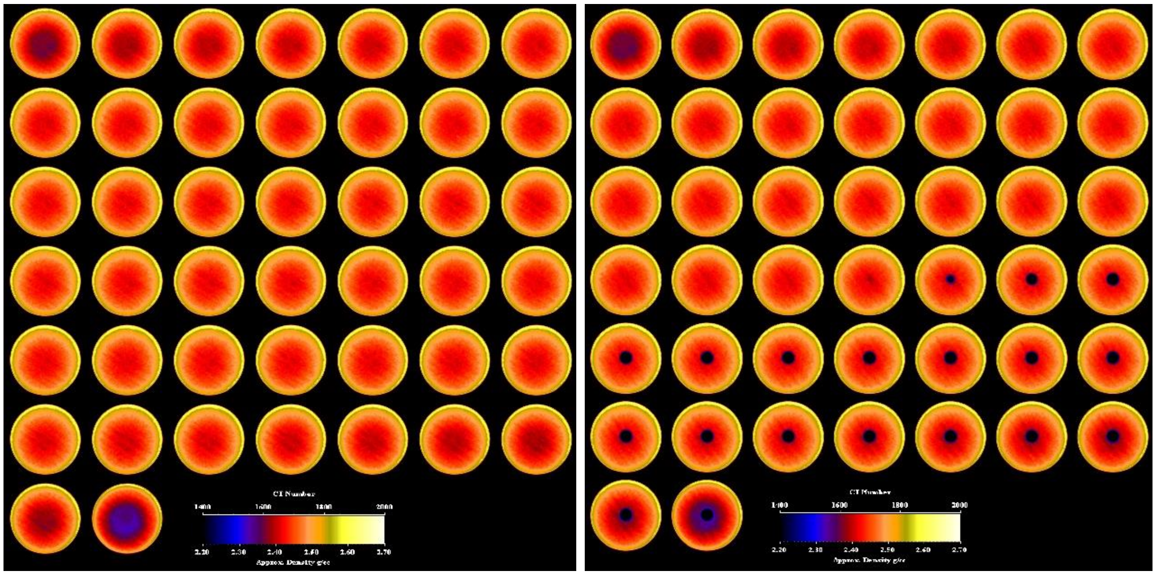

Figure A. 19 CT Scan of Sample 2-21 (before and after drilling)

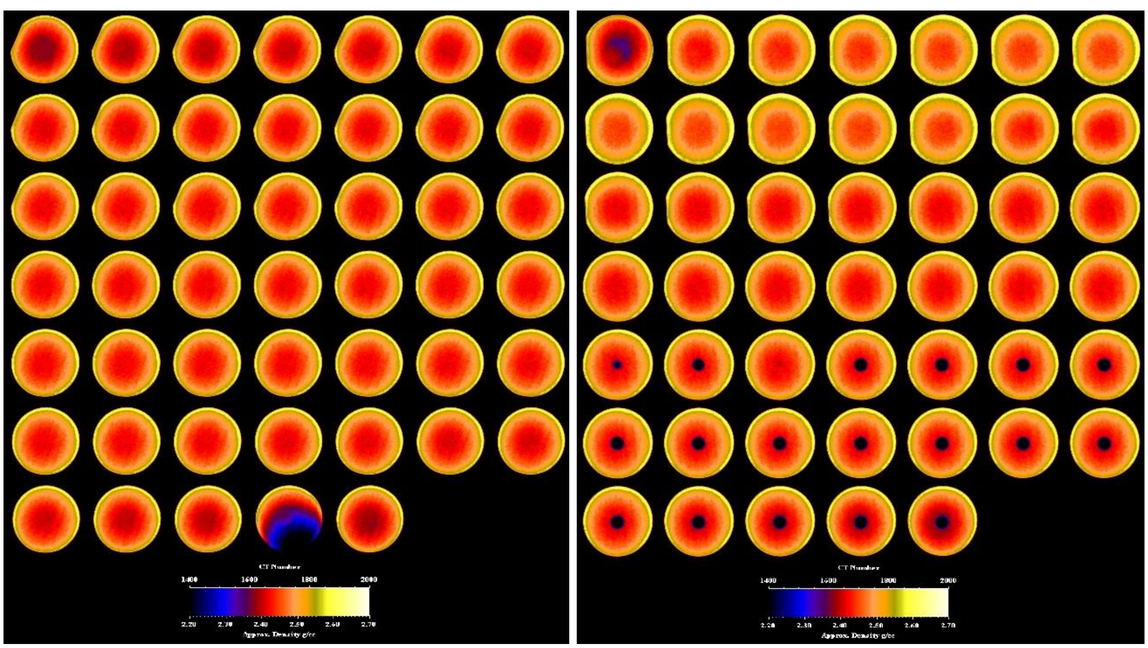

Figure A. 20 CT Scan of Sample 2-22 (before and after drilling)

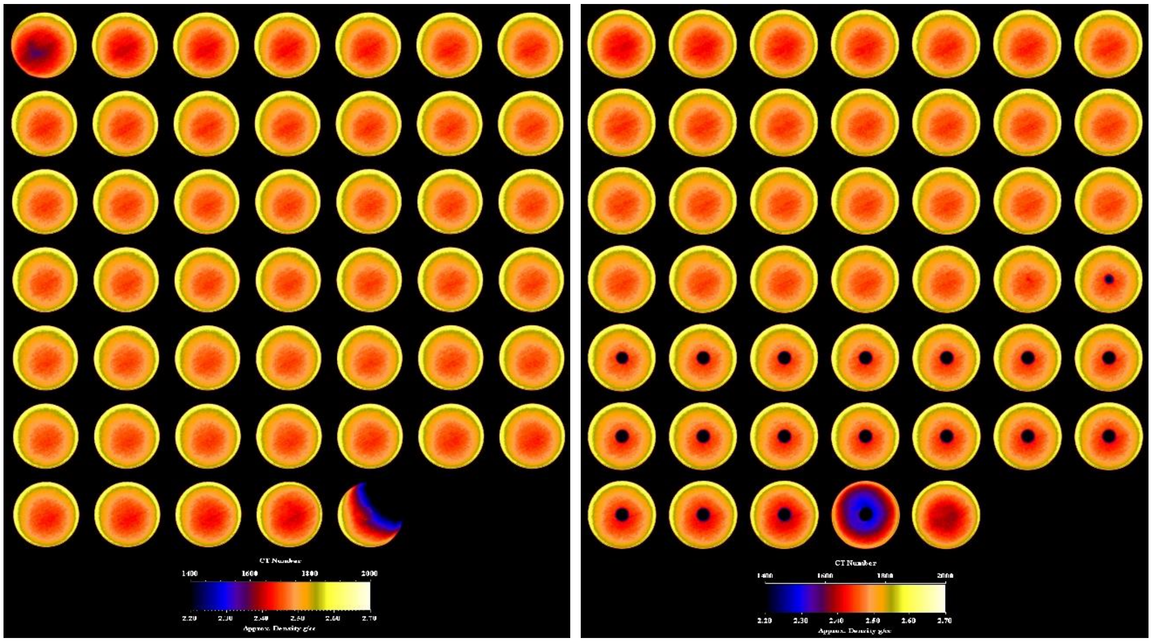

Figure A. 21 CT Scan of Sample 2-23 (before and after drilling)

CT Scans of the samples from the geomechanical group (brine saturated samples)

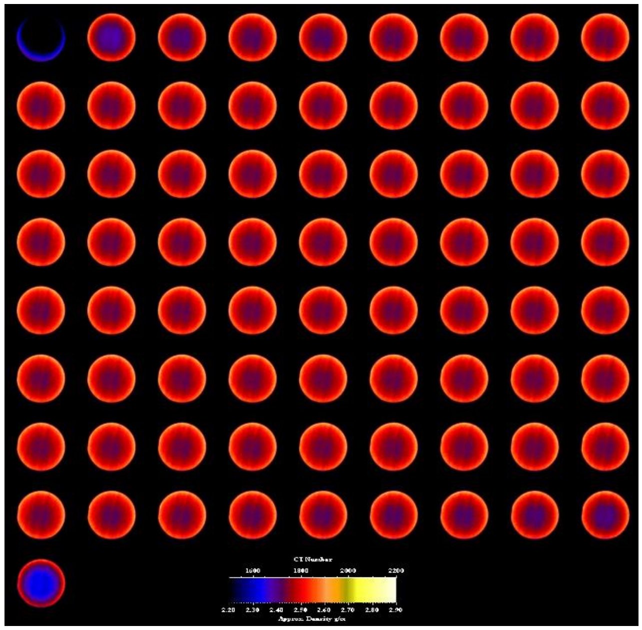

Figure A. 22 CT Scan of Sample 1-1 (Dry)

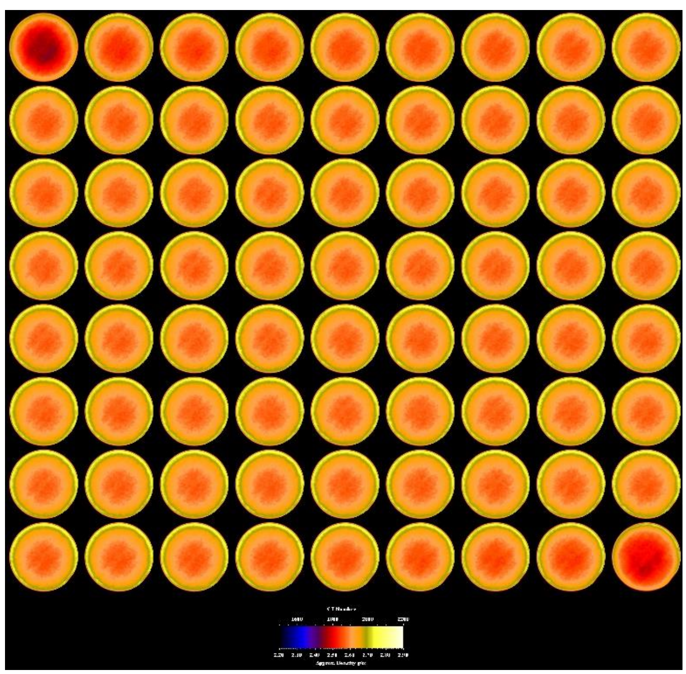

Figure A. 23 CT Scan of Sample 1-1 (Brine Saturated)

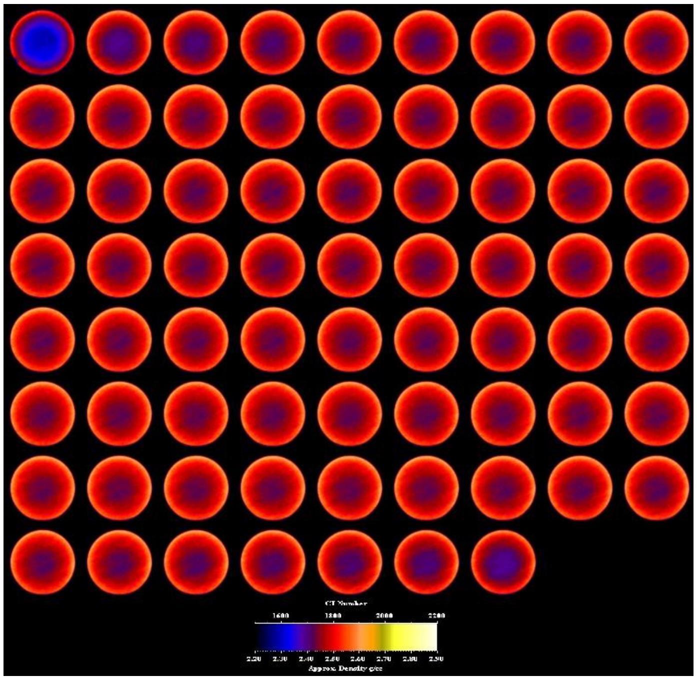

Figure A. 24 CT Scan of Sample 1-12 (Dry)

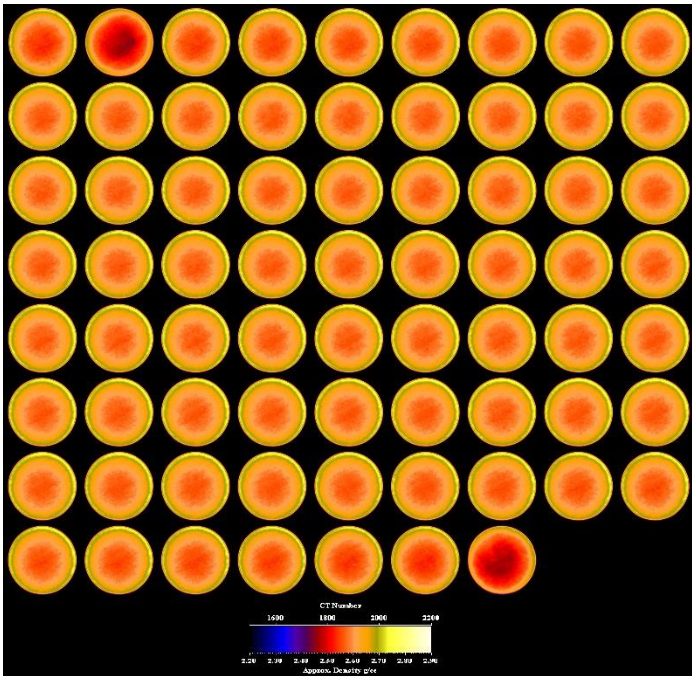

Figure A. 25 CT Scan of Sample 1-12 (Brine Saturated)

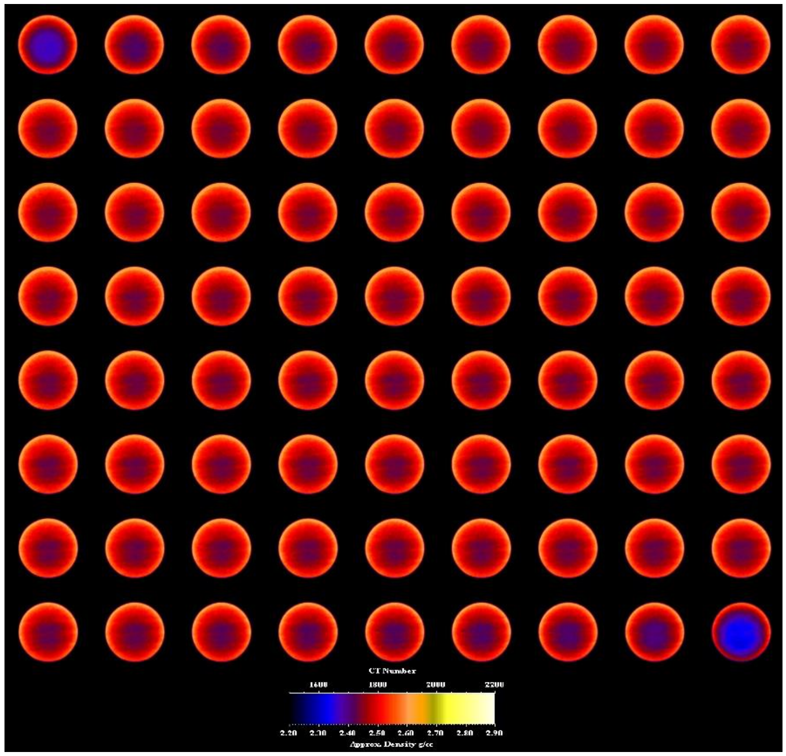

Figure A. 26 CT Scan of Sample 1-13 (Dry)

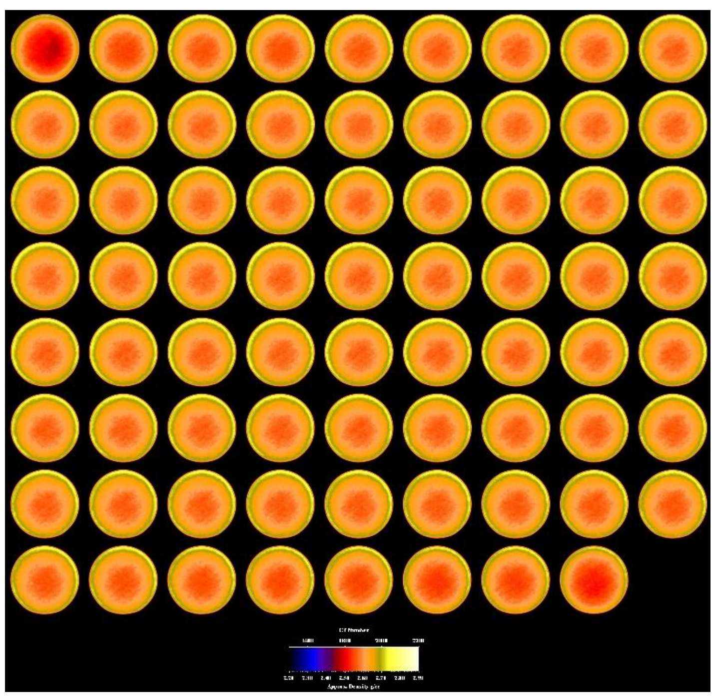

Figure A. 27 CT Scan of Sample 1-13 (Brine Saturated)

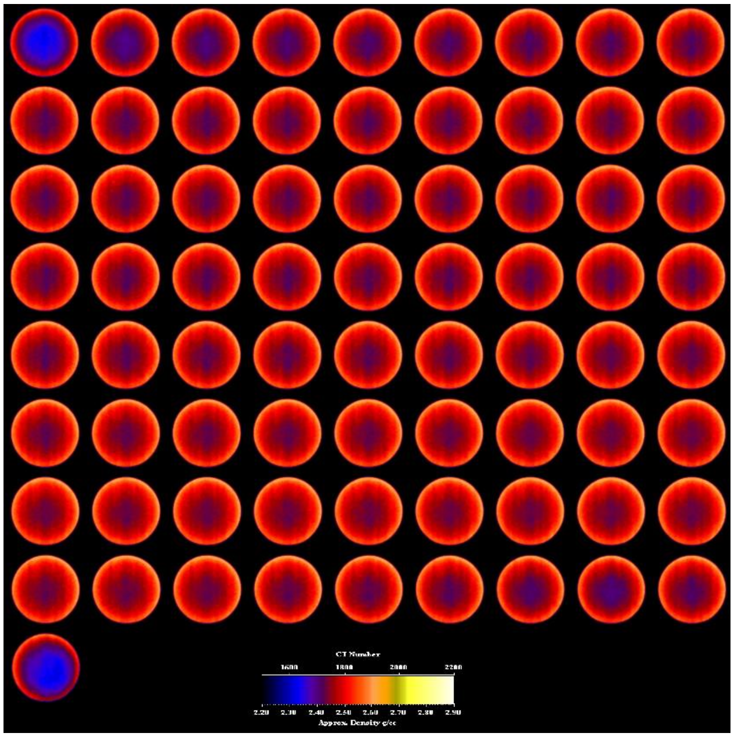

Figure A. 28 CT Scan of Sample 1-14 (Dry)

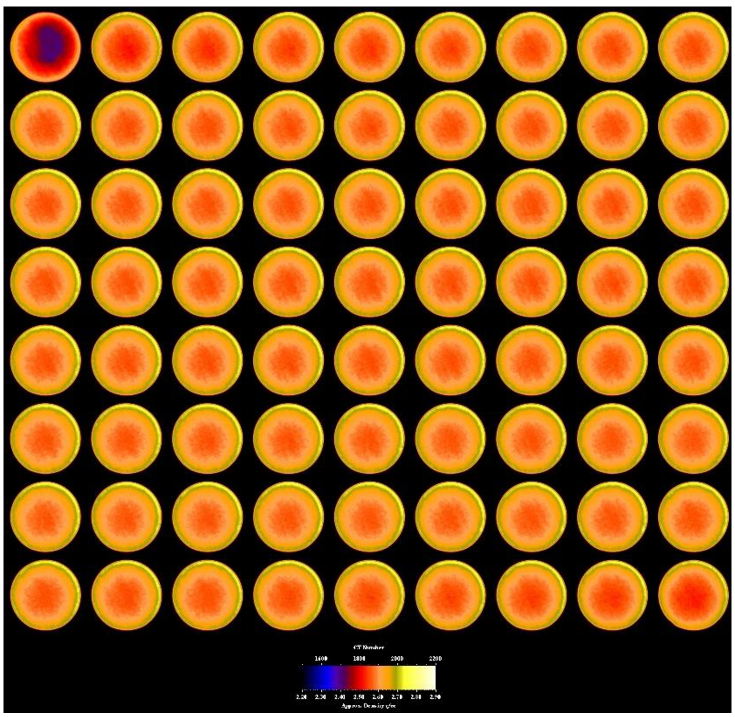

Figure A. 29 CT Scan of Sample 1-14 (Brine Saturated)

CT Scans of the samples from the geomechanical group (oil saturated samples)

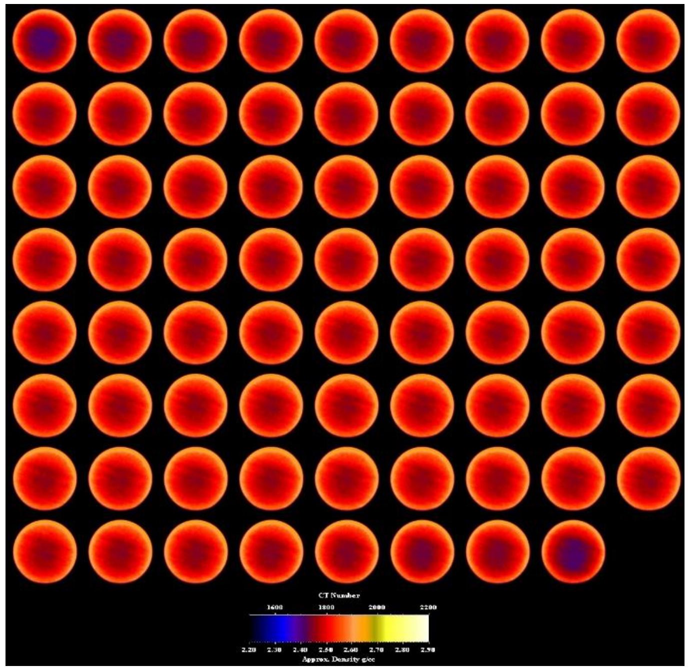

Figure A. 30 CT Scan of Sample 1-2 (Dry)

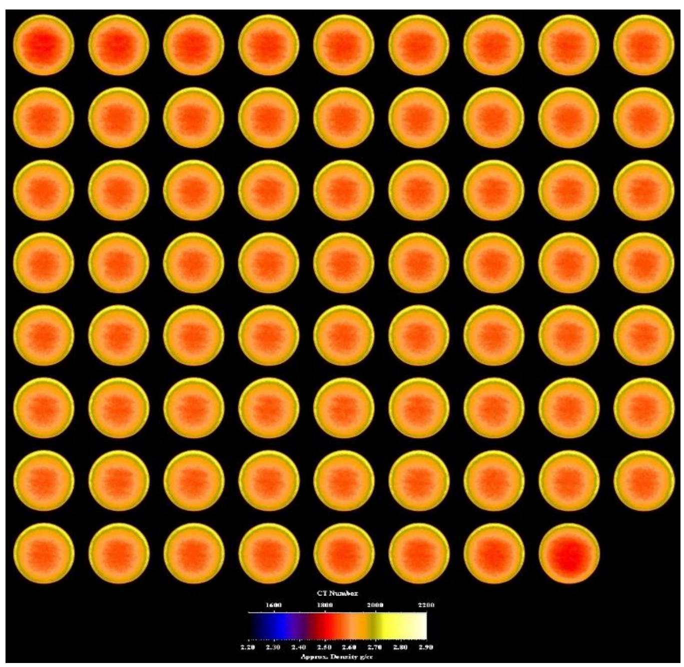

Figure A. 31 CT Scan of Sample 1-2 (Oil Saturated)

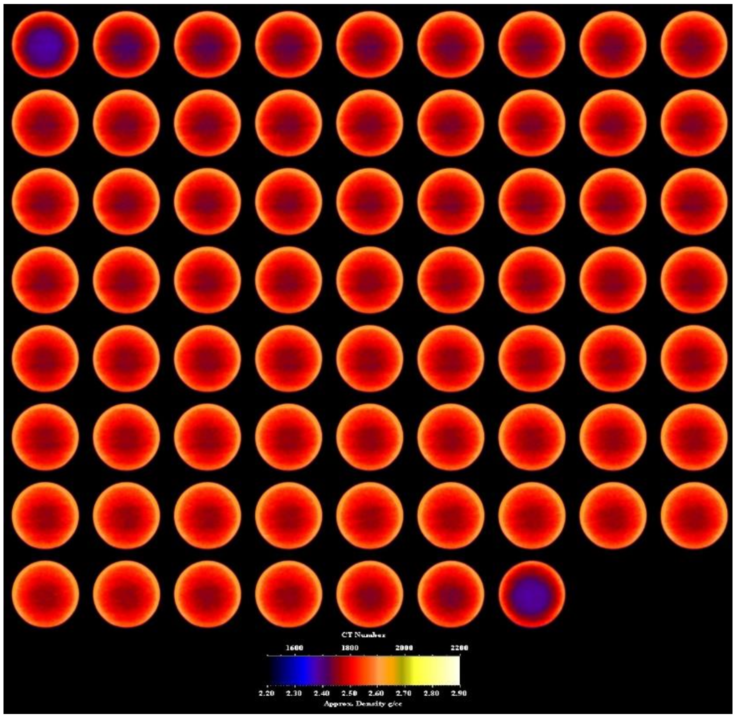

Figure A. 32 CT Scan of Sample 1-5 (Dry)

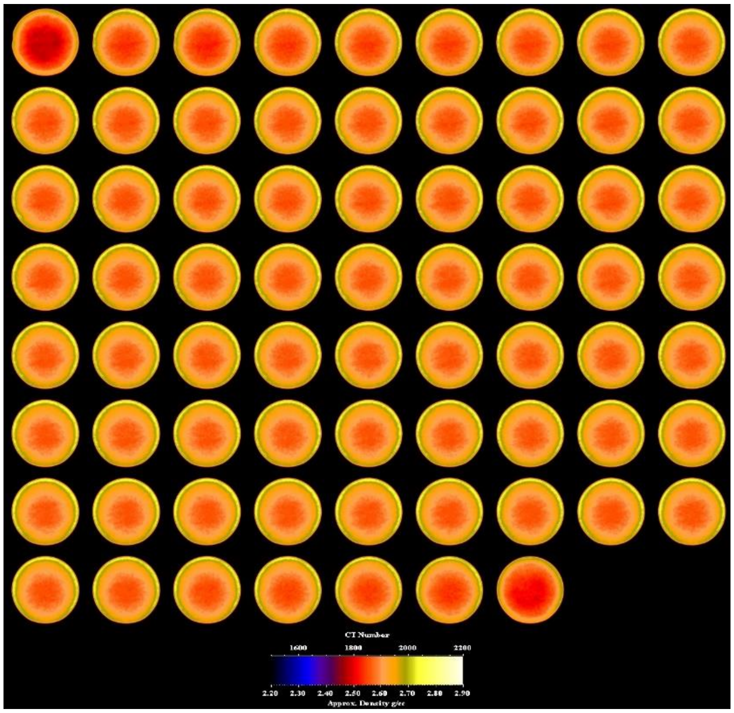

Figure A. 33 CT Scan of Sample 1-5 (Oil Saturated)

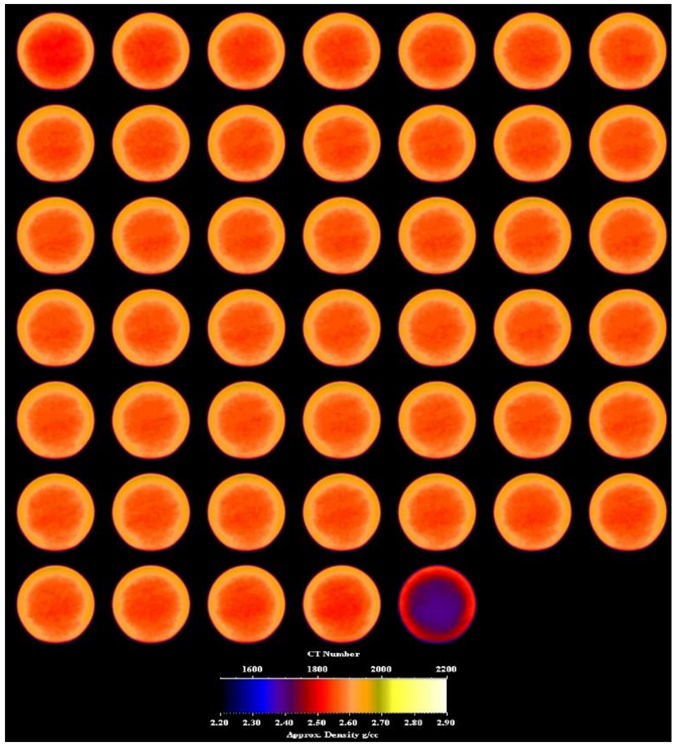

Figure A. 34 CT Scan of Sample 1-15 (Dry)

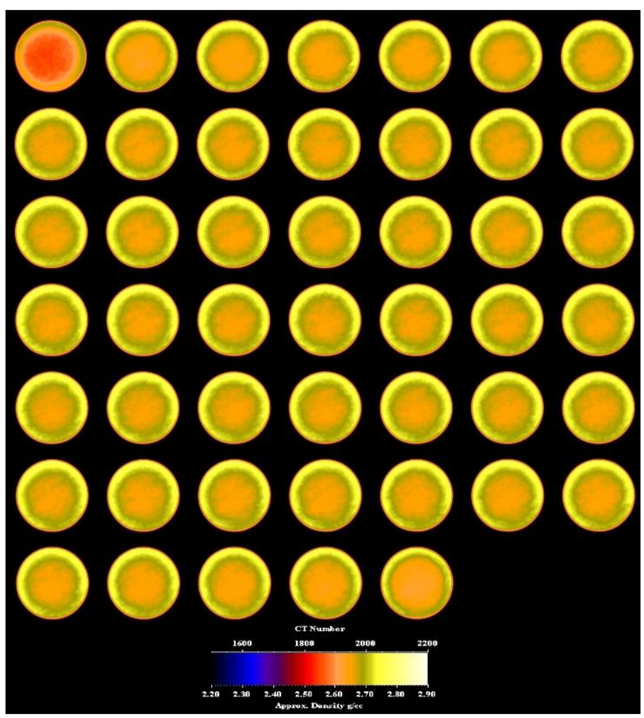

Figure A. 35 CT Scan of Sample 1-15 (Oil Saturated)

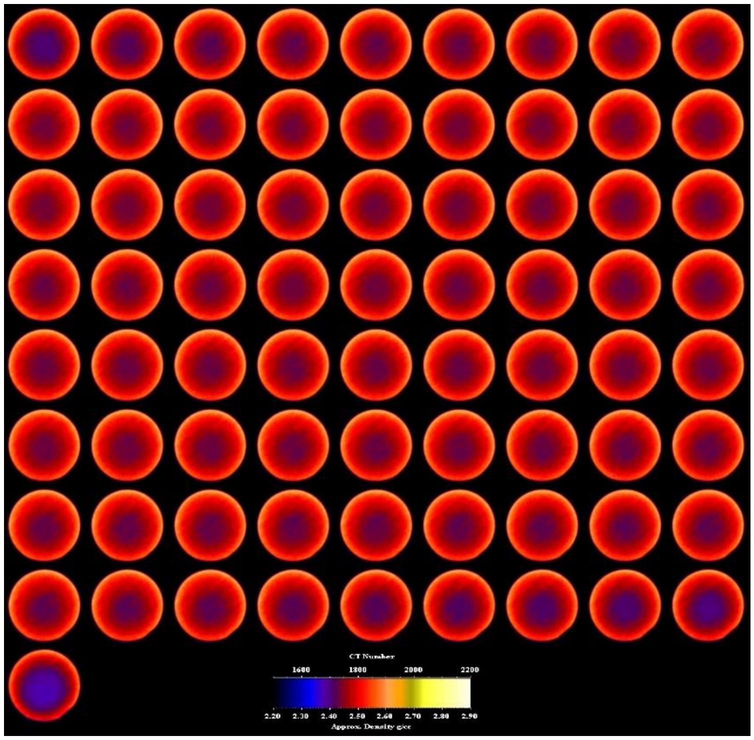

Figure A. 36 CT Scan of Sample 1-16 (Dry)

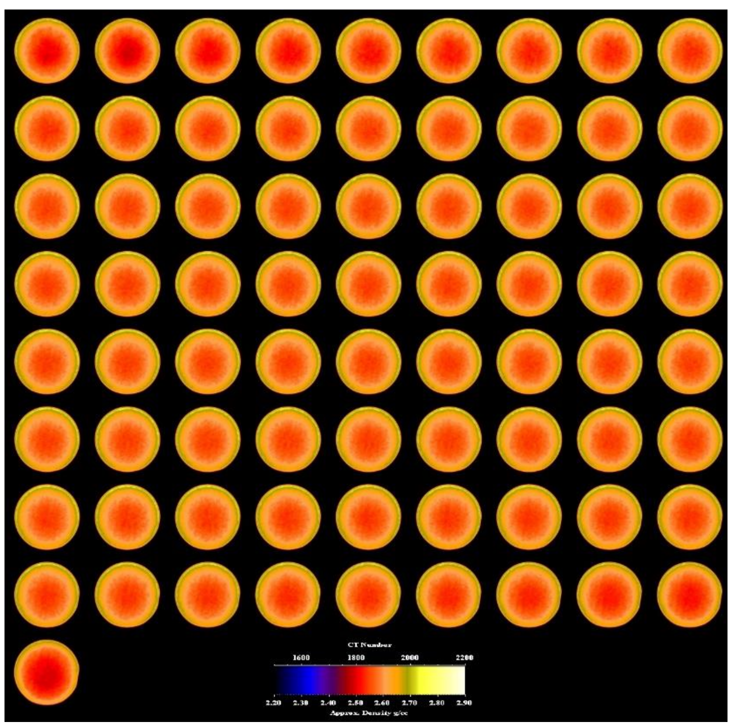

Figure A. 37 CT Scan of Sample 1-16 (Oil Saturated)

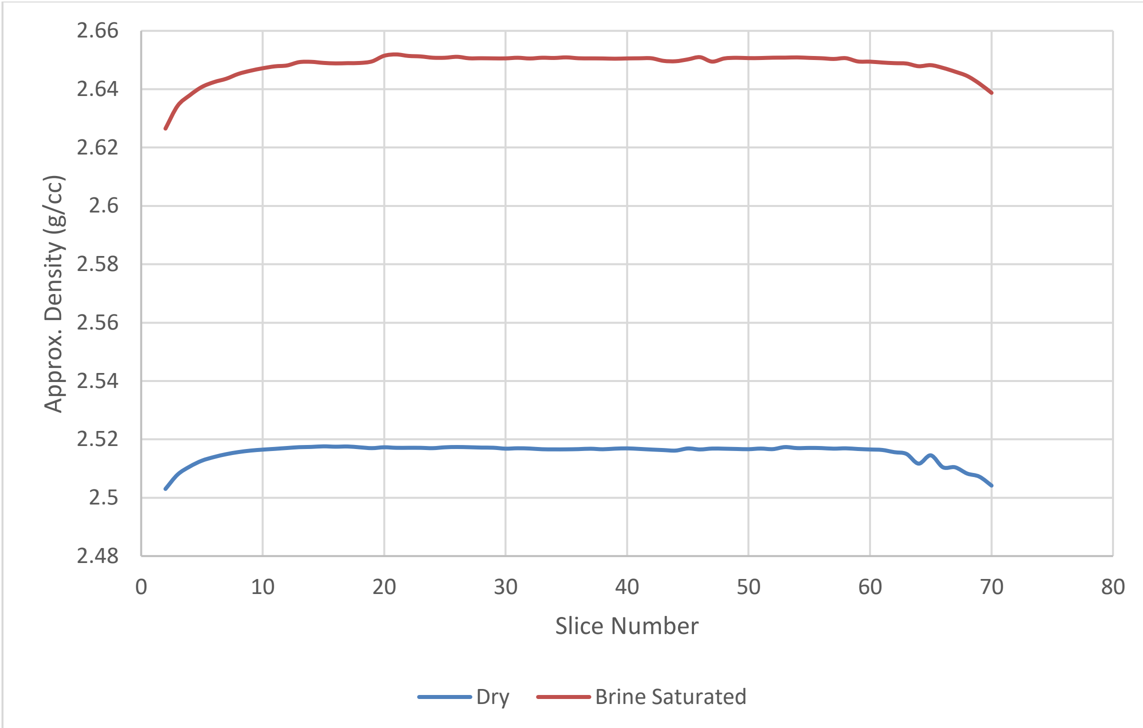

Figure A. 38 Approximate density comparison for dry and brine saturated sample (Sample 1-1)

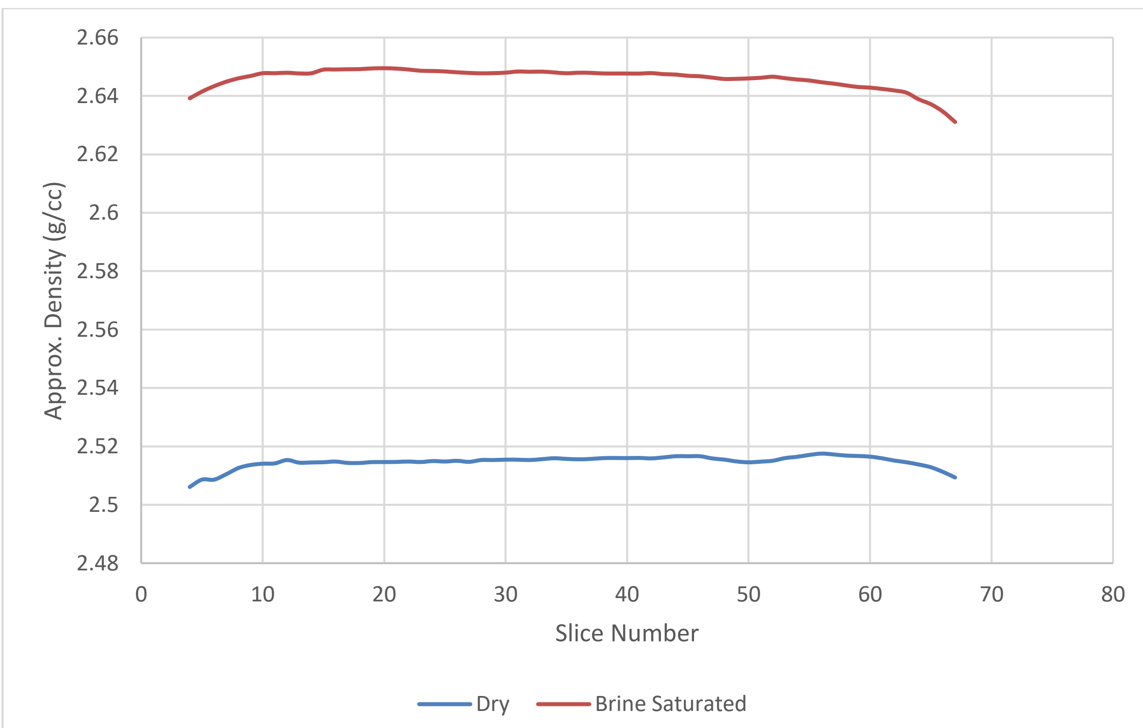

Figure A. 39 Approximate density comparison for dry and brine saturated sample (Sample 1-12)

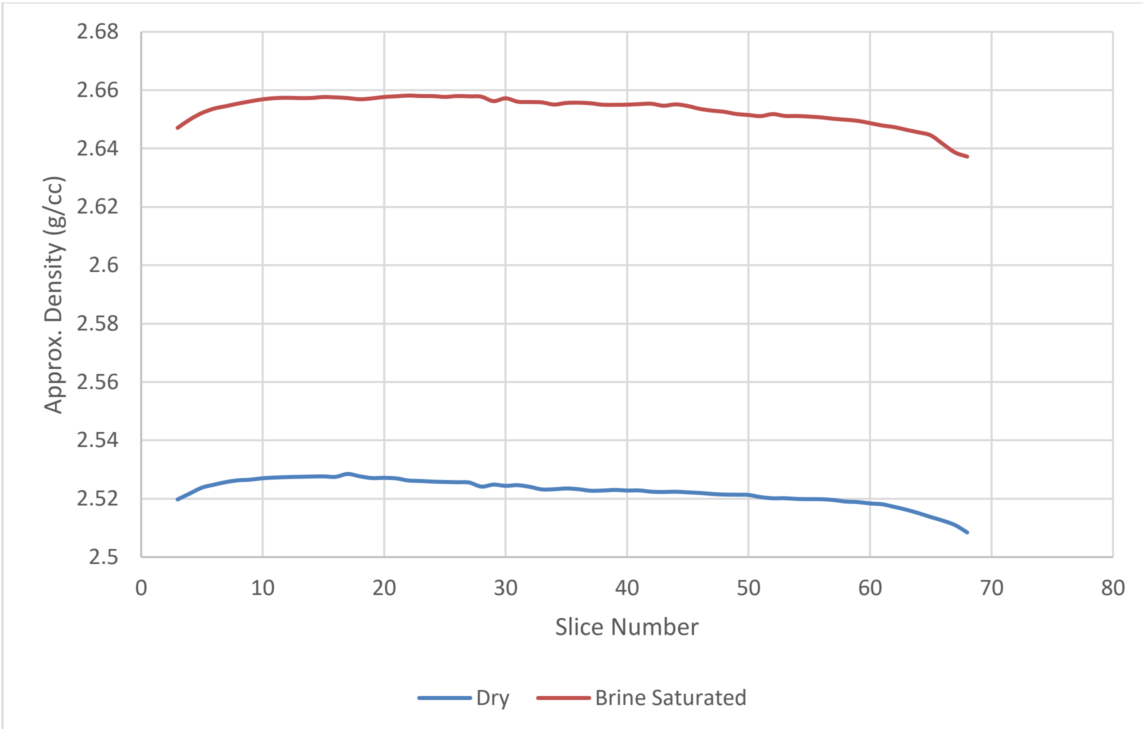

Figure A. 40 Approximate density comparison for dry and brine saturated sample (Sample 1-13)

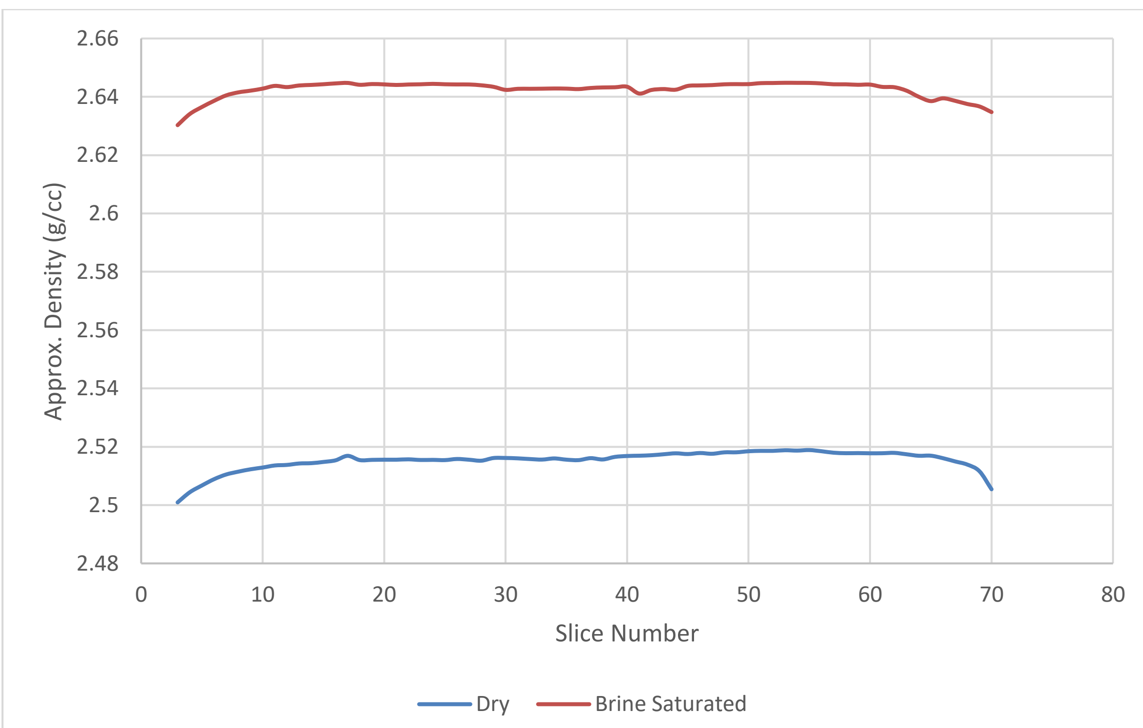

Figure A. 41 Approximate density comparison for dry and brine saturated sample (Sample 1-14)

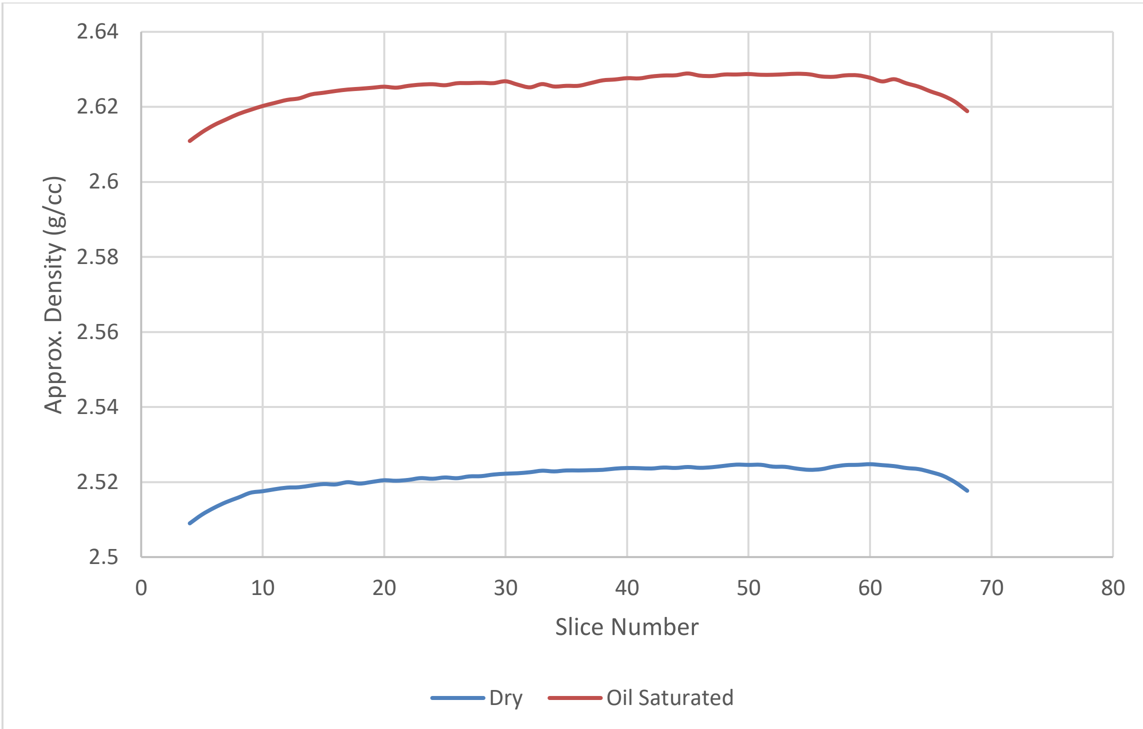

Figure A. 42 Approximate density comparison for dry and oil saturated sample (Sample 1-2)

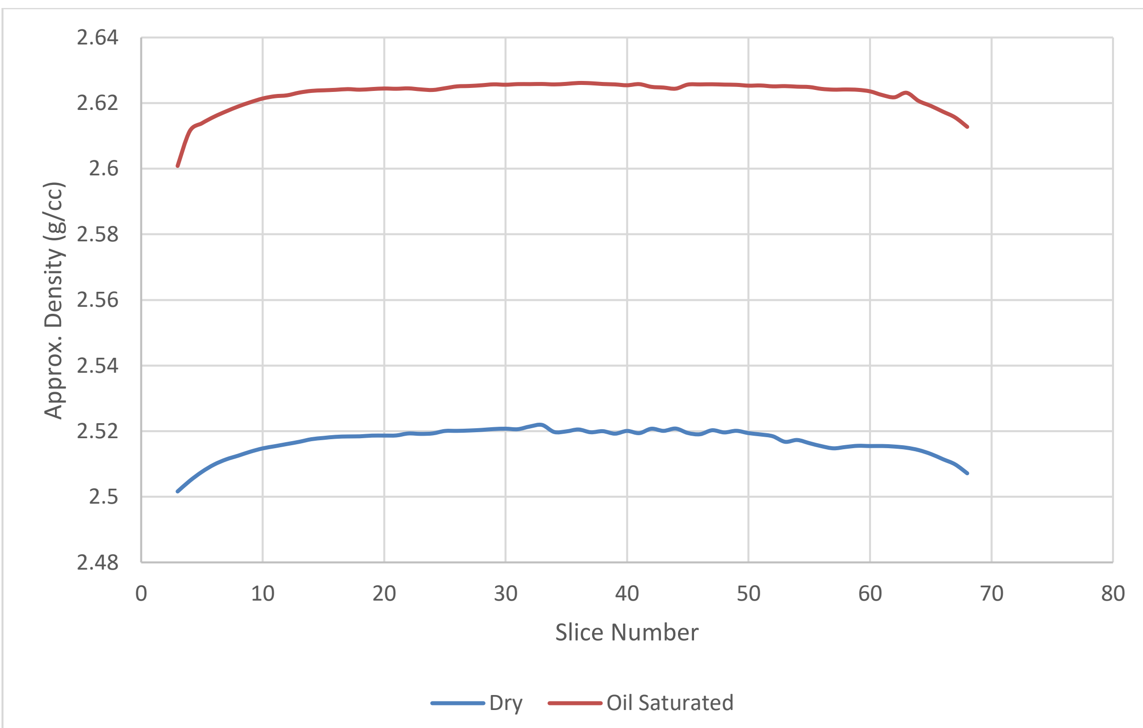

Figure A. 43 Approximate density comparison for dry and oil saturated sample (Sample 1-5)

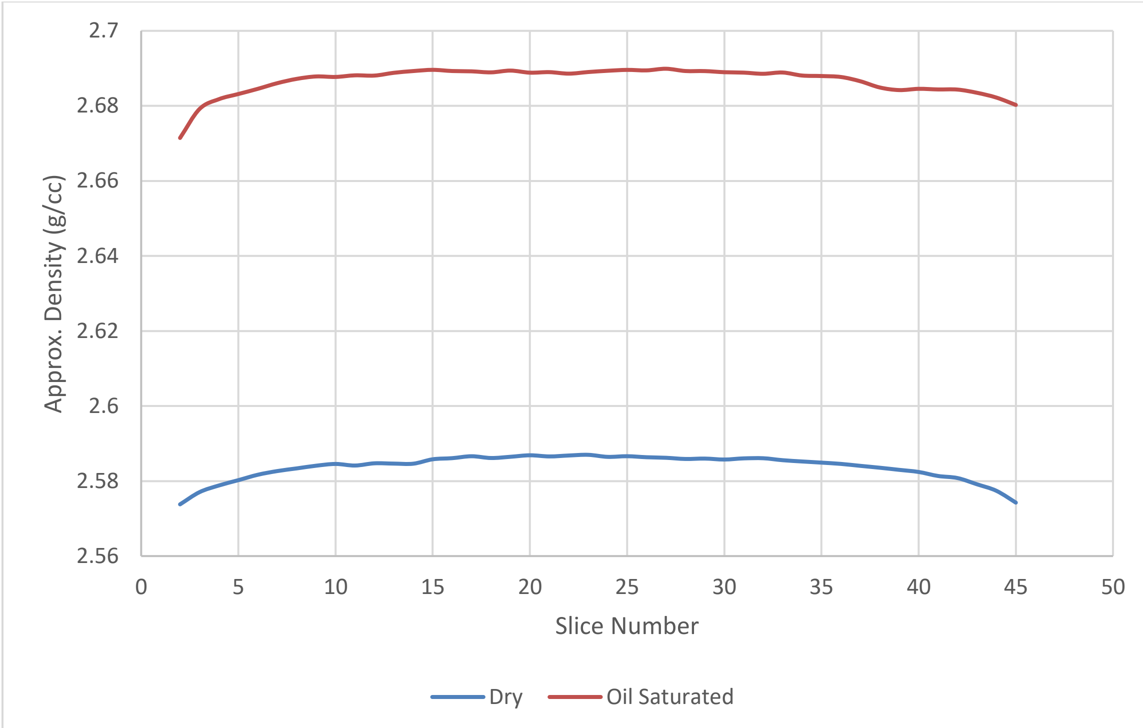

Figure A. 44 Approximate density comparison for dry and oil saturated sample (Sample 1-15)

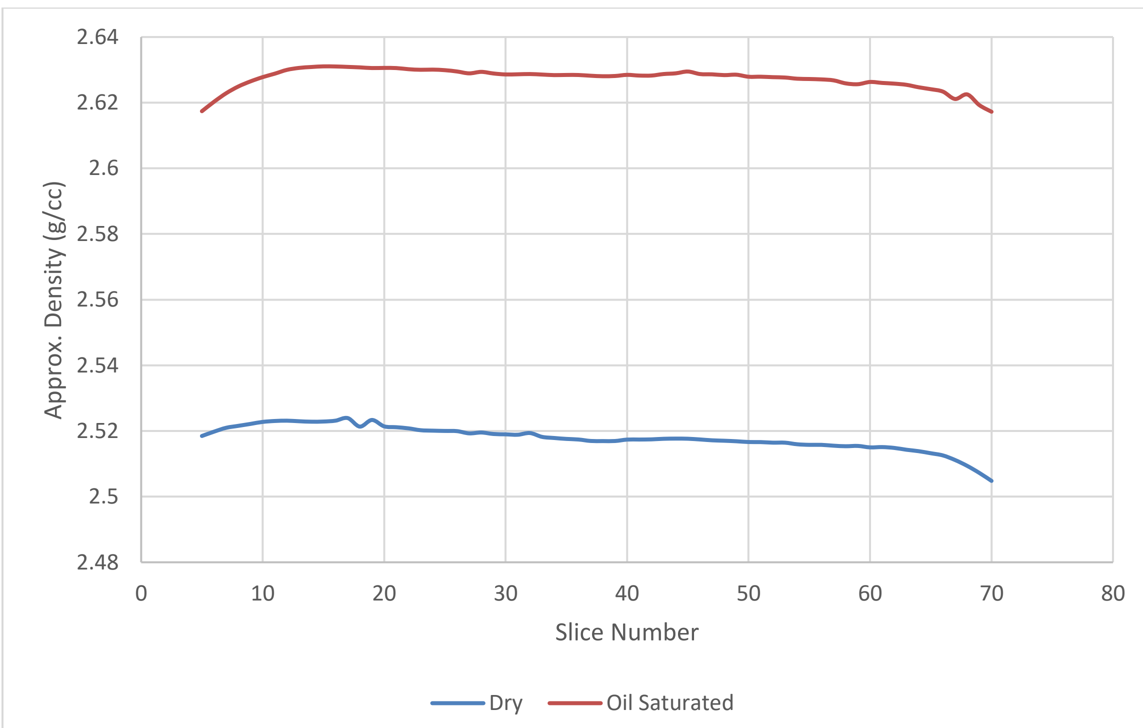

Figure A. 45 Approximate density comparison for dry and oil saturated sample (Sample 1-16)

Appendix B

Ultrasonic tests of Brine Saturated samples

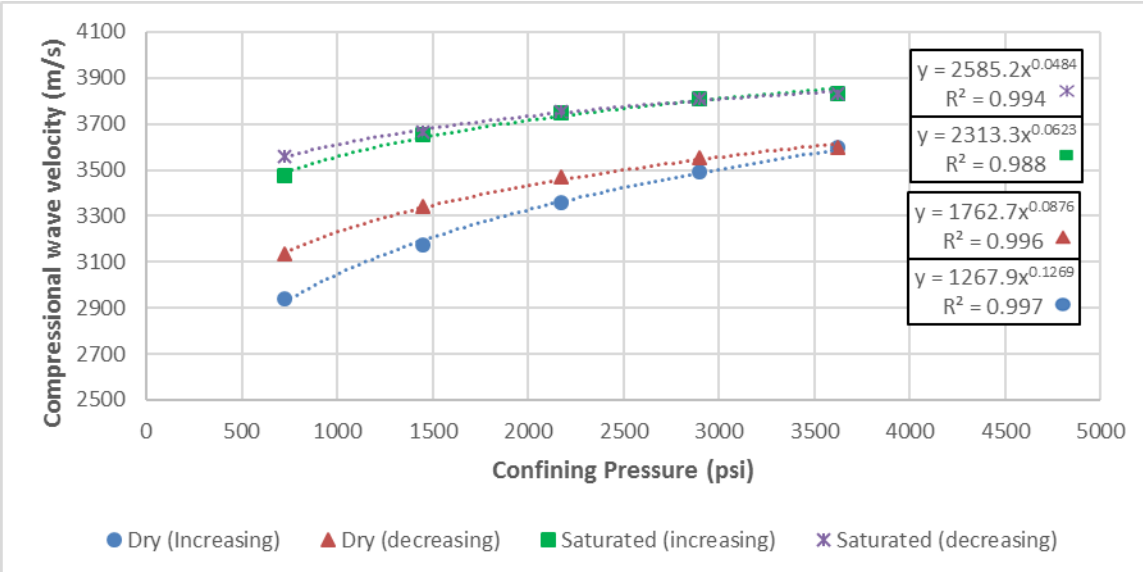

Figure B. 1 Comparison of Compressional wave velocity vs Confining Pressure, Dry vs Brine Saturated (Sample 1-1)

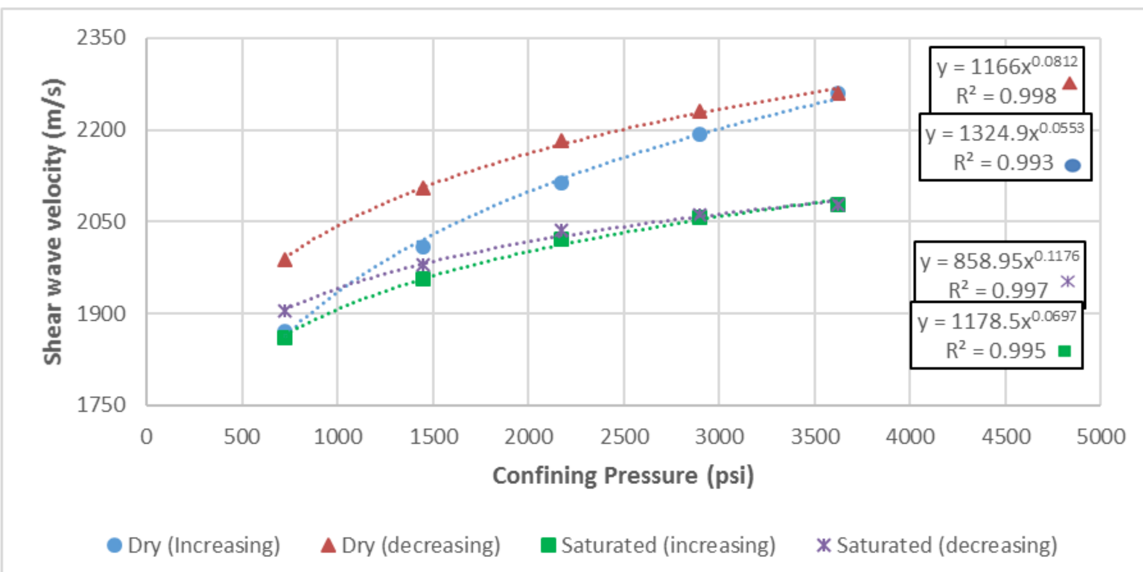

Figure B. 2 Comparison of Shear wave velocity vs Confining Pressure, Dry vs Brine Saturated (Sample 1-1)

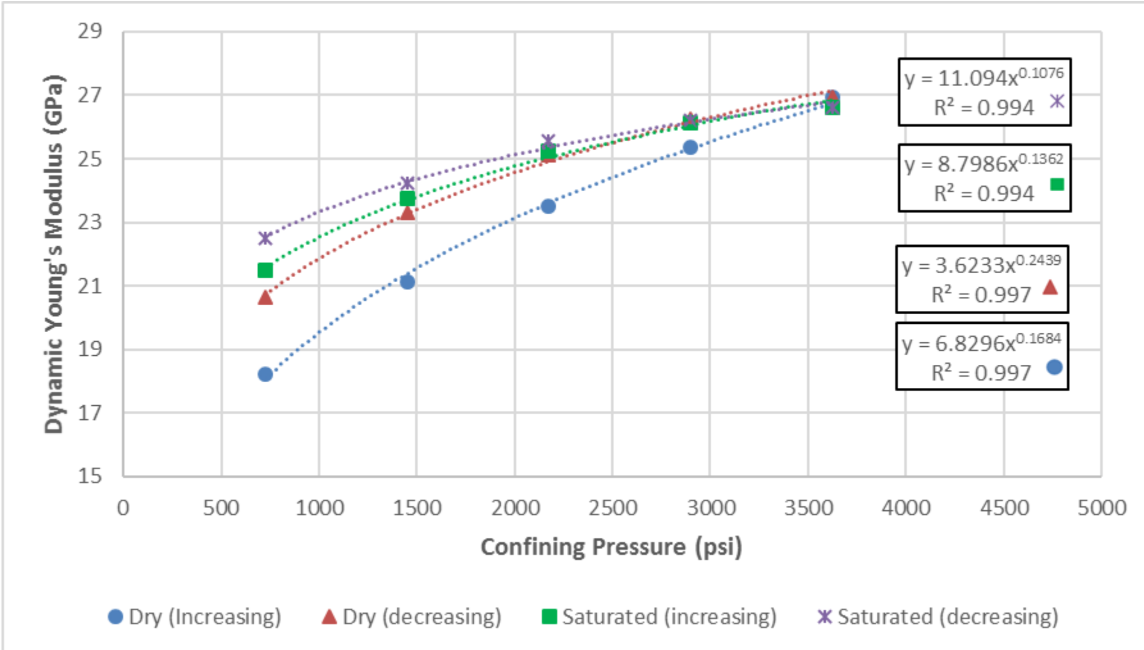

Figure B. 3 Comparison of Young's Modulus vs Confining Pressure, Dry vs Brine Saturated

(Sample 1-1)

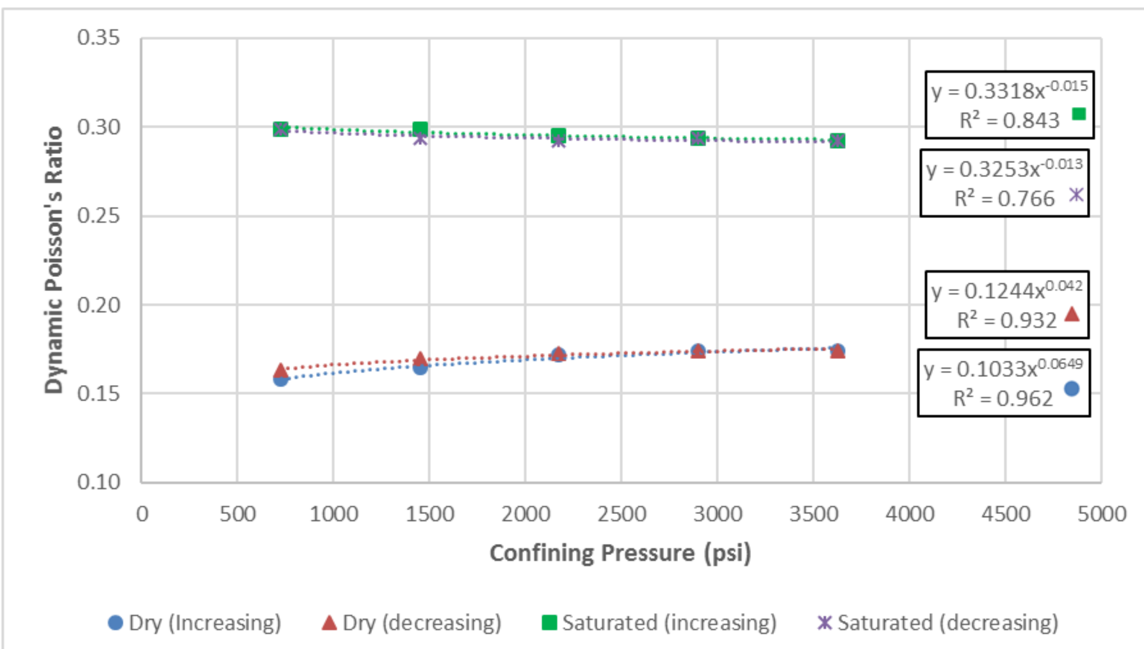

Figure B. 4 Comparison of Poisson's Ratio vs Confining Pressure, Dry vs Brine Saturated

(Sample 1-1)

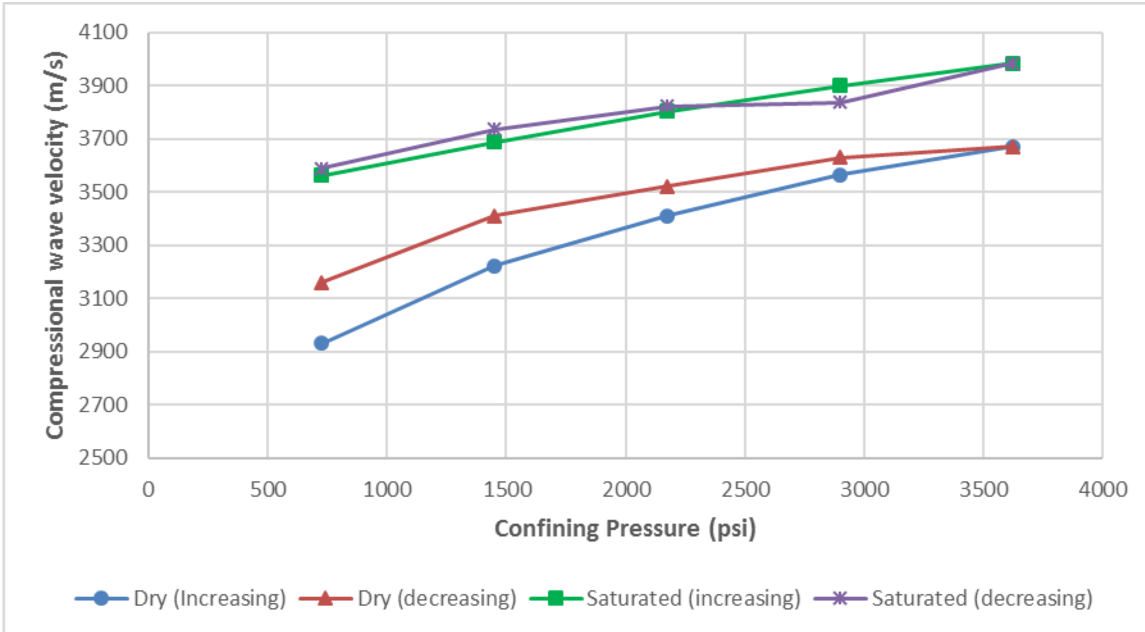

Figure B. 5 Comparison of Compressional wave velocity vs Confining Pressure, Dry vs Brine Saturated (Sample 1-12)

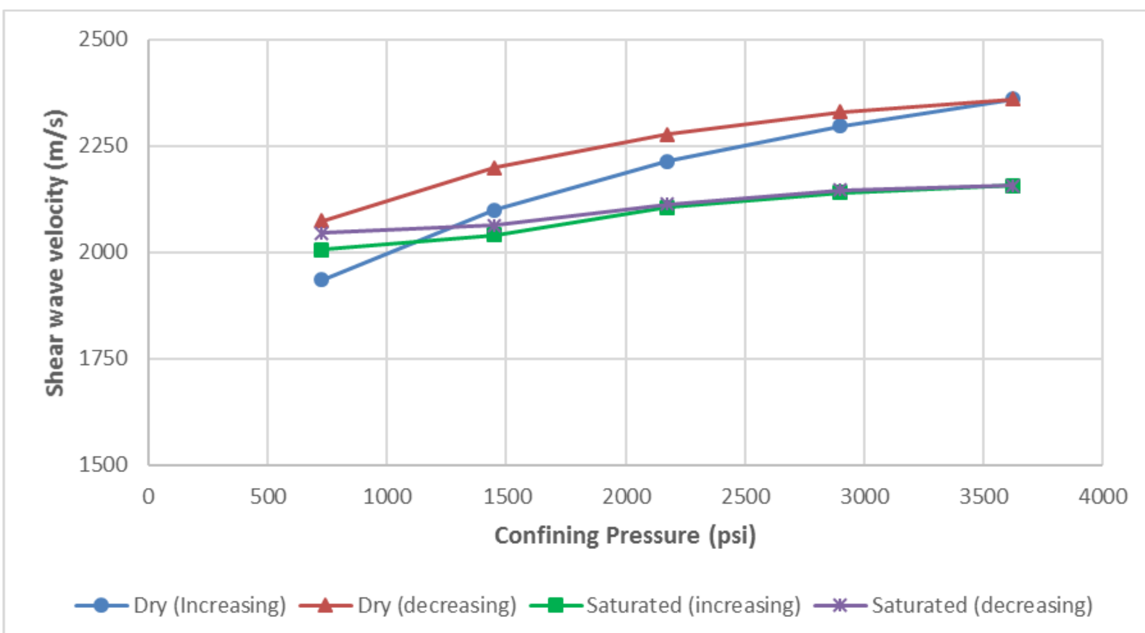

Figure B. 6 Comparison of Shear wave velocity vs Confining Pressure, Dry vs Brine Saturated (Sample 1-12)

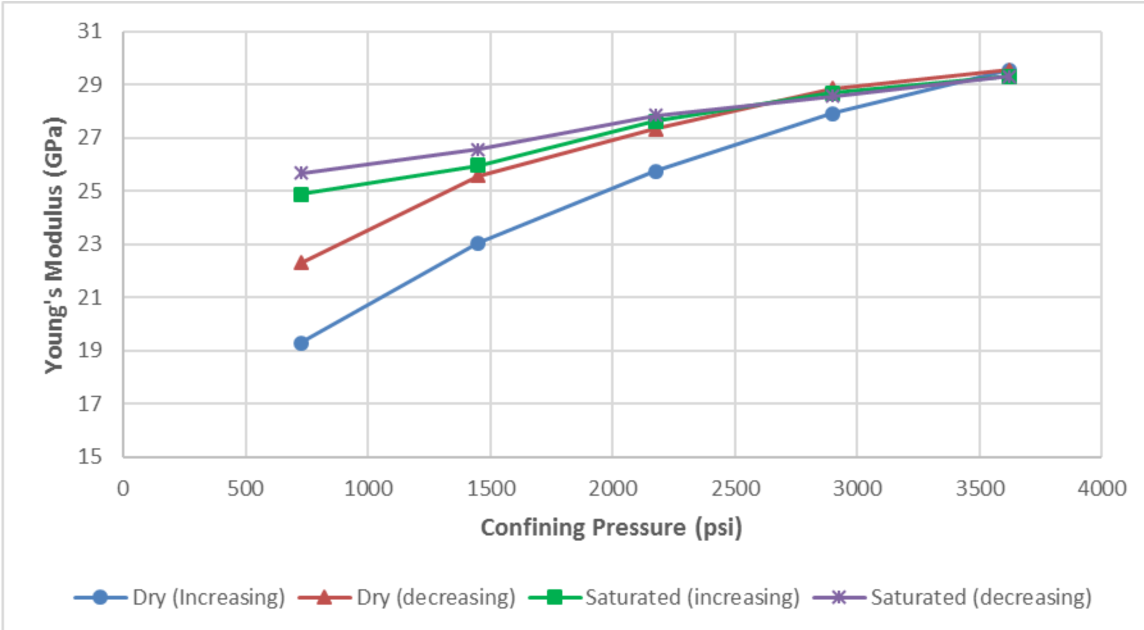

Figure B. 7 Comparison of Young's Modulus vs Confining Pressure, Dry vs Brine Saturated

(Sample 1-12)

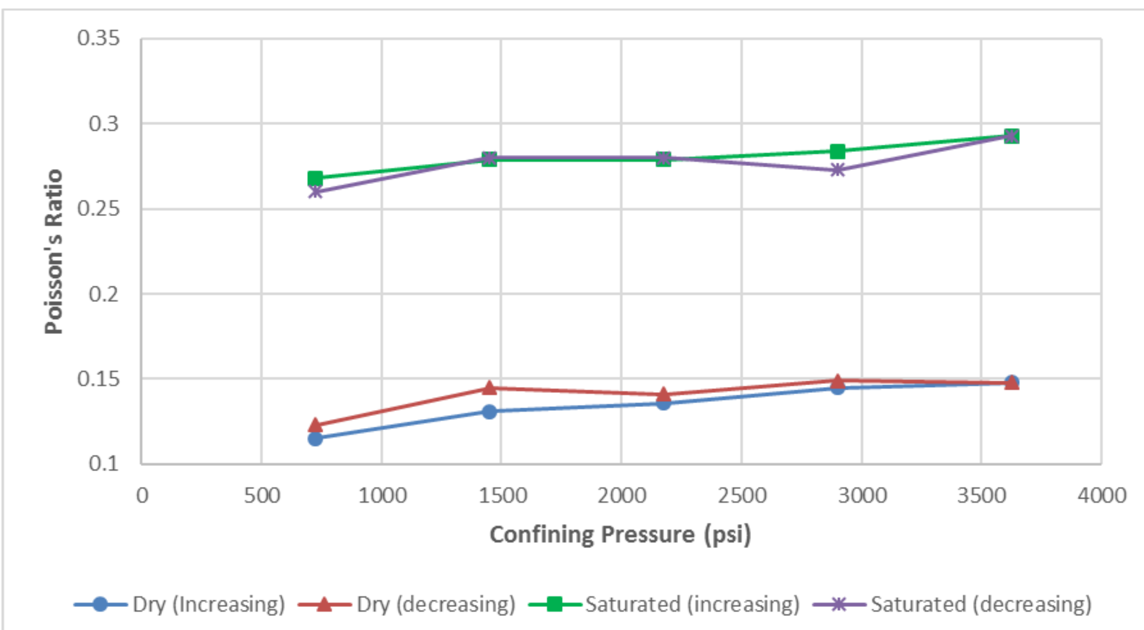

Figure B. 8 Comparison of Poisson's Ratio vs Confining Pressure, Dry vs Brine Saturated

(Sample 1-12)

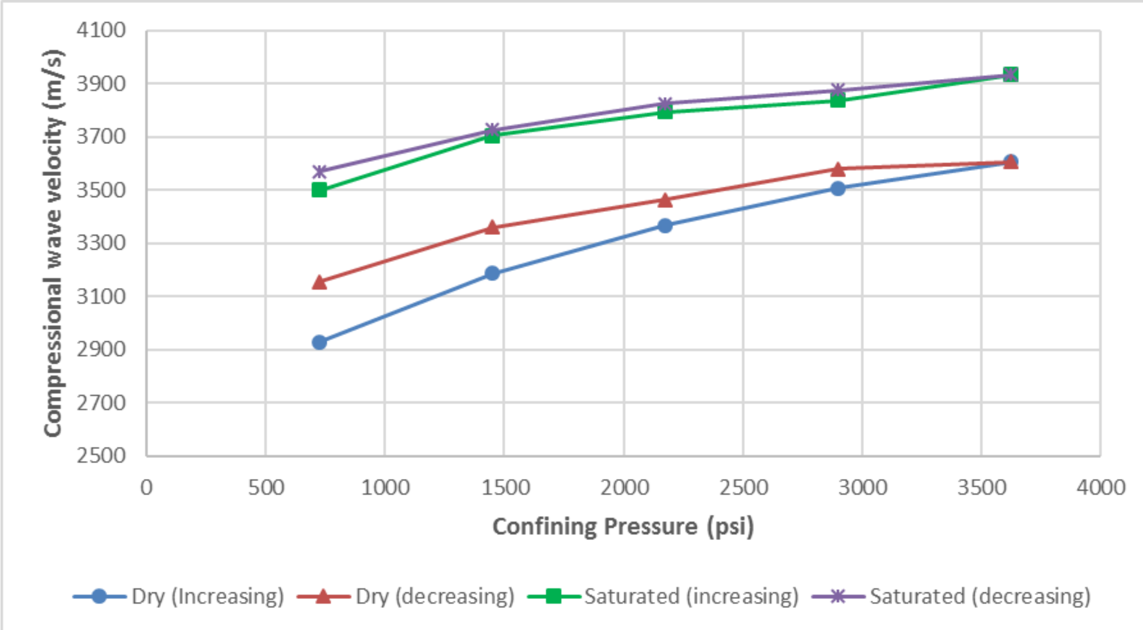

Figure B. 9 Comparison of Compressional wave velocity vs Confining Pressure, Dry vs Brine Saturated (Sample 1-13)

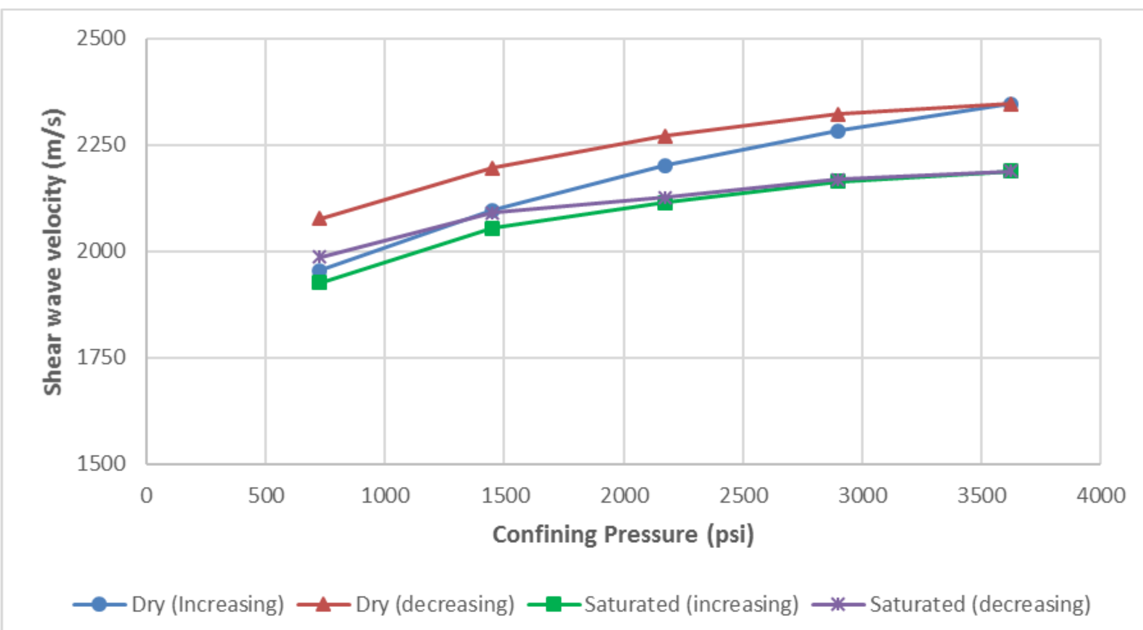

Figure B. 10 Comparison of Shear wave velocity vs Confining Pressure, Dry vs Brine Saturated (Sample 1-13)

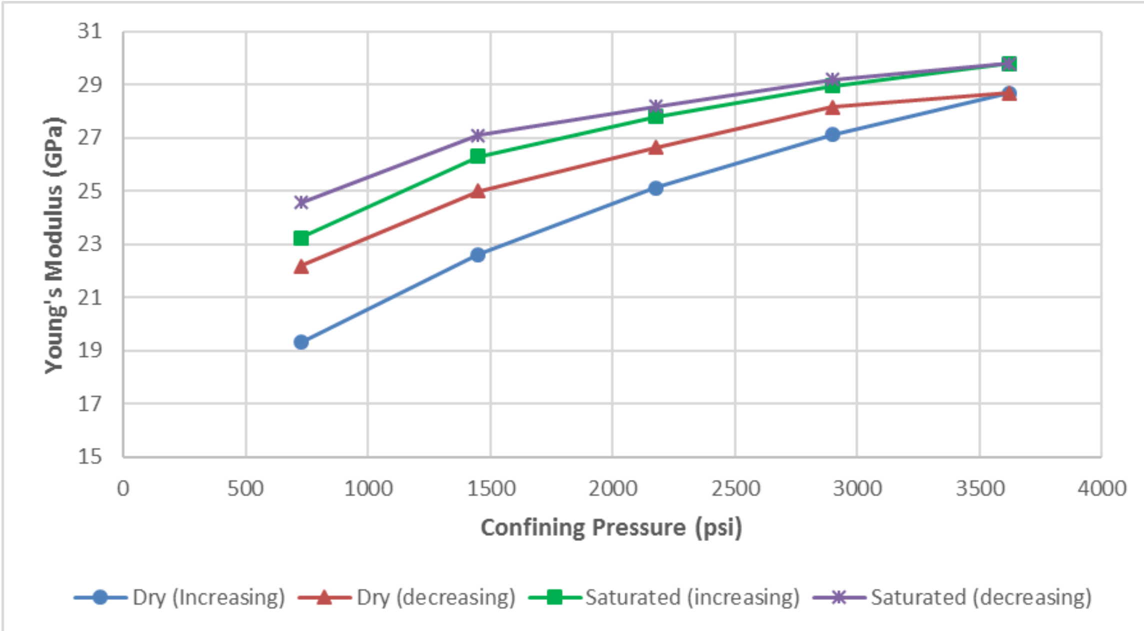

Figure B. 11 Comparison of Young's Modulus vs Confining Pressure, Dry vs Brine Saturated

(Sample 1-13)

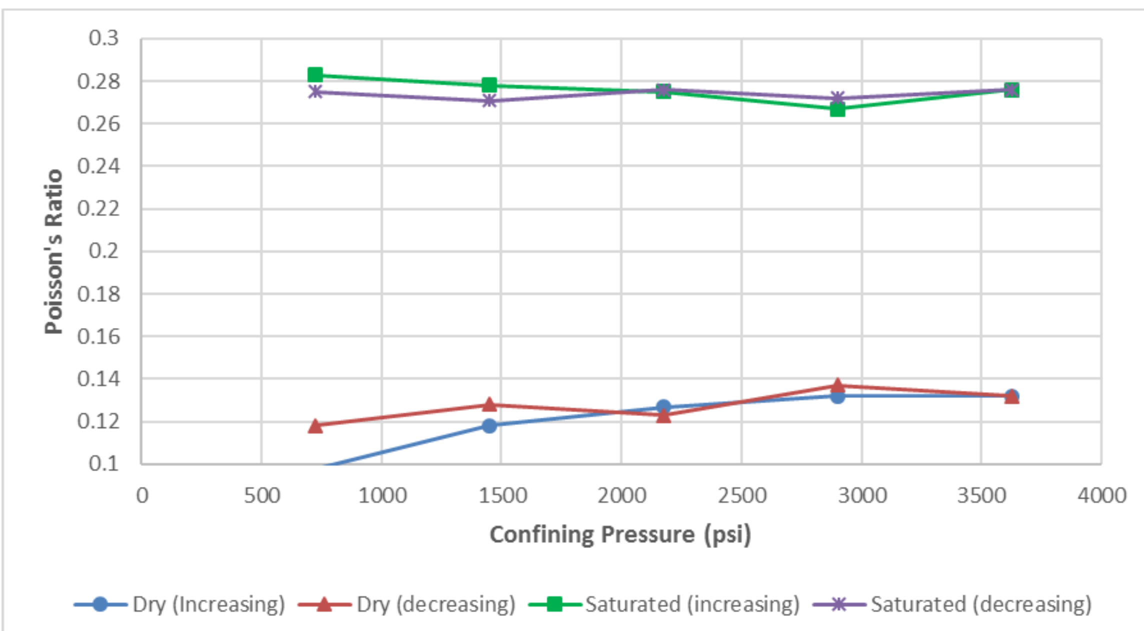

Figure B. 12 Comparison of Poisson's Ratio vs Confining Pressure, Dry vs Brine Saturated

(Sample 1-13)

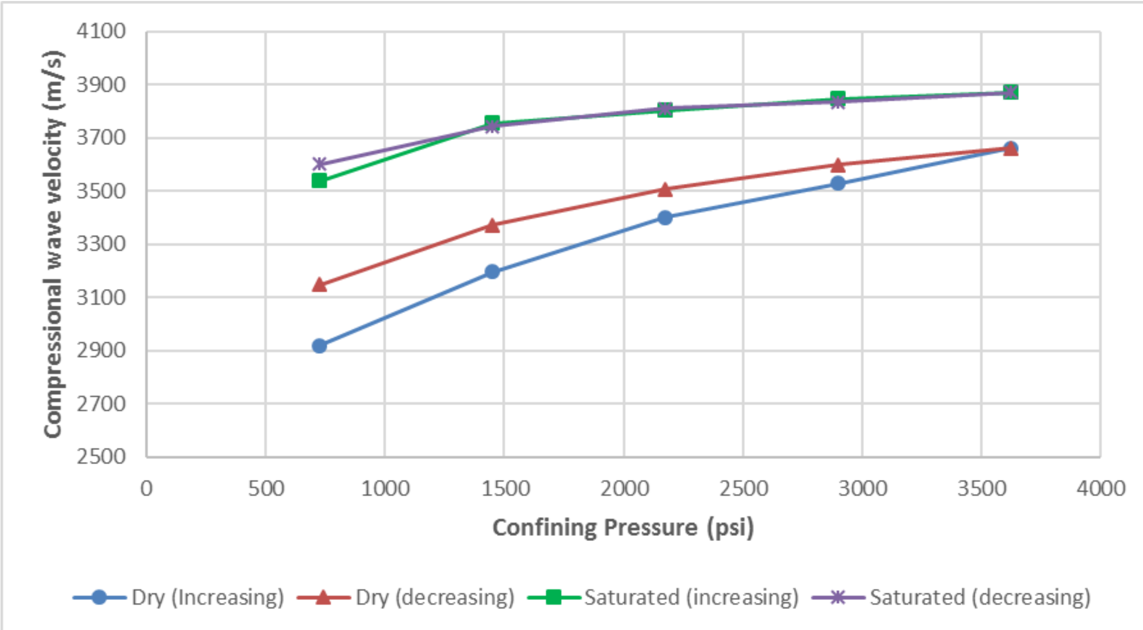

Figure B. 13 Comparison of Compressional wave velocity vs Confining Pressure, Dry vs Brine Saturated (Sample 1-14)

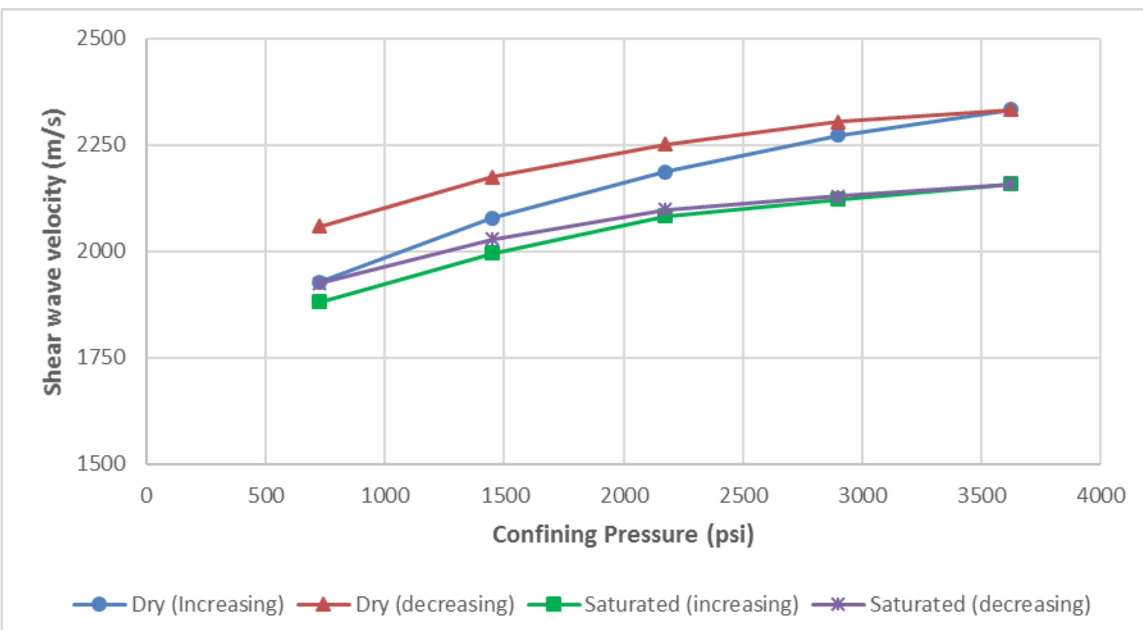

Figure B. 14 Comparison of Shear wave velocity vs Confining Pressure, Dry vs Brine Saturated (Sample 1-14)

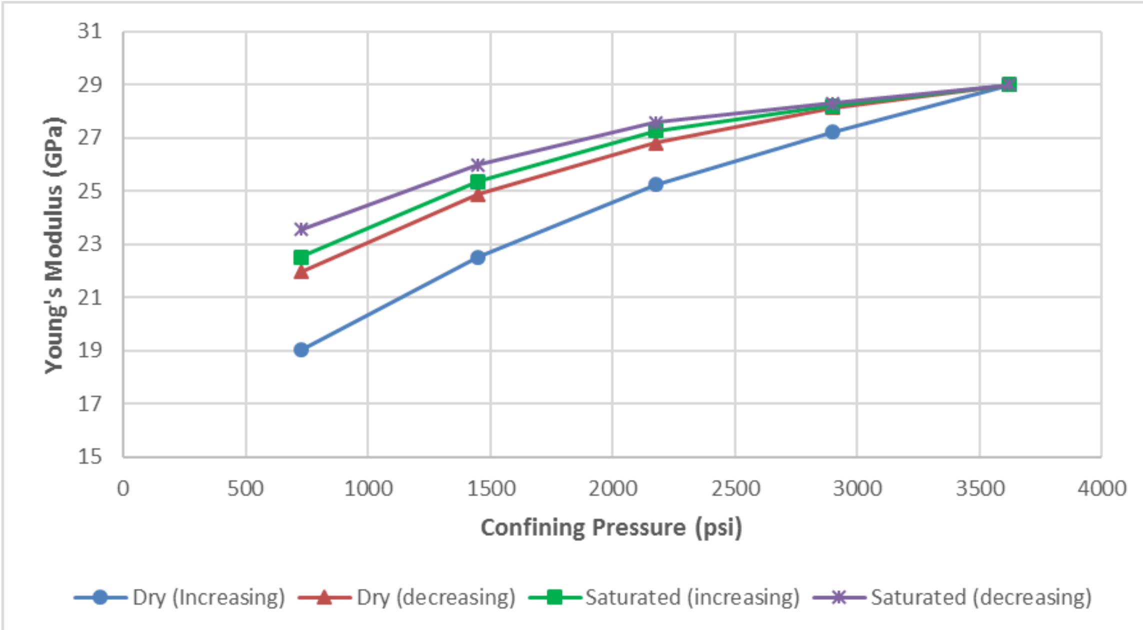

Figure B. 15 Comparison of Young's Modulus vs Confining Pressure, Dry vs Brine Saturated

(Sample 1-14)

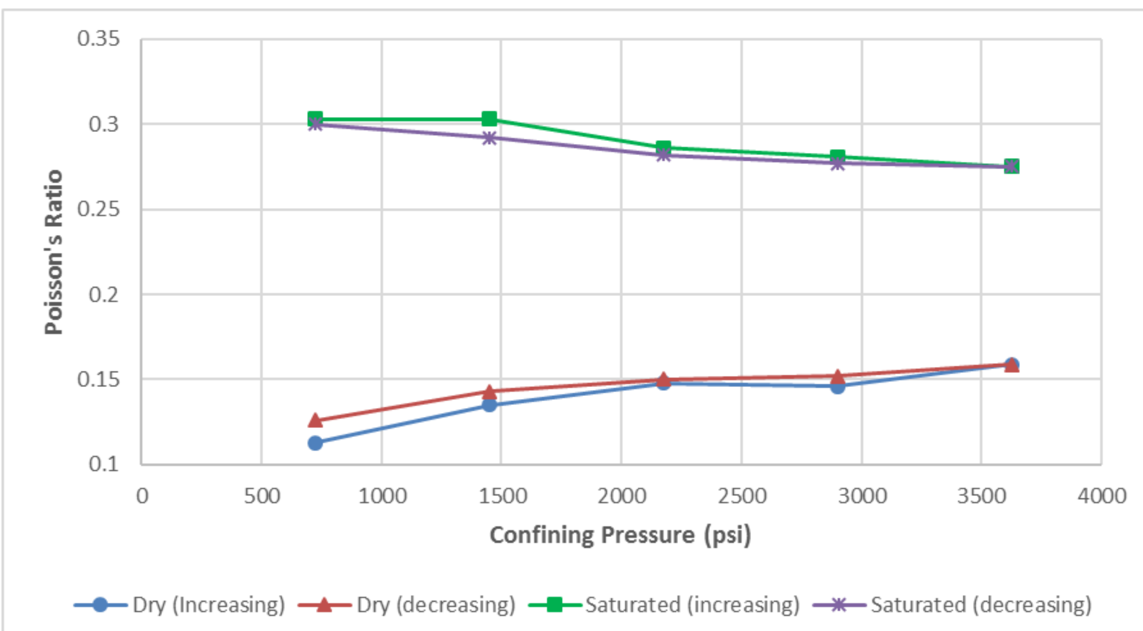

Figure B. 16 Comparison of Poisson's Ratio vs Confining Pressure, Dry vs Brine Saturated

(Sample 1-14)

Ultrasonic tests of oil saturated samples

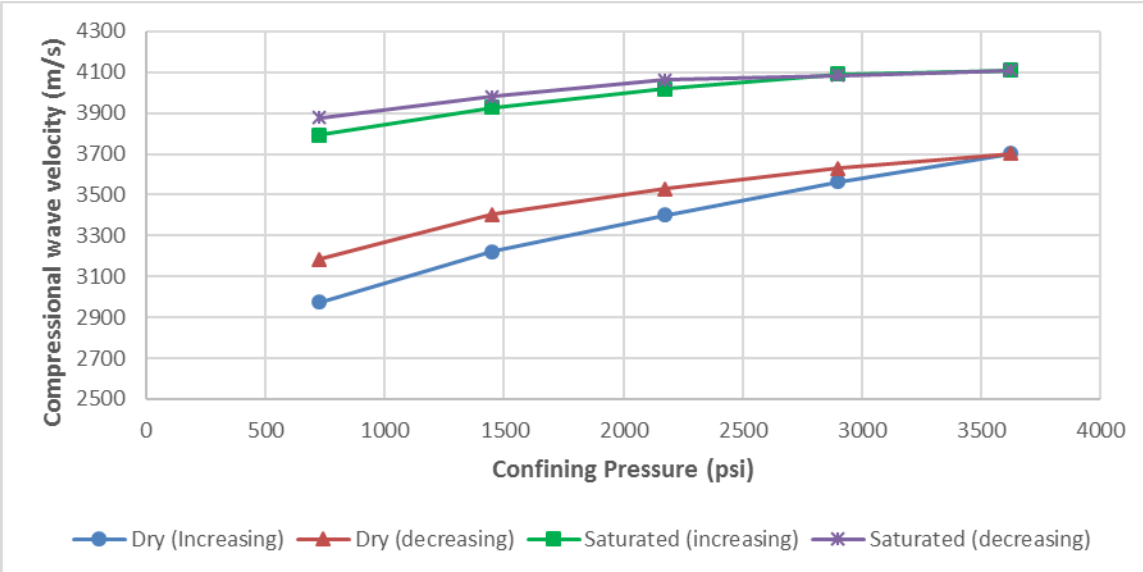

Figure B. 17 Comparison of Compressional wave velocity vs Confining Pressure, Dry vs Oil Saturated (Sample 1-2)

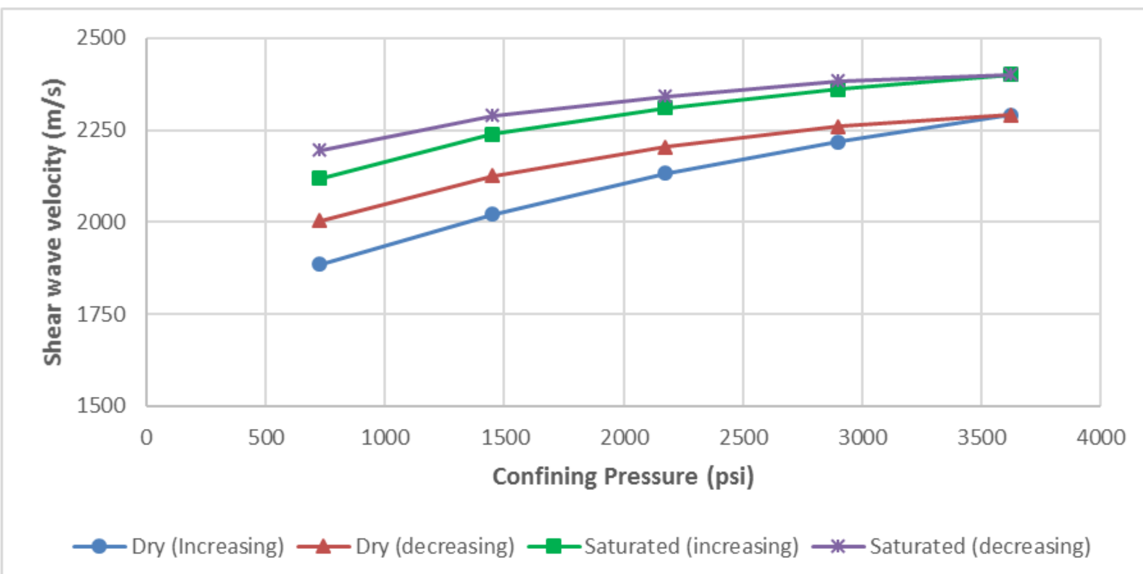

Figure B. 18 Comparison of Shear wave velocity vs Confining Pressure, Dry vs Oil Saturated (Sample 1-2)

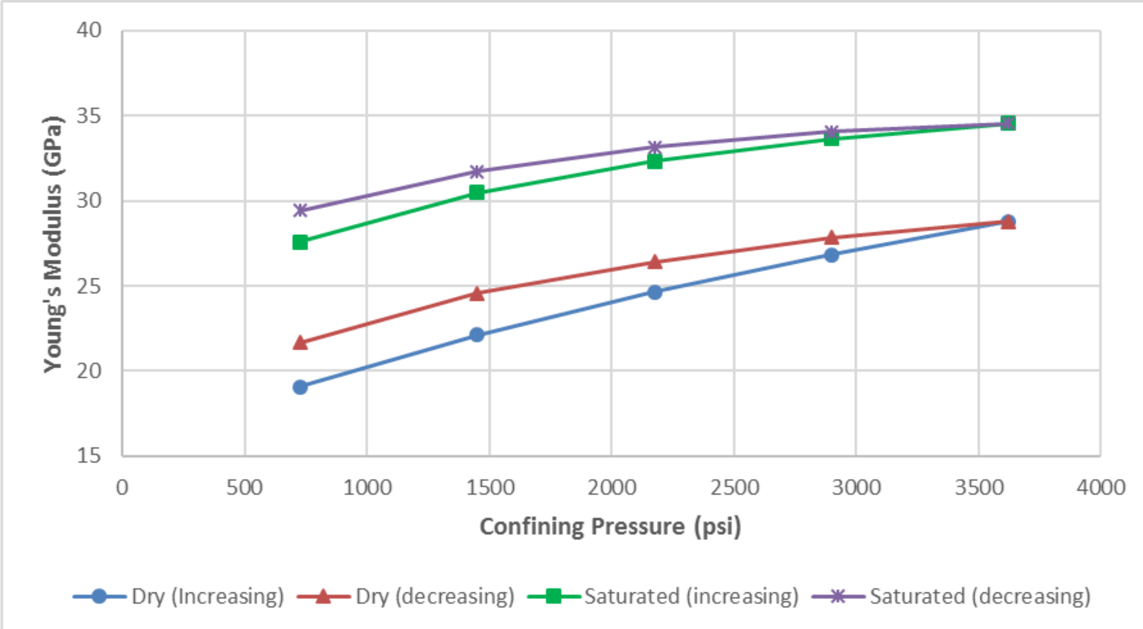

Figure B. 19 Comparison of Young's Modulus vs Confining Pressure, Dry vs Oil Saturated (Sample 1-2)

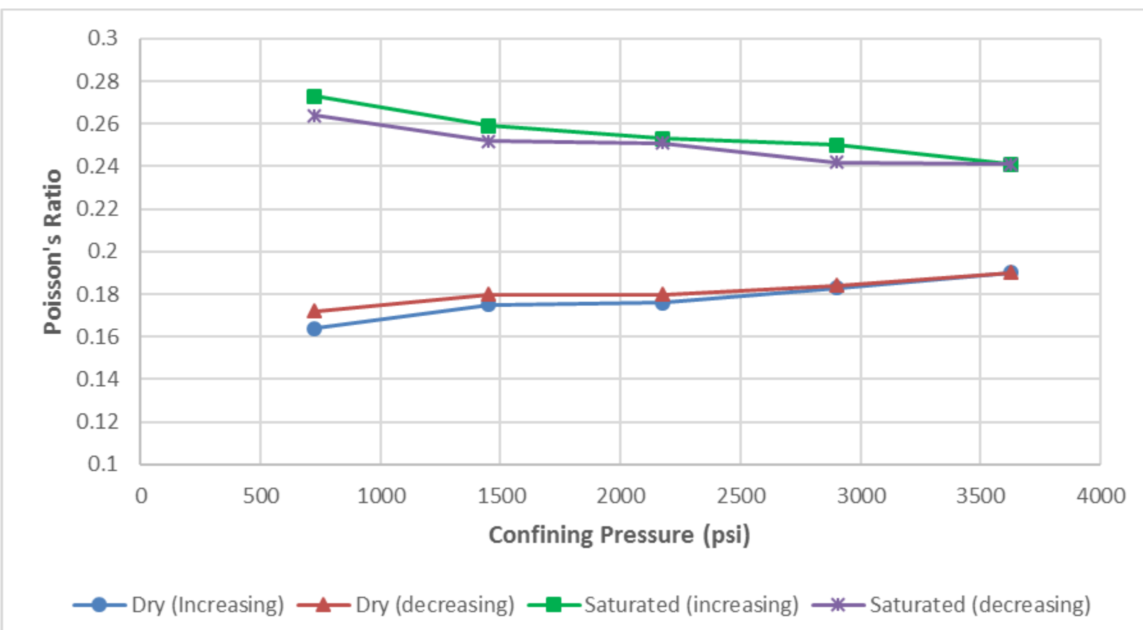

Figure B. 20 Comparison of Poisson's Ratio vs Confining Pressure, Dry vs Oil Saturated (Sample 1-2).

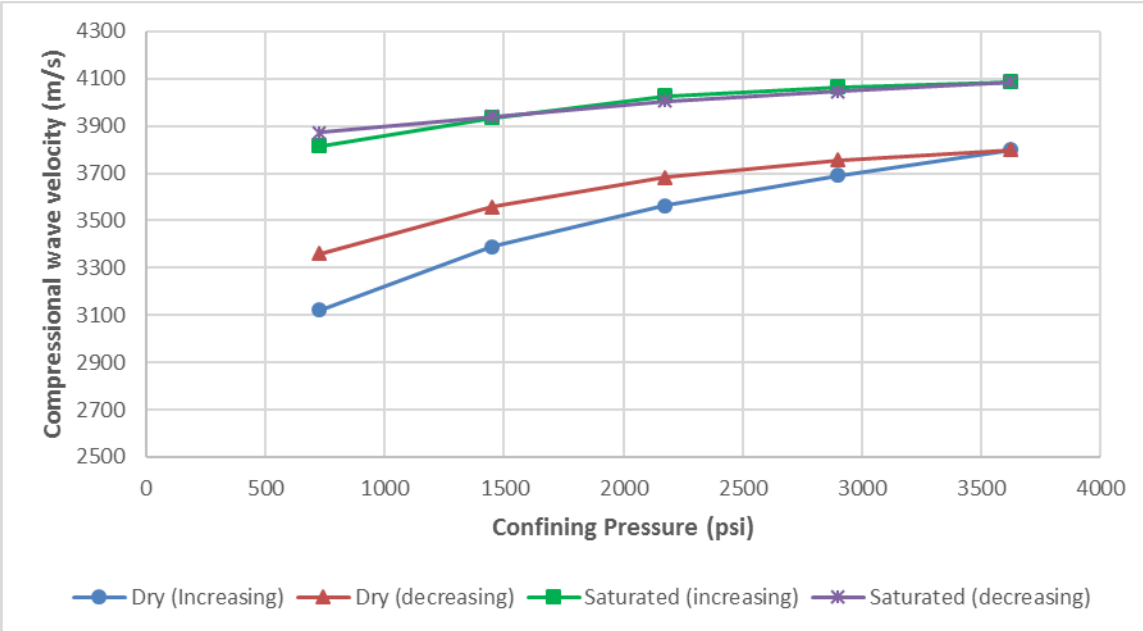

Figure B. 21 Comparison of Compressional wave velocity vs Confining Pressure, Dry vs Oil Saturated (Sample 1-5)

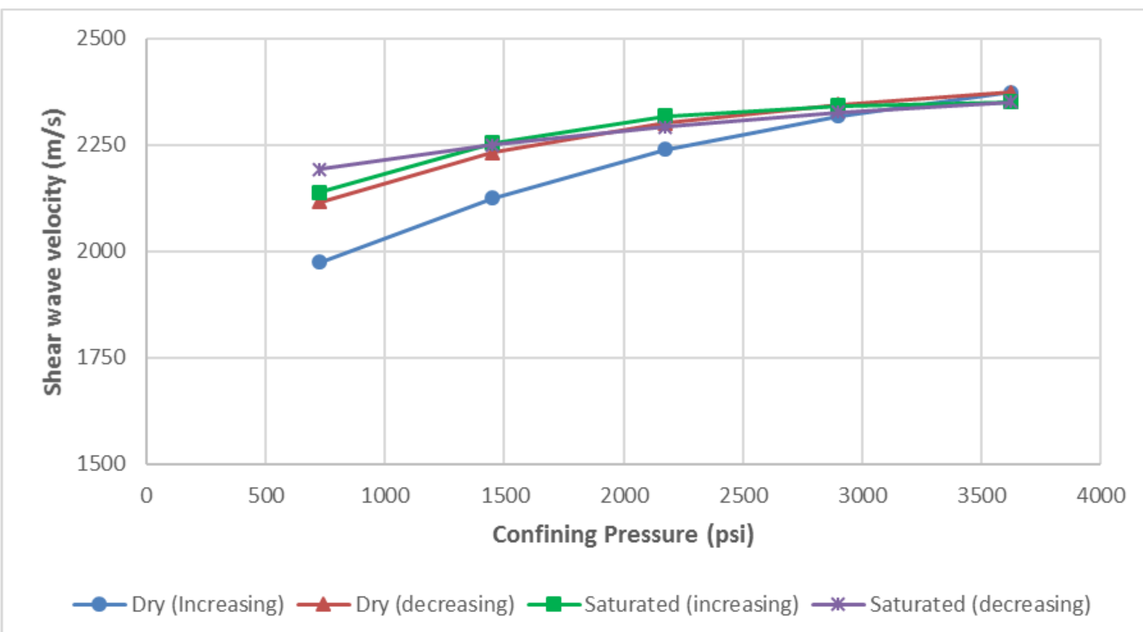

Figure B. 22 Comparison of Shear wave velocity vs Confining Pressure, Dry vs Oil Saturated (Sample 1-5)

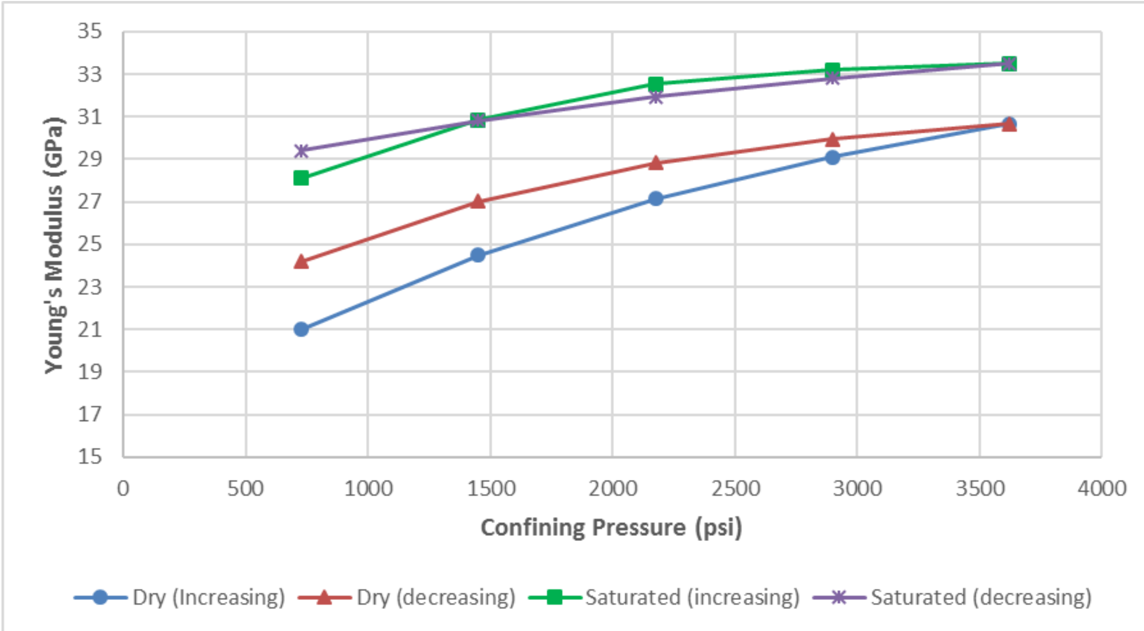

Figure B. 23 Comparison of Young's Modulus vs Confining Pressure, Dry vs Oil Saturated (Sample 1-5)

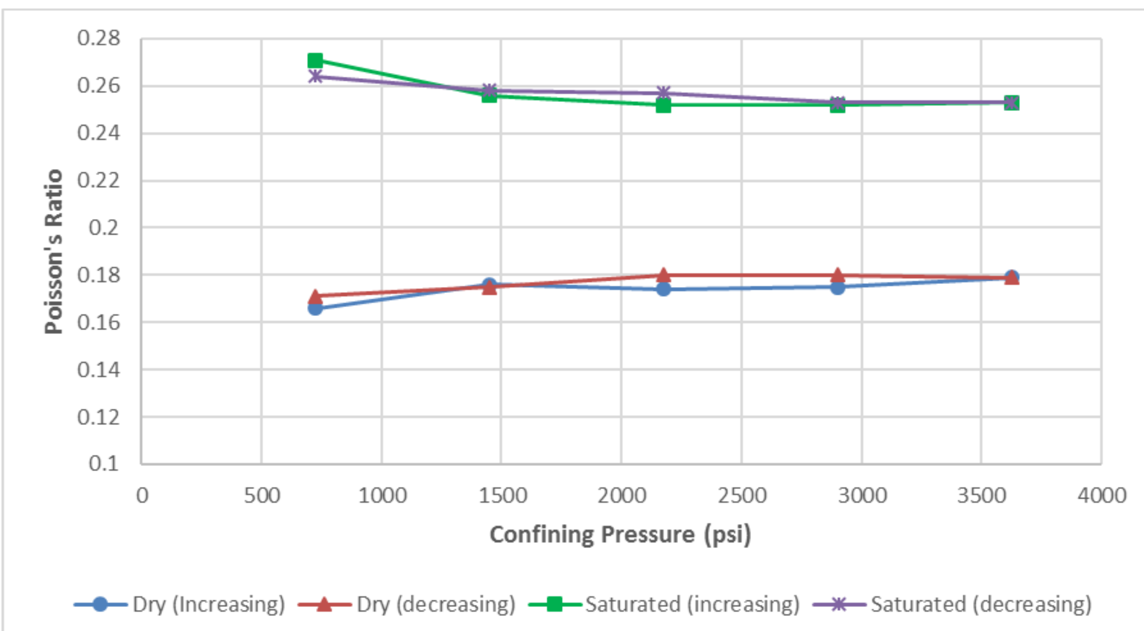

Figure B. 24 Comparison of Poisson's Ratio vs Confining Pressure, Dry vs Oil Saturated (Sample 1-5)

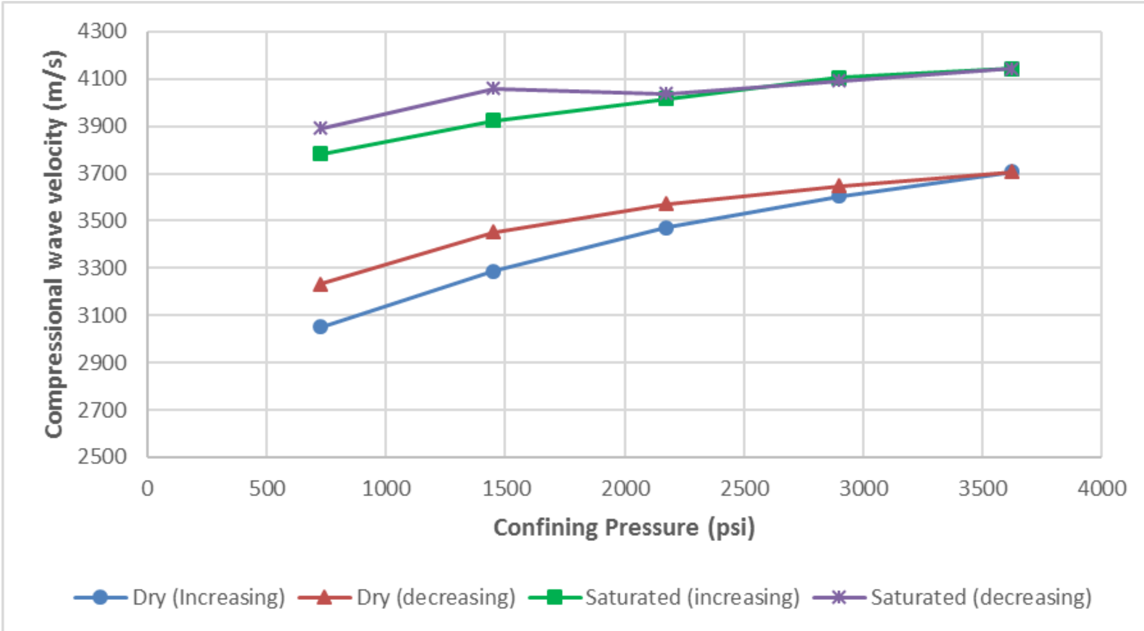

Figure B. 25 Comparison of Compressional wave velocity vs Confining Pressure, Dry vs Oil Saturated (Sample 1-15)

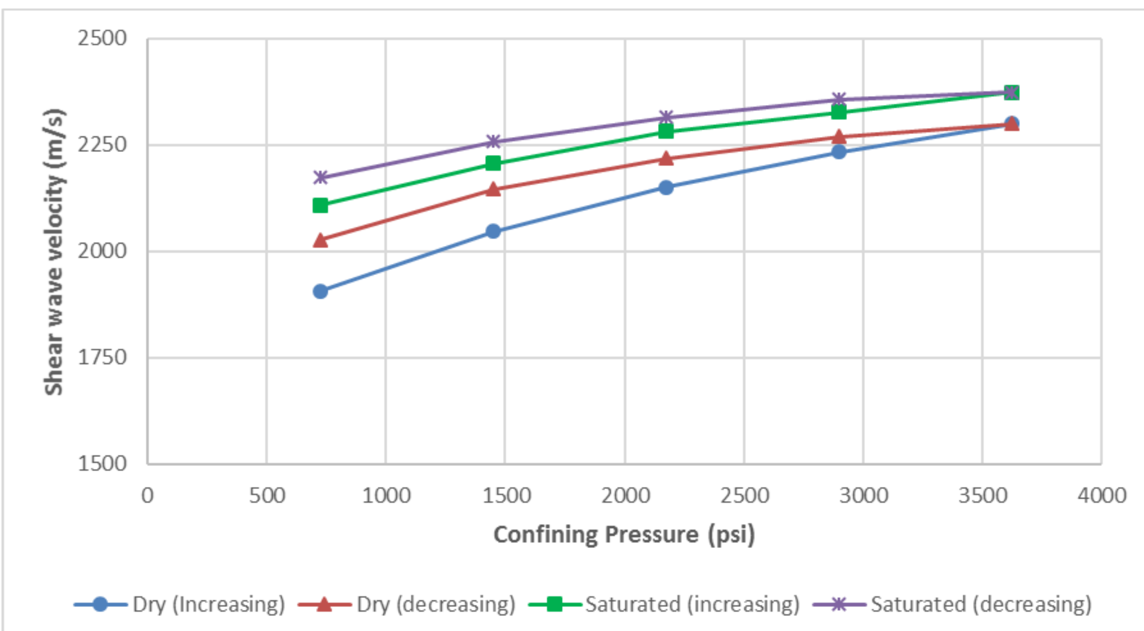

Figure B. 26 Comparison of Shear wave velocity vs Confining Pressure, Dry vs Oil Saturated (Sample 1-15)

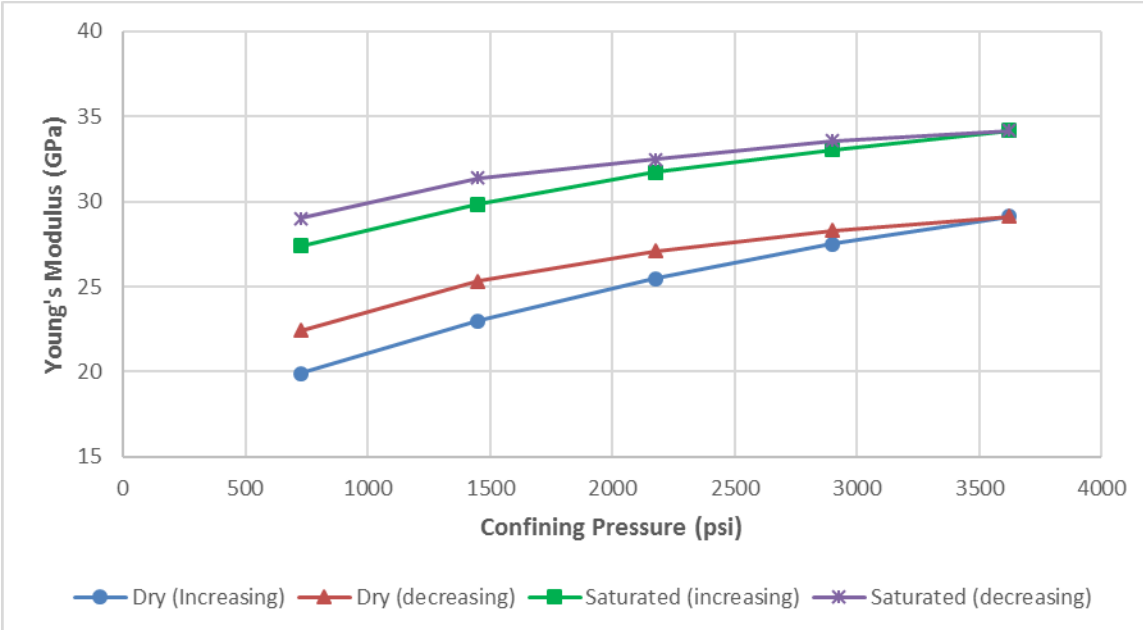

Figure B. 27 Comparison of Young's Modulus vs Confining Pressure, Dry vs Oil Saturated (Sample 1-15)

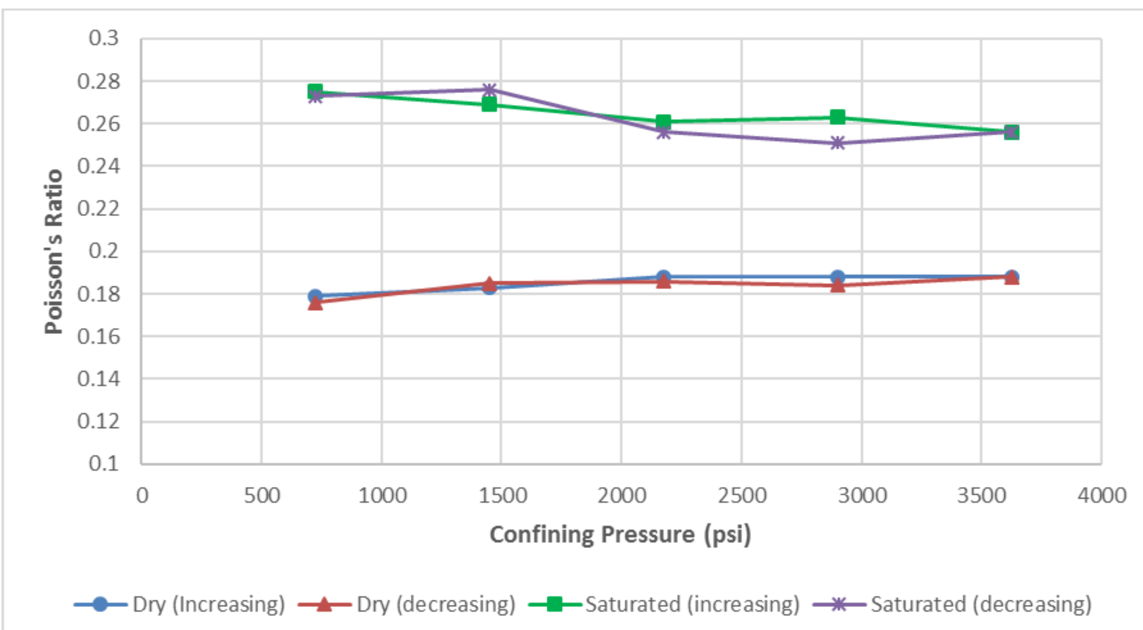

Figure B. 28 Comparison of Poisson's Ratio vs Confining Pressure, Dry vs Oil Saturated (Sample 1-15)

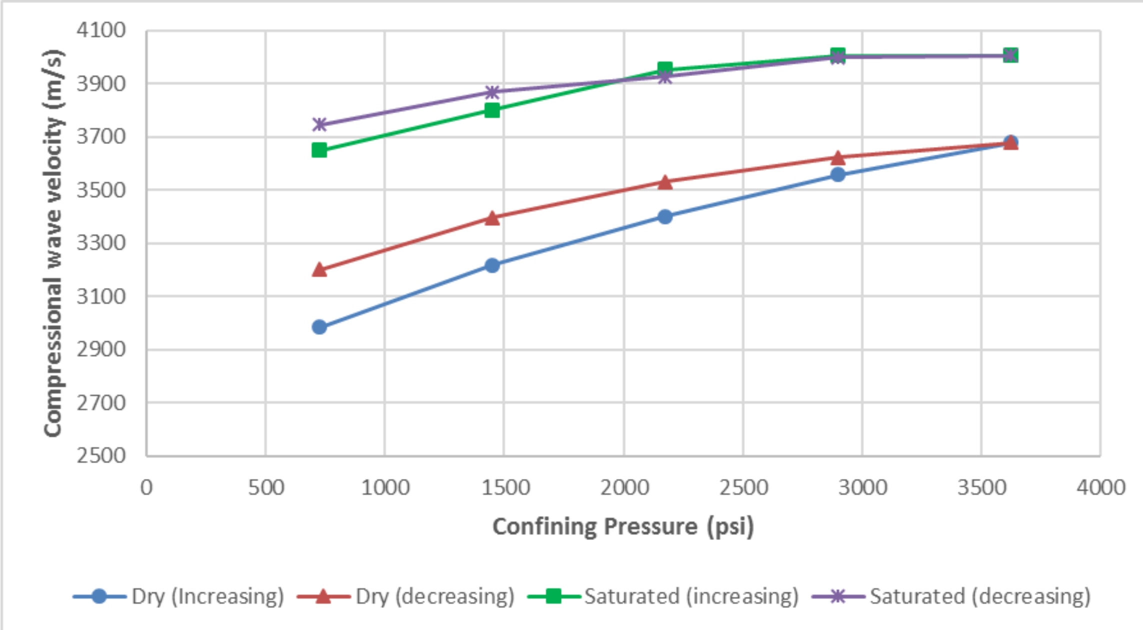

Figure B. 29 Comparison of Compressional wave velocity vs Confining Pressure, Dry vs Oil Saturated (Sample 1-16)

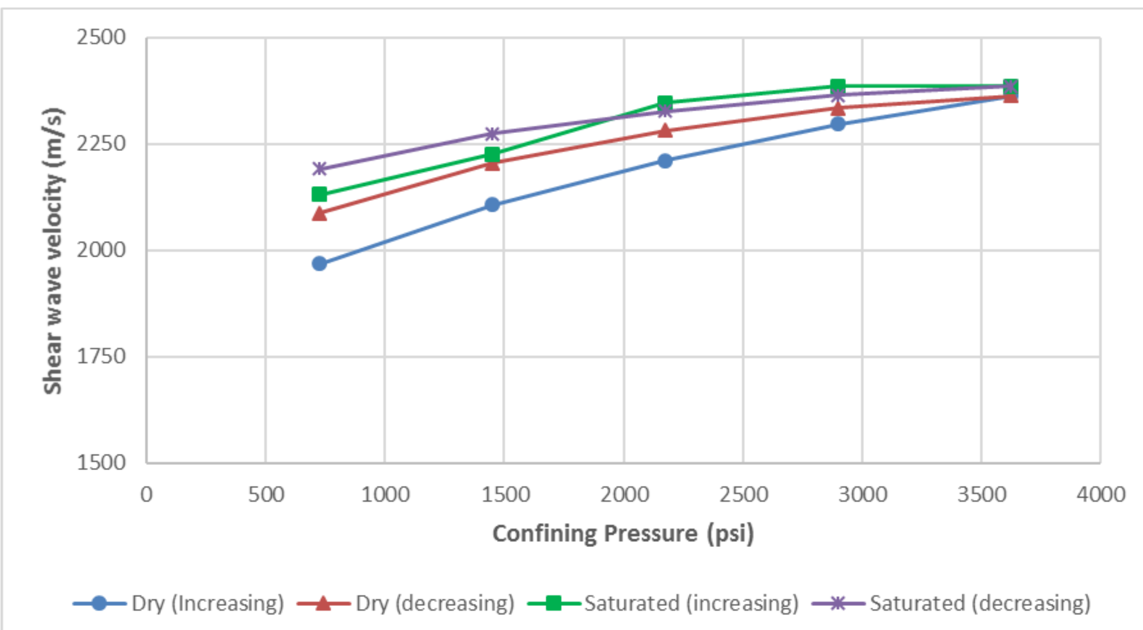

Figure B. 30 Comparison of Shear wave velocity vs Confining Pressure, Dry vs Oil Saturated (Sample 1-16)

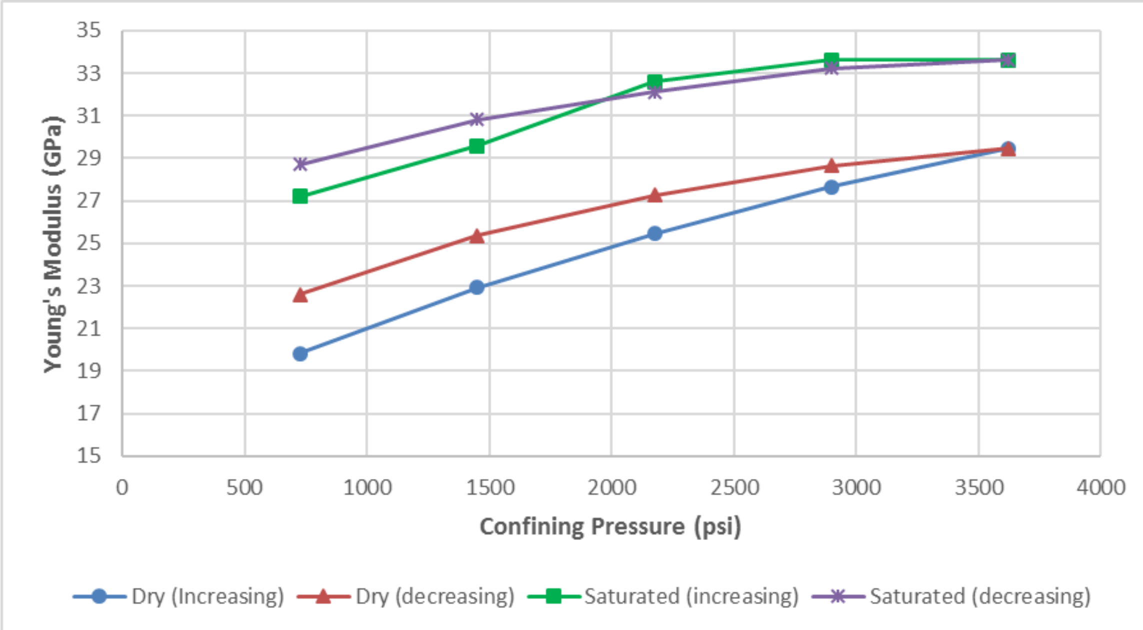

Figure B. 31 Comparison of Young's Modulus vs Confining Pressure, Dry vs Oil Saturated (Sample 1-16)

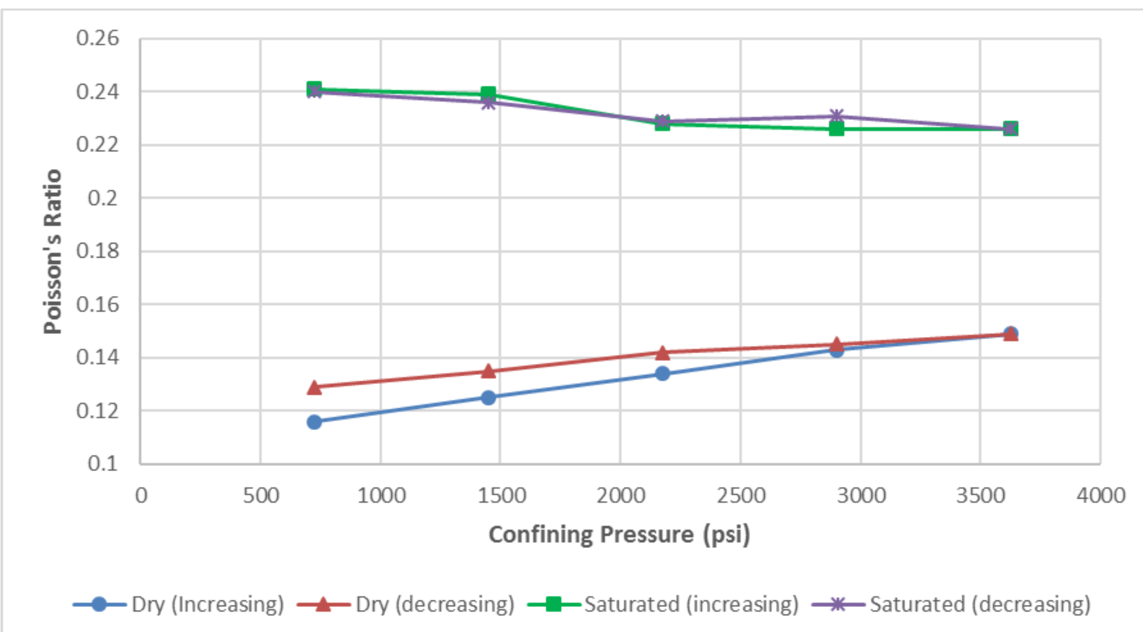

Figure B. 32 Comparison of Poisson's Ratio vs Confining Pressure, Dry vs Oil Saturated (Sample 1-16)

VITAE

Name	: Arqam Muqtadir
Nationality	: Indian
Date of Birth	: 5th July 1992
Email	: arqam_mk@hotmail.com
Address	: A-13, Usman Pura, Aligarh, Uttar Pradesh
Academic Background	: **MS in Petroleum Engineering (December, 2017)**
	BS in Petroleum Engineering (May, 2015)
	King Fahd University of Petroleum & Minerals, Dhahran, Saudi Arabia
Research Interests	: Geomechanics, Well Stimulation, Reservoir Description, Reservoir Simulation and Artificial Intelligence.

Publications

1. Stress-Induced Damage Evolution in Unconventional Shale Monitored by Acoustic Emission (ATCE 2017). **SPE-187336-MS**
2. Application of Artificial Intelligence to Predict Sonic Wave Transit Time in Unconventional Tight Sandstones (IADC, 2018). **SPE-191069-MS**
3. Prediction of Inflow Performance Relationship of a Gas Field Using Artificial Intelligence Techniques (IADC, 2018). **SPE-191000-MS**